



**HAL**  
open science

# In the light of black holes - Accretion discs, coronae and jets around accreting black holes

Julien Malzac

► **To cite this version:**

Julien Malzac. In the light of black holes - Accretion discs, coronae and jets around accreting black holes. Sciences of the Universe [physics]. Université Paul Sabatier - Toulouse III, 2008. tel-00332415

**HAL Id: tel-00332415**

**<https://theses.hal.science/tel-00332415>**

Submitted on 20 Oct 2008

**HAL** is a multi-disciplinary open access archive for the deposit and dissemination of scientific research documents, whether they are published or not. The documents may come from teaching and research institutions in France or abroad, or from public or private research centers.

L'archive ouverte pluridisciplinaire **HAL**, est destinée au dépôt et à la diffusion de documents scientifiques de niveau recherche, publiés ou non, émanant des établissements d'enseignement et de recherche français ou étrangers, des laboratoires publics ou privés.

# IN THE LIGHT OF BLACK HOLES

## Accretion discs, coronae and jets around accreting black holes

Julien Malzac

September 21, 2008



---

# A LA LUMIERE DES TROUS NOIRS

Disques d'accrétion, couronnes et jets  
dans l'environnement des trous noirs accrétants

---

Dossier présenté par

**Julien MALZAC**

pour obtenir

L'HABILITATION A DIRIGER LES RECHERCHES

Université de Toulouse Spécialité: ASTROPHYSIQUE

Soutenue le 8 Janvier 2008

COMPOSITION DU JURY :

M. Dominique LEQUEAU	Directeur de Recherche CNRS	President
Mme Christine DONE	Professeur Universite de Durham	Rapportrice
Mme Isabelle GRENIER	Professeur Universite de Paris	Rapportrice
M. Michel TAGGER	Ingenieur CEA	Rapporteur
Mme Annalisa CELOTTI	Professeur SISSA, Trieste	
Mme Elisabeth JOURDAIN	Chargee de Recherches CNRS	
M. Jean-François OLIVE	Professeur Universite de Toulouse	
M. Andrzej ZDZIARSKI	Professeur Universite de Varsovie	

Centre d'Etude Spatiale des Rayonnements (UPS/CNRS)  
9, av. du Colonel Roche, BP4346, F-31028, Toulouse, CEDEX 4



# Aknowledgements

I thank the members of the habilitation committee for showing interest in this work and managing to attend the defense in spite of their tight schedule.

I am also grateful to Sean Farrel, Elisabeth Jourdain, and Marie-Pierre Moreau for a careful reading of an earlier version of this report. Their corrections and comments significantly improved its presentation. Marie-Pierre Moreau also provided the old Opel Corsa that was used in this work.

I would like to take this opportunity to thank all of those who made it possible for me to follow the path described in this report. I must express again all my gratitude to Elisabeth Jourdain for her indefectible support during all these years. I am also indebted to all my collaborators for their dedicated work, ideas, inspiration and friendship.



*A petite Toumie*



# Contents

<b>1</b>	<b>CURRICULUM VITAE</b>	<b>13</b>
1.1	Personal information . . . . .	13
1.2	Summary . . . . .	13
1.3	Education . . . . .	14
1.4	Professional history . . . . .	15
1.5	Experience and achievements . . . . .	15
<b>2</b>	<b>TEACHING, SUPERVISION AND DISSEMINATION ACTIVITIES</b>	<b>19</b>
2.1	Supervision of students and post-docs . . . . .	19
2.1.1	B.Sc./Licence Level . . . . .	19
2.1.2	Master level . . . . .	19
2.1.3	PhD students . . . . .	20
2.1.4	Post-docs . . . . .	20
2.2	Teaching . . . . .	21
2.3	Refereeing . . . . .	22
2.4	Organising conferences . . . . .	22
2.5	Talking to the media . . . . .	23
<b>3</b>	<b>RESEARCH</b>	<b>25</b>
3.1	Introduction . . . . .	25
3.1.1	Light from black holes . . . . .	25
3.1.2	X-ray spectral states and the structure of the accretion flow . . . . .	26
3.2	Developing numerical tools for high energy radiative transfer . . . . .	30
3.2.1	PhD work: the Non-Linear Monte-Carlo code . . . . .	30
3.2.2	Recent numerical developments: a Fokker-Planck code . . . . .	31
3.3	Modelling the high energy continuum and variability of accreting black holes . . . . .	33
3.3.1	The anisotropic illumination model . . . . .	33
3.3.2	Accretion disc corona models . . . . .	36
3.3.3	Clumps and clouds in AGN . . . . .	42
3.3.4	Effects of general relativity . . . . .	48
3.4	Observations and interpretation of data . . . . .	52
3.4.1	The jet corona connection . . . . .	52
3.4.2	From Beppo-SAX and RXTE, to INTEGRAL and XMM . . . . .	58
3.4.3	Preparing for the future: Simbol-X . . . . .	60
3.5	Conclusion - Summary . . . . .	60
3.6	Research Plans . . . . .	61
3.6.1	Introduction . . . . .	61

3.6.2	The two flow model . . . . .	61
3.6.3	Lightbending . . . . .	62
3.6.4	Absorption . . . . .	62
3.6.5	Back to the clumpy disc model . . . . .	63
3.6.6	Further developments of the Fokker-Planck code and its applications . . .	63
3.6.7	Observation of X-ray binaries with Simbol-X . . . . .	64
3.6.8	Conclusion . . . . .	67
<b>4</b>	<b>LIST OF PUBLICATIONS AND CONFERENCE CONTRIBUTIONS</b>	<b>69</b>
4.1	Articles in refereed international journals . . . . .	69
4.2	Invited talks or reviews at international conferences . . . . .	71
4.3	Refereed conference proceedings . . . . .	72
4.4	Non-refereed publications . . . . .	74
4.5	Communications in conferences . . . . .	77
4.5.1	Talks in international conferences . . . . .	77
4.5.2	Talks in national conferences . . . . .	79
4.5.3	Posters in international conferences . . . . .	79
4.6	Seminars . . . . .	81
4.7	Software . . . . .	83
4.8	Others . . . . .	83
4.8.1	Newsletters . . . . .	83
4.8.2	Thesis and dissertations . . . . .	83
<b>5</b>	<b>FIVE SIGNIFICANT PUBLICATIONS</b>	<b>85</b>
5.1	“X-ray spectra of accretion discs with dynamic coronae” . . . . .	87
5.2	“The optical and X-ray flickering of XTE J1118+480” . . . . .	101
5.3	“Jet-disc coupling through a common energy reservoir in the black hole XTE J1118+480” . . . . .	115
5.4	“Full radiative coupling in two-phase models for accreting black holes” . . . . .	129
5.5	“Bimodal spectral variability of Cygnus X-1 in an intermediate state” . . . . .	141
	<b>Bibliography</b>	<b>156</b>

*Il y a un autre monde mais il est dans celui-ci.*

*Paul Eluard*



# Chapter 1

## CURRICULUM VITAE

### 1.1 Personal information

Name: **Julien MALZAC**  
Citizenship: French  
Date of Birth: 13/04/1973  
Present position: Chargé de Recherche au CNRS  
based at Centre d'Etude Spatiale des Rayonnements (CESR)  
(UMR 5187 UPS/OMP/CNRS)  
Address: CESR, 9 Avenue du Colonel Roche, BP44346,  
31028 Toulouse Cedex 4, France  
Telephone: +33 (0)561557536 Fax : +33 (0)561556701  
E-mail: malzac@cesr.fr

### 1.2 Summary

My research is about studying the radiation (essentially hard X-rays) coming from accreting black holes with the aim of extracting information about the physical conditions in their immediate vicinity. The main questions I am trying to answer are the following. What is the structure and geometry of the accreting material close to the black hole ? What is the nature of the connection between accretion processes and the formation of jets observed in those systems ? My approach is centered on a detailed comparison of the observations with the predictions of various models. My research programme is threefold:

**(i) Development of numerical tools for radiative transfer in relativistic plasmas:**

During my PhD in Toulouse, I developed, starting from scratch, a radiation code based on the non-linear Monte-Carlo method. This code takes consistently into account most of the radiation physics relevant for the emission of accreting black holes, as well as other high energy sources such as neutron stars or gamma-ray bursts. I am still improving this code, coupling it with other codes, and also developing new codes to allow us to deal with more and more realistic situations.

**(ii) Modeling:** I use those tools, as well as others, to study the predictions of different models for **the spectra and the variability of accreting black hole sources**. While I was a post-doc in Milan (OAB) and then in Cambridge (IoA), I studied different models for the hard X-ray emission of accreting black holes sources (both in Seyfert galaxies and X-ray binaries). The observed spectral and temporal characteristics of the sources were compared with the results

from simulations. This work has significant implications for the structure and geometry of the innermost region of the accretion flow. It is still pursued now that I am back in Toulouse with a permanent research position at CNRS.

**(iii) Data analysis and interpretation:** I am directly involved in the analysis and interpretation of observations performed with space-based X-ray and  $\gamma$ -ray telescopes such as XMM and INTEGRAL. I am committed to the scientific preparation of Simbol-X which will be the first hard X-ray ( $>10$  keV) focussing telescope ever. I also participate in multi-wavelength (radio to hard  $\gamma$ -rays) observations of the spectral energy distribution and fast variability of micro-quasars and their interpretation.

I am author or co-author of 43 refereed publications, have been a speaker in 24 international conferences (12 were invited talks). I have an experience of teaching at all levels. I started during my PhD thesis as a ‘moniteur’ (teaching assistant) and later as an **ATER (teaching and research fellow) at Université Toulouse III**. I also had several opportunities to **supervise or co-supervise post-docs and students** doing research training periods, or preparing their PhD.

### 1.3 Education

1996/99 **Doctorat en Astrophysique de l’Université Paul Sabatier, Toulouse III**, prepared at CESR, under the supervision of Elisabeth Jourdain:

“Modélisation de l’émission X et  $\gamma$  des objets compacts  
par les méthodes Monte-Carlo”

PhD defended on 08/10/1999, and obtained with first-class honours  
 (“mention très honorable et les félicitations du Jury”)

The thesis committee consisted of:

Gilles Henri	President
Jean-Marie Hameury	Rapporteur
Laura Maraschi	Rapporteuse
Elisabeth Jourdain	Directeure de These
Philippe Laurent	Examineur
Dominique Lequeau	Examineur
Michel Tagger	Examineur
Gilbert Vedrenne	Examineur

Teaching activities as ‘moniteur’ at UPS (Teaching assistant).

1995/96 **DEA Astrophysique, Géophysique et Planétologie**,

Major: Astrophysics,  
Université Paul Sabatier, Toulouse III,  
‘Mention Bien’ (magna cum laude)

1994/95 **Maîtrise de Physique**,

Elective: Astrophysics,  
Université de Bordeaux I,  
‘Mention Assez Bien’ (cum laude).

1993/94 **Licence de Physique**, Université de Bordeaux I, ‘Mention Bien’ (magna cum laude).

1993 **DEUG A**, Université de Bordeaux I.

1992/1993 **Mathématiques Supérieures et Spéciales**, Lycée Michel Montaigne, Bordeaux

1991 **Baccalauréat C** (Sciences), Lycée Evariste de Parvy, St Paul, Réunion, ‘Mention Bien’ (magna cum laude).

## 1.4 Professional history

2004/2007 **Chargé de Recherche CNRS**

based at **Centre d’Étude Spatiale des Rayonnements (CESR), Toulouse** April

2005: visiting researcher at the Kavli Institute for Theoretical Physics, Santa-Barbara, California

July 2005: visiting researcher at the Aspen Center for Physics, Aspen, Colorado

2002/04 **Associate Researcher, Institute of Astronomy, Cambridge, UK**

Funded under the PPARC Theory rolling grant of IoA

2000/02 **Post Doc, Brera Observatory, Milan, Italy**

Funded by the Italian Research Council

and the European Commission

(grant from the TMR network ‘Accretion onto black holes, neutron stars and protostars’)

1999/2000 **ATER (Teaching and Research Fellow), Université Toulouse III, France**

research at Centre d’Étude Spatiale des Rayonnements (*CESR*)

Dec. 1999 – Jan. 2000: visiting researcher at Stockholm Observatory, Sweden

## 1.5 Experience and achievements

### Teaching experience

More than 380 hours teaching physics, statistics, instrumentation, scientific computing in the form of lectures (‘cours’), tutorials (‘Travaux Dirigés’), or practical works (‘Travaux Pratiques’) at all levels i.e. DEUG, Licence (B.Sc.), Maîtrise and Master of Physics . See Sec. 2.2.

### Supervising experience

Supervision or co-supervision of 6 students (among which 2 PhD students), and 2 post-docs. See Sec. 2.1.

### Publications

24 publications in international refereed journals, including 10 as lead author

19 publications in international refereed conference proceedings including 9 as lead author

34 publications in non-refereed conference proceedings including 22 as lead author

### Conferences, seminars and oral communications

24 talks in international conferences of which 12 were invited or solicited talks or reviews

8 talks in national conferences

25 poster presentations in national or international conferences

27 seminars given in various institutions around the world

### Experience abroad

2005 Aspen Center for Physics, Colorado: 20 days in July 2005 to participate in the Aspen summer programme: “Revealing Black Holes” which aimed at gathering international experts on accreting black holes.

2005 Kavli Institute for Theoretical Physics, University of Santa-Barbara, California: one month in April 2005 to participate in the research programme “Physics of Astrophysical Outflows and Accretion Disks” gathering international experts of accretion discs and jets.

2002/2004 ‘Associate Researcher’ at the Institute of Astronomy (Cambridge, UK) where I was working mainly with Andy Fabian

2000/2002 Post-doc at Osservatorio Astronomico di Brera (Milan, Italy). My main collaborators were Laura Maraschi, Gabriele Ghisellini and Tomaso Belloni.

2001 During summer two weeks in the United Kingdom at the Open University (Milton Keynes), collaborating with Sylvain Chaty and Carole Haswell.

1999/2000 Two stays of one month each at Stockholm observatory (Sweden) for a collaboration with Juri Poutanen, Boris Stern and Andrei Beloborodov.  
(from 21/11/99 to 21/12/99, and from 10/01/00 to 7/02/00).

### Collaborations

During my peregrinations, I had the opportunity to develop collaborations with many researchers. I have particularly strong links with the institutes in which I did my PhD and post-docs (CESR, OAB, IoA), but I also have long term collaborations with other institutes in France and abroad. My main collaborators are:

Volker Beckman (ISDC, Versoix)

Tomaso Belloni (OAB, Merate)

Andrei Beloborodov (University of Columbia, New York)

Marion Cadolle Bel (ESAC, Madrid)

Annalisa Celotti (SISSA, Trieste)

Sylvain Chaty (AIM, Saclay)

Melania Del Santo (IASF, Rome)

Anne-Marie Dumont (LUTH, Meudon)

Andy Fabian (IoA, Cambridge)

Philippe Ferrando (APC, Paris)

Gabriele Ghisellini (OAB, Merate)

Elisabeth Jourdain (CESR, Toulouse)  
Alexandre Marcowith (LNPT, Montpellier)  
Laura Maraschi (OAB, Milan)  
Andrea Merloni (MPE, Garching)  
Giovanni Miniutti (IoA, Cambridge)  
Martine Mouchet (APC, Paris)  
Pierre-Olivier Petrucci (LAOG, Grenoble)  
Juri Poutanen (University of Oulu, Oulu)  
Jean-Pierre Roques (CESR, Toulouse)  
Henk Spruit (MPA, Garching)  
Andrzej Zdziarski (CAMK, Warsaw)

### **Professional memberships**

Member of the Société Française d’Astronomie et Astrophysique (SF2A), of the European Astronomical Society (EAS) and of the CNRS research group ‘Groupement de Recherche Phénomènes Cosmiques de Haute Energie’.



## Chapter 2

# TEACHING, SUPERVISION AND DISSEMINATION ACTIVITIES

### 2.1 Supervision of students and post-docs

#### 2.1.1 B.Sc./Licence Level

2007 Baptiste Schubnel and Thomas Ristorcelli, SupAero engineering students, 'Projet d'Initiation à la Recherche', April to June 2007

Aim: bibliographic work on the Blandford-Payne, Blandford-Znajek effects, the magneto-rotational instability, simulations of the 'synchrotron boiler effect' using a Fokker-Planck code.

Report: "Etude des disques d'accrétion et des processus radiatifs au sein des couronnes des binaires X/AGNs"

Supervisors: Renaud Belmont, Julien Malzac

2000 Romain Ferran, Licence training period, April to June 2000.

Aim: application of the numerical simulation code developed during my PhD to the truncated disc and hot flow geometry. Study of the spectra predicted by such models.

Report: "Modélisation des émissions hautes énergies des trous noirs"

Supervisor: Julien Malzac, Elisabeth Jourdain

#### 2.1.2 Master level

2005: Adnan Ghribi, Master 1 training period, April to June 2005

Aim: study of the flux-flux correlation in the rapid optical and X-ray variability of the black hole binary XTE J1118+480.

Report: "La variabilité X et optique du trou noir XTEJ1118+480"

Supervisor: Julien Malzac

2000: Sébastien Bardeau and Emmanuel Lavallette, Maîtrise training period, April to June 2000.

Aim: study the properties of Cyclo/Synchrotron radiation

Report: "L'émission cyclo/synchrotron"

Supervisors: Alexandre Marcowith, Julien Malzac

1998 Katia Pecqueron and Inès Prieto, Maîtrise training period, May to June 1998.

Aim: use a Non-linear Monte Carlo Code to simulate the emission of a pair plasma under

various conditions.

Report: “Etude d’un modèle de Comptonisation”

Supervisor: Julien Malzac, Elisabeth Jourdain

1998 Denis Rouquette, Maîtrise training period, May to June 1998.

Aim: study of the properties of the geodesics around a rotating black hole.

Report: “Calcul de géodésiques autour d’un trou noir de Kerr”

Supervisors: Elisabeth Jourdain, Julien Malzac

### 2.1.3 PhD students

2004-2006 Thitiwat Suebsubwong, PhD student at the University of Toulouse III, defended in November 2006.

Aim: study of the general relativistic effects on the appearance of accreting black holes

Report: “Effets relativistes sur l’émission haute énergie des trous noirs”

Advisors: Elisabeth Jourdain, Alexandre Marcowith and Julien Malzac.

My contribution was to help him check his numerical results, find some interesting astrophysical applications to his calculations and write his paper. See Sec. 3.3.4.1. Thitiwat is now a Professor at the University of Bangkok

2006-2008 Giovanni De Cesare, PhD student, joint PhD between University of Bologna and Toulouse, defense expected in 2008.

Aim: observation of compact objects with IBIS/INTEGRAL

Advisors; Pietro Ubertini (CNR, Rome), Peter von Balmoos (CESR), G. Palumbo (U. Bologne), Julien Malzac

My contribution was to advise him on his research project and on the interpretation of the data.

### 2.1.4 Post-docs

2006-2008 Renaud Belmont, CNRS post-doc at CESR.

Aim: working on the development of a Fokker Planck code to simulate particle acceleration and radiation processes in relativistic plasma (see Sec. 3.2.2 and 3.6.6).

Advisors: Julien Malzac, Alexandre Marcowith (LPTA, Montpellier)

2005-2007 Angélique Joinet, CNES post-doc at CESR.

Aim: analysis and interpretation of INTEGRAL data on X-ray binaries. See Sec. 3.4.2.

Advisors: Elisabeth Jourdain, Jean-Pierre Roques, Julien Malzac

## 2.2 Teaching

1999/2000 **Attaché Temporaire d’Enseignement et de Recherche**  
at Université Paul Sabatier, Toulouse III.

My teaching duties of 96 hours (‘équivalent TD’) were performed in DEUG, Licence and Maîtrise of Physics. The subjects were essentially in instrumentation, numerical modelling and computing.

During the first semester I taught 6 hours of ‘cours’ (lectures) and 6 hours of ‘travaux dirigés’ (TD, tutorials) for the Licence of Physics. This teaching constituted an introduction to spectroscopy as a part of the Licence instrumentation course. It was about briefing the students on the main mechanisms for the production and absorption of radiation of wavelengths ranging from the radio to the  $\gamma$ -ray domain and the properties of blackbody emission. I also had to present the various types of spectra that can be observed (continuum, lines in absorption/emission) and show that those spectra contain a lot of information on the emitting medium. In addition, I had to introduce various spectroscopy techniques, presenting the different physical processes used to detect photons as well as the principles of operation of common spectrographs with an emphasis on the problems of deconvolution. Most of this teaching was new to the University, and I participated in setting it up. My main contribution was the development of all the exercises for the tutorials.

I also got involved in a new teaching module at DEUG level which aimed at helping students to get familiar with basic statistical notions (probability densities, mean, variance, correlation...) and their applications to measurement (uncertainties, propagation of errors ...). This teaching comprised lectures and practical works (‘Travaux Pratiques’, TPs). The TPs were dealing with statistical processing of data (using EXCEL), the last sessions were devoted to small projects consisting of the description of an experiment and the analysis of its results using the statistical and computational tools introduced during the course. This teaching represented 40 hours (‘équivalent TD’).

I completed my service with 40 hours of TPs of scientific computing for the Licence of Physics where I supervised students carrying out a project of numerical computation with MATLAB. The students, working in pairs, had chosen their project among a few dozen covering different fields of physics. Each teacher of the course was responsible for several of these topics. For questions and help, the students were keeping in touch with the teacher in charge of their subject. I was responsible for the following projects:

- The prism: simulation of the propagation of light in a prism (application of the Snell-Descartes and Cauchy laws).
- The refracting telescope: modelling of lenses and application to refractor telescopes.
- Evolution of the universe: resolution of the Friedmann equations and study of the different solutions.

I also participated in tutorials (TDs) in Licence (8 hours) which were an introduction to computing (MATLAB), mathematical and numerical techniques for instrumentation (Fourier analysis). I also devoted 6 hours to TDs in scientific computing for the Maîtrise of Physics. The aim was to let the students apply the concepts of statistical physics to the numerical resolution of various problems (*e.g.* the internal structure of a white dwarf).

1996/99: **Moniteur CIES** at Université Paul Sabatier, Toulouse III.

During the three years of preparation of my PhD thesis, I was teaching 96 hours of TPs per year as ‘moniteur’. I was overseeing practical works (TPs) of general physics in DEUG. I had to present experiments in hydrodynamics, undulatory optics and electricity. Then help the students to carry them out. Those experiments often involved the use of computers (numerical simulations, data acquisition). I also taught in some TDs of the same course. My service was 96 hours of TPs per year. To make the presentation of the optics experiments easier, I designed a poster presenting the different diffraction and interference patterns in 3D. My pedagogy tutors were Prof Elefterion during the first 2 years and then Prof Brustet during the last year.

## 2.3 Refereeing

I am a referee for the *Astrophysical Journal*, *Monthly Notices of the Royal Astronomical Society*, *Astronomy and Astrophysics*, *Astronomy and Astrophysics Reviews*, *Astrophysics and Space Sciences*, as well as various conference proceedings. The rate is about 2 to 3 articles per year.

I was a member of the PhD thesis committee of Clément Cabanac entitled “Variabilité temporelle des binaires-X: observations avec INTEGRAL, modelisation” which was defended on 26 april 2007 at Université Joseph Fourier in Grenoble.

I was a referee for the PhD thesis of Ascension Camero Arranz entitled “Accreting X-ray pulsars. The high energy picture”, defended at the University of Valencia (Spain) on 31 October 2007.

## 2.4 Organising conferences

I participated in the organisation of the PhD school “Observing the X- and Gamma-ray Sky” that took place in Cargèse, Corsica on 3-14 April 2006. As both a member of the Local Organising Committee and Scientific Organising Committee, I participated in the elaboration of the scientific program, the selection of speakers, and the search for funding. The school was a success (see <http://lheawww.gsfc.nasa.gov/users/beckmann/school/> )

When I arrived at CESR in 2004, I proposed to organize group seminars in the ‘Département des Hautes Energies’. During those fortnightly meetings, group members as well as visitors are invited to present their research. Those seminars rapidly became quite popular and helped improve communication and social life in the group. I am also in charge, together with Natalie Webb, of the planning of the institute seminars at CESR.

In addition, I am part of the organising team of the ‘Soirées Scientifiques’ (conferences of broad interest for the general public) and the ‘Grands Séminaires de l’Observatoire Midi-Pyrénées’ (conferences of broad interest for a scientific audience).

See <http://www.omp.obs-mip.fr/grandsseminaires/>.

## 2.5 Talking to the media

- ‘Le chant du trou noir’, interview in ‘Les Années lumières’ on Radio Canada, broadcasted on 21 September 2003.  
<http://www.radio-canada.ca/radio/lumiere/archives/archives2003/septembre2003.html>
- NASA and ESA press release, July 2004, “ESAs high-energy observatories spot doughnut-shaped cloud with a black-hole filling”. Lead scientist: V. Beckmann, <http://www.esa.int/esaSC/SEM962>
- Press conference, October 2004: “Il dipartimento delle alte energie del CERN”, popularisation of the research activities performed at CERN in the field of high energy astrophysics (presentation to members of the Italian press).



# Chapter 3

## RESEARCH

### 3.1 Introduction

#### 3.1.1 Light from black holes

I specialise in the study and modelling of X-rays and  $\gamma$ -rays coming from astrophysical black holes. There are two main types of black holes emitting high energy radiation. On the one hand, there are solar mass objects formed at the end of the life of a massive star. On the other hand, there are the super-massive black holes located at the center of galaxies with masses larger than a million times the mass of the sun. A black hole may accrete gas from its environment (or from a companion star in the case of stellar black holes) and then radiate a fraction of the gravitational energy of the infalling material. Due to viscosity (and other dissipation processes) the infalling gas can be heated up to a very high temperature. The observations indicate the presence of a very hot plasma with a temperature of a few billion Kelvin in the inner parts of the accretion flow leading to copious X-ray and  $\gamma$ -ray emission. Those sources provide a unique laboratory to study physics in extreme conditions (temperature, energy density, strong gravity ...). Learning about the physical conditions in the environment of a black hole is of fundamental importance for at least two reasons: first, the existence of black holes is the most far-reaching implication of the theory of general relativity, and we would like to use the observations to test this theory. Second, black holes are present in the nuclei of probably all galaxies. The evolution of black holes and galaxies appears intrinsically linked. Understanding how black holes interact with their environment is a prerequisite to the study of the formation and evolution of the first structures of the universe.

For the astrophysicist the main questions are the structure and geometry of the accretion flow, as well as its evolution. My approach attempts to link the theoretical models, describing the complicated processes occurring in the black hole environment, with the increasingly detailed observations obtained with the new generations of space-based X-ray and  $\gamma$ -ray telescopes. It focuses on the study of high energy radiation processes in relativistic plasmas.

In Sec. 3.2, I present the efforts I have been pursuing for almost 10 years in order to develop numerical simulation tools for radiative transfer in the hot X-ray emitting plasma surrounding black holes. Then, in Sec. 3.3, I will show how these tools have been applied to the modelling of the high energy continuum and variability of accreting black holes. In Sec. 3.4, I will describe more observational activities mainly related to the jet and disc coupling in black hole binaries. A summary of the main results will be provided in Sec. 3.5. Finally, my research project is presented in Sec. 3.6. But before going through my own work, some readers will probably be

happy to have an introduction to the hard X-ray properties of accreting black holes in the following section.

### 3.1.2 X-ray spectral states and the structure of the accretion flow

A large fraction of the luminosity of accreting black holes is emitted in the X-ray band. This radiation is now routinely detected thanks to space based X-ray and Gamma-ray telescopes such as XMM and INTEGRAL. This X-ray emission is strongly variable. A single source can be observed with very different X-ray spectra (see Done, Gierliński and Kubota 2007 for a recent, comprehensive review). Because of the shorter time scales in smaller black holes, this spectral variability is more easily studied in Black Holes in X-ray Binaries (BHBs) than in super-massive black holes in Active Galactic Nuclei (AGN). Fig. 3.1 shows various spectra from the prototypical source Cygnus X-1 observed at different times. In most BHBs, there are two main spectral states that are fairly steady and most frequently observed. The occurrence of those spectral states depends, at least partly, on the variable bolometric luminosity of the source.

At luminosities exceeding a few percent of the Eddington luminosity<sup>1</sup> ( $L_{\text{Edd}}$ ), the spectrum is generally dominated by a thermal component peaking at a few keV<sup>2</sup> which is believed to be the signature of a geometrically thin optically thick disc (Shakura & Sunyaev 1973). At higher energies the spectrum is non-thermal and usually presents a weak steep power-law component (photon index  $\Gamma \sim 2.3 - 3$ ) extending at least to MeV energies, without any hint for a high energy cut-off. This soft power law is generally interpreted as inverse Compton up-scattering of soft photons (UV, soft X) by a non-thermal distribution of electrons in a hot relativistic plasma (the so-called “corona”). Since in this state the source is bright in soft X-rays and soft in hard X-rays it is called the High Soft State (hereafter HSS).

At lower luminosities ( $L < 0.01 L_{\text{Edd}}$ ), the appearance of the accretion flow is very different: the spectrum can be modelled as a hard power-law  $\Gamma \sim 1.5 - 1.9$  with a cut-off at  $\sim 100$  keV. The  $\nu F_{\nu}$  spectrum then peaks at around a hundred keV. Since the soft X-ray luminosity is faint and the spectrum is hard, this state is called the Low Hard State (hereafter LHS). LHS spectra are generally very well fitted by thermal Comptonisation (i.e. multiple Compton up-scattering) of soft photons by a Maxwellian distribution of electrons in a hot ( $kT_e \sim 100$  keV) plasma of Thomson optical depth  $\tau_T$  of order unity (Sunyaev & Titarchuk 1980). As it will be discussed in Sec 3.4.1, the LHS is associated with the presence of a compact radio jet that seems to be absent in the HSS. In addition to the dominant Comptonisation spectrum, there are other less prominent spectral features: a weak soft component associated with the thermal emission of a geometrically thin optically thick disc is occasionally detected below 1 keV, as observed for instance in Cygnus X-1 (Balucinska-Church et al. 1995, see Fig. 3.1) or in XTE J1118+480 (McClintock et al. 2001, Chaty et al. 2003, see Fig. 3.2).

Finally, in both states, reflection features are generally detected in the form of a Fe  $K\alpha$  line around 6.4 keV and a Compton reflection bump peaking at about 30 keV, see Fig. 3.1. These components are believed to be produced when the hard X-ray emission of the corona interacts and is reflected by the cold optically thick accretion disc. They often appear to be broadened through special and general relativistic effects, in which case their origin must be very close to the black hole. These reflection features seem to be weaker in the LHS than in the HSS.

To summarize, at high luminosities the accretion flow is in the HSS, characterised by a strong

<sup>1</sup>The Eddington luminosity is  $L_{\text{Edd}} = 1.3 \times 10^{38} M \text{ erg.s}^{-1}$  where  $M$  is the black hole mass expressed in units of solar masses

<sup>2</sup>1 keV =  $2.4 \times 10^{17} \text{ Hz} = 1.16 \times 10^7 \text{ K}$

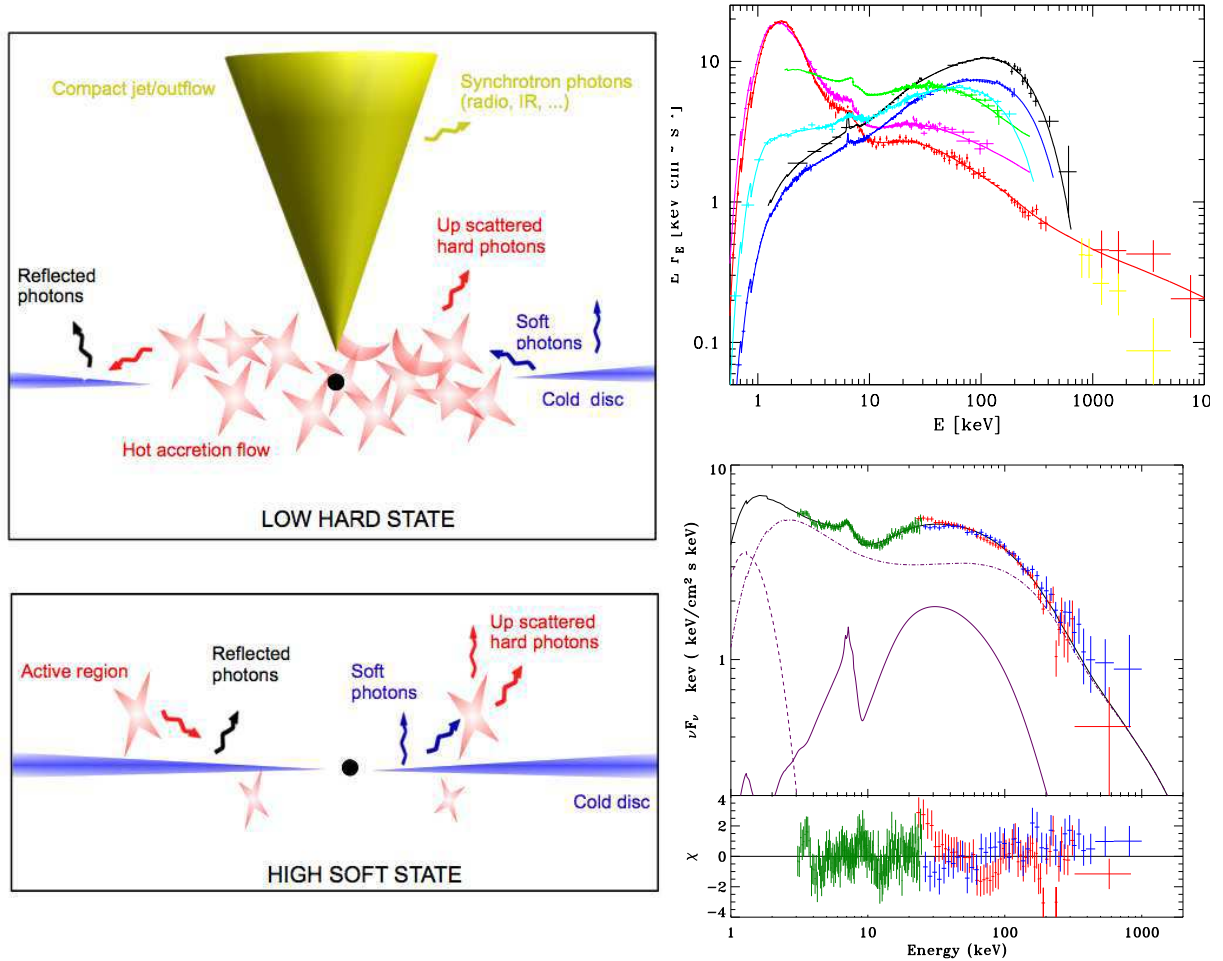


Figure 3.1: Left hand side panels: Structure of the accretion flow during LHS (top) and HSS (bottom) according to the standard scenario. Right hand side panels: Observed spectra of Cygnus X-1 . Upper panel from Zdziarski et al (2002): the LHS (black and blue), HSS (red, magenta), intermediate states (green, cyan). The solid curves give the best-fit Comptonisation models (thermal in the hard state, and hybrid, thermal-nonthermal, in the other states). Lower panel: time averaged INTEGRAL spectrum of Cygnus X-1 during a mini-state transition (intermediate state). The data are fitted with the thermal/non-thermal hybrid Comptonisation model EQPAIR with *mono-energetic* injection of relativistic electrons. The lighter curves show the reflection component (solid), the disc thermal emission (dashed) and the Comptonised emission (dot-dashed). The green, red and blue crosses show the JEM-X, IBIS/ISGRI and SPI data respectively. See Malzac et al. (2006) for details.

thermal disc and reflection component and a weak non-thermal (or hybrid thermal/non-thermal) Comptonising corona. At lower luminosities the disc blackbody and reflection features are weaker, while the corona is dominant and emits through thermal Comptonisation. Beside the LHS and HSS, there are several other spectral states that often appear, but not always, when a source is about to switch from one of the two main states to the other. Those states are more complex and difficult to define. We refer the reader to McClintock & Remillard (2006) and Belloni et al. (2005) for two different spectral classifications based on X-ray temporal as well

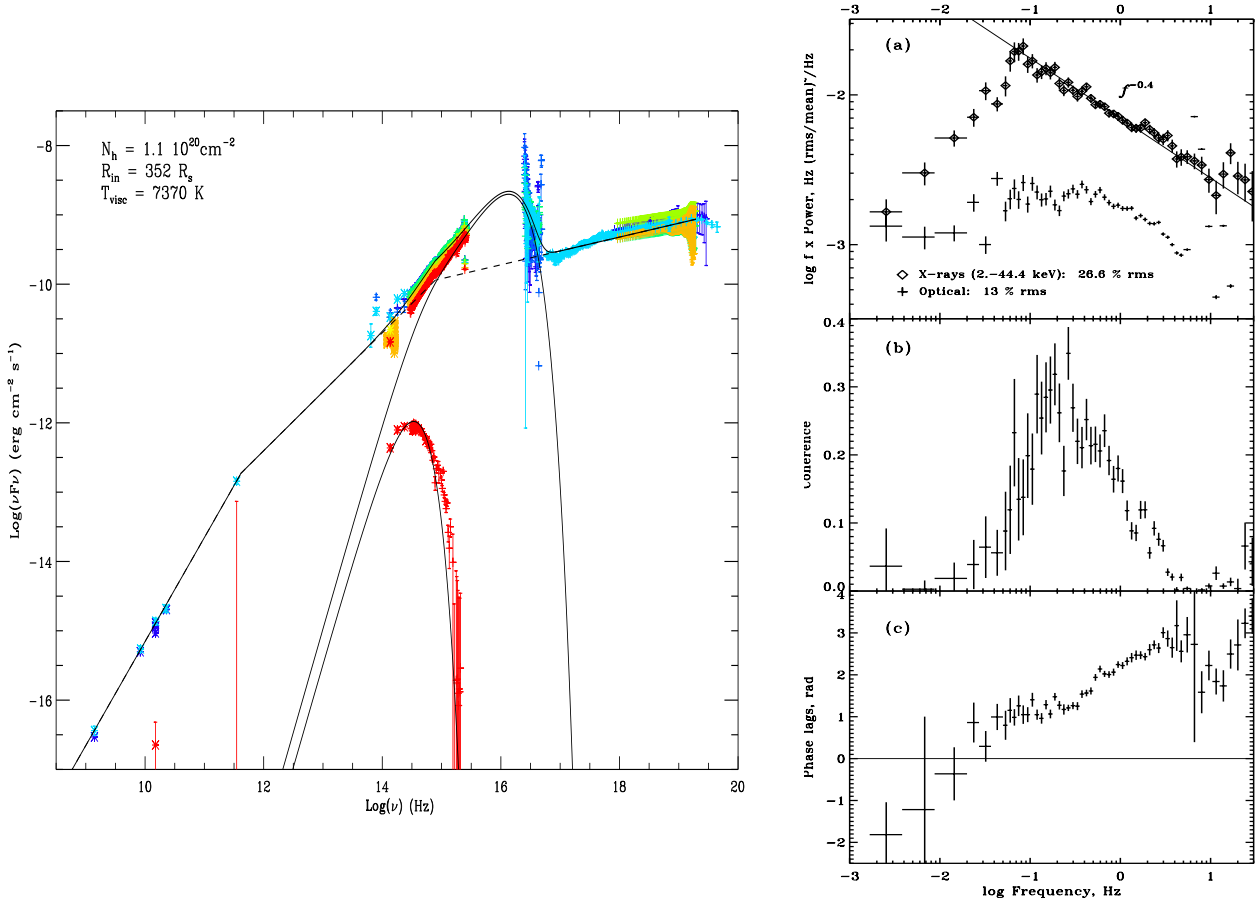


Figure 3.2: Left: Spectral Energy Distribution of XTE J1118+480 during its 2000 outburst (from Chaty et al. 2003). Right: The optical/X-ray correlations of XTE J1118+480 in the Fourier domain (from Malzac et al. 2003). **a)** X-ray and optical power spectra. The counting noise was subtracted. **b)** X-ray/optical coherence (degree of linear correlation between optical and X-rays as a function of Fourier frequency). **c)** Phase-lags as a function of Fourier frequency. A positive lag implies that the optical emission is delayed with respect to the X-rays. The light curves are mostly correlated for fluctuation of time-scales in the range 1–10 s (or 0.1–1 Hz). In this range of time-scales the phase lag is about  $\pi/2$ .

as spectral criteria and radio emission (Fender 2006). In general, their spectral properties are intermediate between those of the LHS and HSS.

Regarding AGN, their X-ray spectra are similar to that of BHBs since they usually show a non-thermal power-law emission interpreted as Comptonised radiation, and reflections features. However, the statistics rarely allow the detection of any high energy cut-off (a notable exception is NGC4151 in which a high energy break was first detected by Jourdain et al. 1992). Contrary to BHBs, the thermal disc emission never shows up in the X-ray band. This is in agreement with basic accretion theory predicting that the disc temperature scales like  $M^{-1/4}$ , and  $kT$  is of the order of few eV in AGN. X-ray spectroscopy alone makes it difficult to tell if AGN also have spectral states comparable to the HSS and LHS. However, evidence based on timing properties and radio emission suggests a similar bi-modal behaviour showing a state transition

at a luminosity of order of a few percent of  $L_{\text{Edd}}$  as in BHBs (Maccarone, Gallo & Fender 2003).

The different spectral states are usually understood in terms of changes in the geometry of the accretion flow. In the HSS, according to the standard scenario sketched in Fig. 3.1, a geometrically thin disc extends down to the last stable orbit and is responsible for the dominant thermal emission. This disc is the source of soft seed photons for Comptonisation in small active coronal regions located above and below the disc. Through magnetic buoyancy the magnetic field lines rise above the accretion disc, transporting a significant fraction of the accretion power into the corona where it is then dissipated through magnetic reconnection (Galeev et al. 1977). This leads to particle acceleration in the corona. A population of high energy electrons is formed which then cools down by up-scattering the soft photons emitted by the disc. This produces the high energy non-thermal emission which in turn illuminates the disc, forming strong reflection features (see e.g. Done, Gierliński and Kubota 2007)

In the LHS, the standard geometrically thin disc does not extend to the last stable orbit. Instead, the weakness of the thermal features suggests that it is truncated at distances ranging from a few hundred to a few thousand gravitational radii from the black hole (typically 1000–10000 km). In the inner parts, the accretion flow takes the form of a hot geometrically thick, optically thin disc. A solution for such hot accretion flows was first discovered by Shapiro, Lightman and Eardley (1976). In these hot accretion flows the gravitational energy is converted through the process of viscous dissipation into the thermal energy of ions. The main coupling between the electrons and the ions is Coulomb collision which is rather weak in the hot thin plasma. Since radiative cooling of the ions is much longer than that of the electrons, the ion temperature is much higher than the electron temperature. This two temperature plasma solution is thermally unstable (Pringle 1976) but can be stabilized if advection of the hot gas into the black hole dominates the energy transfer for ions as it is the case in advection dominated accretion flow (ADAF) solutions (see Ichimaru 1977; Narayan and Yi 1994; Abramowicz et al 1996). Emphasising the fact that in the ADAF solution the accreting gas has a positive Bernoulli parameter, Blandford and Begelman (1999) proposed a variant of the ADAF model in which a significant fraction of the accreting material is advected into an outflow rather than in the black hole (ADIOS). In these hot accretion flow solutions most of the accretion power is either swallowed by the black hole or converted into kinetic power of an outflow. They are therefore radiatively inefficient accretion flows (RIAF). Yuan (2001) has shown that a hot flow may also exist in the higher accretion rate regime where the coupling between electrons and ions becomes effective: the flow is then radiatively efficient.

In the hot flow model, the electrons have a thermal distribution and cool down by Comptonisation of the soft photons coming from the external geometrically thin disc, as well as IR-optical photons internally generated through self-absorbed synchrotron radiation. The balance between heating and cooling determines the electron temperature which turns out to be close to  $10^9$  K, as required to fit the LHS spectra. The weak reflection features of the LHS are produced through illumination of the cold outer disc by the central source. By extension, the hot accretion flow of the LHS is frequently designated as “corona” despite the lack of a direct physical analogy with the rarefied gaseous envelope of the sun and other stars or the accretion disc corona of the HSS.

It is worth noting, that although it is currently very popular, this ‘hot flow plus truncated disc’ model (Esin, McClintock and Narayan 1997; Poutanen, Krolik and Ryde 1997) is far from being the only possibility. For instance, recently Ferreira et al. (2006) have proposed a new framework for the understanding of the X-ray spectral states and jet activity of BHBs in which a thin disc is present down to the last stable orbit in all spectral states (but not seen in the LHS because it is much colder than in the HSS). As will be discussed in section 3.3.2, Accretion Disc

Corona models (ADC) may also be a viable possibility for the LHS. These alternative models are supported by recent observational evidence showing that a thin accretion disc may be present close to the black hole in the LHS (see e.g. Miller et al. 2006; Rykoff et al. 2007). In addition there are also jet models (see section 3.4.1) and clumpy disc (or cloud) models that will be discussed in section 3.3.3. Actually, the evolution of the structure and geometry of the accretion flow as a function of mass accretion rate remains a very controversial issue. It constitutes one of my main research interests.

## 3.2 Developing numerical tools for high energy radiative transfer

### 3.2.1 PhD work: the Non-Linear Monte-Carlo code

When I started my PhD thesis at CESR in 1996 under the supportive supervision of Elisabeth Jourdain, the phenomenological picture of accretion onto black holes was not as clear as it is today, but the basic features, such as the existence of two spectral states in BHBs were already known. The SIGMA/GRANAT<sup>3</sup> telescope and CGRO<sup>4</sup> missions were finishing their operations after having opened a new window in the hard X-ray band. RXTE<sup>5</sup> had just been launched and was about to produce a revolution in X-ray timing. A wealth of high quality data were becoming available.

The two main questions raised by those observations were (and still are, for a large part), the nature of the energy dissipation mechanism in these sources (viscosity, shocks, magnetic reconnection...), and the geometry and structure of the hot plasma and surrounding cold material. It was also becoming evident that simple analytical models (such as the Sunyaev and Titarchuk (1980) formula) were not suitable anymore to interpret those data, and would not provide an answer. On the other hand, a complete modelling/simulation starting from the first principles and taking into account every aspect of accretion is still impossible today owing to the complexity of the physics which is involved. It seemed that a semi-empirical approach based on the comparison of detailed radiative transfer calculations with data of improving quality would bring some elements of answer and, in the longer term, would bring a better knowledge of the physics in such extreme conditions (high temperature, strong radiation and gravity field...)

In order to reach those goals it was necessary to be equipped with quite heavy numerical tools. The aim of my PhD thesis was precisely to develop such numerical simulation codes dedicated to the study of high energy radiative processes in relativistic plasmas thought to be present in the vicinity of compact objects (neutron stars, BHBs, AGN...).

By that time, several groups had already developed different numerical methods in order to deal accurately with similar problems. In Caltech, Paolo Coppi (1992) had developed a very fast code based on the resolution of the kinetic equations of photons and electrons, but with a poor handling of spatial radiative transfer. Juri Poutanen and Roland Svensson (1996) in Stockholm had just published a paper presenting a code based on the resolution of the full radiative transfer equations for an ADC geometry. Meanwhile in Moscow, Boris Stern had spent 10 years developing the so called Non Linear Monte-Carlo method (NLMC). He had finally published an impressive article (Stern et al. 1995a) that I would keep within reach on my desk during the next three years.

<sup>3</sup>see [http://astrophysics.gsfc.nasa.gov/cai/coded\\_sigma.html](http://astrophysics.gsfc.nasa.gov/cai/coded_sigma.html)

<sup>4</sup>see <http://cossac.gsfc.nasa.gov/docs/cgro/index.html>

<sup>5</sup>see <http://heasarc.gsfc.nasa.gov/docs/xte/XTE.html>

Indeed, among the existing methods, the NLMC appeared to be not only very accurate, but also the most versatile. I had already some experience with simple radiative transfer Monte-Carlo methods. The previous year, during my DEA training period ( $\sim$  master thesis), I had written a linear Monte-Carlo code computing Comptonisation spectra produced by hot electrons with an arbitrary fixed energy distribution and optical depth, in various geometrical configurations, including density gradients and anisotropy. I knew that Monte-Carlo methods are the most convenient to deal easily with various complicated geometries. I therefore decided to develop my own implementation of the NLMC. Most of my PhD work was dedicated to this task. Besides Compton scattering, this code also accounts for electron positron pair production and annihilation and Coulomb interactions between leptons (Möller and Bhabha effects). Unlike standard Monte-Carlo methods where the radiation transfer is solved for an arbitrary fixed distribution of leptons, the NLMC takes into account the effects of radiation on the lepton distribution. With the NLMC no assumption on the shape of this distribution is required. The distribution is computed self-consistently using energy and pair balance. The free parameters are then the power provided to the plasma and the way it is provided (thermal heating, high energy particle injection or acceleration ...). The computed spectra compared to observations can provide information on the particle distribution and energy dissipation processes. The code is extensively described in my PhD thesis, in Malzac & Jourdain (2000) and Malzac (2001a).

X-ray binaries harbour a strong rapid X-ray variability which presents a very complex and richly documented phenomenology (see e.g. van der Klis 2006). Modelling this fast variability is very challenging. Motivated by the first results from RXTE and the scarcity of models attempting to explain these timing features, my attention focussed on attempting to solve time-dependent problems with the NLMC. Time is a natural ingredient of the method, however, due to statistical errors that are inherent to the Monte-Carlo methods, I had to improve it by introducing some analytical calculations in the code in order to reduce these errors. In Malzac & Jourdain (2000), we showed that this modified method was efficient in dealing with different non-stationary situations likely to arise in the framework of ADC models. For instance, the code allowed me to simulate for the first time the response of the system to a flare of soft photons coming from the disc or a sudden increase of the heating rate of the corona. The code allowed us to study the temporal evolution of the physical parameters controlling the shape of the escaping spectrum, as well as the associated light curves in various energy bands. The main results from these simulations will be summarized in section 3.3.2.2

Simultaneously, I was working on another Monte-Carlo code previously developed at CESR by Elisabeth Jourdain and Jean-Pierre Roques (Jourdain & Roques 1995) dedicated to the calculation of the reflection component produced by the illumination of an accretion disc. This reflection code was later coupled with the NLMC code.

### 3.2.2 Recent numerical developments: a Fokker-Planck code

When I finished my PhD thesis, an important process was absent from the NLMC code. This process was cyclo/synchrotron emission and absorption by leptons in a magnetic field. These effects are important because most of the relativistic plasmas responsible for the high energy emission of compact sources are magnetised. Thus, some level of emission from the relativistic leptons spiraling in the magnetic fields is expected. Synchrotron emission is believed to be a dominant emission mechanism in several classes of high energy sources, in particular those presenting a strong jet emission such as Gamma-ray bursts or radio loud AGN, like blazars. But even in radio quiet AGN and BHBs, those processes may have significant effects. For

instance, self-absorbed cyclo/synchrotron emission from mildly relativistic particles will produce an additional source of soft cooling photons available for the Comptonisation process. In some models such as the original ADAF model this is the only source of Compton seed photons. There is evidence that this is indeed the case in low luminosity sources (Wardziński & Zdziarski 2000). In addition, rapid absorption and emission of soft synchrotron photons may play an important role in the plasma thermalization process. For instance in BHBs in the LHS, the shape of the high energy spectrum indicates that the electron distribution is essentially thermal. Yet all known acceleration processes lead to a non-thermal, power-law like distributions of particles. If the particles are powered by such a process, as expected for instance in ADC models, this requires a very efficient mechanism of energy redistribution between particles. Coulomb interactions are much too slow. A good candidate seems to be the ‘synchrotron boiler effect’ (Ghisellini, Guilbert & Svensson 1988; Ghisellini, Haardt and Svensson 1998; Katarzyński et al. 2006): in the presence of a magnetic field high energy particles emit synchrotron radiation which is almost instantaneously auto-absorbed by lower energy particles, leading to a very effective transfer of energy between particles. This strong coupling is able to thermalise a distribution on a time-scale of the order of the light crossing time of the hot plasma. It is therefore important to be able to take into account these effects and their consequences on the equilibrium lepton distribution. When I first attempted to introduce the effects of synchrotron emission and absorption in the NLMC in 2002, I ran into two difficulties.

The first one was to evaluate accurately the cyclo-synchrotron emissivity and absorption coefficients. Simple formulae exist both in the non-relativistic (cyclotron) and ultra-relativistic (synchrotron) limits. Dealing with the intermediate regime requires complex and time consuming numerical calculations. Unfortunately, for most of the applications that I could envision, the particles were only mildly relativistic. Therefore with Alexandre Marcowith, the lone theorist of the high energy department at CESR<sup>6</sup>, we attempted to find analytic fitting functions that would provide a good approximation to the synchrotron emissivity and absorption cross section in this regime. This was quite a difficult task due to the complex harmonic structures in the cyclo/synchrotron spectrum. But eventually we succeeded and our results were published in *Astronomy and Astrophysics* (Marcowith and Malzac 2003).

Having implemented those formulae in the NLMC, I realised that there was a second and bigger problem. Due to the numerous very rapid emission and absorption events that had to be simulated by the Monte-Carlo method, the code was spending most of its running time generating synchrotron photons that were immediately absorbed. The code was therefore extremely inefficient and time-consuming. I managed to devise a trick to make the code efficient for the special case in which a pure Maxwellian lepton distribution is assumed. Then, however, the thermalising processes could obviously not be studied. We were reaching the limits of Monte-Carlo methods.

With Alexandre, we soon realised that methods based on the resolution of the kinetic equations would be much more efficient to deal with those effects. Several codes based on the kinetic equations already existed but none of them had a proper implementation of the cyclo/synchrotron effects (Coppi 1992, 1999; Nayakshin & Melia 1998; Böttcher, Jackson and Liang 2003). These methods are quite efficient when dealing with the fast dynamics of the lepton distribution. Nevertheless, they are not very accurate for the radiative transfer. They use a ‘one zone’ approximation in which only the energy (and not the spatial) distribution is solved for photons and leptons. Radiation transfer is usually dealt with using a simple escape

---

<sup>6</sup>Now a happy theorist in Montpellier

probability formalism. This is not however a critical problem, since in many practical situations, the geometry of the emitting region is not known and not extremely relevant. When accurate radiative transfer is needed (as for example when dealing with accretion disc corona models, see section 3.3.2), it is in principle possible to use the kinetic equation method to compute the particles energy distribution and the NLMC to solve the radiative transfer (see Böttcher et al. 2003)

In 2002, Alexandre and myself started to develop a code based on the resolution of a kinetic Fokker-Planck equation using a semi-implicit algorithm proposed by Chang and Cooper (1970; see also Park and Petrosian 1996). However, due to our other works and duties, the project was progressing very slowly. We finally decided that this was the kind of work that could be better performed by someone that would be able to work full time on this project. We applied for funding for PhD students and post-docs. After a few trials it worked out and we obtained some funding from CNRS for a post-doc. In November 2006, we recruited Renaud Belmont, a young and smart plasma astrophysicist. From then, Renaud took over the development of the Fokker-Planck code. He obviously ran into many tricky numerical problems. For example, we realised that the Chang-Cooper method we had been using is inaccurate when synchrotron emission is dominant and leads to a poor energy conservation. Finally, Renaud invented his own numerical scheme which appears to be very fast and conserving both particle number and energy. At the time of writing, we have a preliminary version of the code solving the Fokker-Planck equations for both electrons and photons and taking into account the cyclo-synchrotron and Compton effects. This code was presented in several conferences (e.g. Belmont, Malzac & Marcowith 2007) and we are now close to start working on its applications.

### 3.3 Modelling the high energy continuum and variability of accreting black holes

#### 3.3.1 The anisotropic illumination model

In September 1996, during the 2nd INTEGRAL Workshop, in St Malo, I had met Gilles Henri and Pierre-Olivier Petrucci from the Grenoble observatory. They were proposing a new model to explain the emission of Seyfert galaxies<sup>7</sup> from the UV to hard X-ray band. This model was based on the presence of an X-ray source located at some height above the black hole (Henri & Petrucci 1997). Such a source was supposed to be associated with a form of aborted jet. In this hot source a non-thermal distribution of electrons was up-scattering the soft thermal UV photons from the accretion disc. Due to the assumed geometry and relativistic energies of the particles, the X-ray source was strongly anisotropic, with most of the power being emitted toward the disc. I offered to improve upon their analytical estimates of the model spectra by using numerical Monte-Carlo simulations. More specifically, I computed the reflection component expected from their model and then compared the result to the available data of several sources. Unfortunately, it turned out that the results were negative: the strong anisotropic illumination of the disc was producing extremely strong reflection features which were not observed, making the model extremely unlikely. These results led to my first publication (Malzac, Jourdain, Henri & Petrucci 1998). A second problem arose when I attempted to simulate the primary non-thermal inverse Compton emission. Indeed, using the NLMC, I was able to show that, contrary to what was

---

<sup>7</sup>Seyfert galaxies are a class of AGN characterised by extremely bright nuclei, and optical spectra which have very bright emission lines of hydrogen, helium, nitrogen, and oxygen.

assumed in earlier analytical calculations, multiple Compton scattering was not negligible in this model. The higher Compton orders would lead to a strong emission at MeV energies which is not observed (Malzac et al. 1999). The model in the formulation by Henri & Petrucci was therefore hard to reconcile with the observations. However the idea that the X-ray emission of Seyfert galaxies (and possibly also X-ray binaries) could arise in a jet like structure above the black hole survived and was latter revisited by several authors. In particular, Ghisellini, Haardt and Matt (2004) proposed a modified version of this model in which the electron distribution is thermal, reducing the anisotropy and making the model in agreement with the observations of radio quiet AGNs. Although I had falsified the model he had been working on during all his PhD thesis, Pierre-Olivier Petrucci was not resentful and, fortunately, he is still among my closest and most valued collaborators

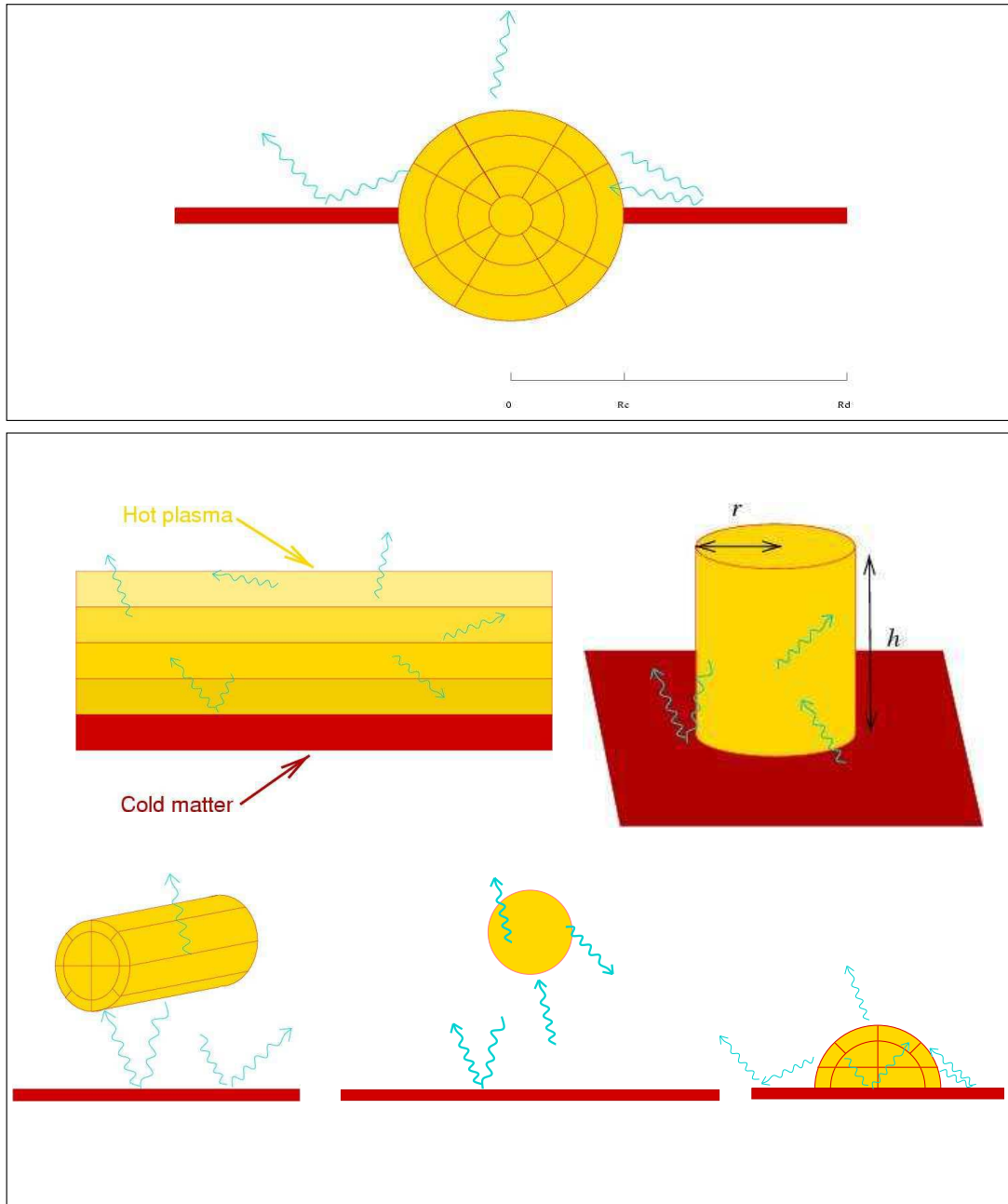


Figure 3.3: X-ray emitting region of the accretion flow around a black hole. The figure shows various idealised geometries that were studied with the NLMC code. Top: hot spherical flow plus truncated disc model (the black hole is at the center of the hot sphere). Bottom: ADC models: infinite slab corona geometry and a patchy corona (different shapes for the active region above the disc are represented). The hot active regions emit X-rays through thermal Comptonisation. A fraction of this radiation intercepts the cold accretion disc where it is partly Compton back scattered, forming the reflection component, partly absorbed and thermally reemitted at lower energy (UV to soft X-rays). Some of this reprocessed radiation returns the active regions to be up-scattered again and so regulates the temperature of the Comptonising plasma.

### 3.3.2 Accretion disc corona models

The presence of a hot accretion disc is not the only possible model for the LHS of BHBs. It was suggested long ago that instead, a real Accretion Disc Corona (ADC) system similar to that of the HSS may reproduce the spectra as well (Bisnovatyi-Kogan & Blinikov 1976; Liang & Price 1977). This would imply a cold, geometrically thin disc extending down very close to the black hole in the LHS. Unlike in the HSS, this disc does not produce a strong thermal component in the X-ray spectrum because it is too cold. It is cold because most of the accretion power is not dissipated in the disc, rather it is transported away to power both the corona and the compact jet. This, at least in principle, could be achieved either through transport via buoyancy of the magnetic field (Miller & Stone 2000; Merloni & Fabian 2002) or through the torque exerted on the accretion disc by a strong magnetic field threading the disc and driving the jet (Ferreira 1997), or even through a disc instability transporting power and angular momentum toward the corona and the jet in the form of Alfvén waves (Tagger and Pelat 1999; Tagger et al. 2004).

Due to the complexity of the ADC physics it is not possible to obtain simple analytical solutions giving the main properties of the corona unless some parametrization of the energy transfer between the disc and the corona is used (see e.g. Svensson & Zdziarski 1994). However, from an observer perspective it does not really matter because the appearance of the ADC does not depend on the details of the energy transport and dissipation mechanisms. Indeed, Haardt & Maraschi (1991) realised the existence of a strong radiative feedback between the cold disc and the hot corona. A fixed fraction of the power dissipated in the corona in the form of hard X-ray photons, impinges on the cold disc where it is absorbed, heating the cold disc, and is finally re-emitted in the form of thermal soft photons. A fraction of those soft photons re-enters the corona providing the major cooling effect to the corona through inverse Compton scattering. As a consequence, the cooling rate of the corona scales like the heating rate. The coronal temperature is determined only by the geometry of the ADC (controlling the fraction of coronal power that returns to the corona in the form of soft photons). For instance, an extended corona sandwiching the cold accretion disc would intercept more cooling photons than a patchy corona made of a few compact active regions covering a small fraction of the disc, and therefore would have a lower temperature and hence a softer Comptonised X-ray spectrum.

During the nineties several groups (Haardt & Maraschi 1993; Stern et al. 1995a; Poutanen et al. 1996) performed detailed computations of the resulting equilibrium spectra for various geometries (see Fig. 3.3). They concluded that the corona has to be patchy in order to produce spectra that are hard enough (Haardt et al. 1994; Stern et al. 1995b). Yet those ADC models had an important problem: the production of an unobserved strong thermal component due to reprocessing of the radiation illuminating the disc. In the case of an active region emitting isotropically, about half of the luminosity intercepts the disc and the thermal reprocessing component is comparable in luminosity to the primary emission. Yet in the LHS spectra of BHBs the thermal component from the disc is barely detectable and much lower than expected from this model. Moreover, the amplitude of the reflection features observed in the LHS are also lower than expected from an isotropic corona by at least a factor of 3, in some cases they are so weak that they are not even detected. This led us to consider models where the coronal emission is not isotropic. Beloborodov (1999) pointed out that the corona is unlikely to stay at rest with respect to the accretion disc. Due to the anisotropy of the dissipation process or simply to radiation pressure from the disc, the hot plasma is likely to be moving at mildly relativistic velocities. Then, due to Doppler effects, the X-ray emission is strongly beamed in the direction of the plasma velocity. In the case of a velocity directed away from the accretion disc

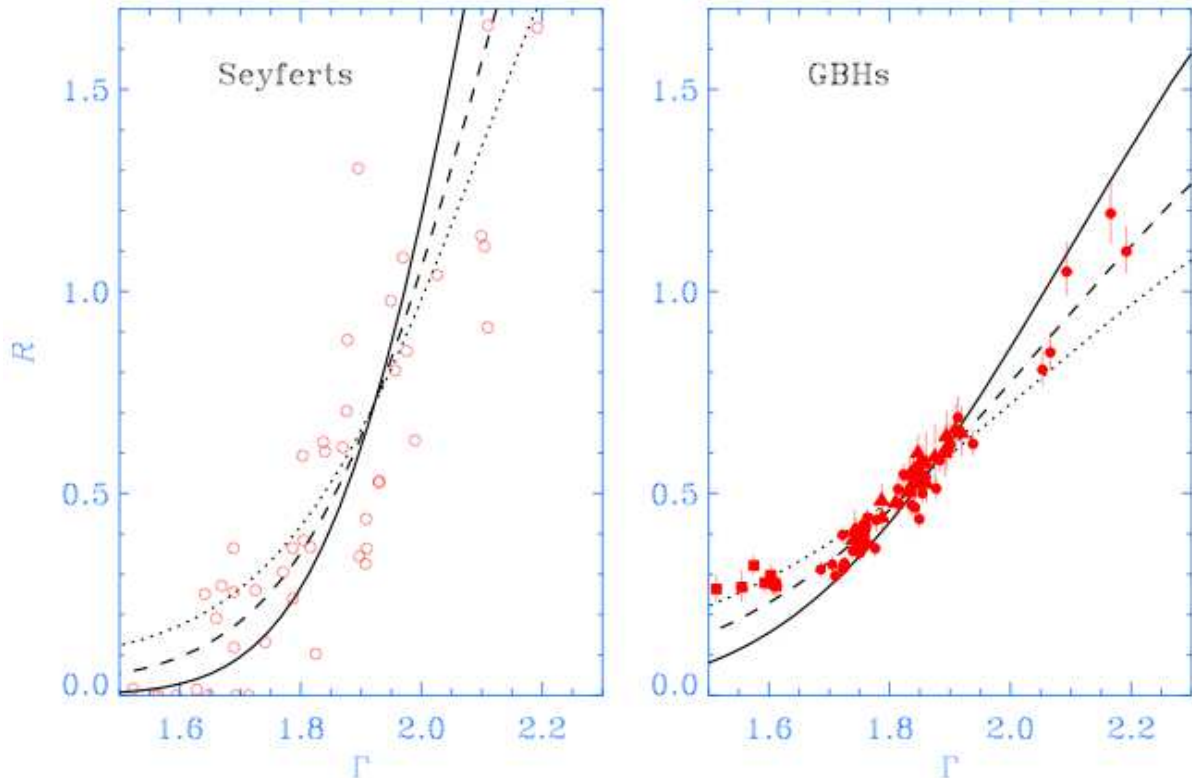


Figure 3.4: (a) The observed  $R$ - $\Gamma$  correlation for Seyfert galaxies (circles). Data from Zdziarski et al. (1999). The curves show the correlation predicted by the dynamic ADC model. The solid, dashed, and dotted curves correspond to inclination angles  $i=32$ ,  $57$ , and  $70$  deg. respectively. (b) The observed  $R$ - $\Gamma$  correlation for GBHs, Cyg X-1 (circles), GX 339-4 (triangles), and GS 1354-644 (squares). Data from Gilfanov et al. (2000). The curves correspond to the same three inclinations as on the left panel (see Malzac, Beloborodov & Poutanen 2001 for details).

(outflowing corona), the reprocessing features (both reflection and thermalised radiation) are strongly suppressed. Moreover, due to the reduced feedback from the disc, the corona is hotter, and harder spectra can be produced.

### 3.3.2.1 The dynamic corona

During the winter of 1999-2000, just a couple of months after my PhD defense, I went to Sweden and spent two months at Stockholm Observatory. The institute was then located close to the seaside resort of Saltsjöbaden, on top of a hill with scenic views on the frosty pine forests and the sea. I had come there to work with Juri Poutanen. Boris Stern was there as well and we were sharing the guest house of the observatory. Like many Russian scientists in this early post cold war era, he had to work abroad a few months a year in order to make a living. As he was the main inspiration for my PhD thesis work, I was quite excited to meet him in person. It was an excellent opportunity to compare and check our codes. It also turned out to be an excellent opportunity for vodka tasting.

Andrei Beloborodov was also there as a postdoc working with Roland Svensson. He had just published his famous paper on the outflowing corona model. In this paper, he had found simple

analytic formulae estimating the relative flux in the different emission components (primary, reflection and reprocessing) and the slope of the photon spectrum of the outflowing corona. However, he had no mean to calculate the actual spectrum and test the model further. Juri Poutanen suggested me to try to compute spectra of this dynamic corona model with my NLMC code. It took us two months to figure out how to do this exactly. One year later, we finally published a paper (Malzac, Beloborodov & Poutanen 2001, publication enclosed in Sec. 5.1) in which we presented detailed non-linear Monte-Carlo simulations of this dynamic ADC equilibrium, and compared the results with observations. We found that compact active regions of aspect ratio of order unity, outflowing with a velocity of 30 percent of the speed of light could reproduce the LHS spectrum of Cygnus X-1. A similar agreement was found for the Seyfert 1 galaxy IC4329a.

Moreover, since the velocity of the coronal plasma controls both the strength of the reflection features and the feedback of soft cooling photons from the disc, the model predicts a correlation between the slope of the hard X-ray spectrum and the amplitude of the reflection components. Such a correlation had just been discovered and is indeed observed both in individual objects and a sample of AGN and BHBs (Zdziarski et al. 1999, 2003; Gilfanov, Churazov & Revnitsev 2000; see Fig. 3.4). Sources with stronger reflection features (iron line or reflection bump) tend to have softer spectra. This so called  $R$ - $\Gamma$  correlation brings important information on the physical processes operating in accreting black holes. It suggests, or rather confirms, that the flux of soft seed photons for Comptonisation is emitted by the cold reflecting material.

In the standard truncated disc scenario described in section 3.1.2, this correlation could be the consequence of the inner truncation radius of the disc moving in inside the hot flow, varying simultaneously the flux of soft cooling photons in the hot phase and the surface area of the reflector. However, detailed calculations performed independently by Andrei Beloborodov and myself, under different assumptions, showed that the shape of the  $R$ - $\Gamma$  correlation produced in this framework differs significantly from the observations (Malzac 2001b; Beloborodov 2001).

Furthermore, we also showed that changing the geometry of a *static* ADC would produce an unobserved  $R$ - $\Gamma$  *anti-correlation*. Therefore a static ADC (i.e. not out-flowing) can be ruled out on this ground. On the other hand, we found that the correlation is very well matched by the dynamic corona model (as shown on Fig 3.4.)

Recently, ADC models for the LHS obtained more observational support, with the discovery of relativistically broadened iron lines in the LHS of GX339-4 (Miller et al., 2006). Such relativistically broadened lines require that disc illumination takes place very close to the black hole. Such observations suggests that, at least in some cases, a thin disc is present at, or close to, the last stable orbit in the LHS.

### 3.3.2.2 Time dependent comptonisation

The fast variability of BHBs occurs on surprisingly long time-scales. Most of the high energy photons (and variability) must originate deep in the potential. The variability is therefore expected to occur on time-scales of the order of the dynamical time-scale close to the black hole, which is of order of 1 ms for a ten solar mass black hole. On the other hand, observations show that most of the X-ray variability occurs on time-scales ranging from 0.1 to 10 s (see e.g. the power density spectrum of XTE J1118+480 on panel *a* of the right hand side of Fig. 3.2). In comparison there is virtually no variability on time-scales shorter than 0.01 s. Thinking in terms of Power Density Spectrum (PDS), the observed power requires short distances from the black hole, but the observed frequencies imply large distances. Another intriguing feature of the rapid

variability of BHBs is the existence of delays between energy bands that are measured up to frequencies of a few hertz. The hard photons tend to lag behind the softer photons (Miyamoto and Kitamoto 1989).

In 1999, when I was working at making the NLMC time-dependent, most of the models for the aperiodic variability assumed that this variability was driven by the variability of the soft seed photon luminosity. A then popular explanation for the absence of long time-scales in observed power spectra was that if the Comptonising corona was large enough (i.e.  $10^3$  to  $10^4 R_g$ ), it would act as low-pass filter on the variability of the soft seed photons (their fast variability being smeared out in the multiple scattering process). In this model, time-lags would be associated to the time required for a photon to gain energy through multiple Compton scattering as it travels in the corona (see e.g. Kazanas et al 1999).

However, these models did not take into account the response of the corona to this fluctuating soft photon field. In Malzac and Jourdain (2000), we have shown that, in a real situation, the corona responds to the fluctuations of the soft photon field and damps out any variability. For example, if the soft photon density is suddenly increased while the dissipation rate in the corona is kept constant, then the temperature drops almost instantaneously (on a Compton cooling time scale which is much shorter than the light crossing time). In a fluctuating soft photon field, the coronal temperature tends to adjust very quickly to keep the comptonised luminosity constant. Models in which the variability is driven by the soft photon field might be successful in reproducing the shape of the power spectra or time-lags (see e.g. Böttcher 2001) but they *cannot* produce the strong variability rms amplitudes of 10 to 40 percent that are typically observed. Therefore, independently of the assumed geometry, the rapid variability must be driven by changes in the physical parameters of the corona (most likely the hot plasma heating rate), rather than by fluctuations of the soft seed photon input.

In the framework of ADC models, we then investigated the radiative response of the corona to a sudden and brief increase of the coronal heating rate. We found that combining detailed Monte-Carlo calculations and time-lags measurements can provide some constraints on the size and structure of the active region(s). Indeed, we found that, for ‘flares’ occurring on a time-scale shorter than  $t_c \sim 50R/c$ , the<sup>8</sup> escaping spectrum follows a hard to soft evolution (in other words the escaping photons are, on average, more energetic at the beginning of the flare). This would lead to the appearance of time-lags between high and lower energy bands. Observations usually show the opposite behaviour (i.e. the hard photons lagging behind the lower energy ones). However these hard lags are detected only for fluctuations occurring on time-scales larger than  $\sim 0.2$  s. Unfortunately, the detection of lags on shorter time-scales is prevented by lack of sensitivity. Since we expect soft lags on times scales shorter than  $t_c$  and since we observe hard lags down to  $\sim 0.2$  s, this implies  $t_c < 0.2$  s and  $R < 10^8$  cm. This constraint on the size of the emitting region could be very much tightened if measurements of time-lags occurring on time-scales shorter than 0.2 s become possible with better instruments.

We have also shown that the shape of the time averaged spectrum can be significantly affected by the fact that the ADC system is not in a steady state. In such conditions, a pure thermal Comptonisation model can produce spectral features such as high-energy tails at MeV energies or even annihilation lines which are generally considered as the signature of non-thermal processes. For instance, the observed tail in the LHS of Cyg X-1 (Ling et al. 1997; McConnell et al. 2002; Malzac et al. 2006) can probably be explained by pure non-equilibrium thermal Comptonisation without need for hybrid models.

---

<sup>8</sup>where  $R$  is the typical size of the emitting region and  $c$  the speed of light

### 3.3.2.3 What if the disc is ionised ?

During summer 2000, I moved from Toulouse to Milan. Laura Maraschi, who knew about my work for being a referee of my PhD thesis, had offered a postdoc position in her group at Brera Observatory. I was very happy to go there, and not only because I like Italian food. As already mentioned, Laura Maraschi is the co-inventor of the two phase accretion disc corona models (with Francesco Haardt based in the close by city of Como). In Brera, I would also find Pierre-Olivier Petrucci who had already been there as a post-doc for two years. This stimulating environment would be the best place to use my code to study various two-phase models that I had in mind (which I did, eventually).

Yet, I was a bit perplexed because, so far, in all the calculations of the radiative coupling between a cold phase and a hot plasma, including mine, it was always assumed that the reflecting material was neutral. Actually, due to illumination, the reflecting material could easily have a high degree of ionisation. Ionisation has important effects on the shape of the reflected component and the line properties. Moreover, the gas albedo is increased, and therefore, the fraction of soft reprocessed photons returning to the hot plasma is decreased. This, in turn, for a given geometry, may increase the equilibrium temperature of the hot Comptonising plasma and affect the shape of the primary spectrum (making it harder). If this effect was strong, all the constraints that we had obtained on the geometry of the ADC systems (i.e. the requirement for outflowing active regions of aspect ratio  $\sim 1$ ) could possibly be relaxed. Could, for example, an extended slab corona sandwiching the disc be a viable possibility if the disc is ionised ?

The ionisation structure of the reflecting material depends on the density structure of this medium as well as on the shape of the incident spectrum. The consistent calculation of this ionisation structure is a highly complex problem, which was out of reach of my own reflection Monte-Carlo code which can handle only pure neutral matter and no line emission (except for the 6.4 iron line).

In January 2001, as part of my early campaign in an attempt to win a permanent position in France, I visited Meudon observatory to give a seminar. There, I met three very interesting ladies: Suzy Collin, Martine Mouchet and Anne-Marie Dumont. This meeting was highly inspirational. First Suzy Collin had been a proponent of a model (the cloud model, Collin-Souffrin et al 1996) on which I was to work later and that will be discussed below (see Section 3.3.3). Anne-Marie Dumont had been working on a code for radiative transfer in optically thick and hot photoionized media (TITAN/NOAR, Dumont, Abrassard & Collin 2000). This code constitutes a very accurate tool to compute the reflection (or even transmission) spectrum of an illuminated accretion disc. This is done taking into account ionisation and energy balance.

By that time, the shape of ionised reflection spectra had been studied by several authors (Ross & Fabian 1993; Zycki et al. 1994). Actually, strong ionisation had already been proposed as a possibility to reduce both reflection and reprocessing features in an ADC like geometry (Malzac, Jourdain, Petrucci & Henri 1998; Ross, Fabian & Young 1999; Nayakshin 2000; Done & Nayakshin 2001). Anne-Marie Dumont was refining those studies. She was also considering the effects of different assumptions for the ionisation equilibrium of the gas (such as constant gas density versus constant pressure). But so far, all the calculations of ionised reflection had been performed for an arbitrary fixed incident spectrum. The possibly important effect of feedback on the primary emission had been ignored. In order to make a fully consistent calculation, I suggested to couple the NLMC code computing the radiative transfer and energy balance in the corona, to the TITAN/NOAR code computing the ionisation and thermal balance in the disc and the associated reflection spectrum (see Fig. 3.5).

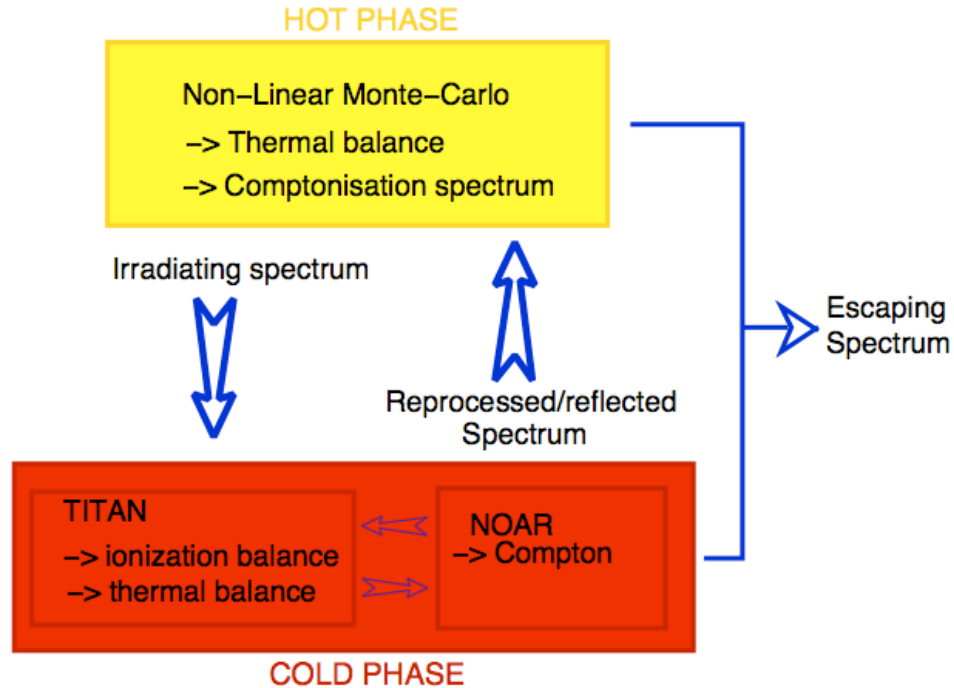


Figure 3.5: In order to take self-consistently into account the ionisation of the disc reflector, it was necessary to couple the NLMC, with the photoionisation code, TITAN computing ionisation and thermal balance in the cold phase as well as the reprocessed/reflected spectrum (Dumont, Abrassard & Collin 2000). To account accurately for the Compton reflection in the cold phase, TITAN is itself coupled with a linear Monte Carlo-Code (NOAR). The physical conditions and escaping spectra at radiative equilibrium are determined by multiple iterations between the NLMC and TITAN/NOAR code, as indicated on the figure. The NLMC was later coupled with another similar photo-ionisation code developed by Randy Ross and Andy Fabian (Ross & Fabian 2005 see Sec 3.3.3.4).

Unfortunately, this coupling between the two codes turned out to be extremely tedious. The TITAN/NOAR code had not yet been optimised. It was very time consuming and not user friendly (requiring human intervention at different stages of the simulation). Running this code required a high level of expertise: Anne-Marie and Martine kindly accepted to do it for me. Typically, a TITAN/NOAR simulation would take one week. Anne-Marie and Martine would then send me the results that I would inject into the MCNL code which would be running for a few hours. I would then send the output back to Meudon. As several iterations were required before convergence, a full calculation could easily take several months, specially if some of us had conferences, other duties, or simply holidays in between. One year later we had enough results to submit a paper to *Astronomy and Astrophysics* (Malzac, Dumont & Mouchet, 2005).

We had found that the hardening effects of ionisation on the primary emission are quantitatively important, even at low ionisation parameters and should definitely be taken into account. The effect, however, is not strong enough to reconcile the slab corona model with the hardest observed LHS spectra, unless the reflector has a constant density and the ionization parameter is large (of the order of  $10^4 \text{ erg s}^{-1} \text{ cm}$ ). A couple of months later, we received a referee report

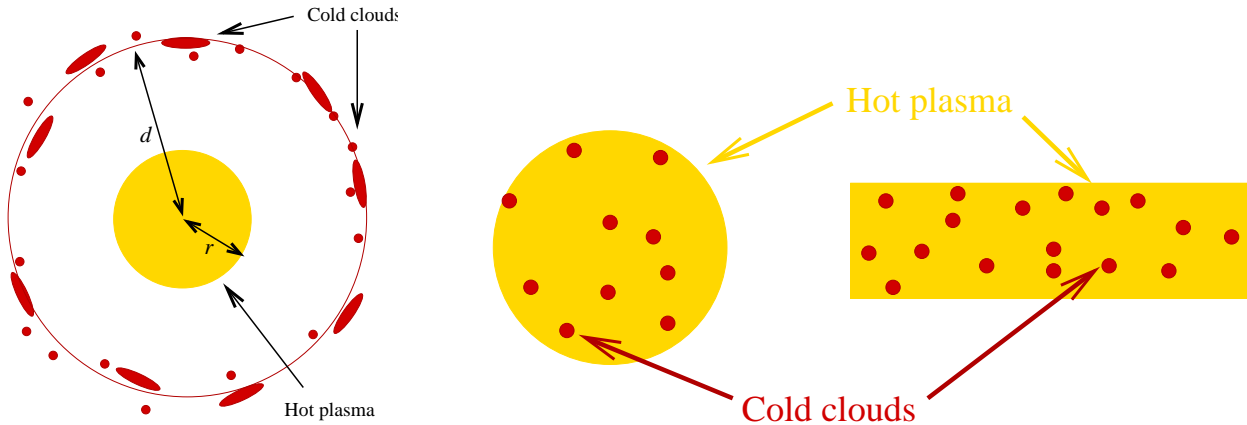


Figure 3.6: Various geometries of cloudy and clumpy models. Left hand side: idealised geometry for the spherical cloud model: the black hole is at the centre of a spherical hot plasma cloud, with radius  $r$ , forming the hard X-ray source. Cold clouds are spherically distributed at some distance  $d$  from the centre. Right hand side: the hot plasma emitting the hard X- and soft  $\gamma$ -ray emission is pervaded by small lumps of cold dense matter. The geometry of the hot plasma could be close to spherical (left) or slab (right). In all geometries the cold clouds provide the seed photons for Comptonisation in the hot phase. They intercept a fraction of the primary X-ray radiation. The main part of the intercepted X-ray flux is reprocessed as low energy (UV) radiation, the rest is reflected in the X-ray domain.

that was quite favourable but requested more simulations. It took us one more year to complete those. The paper (enclosed within this report, see Sec. 5.4) was finally accepted in July 2004. By then, I had won a permanent position and was back in the beautiful pink city of Toulouse.

### 3.3.3 Clumps and clouds in AGN

While a Post Doc in Milan, my attention was attracted to another possible explanation for the broad band spectra of Seyfert galaxies. I got interested in a configuration in which a soup formed by a hot plasma contains small grains constituted by small dense clouds of much colder matter. Such a configuration had been often considered in the literature (e.g. Guilbert & Rees 1988). It is referred to under various denominations such as ‘clumpy disc’, ‘inhomogeneous accretion flow’, or ‘cloud model’. Several earlier works were devoted to explain how such a configuration could be physically realized and compute the spectrum emitted by the clouds for different cloud optical depths (see e.g. Rees 1987; Ferland & Rees 1988; Rees, Netzer & Ferland 1989; Celotti, Fabian & Rees 1992; Kuncic, Blackman & Rees 1996; Collin-Souffrin et al. 1996; Kuncic, Celotti & Rees 1997; Krolik 1998).

The main observable effect of optically thick cold clouds is the reprocessing into soft UV photons of the hard X-ray radiation produced in the hot phase by the Comptonisation process. This reprocessed emission is likely to contribute, at least partly, to the big blue bump observed in AGN. In addition, the presence of such clumps inside the hot plasma may also contribute to the formation of the reflection component (see e.g. Nandra & George 1994).

Most of the previous works on cloud models had focused on the physics and radiative processes in the clouds themselves, without taking into account the possible effects of the clouds on

the characteristics of the hot phase. Indeed the soft radiation re-emitted by the cold material can constitute the main radiation field responsible for the Compton cooling of the hot gas. This in turn affects the temperature of the hot plasma, and thus the emitted X-ray Comptonised spectrum. This feedback loop is identical to that found in ADC models (Haardt & Maraschi 1993). Similarly, the conditions at radiative equilibrium depend mainly on the cold matter distribution relative to the hot plasma.

### 3.3.3.1 A simple spherical model

In this context, I started by studying analytically a simple geometry in which the clouds are external to the hot Comptonising plasma and spherically distributed around it (see left hand side of Fig. 3.6). This particular spherical geometry was first proposed by Collin-Souffrin et al. (1996). It had been shown to present a range of advantages regarding the observations (e.g. Czerny & Dumont 1998; Abrassart & Czerny 2000; Collin et al. 2000). However, again, in all of these studies the authors focused on the cold blobs themselves and not on the problem of energy balance in the hot phase.

Taking the radiative feedback into account, I derived analytical estimates for the luminosity of the different spectral components (reprocessed, reflected and primary emission) as well as estimates for the X-ray photon index  $\Gamma$  and the amplitude of reflection features. The two main quantities controlling the value of the spectral parameters are the average cloud distance to the hot plasma size ratio  $d/r$ , and the cloud covering factor  $C$ . I found that this model successfully reproduces the range of observed spectral slopes and reflection amplitudes, the  $R$ - $\Gamma$  correlation and the individual  $R$  and  $\Gamma$  distributions. The same model is also consistent with the  $R$ - $\Gamma$  data of galactic black holes. Wide changes in the covering factor  $C$  from source to source would be responsible for the observed spectral differences. Without dissipation in the cold phase (i.e. if the clouds radiate only through reprocessing), the clouds are constrained to be in the immediate vicinity of the central hot plasma. The data indicate an average relative distance  $d/r=1.7$  with a small spread in distance from source to source. If there is some form of internal dissipation in the clouds this constraint can be relaxed somewhat. But in any case the distance is constrained to be lower than  $d \sim 13r$ , by the maximum observed UV to X flux ratios. These results are detailed in Malzac (2001). For me, it was really surprising that such an over-simplistic model could be so successful in reproducing such a large amount of data.

### 3.3.3.2 The clumpy disc model

The next step was to study the effects of the presence of cold optically thick clouds homogeneously distributed *inside* the hot phase (see Fig. 3.6). In order to do this, I teamed up with Annalisa Celotti, from SISSA in Trieste, who had a long history of cloud modelling. Under assumptions of neutral, optically thick, small scale, homogeneously distributed clouds inside the hot plasma, we could use the Non-Linear Monte-Carlo code to compute the emitted spectra. These numerical results were completed by analytical formulae giving the slope of the primary X-ray Comptonised spectrum  $\Gamma$  and the reflection amplitude  $R$ . The results were presented in a paper published in MNRAS (Malzac & Celotti 2002). They can be summarised as follows: The spectrum depends mainly on the amount of cold clouds filling the hot phase. Cold clouds pervading the hot plasma have a much stronger cooling effect than the external reprocessor previously studied. The clouds filling factor is therefore constrained to be low in order to produce spectra similar to those observed in Seyfert galaxies and X-ray binaries in the hard state (i.e.

not too soft). This implies that, contrary to what is observed, the amplitude of the reflection component is always very weak.

An important contribution from an additional external reflector is therefore required to explain the relatively strong reflection features observed in many sources. This reflector could take the form of an external accretion disc or the molecular torus postulated in AGN unification models (Antonucci 1993). Then, however, the observed  $R$ - $\Gamma$  correlation is *a priori* not expected, and becomes very difficult to explain. In the case of Seyfert galaxies, the problem can be partly solved. Indeed, at the same epoch, I was also finishing a paper in collaboration with Pierre-Olivier Petrucci (Malzac & Petrucci 2002) showing that at least part of the observed  $R$ - $\Gamma$  correlation in Seyfert galaxies could be understood in terms of the effects of time-delays between the fluctuations of the primary emission and the response of a large-scale distant reflector (e.g. a molecular torus). Obviously, because of the time-scales involved, this interpretation could not hold for black-hole binaries.

Therefore it seemed unlikely that both soft photons and reflection would arise from cold material mixed inside the hot Comptonising plasma. A situation in which the cold clouds were external as in the simple spherical model that I had studied before appeared to be much more favoured. The clumpy disc model had failed to match the observations of hard state like sources. However, this was far from being its end: we would soon find how to use it for a different purpose.

### 3.3.3.3 How the X-ray spectrum of a narrow-line Seyfert 1 galaxy may be reflection-dominated

During summer 2001, I spent two weeks in Milton Keynes, England. I had been invited by Sylvain Chaty and Carole Haswell to help them with the amazing multi-wavelength data they had collected on a recently discovered microquasar (this story will be told in Section 3.4.1.1). It was my first stay ever in the UK. I had been told that Cambridge was a very pretty city that deserved a visit. As it was not very far from Milton Keynes, I dropped an e-mail to Andy Fabian, offering to give a seminar at the Institute of Astronomy of the University of Cambridge. I did not know him personally and was not expecting an answer. He replied apologising that it was too late to organise a seminar at the institute, but he would arrange a small informal ‘bunclub’ group meeting with his students. I had not realised that his group was so big. As a matter of fact, I never had such a large audience for a seminar. Among the students was Andrea Merloni who would become a close collaborator.

During this talk, I presented my early results on the clumpy disc and cloud models. Andy Fabian and Andrea Merloni seemed particularly interested by the fact for large cloud covering fraction, the spherical cloud model would produce a very strong reflection component. Actually XMM had been launched in December 1999, and they were starting to receive a wealth of very interesting data on luminous AGN, namely bright Seyferts and Narrow Line Seyfert 1s (NLS1)<sup>9</sup>. These data were often showing strong reflection and iron lines. In some of these sources the primary emission appeared to be strongly suppressed leaving a bare reflection spectrum. Hence, in Andy Fabian’s group, some people were starting to think about ways of producing reflection dominated spectra. Six months later they would publish a paper precisely entitled “How the X-ray spectrum of a narrow-line Seyfert 1 galaxy may be reflection-dominated” (Fabian et al. 2002), in which they used analytical arguments to show that a clumpy disc model with very high filling factor could do the trick. Indeed, if the covering factor is such that the X-ray source is hidden, then the detected X-ray emission is dominated by reflection off the surface of the

---

<sup>9</sup>A subclass of Seyfert 1s with luminosity close to Eddington and showing extreme variability

clouds. Of course for such high filling factors, the radiative cooling in the hot plasma is very strong, leading to a primary spectrum that is much softer ( $\Gamma > 2$ ) than the typical hard state spectra that I was trying to model with Annalisa Celotti, but consistent with what is observed in NLS1s.

If this was correct, then the question arised of why this kind of clumpy disc would appear only in highly luminous objects. Latter developments in accretion theory would soon provide us with an answer. Indeed black hole systems, either in X-ray binaries or in active galactic nuclei, when shining at luminosities close to the Eddington limit are thought to be powered by accretion through geometrically thin, optically thick discs. Nonetheless, according to the standard accretion disc solution, such highly luminous discs should be radiation pressure dominated and therefore unstable to perturbations of both mass flow (Lightman & Eardley 1974) and heating rates (Shakura & Sunyaev 1973). Thus, it is not clear yet to what extent this standard solution represents a realistic description of the observed systems. In recent years, both analytic works (Blaes and Socrates 2001, 2003) and simulations (Turner, Stone and Sano 2002, Turner et al. 2003, Turner 2004) have shown that magnetized, radiation pressure dominated accretion discs may be in fact subject to violent clumping instabilities if magnetic pressure exceeds gas pressure and photons are able to diffuse from compressed regions. Large density variations may also be caused by photon bubble instabilities (Gammie 1998), which may develop into a series of shocks propagating through the plasma (Begelman 2001,2002; Turner et al. 2005). These instabilities may in turn have profound effects not only on the nature of the cooling mechanism of luminous discs, but also on their observational appearance (see e.g. Ballantyne et al. 2004).

In the following years the accumulation of data confirmed that the spectra of luminous Seyfert galaxies are very well described by photoionized and strongly relativistically blurred reflection models (Fabian et al. 2004, 2005; Crummy et al. 2006; Porquet 2006). In addition, the spectral variability studies evidenced some rather puzzling properties. In a number of NLS1 galaxies and galactic black holes in the very high state<sup>10</sup>, the variabilities of the continuum and of the iron line are decoupled, in apparent contradiction with the predictions of simple disc reflection models (see e.g. Miniutti, Fabian & Miller 2004; Fabian et al. 2004). In particular, the monitoring of Seyfert galaxies indicates that the reflection flux can be weakly variable when the primary emission changes dramatically (Papadakis et al. 2002). Moreover, in at least two AGN, MGC 6-30-15 (Miniutti et al 2003) and NGC4051 (Ponti et al. 2006) and one X-ray binary (XTE J1650-500, Rossi et al. 2005) the reflection flux is correlated to the primary emission at low fluxes and saturates at higher fluxes. In 2004, Miniutti & Fabian (2004) proposed the so-called ‘light bending’ model in which all these properties (including the occurrence of reflection dominated spectra) are interpreted in terms of general relativistic effects (see Section 3.3.4.2). This model quickly became very popular and nobody was talking about the clumpy disc model anymore.

### 3.3.3.4 The inhomogeneous accretion flows are back

Yet, Andrea Merloni and I had the intuition that all these properties could also be the result of the complex structure of near Eddington clumpy accretion flows. Since 2002, we had the project of exploring in detail the consequences of the hypothesis that accretion flows close to the Eddington rate are indeed inhomogeneous both in density and heating structure. I could have performed calculations similar to those of Malzac and Celotti (2002) with a larger cloud filling factor. However, I was already aware from my work with Martine Mouchet and

---

<sup>10</sup>The very high state is an intermediate or transition spectral state observed at high X-ray luminosity

Anne-Marie Dumont that ionisation effects could not be neglected in the two phase radiative equilibrium. Moreover, since the observations were showing ionized reflection, I had to couple the NLMC simulations with a photoionisation code. Coupling the NLMC with the TITAN/NOAR code was not an option. The simulation of inhomogeneous disc was much more complicated than the simple slab corona model I had been simulating with Anne-Marie and Martine. The inhomogeneous heating rate implied a spatial gradient of the ionisation properties of the clumps which would imply many more time-consuming iterations with TITAN/NOAR.

In October 2002, I had been awarded a postdoctoral theory rolling grant from the Institute of Astronomy in Cambridge. I packed all my stuff in the old Opel Corsa and moved from Italy to England. Andrea Merloni had already left Cambridge for Garching in Germany. Nevertheless, I talked about our project with Andy Fabian who suggested we use the photoionisation code of Ross & Fabian (1993, 2005). This code was supposed to be slightly less accurate but much faster and easy to use than TITAN/NOAR. I started to work on this code with Randy Ross (based in the US) and managed to automatise the complicated iteration process between the NLMC and photoionisation codes for each cell of the accretion disc. Then I just had to let the code run in the background for weeks to months and wait for the results. But then Andrea and I stopped everything to work on a different and very hot topic (see Section 3.4.1). It is only two years later, during Andrea’s visit in Toulouse, that we started working again on the appearance of inhomogeneous accretion flows. This work led to a publication (Merloni, Malzac, Fabian and Ross 2006) in which we present a detailed study of their expected X-ray spectra and variability, taking into account the radiative coupling between the two phases. As already mentioned a crucial factor in determining the broad band spectral properties of an inhomogeneous flow is the amount of cold clouds pervading the hot plasma. In the limit of small scale optically thick clumps, this is quantified by the cloud optical depth  $\tau_B = nSH$ , where  $H$  is the disc scale height,  $n$  is the number density of cold clouds and  $S$  their average geometrical cross section. Figure 3.7 shows a sequence of spectra obtained by varying  $\tau_B$ . As the cloud covering fraction (i.e.  $\tau_B$ ) increases, the primary spectrum becomes softer, because of the enhanced cooling in the hot phase, and at the same time the reflection/reprocessing features become more and more prominent. Reflection dominated spectra are achieved for  $\tau_B > 1$ . As these spectra are supposed to be formed in the central part of the accretion flow, one naturally expect some relativistic blurring that is not taken into account in the spectra of Fig. 3.7.

In Merloni et al. (2006), we also derived analytical formulae to estimate the luminosity of the different spectral components of the radiation emerging from the inhomogeneous accretion flow. Fig. 3.8 shows the reflected luminosity, the soft reprocessed luminosity and the reflection fraction as a function of the X-ray (Comptonised) luminosity. The fact that the reflected luminosity has a broad maximum, implies that large variations of the emergent X-ray luminosity,  $L_X$ , associated with changes in the cold clump integrated optical depth correspond to only modest variations of the reflection component, at least around the maximum. On the other hand, for lower values of the Comptonised X-ray luminosity, the reflected luminosity correlates with  $L_X$ , while at high  $L_X$ , the trend is the opposite. This global behaviour of  $L_R$  vs.  $L_X$  is strikingly similar to that of the light bending model (see Section 3.3.4.2 and Fig 3.10) and reproduces the variability properties of the continuum and of the iron line in a number of Narrow Line Seyfert 1 (NLS1) galaxies and galactic black holes in the very high state.

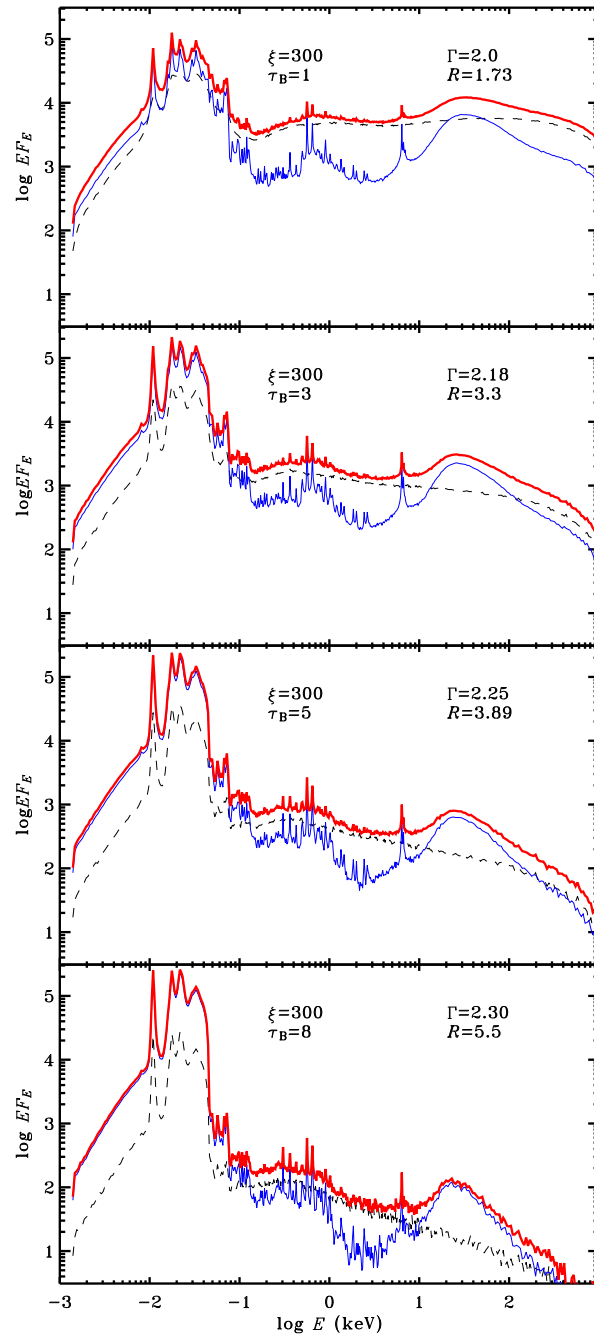


Figure 3.7: Inhomogeneous disc model: angle averaged spectra for  $\tau_B$  ranging from 1 to 8 as indicated. The best fit parameters  $R$  and  $\Gamma$  obtained when these spectra are fitted with PEXRAV in the 2-30 keV range are shown as well. The other fixed model parameters are the vertical Thomson optical of the disc  $\tau_T = 1$ , the ionisation parameter of the cold clumps  $\xi = 300$ , and the size of the regions where the plasma is heated  $h = 0.1H$  (see Merloni et al. 2006 for details).

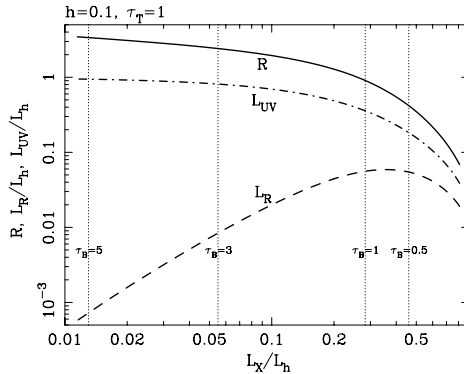


Figure 3.8: Inhomogeneous disc: the relative intensity of the reflection component ( $R$ , solid line), of the reprocessed UV ( $L_{UV}$ , dot-dashed line) and reflected ( $L_R$ , dashed line) luminosities are plotted as functions of the emergent X-ray (Comptonised power-law) luminosity above 1 keV ( $L_X$ ) for a varying cloud optical depth  $\tau_B$ . All luminosities are renormalized to the total heating rate  $L_h$  (see Merloni et al. 2006 for details). The vertical dotted lines mark the X-ray luminosities corresponding to  $\tau_B=0.5, 1, 3, 5$

### 3.3.4 Effects of general relativity

#### 3.3.4.1 Tracking photons in a curved space time

Potentially, compact objects represent a unique laboratory to probe physics in strong gravitational fields. General relativity can imprint specific signatures on the spectra or the temporal properties of the sources. The observation of relativistically broadened and redshifted iron lines is the best known example (see Miller 2007 for a recent review). But other effects, associated to the geometry of the accretion flow and affecting the variability of the iron line and the continuum are also expected. They have possibly already been observed. When, in January 2004, I moved back to Toulouse to take my current position at CNRS, a Thai student, named Thitiwat Suebsuwong, was preparing a PhD (under the supervision of Elisabeth Jourdain and Alexandre Marcowith) with the goal of studying some observational consequences of general relativity. I started to work with him on the possibility of including GR effects in accretion disc corona models. At that time he had already written and validated routines to compute the path of photons in the Kerr metric. In principle, these routines could be coupled with our Monte-Carlo codes. However we quickly realised that introducing these routines in the NLMC code would constitute a difficult and time-consuming problem. As a first step, I suggested to neglect GR effects and radiative transfer in both the corona and the disc and only implement GR photon travel between the corona and the disc or from the disc-corona to the observer. As long as the corona is compact (i.e. can be represented by one or several point sources), this is a good approximation.

#### 3.3.4.2 Light bending model

At the same time, I was well aware of Giovanni Miniutti's work on the light bending model (he had been my colleague as well as a good cigarette provider at IoA). In this model, the active

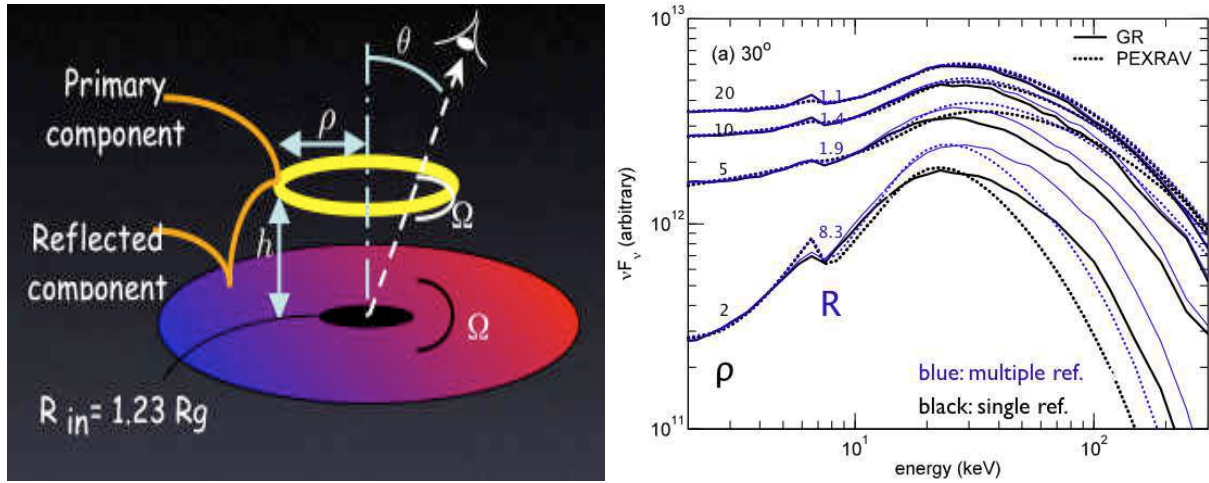


Figure 3.9: Left: assumed geometry of the light bending model. The primary X-ray source forms a ring of radius  $\rho$  at a height  $h$  above, and in corotation with, the accretion disc that extends down to the last stable orbit of a maximally spinning Kerr black hole. Right: light bending model spectra (light blue lines) for a ring height of  $2 R_g$  and various radii  $\rho = 2, 5, 10$  and  $20 R_g$ , from bottom to top respectively. The thick black lines show the spectra obtained when multiple reflections, due to radiation returning to the disc, are neglected. The effects of multiple reflections are very significant above 10 keV. The dotted curves show the Newtonian model (PEXRAV) providing the best fit of the light bending spectra in the 2-30 keV band. The reflected spectra are for neutral material and standard abundances. The primary emission consists in an e-folded power law with photon index  $\Gamma = 2$  and  $E_c = 200$  keV. The inclination angle is  $30^\circ$ . The spectra are reflection dominated when the ring radius is low, as can be seen from the reflection coefficients  $R > 1$ , shown on the figure.

coronal region(s) illuminating the disc are idealised as a ring source at some height above, and corotating with the accretion disc (see Fig. 3.9). When the source is close enough to the black hole, the primary component is strongly suppressed leading to reflection dominated spectra. Moreover, as shown by Miniutti & Fabian (2004), fluctuations in the height of the source can lead to strong variability in the primary component with little variability in the reflected flux, as observed.

In their calculations of the light bending model, Miniutti and Fabian focused on the iron line profile and flux and were not able to compute the full shape of the reflected continuum which is useful for a more detailed comparison with the data. I therefore encouraged Thitiwat to implement this model and helped him to produce detailed calculations of the light bending model spectra. This resulted in a paper (Suebsuwong, Malzac, Marcowith & Jourdain 2006) which largely confirms the results of Miniutti & Fabian (2004). These calculations improved upon the previous works by fully computing broad band angle dependent reflection spectra and primary emission as a function of ring radius  $\rho$  and height  $h$  of the ring source.

We also included for the first time the effects of multiple reflection (i.e. reflected photons returning to disc due to light bending). Fig. 3.9 shows some sample spectra obtained when varying the ring radius while keeping a constant height above the disc ( $h = 2 R_g$ ). These spectra show that the smaller the radius, the stronger the reflection component. Indeed, when

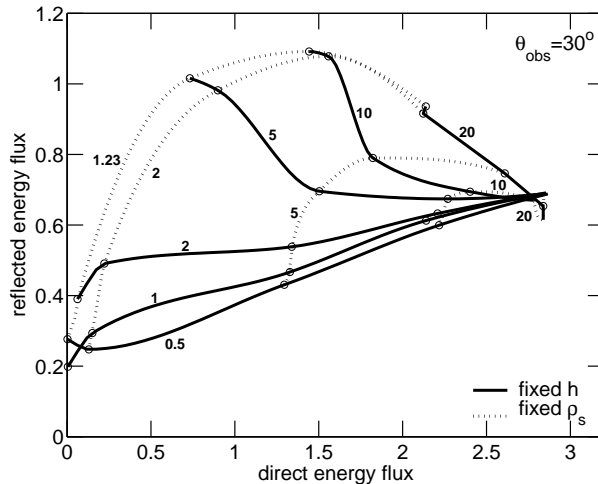


Figure 3.10: The total reflected energy flux as a function of the total direct energy flux, both are in the energy range 1-30 keV, for an observation inclination  $30^\circ$  and different source height and radius. The thin lines represent the fixed source radius and the thick lines indicate the same source height. These curves are spline interpolations between the results of the light bending model spectra simulations lying at their intersections.

the primary X-ray source is located at less than a few  $R_g$  from the black hole horizon, the light bending effects are very strong and tend to beam the primary radiation towards the disc, leading to strongly reflection-dominated spectra. In these extreme cases, the irradiation is concentrated in the central part of the disc. Then, the same light bending effects make it difficult for the reflected photons to escape. A significant fraction of them returns to the disc where they can be reflected again and so on. The reflection spectrum is then made up of the sum of the multiply reflected spectra, which makes it significantly different above 10 keV from what is expected from single reflection models (as shown in Fig. 3.9). These effects should be taken into account when fitting the spectra of extreme sources such as MGC 6-30-15 observed with broad band instrument such as those of BeppoSAX, INTEGRAL or Suzaku.

Figure 3.10 shows the dependence of the observed reflected and primary luminosity upon the height  $h$  and radius  $\rho$  of the ring source. Fluctuations of the geometrical parameters of the source lead to changes in the reflected and primary flux that are not always correlated. Indeed, as can be seen on this figure, depending on the parameter regime, the reflected and primary components can also be anti-correlated or nearly independent. When the source height changes at constant radius and as long as  $\rho_s < 5R_g$ , its track in this plane can be described according to three regimes:

- i) at low fluxes (or low source height) the reflected and primary flux are correlated,
- ii) at higher fluxes the reflection saturates at an almost constant value while the primary can change by a factor larger than 2,
- iii) at even higher fluxes the reflection component is weakly anti-correlated with the primary emission.

This behaviour was first identified and described in details by Miniutti and Fabian (2004). As shown by these authors, many properties of the variability of Seyfert galaxies and black hole

binaries can be understood in terms of fluctuations of the source height. In particular the curious behaviour of MGC 6-30-15, NGC4051 and XTE J1650-500, where the reflection flux is correlated to the primary emission at low fluxes and saturates at higher fluxes, is in qualitative agreement with the predictions of this model. Fig 3.10 enables us to investigate further the model parameter space. If the radius is larger than  $\sim 5R_g$  the variability induced by change in the height is much too weak ( $< 2$ ) to account for the variability observed in most accreting black holes. Let now consider the effects of changes in the source radius at constant height. At small source heights ( $h < 5R_g$ ), overall the reflection and primary emission are weakly correlated: the reflected flux changes by at most 50 % when the primary flux increases by more than one order of magnitude which might be in qualitative agreement with some observations but is inconsistent with the strong non-linear correlation observed for instance in the low state of NGC4051. At higher source heights, the reflected and primary fluxes become anti-correlated, which is not observed. The slope of the anti-correlation increases with  $h$ . At  $h \sim 10R_g$  we could observe large variations of the reflection component at constant primary flux. These results suggest that if the light bending model is to be the correct interpretation of the observations, the driver of the variability should be  $h$  while the source ring radius has to be nearly constant and small ( $< 5R_g$ ). This is precisely what is expected if X-ray emitting active regions continuously form and vanish at various heights above the disc in the innermost part of the accretion flow.

A more indirect way to test the light bending model is through the study of the hard X-ray background, which is believed to be dominated by AGN. In a given AGN, if the X-ray emitting region lies in the deepest parts of the gravitational potential within a few gravitational radii of the event horizon, then the spectrum is reflection dominated and relativistically blurred. If this happens in an important fraction of AGN, this must affect the X-ray background spectrum. Recently Poshak Gandhi, working at RIKEN in Saitama (Japan), and Andy Fabian asked Thitiwat and myself to help them at incorporating general relativistic light bending in AGN synthesis models for X-ray background. We did it by providing the template light bending spectra. The main result is that the X-ray background spectrum allows for a cosmologically-significant fraction of sources with strong light bending (Gandhi, Fabian, Suebsuwong, Malzac, Miniutti & Wilman 2007).

### 3.3.4.3 Light bending or inhomogeneous accretion ?

The similarity between the light bending model and inhomogeneous disc models lends itself to a simple geometrical explanation. In the more general framework of two-phase models for the X-ray spectra of accreting black holes, the main spectral and variability properties are determined by the geometry (and the topology) of the two phases and, in particular, on the sky covering fraction of the cold phase as seen by the hot, Comptonising medium. Reflection dominated spectra are expected when the cold phase intercepts most of the photons coming from the hot phase. This, in the light bending model, is achieved via general relativistic effects, while in the inhomogeneous disc model it is a result of the clumpy and inhomogeneous nature of the inner disc.

In principle, the relativistic blurring induced by the differential rotation of the inner disc should always be taken into account when fitting observed spectra. In the original light-bending model, where the illuminating source is a point-like source above a standard geometrically thin disc, the ratio of the reflected component to the power-law continuum is determined by the same effects that determine the shape of the relativistic lines, while if the disc is truly inhomogeneous, the two effects can be decoupled. Therefore, simultaneous spectroscopic studies of relativistically

blurred emission lines and of the broad band continuum and variability could be effectively used to discriminate between a pure light bending model and a clumpy disc. Detailed predictions for the latter, however, require the combination of sophisticated MHD and radiative transfer simulations.

### 3.4 Observations and interpretation of data

This part describes more observational aspects of my work that are mostly related to the connection between accretion and ejection in BHBs. In section 3.4.1, I provide some general background on this subject before moving to two particularly interesting sources that I have studied. Those two sources are Cygnus X-1 in which I have observed some unusual coupling between the accretion flow and radio jet occurring on a time-scales of a few hours (section 3.4.1.2) and XTE J1118+480 (section 3.4.1.1) in which we have observed what we believe is a signature of jet/disc coupling on time-scales shorter than a second. Finally, I summarise my participation in various observations of BHB and AGNs in section 3.4.2, and my contribution to the Simbol-X mission in section 3.4.3.

#### 3.4.1 The jet corona connection

While I was a postdoc in Milan, the importance of jets and outflows as a significant component of the energy output of BHB was gradually acknowledged. Multi-wavelength observations of accreting black holes in the LHS had shown the presence of an ubiquitous flat-spectrum radio emission (see e.g Fender 1999; Fender 2006), that may extend up to infrared and optical wavelengths (see Fig. 3.2). The properties of the radio emission indicate it is likely produced by synchrotron emission from relativistic electrons in compact, self-absorbed jets (Blandford & Konigl 1979; Hjellming & Johnston 1988). This idea was confirmed by the discovery of a continuous and steady milliarcsecond compact jet around Cygnus X-1 (Stirling et al. 2001). Moreover, in LHS sources a tight correlation has been found between the hard X-ray and radio luminosities, holding over more than three decades in luminosity (Corbel et al. 2003; Gallo, Fender & Pooley 2003). In contrast, during HSS episodes the sources appear to be radio weak (Tananbaum et al. 1972; Fender et al. 1999; Corbel 2000), suggesting that the Comptonising medium of the low/hard state is closely linked to the continuous ejection of matter in the form of a small scale jet. When the importance of the connection between radio and X-ray emission was realised, it was proposed that the hard X-ray emission could be in fact synchrotron emission in the jet, rather than Comptonisation in a hot accretion flow/corona (Markoff, Falke, Fender 2001; Markoff et al. 2003). This model is able to explain quantitatively the correlation between the X-ray and radio emission, it is also able to reproduce at least roughly the shape of the LHS X-ray spectrum of several sources. However, it seems that in most sources the synchrotron emission alone is not enough to reproduce the details of the X-ray spectra. In the most recent version of this model a thermal Comptonisation component was added which appears to provide a dominant contribution to the hard X-ray spectrum (Markoff et al., 2005). This component is supposedly located at the base of the jet which forms a hot plasma very similar to an accretion disc corona.

In the context of ADC/hot disc models the correlation between X-ray and radio emissions, simply tells us that the corona and the compact jet of the LHS are intimately connected. A strong corona may be necessary to launch a jet and/or could be the physical location where the jet is accelerated or launched (Merloni & Fabian 2002). Jet spectral components have recently

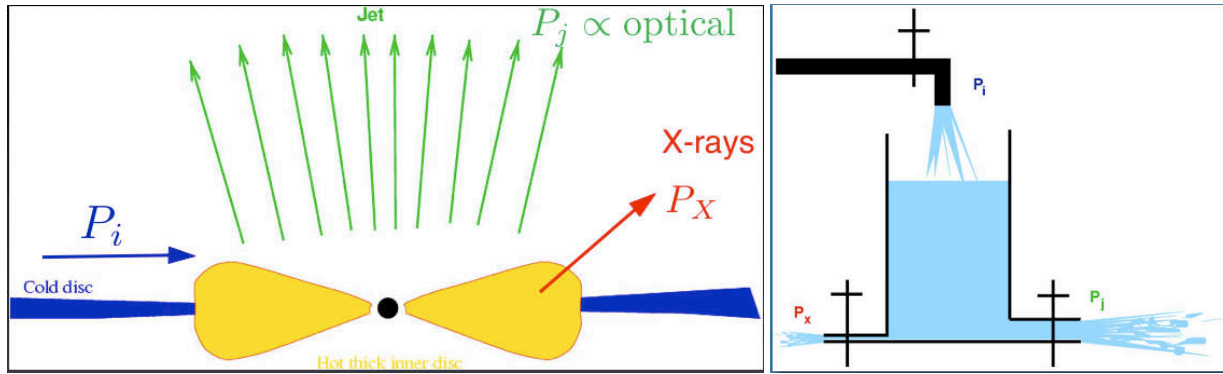


Figure 3.11: A simple energy reservoir model for the complex optical/X-ray correlations observed in the BHB XTE J1118+480. Left: The variable optical emission arises in the jet photosphere and is a tracer of the jet power. The X-rays are produced in the hot accretion flow or corona. Large amounts of accretion energy flows into the system at a rate  $P_i$ . It is stored in the accretion flow and accumulates until it is channelled partly into the jet (triggering the optical emission) and partly into the corona (triggering the X-ray emission). Right: the hydraulic analogue: the accretion flow behaves like a tank with one input pipe and two output pipes. The flow of water in these three pipes represents the incoming accretion power, the jet power and the X-ray luminosity respectively. Taps on the three pipes are randomly opened and closed. As a consequence the flows in the ‘jet’ and ‘X-ray’ pipes are variable. They present correlations that are similar to those between the optical and X-ray light curves of XTE J1118+480. See Malzac et al. 2004 for details.

been added to the hot disc models and make it possible to produce good fits of the whole spectral energy distribution from radio to hard X-rays (Yuan et al 2007), although the physics of the jet/ADAF connection has not been fully worked out yet.

Following a different approach, K rding et al. (2006) show that the observed X-radio correlation can be reproduced provided that the hot flow/corona is radiatively inefficient (i.e. luminosity scales like the square of mass accretion rate) and that a constant fraction of the accretion power goes into the jet (i.e. jet power scales like mass accretion rate). However there is presently no detailed model to explain how the physical connection between jet and corona works. A possible basic explanation was proposed by Meier (2001) for ADAF like accretion flows and later extended to the case of accretion disc coronae by Merloni and Fabian (2002). It goes as follows. Models and simulations of jet production (Blandford & Znajek 1977; Blandford & Payne 1982; Ferreira 1997) indicate that jets are driven by the poloidal component of the magnetic field. If we assume that the magnetic field is generated by dynamo processes in the disc/corona, the strength of the poloidal component is limited by the scale height of the flow (Livio, Ogilvie & Pringle 1999; Meier 2001; Merloni & Fabian 2002). Therefore geometrically thick accretion flows should be naturally more efficient at launching jets.

Despite this strong link between corona and outflow in the LHS, there are indications that in Intermediate States (IS) the jet is connected to the accretion disc rather than the corona (see Malzac et al. 2006 and section 3.4.1.2), suggesting a different mode of coupling between the jet, the cold disc and the corona in Intermediate States.

### 3.4.1.1 XTE J1118+480

**Spectral energy distribution** I met Sylvain Chaty in 1998 while he was an ATER (teaching assistant) in Toulouse and I was finishing my PhD. We were sharing a passion for rugby. But unlike me, he knew how to operate telescopes. He is a real astronomer capable of coordinating complex multi-wavelength observing campaigns. In 2001, he was a post-doc in Milton Keynes. He was working on a very interesting source for which he had just extracted multi-wavelength spectra extending from the radio band to hard X-rays. He called me in Milan to ask if I could help him with their interpretation. I was not familiar with those multi-wavelength data and I was also busy simulating clumpy disc models, I therefore accepted very reluctantly. The name of the source was XTE J1118+480 and I would spend the next four years trying to understand it.

The X-ray nova XTE J1118+480 had been discovered during an outburst by the (*RXTE*) All-Sky Monitor (*ASM*) on 2000 March 29 (Remillard et al. 2000). This discovery would lead to a breakthrough in the understanding of the connection between accretion and ejection in the LHS. The optical spectrophotometry proved a low mass X-ray binary system containing a black hole of at least 6 solar masses (McClintock et al. 2001). This source is located outside of the galactic plane with an exceptionally low interstellar extinction along the line of sight (Garcia et al. 2000). This fact allowed an unprecedented wavelength coverage ranging from the radio to the hard X-ray domain. The resulting spectral energy distribution that I studied with Sylvain Chaty and his collaborators is displayed in Fig. 3.2. In the radio to optical bands, a strong non-thermal component was associated with synchrotron emission from a powerful jet or outflow (Fender et al. 2001). In the optical to EUV bands the spectral energy distribution is dominated by a thermal component from the accretion disc. The X-ray emission consists of a typical powerlaw spectrum with photon index  $\Gamma \sim 1.8$ . During the whole outburst duration, the X-ray properties of the source, as well as the presence of strong radio emission, were typical of black hole binaries in the LHS. For the first time in a BHB in the LHS, it was possible to constrain simultaneously the properties of the disc, the corona and the jet.

Our spectral fits of the thermal disc emission with standard multi-color blackbody disc models suggest that the optically thick geometrically disc is truncated at a relatively large distance from the black hole (about 300 Shwarschild radii i.e.  $\sim 6000$  km). The data were clearly incompatible with a standard disc extending to the last stable orbit. This was in remarkable agreement with the hot disc scenario described in Sec. 3.1. Assuming that a hot spherical flow constitutes the central parts of the accretion flow (i.e. below 300  $R_s$ , see top panel of Fig. 3.3) and fixing the cold disc and corona luminosity to that observed, my NLMC simulations showed that the radiative equilibrium leads to a hard X-ray spectrum compatible with the observations (Chaty et al. 2003). A dynamic ADC model could not be ruled out, but requires the innermost part of the cold accretion disc to be invisible due to a very low temperature (not exceeding  $kT \sim 30$  eV the temperature measured at 300  $R_S$ ). As already mentioned in Sec. 3.3.2, this low temperature can be achieved if most of the accretion power is not dissipated in the thin disc but transported away in the corona or the outflow.

Yet in the case of XTE J1118+480, we know that only a small fraction of the accretion power is radiatively dissipated in the corona. Indeed, the total mass accretion rate onto the black hole can be estimated from the observed luminosity of the cold disc component which, in the case of XTE J1118+480, was known from our fits to the optical, UV and EUV spectra (see Chaty et al. 2003). The result depends on several assumptions regarding the geometry and the physical mechanisms for energy dissipation in the disc and the hot Comptonising medium.

However, for reasonable parameters, the estimated accretion power is much larger than the observed bolometric luminosity (by at least a factor of ten) and therefore the source is radiatively inefficient.

Then, an important question would be to determine whether the missing accretion power escapes the system in the (low radiative efficiency) jet or in other forms of non-radiative losses, such as a slow wind, or large scale convective motions, or advection into the black hole. The answer to this question resides in the exact determination of the jet kinetic power. Unfortunately, there are major uncertainties in this determination, mainly because the jet radiative efficiency is not known. The jet is expected to be a poor radiator because most of the energy is lost in adiabatic expansion. Thus, although the radiation from the jet represents a small fraction of the bolometric luminosity, the jet could dominate the energetics. For the case of XTE J1118+480, a typical efficiency of  $\epsilon_j \sim 0.01$  would already imply that the total jet power dominates over the X-ray luminosity.

**A correlated fast X-ray and optical flickering** As usual for a BHB in the hard state, the source presented a strong X-ray variability on time-scales of seconds (Revnitsev et al. 2000, its power spectrum is shown on the right panel of Fig. 3.2). But in addition, the weak extinction made it possible to perform fast optical and UV photometry of the source. These observations revealed a strong rapid optical/UV variability (Haswell et al. 2000). Interestingly the optical and X-ray variability appeared to be somewhat correlated. At the time I was starting to work with Sylvain on the spectral study, Laura Maraschi drew my attention on an article entitled “Correlated fast X-ray and optical variability in the black-hole candidate XTE J1118+480” (Kanbach et al. 2001) appeared in Nature. This paper reported simultaneous timing observations of XTE J1118+480 with *RXTE* and the rapid optical photometer *OPTIMA*. It showed a complicated optical/X-ray Cross-Correlation Function (CCF) with the optical band lagging the X-ray by 0.5s, but with a dip 2-5 seconds in advance of the X-rays. The authors argued that this correlated variability cannot be caused by reprocessing of the X-rays in the external parts of the disc. Indeed, the autocorrelation functions (see Fig. 1 of Sec. 5.2) showed that on average the optical flickering occurs on shorter time-scales than the X-ray one, and reprocessing models fail to fit the complicated shape of the X-ray/optical cross correlation function (see Fig. 3 in Sec. 5.2). Although they suggested this variability could arise through synchrotron emission in an outflow, they had no explanation for the complex shape of the X-ray Optical correlation they had found.

I had some ideas about the origin of these complex correlations. In order to test them, I needed to gain access to the data. By chance, I knew two of the authors of the Nature paper (Tomaso Belloni who was working in my institute and Henk Spruit who was the administrator of the European RTN Network I was paid by). I asked to have a look at the data and they kindly accepted. I started to work and rapidly realised that none of the models I had in mind could fit these variability patterns. In particular, I was thinking about the possibility (already suggested by Merloni et al. 2000) that the optical could be emitted through synchrotron process by the same coronal electrons emitting the Comptonised X-ray emission. This failed to reproduce the optical X-ray CCF unless all the parameters of the models (magnetic fields, optical depth, size of the emitting region, temperature of the hot electrons...) were all very weirdly correlated.

I explored more in depth the properties of the X-ray/optical correlation, applying a Fourier analysis (see fig. 3.2) as well as several other timing techniques. The result of these investigations was later published in A&A (Malzac et al 2003, reproduced in Sec. 5.2). The data were even more challenging than I had thought. The two most puzzling properties that I had found were

the following:

- The correlation between X-ray and optical light curves appears to have timescale-invariant properties: the X-ray/optical CCF maintains a similar, but rescaled, shape on timescales ranging at least from 0.1 s to a few tens of sec. See Fig. 4 of Malzac et al. 2003 in Sec. 5.2.
- The correlation does not appear to be triggered by a single type of event (dip or flare) in the light curves. Optical and X-ray fluctuations of very different shapes, amplitudes and timescales are correlated in a similar way, such that the optical light curve is related to the time derivative of the X-ray one. Indeed, in the range of timescales where the coherence is maximum, the optical/X-ray phase lags are close to  $\pi/2$  (see Fig. 3.2), indicating that the two lightcurves are related through a differential relation. Namely, if the optical variability is representative of fluctuations in the jet power output  $P_j$ , the data suggest that the jet power scales roughly like  $P_j \propto -\frac{dP_x}{dt}$ , where  $P_x$  is the X-ray power.

**The energy reservoir model** Spectrally, the jet emission seems to extend at least up to the optical band (see Fig. 3.2). Although the external parts of the disc may provide an important contribution to the observed flux at such wavelengths, my opinion was that the jet activity is the most likely explanation for the rapid observed optical flickering. For this reason, I felt that the properties of the optical/X-ray correlation in XTE J1118+480 might be of primary importance for the understanding of the jet-corona coupling and the ejection process.

I spent a lot of time trying to figure out how it could work. I was very puzzled by the differential relationship that I had found between the light curves. This was until one night of 2003, at about 3 a.m., when I woke up with an idea that would explain most of these properties. We just had to assume the presence of an energy reservoir in the innermost part of the accretion flow where large amounts of accretion power are stored before being channelled into either the jet or the X-ray corona (see sketch on Fig 3.11). The optical variability is then produced mainly from synchrotron emission in the inner part of the jet at distances of a few thousands gravitational radii from the hole. I assumed that at any time the optical flux  $O_{pt}$  (resp. X-ray flux) scales like the jet power  $P_j$  (plasma heating power  $P_x$ ). Stochastic fluctuations of the energy dissipation rates in the jet or the corona would then account for the observed variability and optical/X-ray correlations. This simple model is actually largely independent of the physical nature of the energy reservoir. In a real accretion flow, the reservoir could take the form of either electromagnetic energy stored in the X-ray emitting region, or thermal (hot protons) or turbulent motions.

When a few days later I discussed my idea with Andy Fabian, he suggested the following hydraulic analogy (see Fig 3.11): consider a tall water tank with an input pipe and two output pipes, one of which is much smaller than the other. The larger output pipe has a tap on it. The flow in the input pipe represents the power injected in the reservoir  $P_i$ . The flow in the small output pipe represents the X-ray power  $P_x$ , and in the large output pipe the jet power  $P_j$ . If the system is left alone the water level rises until the pressure causes  $P_i = P_j + P_x$ . Now, consider what happens when the tap is opened more, causing  $P_j$  to rise. The water level and pressure (proportional to  $E$ ) drop causing  $P_x$  to reduce. If the tap is then partly closed, the water level rises,  $P_j$  decreases and  $P_x$  increases. The rate  $P_x$  depends upon the past history, or integral of  $P_j$ . Identifying the optical flux as a marker of  $P_j$  and the X-ray flux as a marker of  $P_x$  we obtain the basic behaviour seen in XTE J1118+480. In the real situation, we envisage that the variations in the tap are stochastically controlled by a shot noise process. There are also

stochastically-controlled taps on the input and other output pipes as well. The overall behaviour is therefore complex.

Andrea Merloni helped me to develop this idea and we finally published a paper showing that the observed complex rapid optical X-ray correlation described above and in particular the differential relation between jet power (i.e. optical flux) and X-ray flux, can be explained by this relatively simple basic model involving several energy flows and an energy reservoir (Malzac, Merloni & Fabian 2004 enclosed in Sec. 5.3). An important requirement of the model is that the total jet power should be at least a few times larger than the observed X-ray luminosity. This would be consistent with the overall low radiative efficiency of the source and was also in agreement with contemporary estimates of the energy budget of accreting black holes suggesting that the kinetic jet power constitutes the main energy output of many accreting black holes (Fender, Gallo and Jonker 2003). This requirement of the model is also supported by more recent results on the study of the X-ray radio correlation in black holes and neutron stars indicating that for black holes in the LHS the jet power dominates over the X-ray emission (Körding et al. 2006).

This energy reservoir model may appear a bit simple and naive, but it is still the only explanation we have for the complex Optical/X-ray correlations observed in XTE J1118+480. Probably inspired by this work, Feng Yuan and Ramesh Narayan later proposed a spectral model of coupled jet and ADAF (Yuan & Narayan 2005; Yuan et al. 2007) that was applied to XTE J1118+480 and other BHBs.

### 3.4.1.2 Cygnus X-1

In 2004, I was back in the pink city, as ‘Chargé de Recherche au CNRS’. I was participating in the analysis of data from the INTEGRAL<sup>11</sup> satellite (see section 3.4.2) in collaboration with the SPI team at CESR (SPI is the spectrometer on Board of INTEGRAL<sup>12</sup> developed primarily in Toulouse). It was the best possible environment to start having a look at some INTEGRAL data in my possession. Indeed, I had been the PI of a 300 ks observation of the black hole Cygnus X-1. This prototypical source was the first dynamically proved black hole. Since its discovery (Bowyer et al. 1965), it has been an important target for all hard X-ray missions.

I had requested this observation in the INTEGRAL open observing time when I was in Milan. It was approved and latter performed in June 2003. Its aim was to look for spectral and temporal correlations between the X- $\gamma$  and other wavelengths (radio, IR, UV) This multi-wavelength campaign involved nine european research institutes including CESR (Toulouse), SAp/CEA (Saclay), and LAOG (Grenoble) for the French side.

The data analysis showed that during this observation the source was not in any of the two canonical spectral states. Rather, Cygnus X-1 was displaying spectral properties that were intermediate between the LHS and HSS: presence of a soft component in the 3-10 keV band (probably related to the geometrically thin accretion disc), a thermal Comptonisation component with a spectral index ( $\Gamma = 2.1$ ) softer than in the LHS showing a break or cut-off at about 100 keV. Above 100 keV, the spectrum was dominated by a non-thermal component similar to that of the HSS (see the time averaged spectrum in Fig. 3.1).

The hard X-ray and radio light curves showed a strong activity with many flares of large amplitude. It seems therefore that the source was in an unstable transition state between LHS and HSS. Broad band observations during those intermediate states are still rather rare. This

<sup>11</sup>see <http://www.esa.int/SPECIALS/Integral/index.html>

<sup>12</sup>see <http://sigma-2.cesr.fr/spi/>

observation therefore appeared particularly interesting for the understanding of state transitions in BHBs. Studying spectral transitions of BHBs between states with (LHS) and without (HSS) jets also provides important information on the connection between accretion and ejection processes.

During the four day long observation, the broad band (3-200 keV) luminosity varied by up to a factor of 2.6 and the source showed an important spectral variability. A principal component analysis demonstrates that most of this variability occurs through two independent modes. The first mode consists in changes in the overall luminosity on time-scales of hours with almost constant spectra (responsible for 68% of the variance) that are strikingly uncorrelated with the variable radio flux. We interpreted this variability mode as variations of the dissipation rate in the corona, possibly associated with magnetic flares. The second variability mode consists in a pivoting of the spectrum around 10 keV (27% of the variance). It acts on a longer time-scale: initially soft, the spectrum hardens in the first part of the observation and then softens again. This pivoting pattern is strongly correlated with the radio (15 GHz) emission: radio fluxes are stronger when the INTEGRAL spectrum is harder. We proposed that the pivoting mode represents a “mini” state transition from a nearly HSS to a nearly LHS, and back. This mini-transition would be caused by changes in the soft cooling photons flux in the hot Comptonising plasma associated with an increase of the temperature of the accretion disc. The jet power then appears to be anti-correlated with the disc luminosity and unrelated to the coronal power. The reason for the anti-correlation between jet and X-ray luminosity is most probably that state transitions are associated with a redistribution of the available accretion power between the compact jet and the cold accretion disc. In the standard hot disc scenario described in Sec. 3.1.2, this redistribution of accretion power could occur because the jet shrinks as the inner radius of the outer disc moves closer to the black hole. From this interpretation we also infer that the bolometric luminosity jumps by a factor of about 2 during the transition hard to soft. This suggests that accretion flow radiative efficiency is lower in the LHS.

All those results are detailed in an article published in A&A (Malzac et al. 2006) which is reproduced in Sec. 5.5. Besides this peculiar observation of Cygnus X-1, I also participated in a study of the long term spectral evolution of Cygnus X-1 using all the INTEGRAL data available at that time (Cadolle Bel et al. 2006). Moreover, in an ongoing work in collaboration with Melania del Santo from the IBIS group in Rome, we have found a similar bi-modal variability behaviour during the spectral state transition of the low mass BHB GX 339-4 (Del Santo et al. 2006).

### 3.4.2 From Beppo-SAX and RXTE, to INTEGRAL and XMM

In addition to the major works on Cygnus X-1 and XTE J1118+480 described above, I also took part in several other X-ray observations of BHB and AGN that are briefly described below.

In Milan, I participated in the interpretation of data from the BeppoSAX telescope<sup>13</sup> on Seyfert galaxies in collaboration with Pierre-Olivier Petrucci, Francesco Haardt and Laura Maraschi (Petrucci et al. 2001). We confirmed the existence of a  $R$ - $\Gamma$  correlation when those data are fit with a Comptonisation model with large optical depth ( $\tau_T \gtrsim 1$ ). In this case the data also suggest a correlation between temperature of the hot plasma and the X-ray photon index  $\Gamma$ . Such a correlation could be the signature of a  $e^+e^-$  pair dominated plasma. In addition, still in collaboration with Pierre-Olivier Petrucci, I analysed the data from NGC5548 a Seyfert 1 which was observed a dozen times by RXTE. The result of the spectral variability study shows that

---

<sup>13</sup><http://www.asdc.asi.it/bepposax/>

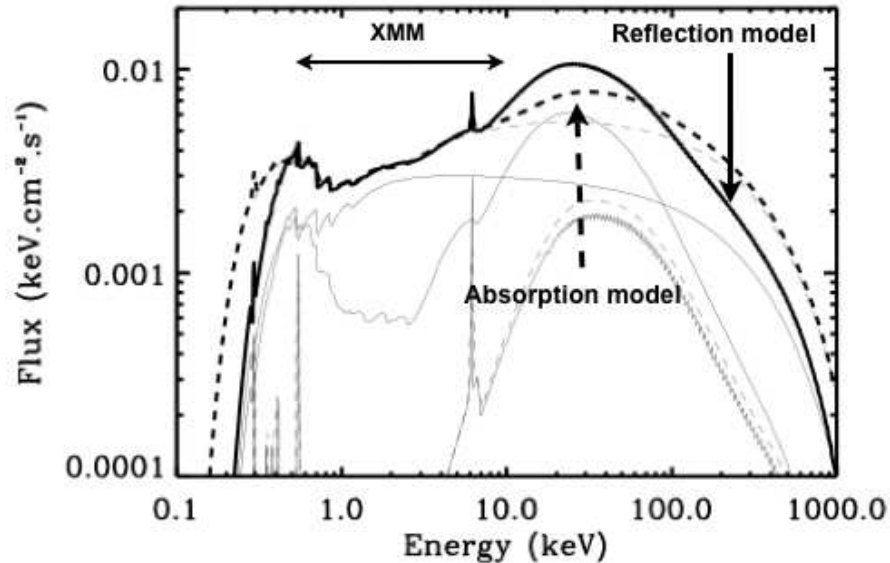


Figure 3.12: Best fit models to the XMM spectra of Mkr 841 (OBS 3 of Petrucci et al. 2007). The thick solid and dashed curves show the relativistically blurred reflection model and absorption model spectra respectively. Over-plotted in thin lines are the different components of each model. Thin solid lines: cut-off power law continuum, relativistically blurred ionized reflection and neutral reflection. Thin dashed lines: cut-off power law continuum, modified by relativistically smeared ionized absorption, and neutral reflection. Both models appear undistinguishable in the XMM band. See Petrucci et al. (2007) for details.

the flux both in the reflection component and the iron line is essentially constant on relatively short time-scales ( $< 1$  month) while the primary emission varies. This suggests that the reflection features are produced mostly at large distances from the central object (Malzac & Petrucci 2002).

Since I arrived in Toulouse in 2004, I collaborate with the SPI team at CESR on the analysis of INTEGRAL data from BHBs. I have worked with Angélique Joinet (CNES post-doc at CESR) on a BHB located close to the galactic centre and named IGR J17464-3213/H1743-322. This source was monitored by SPI and RXTE during an outburst that lasted from March to September 2002 (Joinet et al. 2005). We also analysed data from GX 339-4 at the beginning of its 2004 outburst (Joinet et al 2007).

I also had the opportunity to get involved in some AGN studies with INTEGRAL. I participated in the INTEGRAL and XMM data analysis of two Seyfert galaxies NGC4388 and NGC4151. The PI of those projects was Volker Beckmann, then at Goddard Space Flight Center in Greenbelt. Volker is actually an old acquaintance from the ‘foresteria’ (guest house) of the Merate observatory in Milan. This work led to 2 publications in the *Astrophysical Journal* (Beckmann et al. 2004, 2005) More recently, I have participated in the analysis of XMM data from the bright Seyfert 1 galaxy Markarian 841 led by Pierre-Olivier Petrucci (Petrucci et al. 2007). Among the results, we show that the complex spectrum of this source can be equally well described by reflection dominated models and absorption models (see Sec. 3.6.4).

### 3.4.3 Preparing for the future: Simbol-X

Simbol-X will be a hard X-ray mission, operating in the 0.5-80 keV range, proposed as a collaboration between the French and Italian space agencies with participation of German laboratories for a launch in 2013. Relying on two spacecrafts in a formation flying configuration, Simbol-X uses for the first time a 20-30 m focal length X-ray mirror to focus X-rays with energy above 10 keV, resulting in over two orders of magnitude improvement in angular resolution and sensitivity in the hard X-ray range with respect to non-focusing techniques. The Simbol-X revolutionary instrumental capabilities will allow us to elucidate outstanding questions in high energy astrophysics such as those related to black-holes accretion physics and census, and to particle acceleration mechanisms, which are the prime science objectives of the mission. After having undergone a thorough assessment study performed by CNES in the context of a selection of a formation flight scientific mission, Simbol-X has been selected for a phase A study to be jointly conducted by CNES and ASI.

At the technical level, CESR is involved in the development of on board electronics under the responsibility of Jean-Pierre Roques and Laurent Ravera. Jean-Pierre strongly encouraged me to get involved in the scientific part of the mission. So far my personal commitment regarded the definition of the scientific objectives and requirements of the mission. During the preparation of the phase A selection bid in 2005, I was responsible for the writing of the important section on compact objects and ultraluminous X-ray sources in collaboration with our Italian colleagues in Milan (Sandro Meregheti) and in Bologna (Pino Malaguti). I am now also involved in the ground segment definition.

## 3.5 Conclusion - Summary

I have developed powerful simulation tools for radiative transfer in relativistic plasma. The NLMC code allowed me to address for the first time detailed time-dependent Comptonisation problems. Those simulations lead to rule out models where the fast flickering of BHBs is driven by the variability of soft photons. We were also first to simulate a two-phase radiative equilibrium taking into account the full radiative coupling including both energy balance in the hot phase and the important effects of ionisation balance in the cold phase. The NLMC was then used to test the predictions of several models against the observations. The main results are the following:

- (i) The truncated disc model does not reproduce the observed shape of the  $R$ - $\Gamma$  correlation. Otherwise it provides a good explanation of almost all the data, and in particular the spectra of radiatively inefficient sources such as XTE J1118+480.
- (ii) Accretion disc corona models are also a viable possibility to model the LHS of BHBs. However, the model is tightly constrained by the observations. The constraints are the following: the accretion power cannot be dissipated in the accretion disc (but in the corona or the jet). The corona cannot be extended above the disc, it must be in the form of active regions of aspect ratios of about unity, the plasma in the corona must be outflowing with mildly relativistic velocities.
- (iii) Clumpy disc models do not give a satisfactory description of the spectra of LHS sources, but they may provide an explanation for the extreme properties of bright Narrow line Seyfert 1 galaxies. Very similar properties are actually expected from the effects of light bending in an accretion disc corona.

Besides this rather theoretical work, I have also participated in the analysis of data from orbiting X-ray and  $\gamma$  ray telescopes (RXTE, BeppoSAX, XMM, INTEGRAL). I found that the evolution of the high energy spectrum of Cygnus X-1 during a mini-state transition can be understood as a dramatic change in the cooling soft photon flux in the corona, that may be associated either to a change in the inner disc radius (truncated disc model) or to a change of the temperature of the cold accretion disc (ADC model). In the source XTE J1118+480, I established the properties of the correlation between the X-rays and the optical emission. I concluded that these complex correlations are most likely due to some form of coupling between the jet and the corona. I later proposed a simple phenomenological model involving an energy reservoir. Finally, I am actively participating in the scientific definition of the Simbol-X mission.

## 3.6 Research Plans

### 3.6.1 Introduction

In line with my past activities, my research project consists in continuing to develop numerical tools and use them to compare precisely models and observations of high energy sources. I plan to study various models for the spectra and variability of AGN and BHBs. I will try to make predictions that can be tested with data from present days telescopes (HESS, INTEGRAL, XMM) or future missions (GLAST, Simbol-X or XEUS). These investigations will take place in the context of the scientific preparation of the Simbol-X project to which I am strongly committed. In the longer run, I wish also to widen my research interests by adapting my numerical tools to various kinds of celestial sources of X and  $\gamma$ -rays, such as pulsars, gamma-ray bursts and blazars. This should be made easier by several improvements of the Fokker-Planck code.

My experience of writing and then performing research projects, is that I often end up working on things that have very little to do with the original plan. Nonetheless, in the following, I venture to detail several specific projects on which I plan to work in the forthcoming years.

### 3.6.2 The two flow model

Recently, Ferreira et al. (2006) have proposed a new framework for the understanding of the X-ray spectral states and jet activity of BHBs which represents an alternative to the truncated disc model. This scenario is based on the two-flow model (Sol, Pelletier & Asseo 1989; Henri & Pelletier 1991; Pelletier & Sol 1992) that has been developed for many years at the Observatoire de Grenoble and successfully applied to AGN. In this view, the central regions of the accretion flow have a multi-component configuration consisting in (1) an outer standard accretion disc (SAD) down to a transition radius  $r_{tr}$ , (2) an inner magnetized jet emitting disc (JED) below  $r_{tr}$  driving (3) a self-collimated non relativistic MHD jet surrounding, when conditions for pair creation are met, (4) a ultra relativistic pair beam. Large values of  $r_{tr}$  correspond to LHS while small values correspond to HSS. In between these extremes, in the high intermediate state,  $r_{tr}$  can reach values that switch on a pair cascade process giving birth to ultra-relativistic pair blobs that explain the superluminal events often observed in intermediate states. In this framework the X-ray corona is expected to form naturally in the JED itself. I am part of an ANR funded project led by Pierre-Olivier Petrucci aiming to investigate further this scenario by mean of both MHD and radiative transfer simulations. My task will be to help compute the spectral energy distribution as a function of  $r_{tr}$  (and in particular the emission of the hot corona) given the inputs

of the MHD simulations and analytical estimates of the structure of the accretion-ejection flow.

### 3.6.3 Lightbending

The fact that general relativity may play a dominant role in shaping the hard X-ray spectra of bright AGN is particularly exciting. The light bending model is very promising. However, in its present form, it appears too naive by several aspects. For example, the simulations of model spectra that we performed so far with Thitiwat Suebsuwong used a simple neutral reflection code. As already mentioned, the observations usually show ionised reflection. In order to confront directly the model with data we have to use a ionised reflection code. Previously, this was quite difficult because photoionisation codes are generally not very accurate when it comes to the angular distribution of the reflected radiation. This distribution is of prime importance when general relativistic effects are taken into account. However, it seems now that the recent version of the TITAN code has much improved capabilities in this respect. I would therefore be interested in performing simulations using this ionised reflection code.

Another important simplification in the present implementation of the light bending model is that the radiative cooling of the hot X-ray source by the soft photons coming from the disc is ignored. The shape of the primary emission is arbitrarily fixed and assumed to be independent of other parameters such as the height or radius of the source. In fact, the energy density of soft cooling photons is larger in the regions close to the innermost part of the disc. Therefore, if all the other parameters are constant, one could expect the primary emission to be softer when the source is located at a low height above the disc. The influence of this effect should be evaluated by implementing the general relativistic photon tracking routines of Suebsuwong et al. (2006) in the NLMC. This kind of calculations compared to broad band spectro-temporal observations of bright AGN may constitute a good test for the model, or at least put some more constraints on the nature and geometry of the active regions.

### 3.6.4 Absorption

Reflection by a ionised medium depends on the density structure of the gas. So far, all detailed comparisons of the light bending model with data used constant density models. However, in accretion discs, a pressure equilibrium is expected and it was recently claimed that ionised reflection spectra of a disc in hydrostatic equilibrium may have difficulties in reproducing the data (Done & Nayakshin 2007). This should be investigated by reanalysing the available data with this hydrostatic equilibrium model.

Moreover, relativistically blurred ionised reflection models are not the unique possibility to interpret the complex X-ray spectra of luminous AGN. Indeed, an alternative to reflection models uses similar partially ionised, velocity-smearred material seen in absorption rather than reflection (Gierliński & Done 2004; Sobolewska & Done 2007). It was initially suggested that this absorbing material would be the signature of a line driven accretion disc wind. But this specific physical explanation for the presence of the absorber seems to meet some difficulties in reproducing extremely blurred spectra that are observed (Schurch & Done 2006, 2007). The fact is that both reflection and absorption models fit the XMM spectra equally well (Middleston et al. 2007; Petrucci et al. 2007). Discriminating between the two models will be difficult. It will probably require high sensitivity spectra with a broader band than what is available today. It will also be important to compare the predictions of both models regarding the spectral variability, with high quality, time resolved, spectroscopic data. For me, the investigation of the predictions of both models will represent a preliminary to future observational studies with

Simbol-X. Another possible way of discriminating between those two models could be to use the fact that reflection and absorption have different polarimetric signatures. The advent of new telescopes allowing X-ray polarimetry (such as XEUS) may prove crucial in settling this issue. While waiting for these advances in instrumentation, I propose to take a first step and compute the polarization predicted by both models as a function of energy to see whether the results are different enough to be observationally discriminated.

### 3.6.5 Back to the clumpy disc model

A likely possibility could be that both reflection and absorption effects are important for the formation of the X-ray spectra of bright AGN. It would be very unpleasant because of the increased complexity and the difficulty of disentangling both components. However this is a situation that would be naturally expected in the framework of the clumpy disc model. Indeed, for the sake of simplicity, we had neglected absorption in our previous calculation of clumpy disc spectra. We had assumed that all clouds were optically thick. Instead, in a real situation, a range of sizes and optical depths are expected for the clouds. Some clumps will be thick, producing mainly reflected features, while others are optically thin, possibly imprinting absorption features in the escaping spectra. Those effects are not difficult to introduce in the NLMC code. We need however to have an idea of the distribution of the cloud optical depths. At present, it is not clear what this distribution looks like. More efforts in understanding these clumpy disc solutions are required. Hopefully this work will lead to a physically motivated prescription that we will be able to use in our simulations. Another option would be to use directly the density maps produced by MHD simulations of radiation pressure dominated accretion discs. The ultimate (and necessary) step of course would be to couple the radiation transfer and magneto hydrodynamics. Again, all this work will be pursued in the context of the scientific preparation of Simbol-X which I believe will be very important in discriminating between these models.

### 3.6.6 Further developments of the Fokker-Planck code and its applications

In the upcoming year, my priority will be to work with Renaud Belmont and Alexandre Marcowith on the development of the Fokker-Planck code. New radiation processes such as pair-production or bremsstrahlung as well as Coulomb interactions will have to be implemented. We also plan to take into account the presence of ions in the plasma that may interact with the leptons through Coulomb collisions. Another useful improvement of the code will be to implement self-consistent stochastic particle acceleration. Indeed, the Fokker-Planck formalism is particularly suited to the implementation of such processes. Currently, in the literature, radiation and acceleration models are not coupled. On the one hand, in radiation models, one assumes that electrons or pairs are instantaneously accelerated to ultra-relativistic energies with an ad-hoc distribution. On the other hand, in acceleration models, radiative losses are neglected or taken into account very roughly. In the code we plan to develop, particles will be able to cool at the same time they are being accelerated. This kind of simulations compared to observations will certainly provide constraints on the acceleration mechanisms in high energy sources. As already mentioned, the drawbacks of the Fokker-Planck code is that radiative transfer is dealt with a simple escape probability formalism. In the longer term the Fokker-Planck code should be coupled with the NLMC in order to achieve accuracy of the dynamic of particles and photons both in the momentum and position spaces.

The first applications of the Fokker-Planck code will certainly be devoted to a comparisons of hybrid thermal-nonthermal models accounting for the effects of magnetic field with INTEGRAL

data from BHBs such as GX339-4 or Cygnus X-1 in various spectral states. The aim will be to see if the ‘synchrotron boiler’ effect (see Sec. 3.2.2) could provide the right explanation for the quasi Maxwellian electron distributions observed in the LHS and also put constraints on the strength of the coronal magnetic field in both spectral states.

Besides X-rays, the Fokker-Planck code could turn out to be a useful tool when interpreting the data for very high energy telescopes such as HESS<sup>14</sup> or Glast<sup>15</sup>. For instance, the giant radio galaxy M87 harbours many distinct regions of broad-band nonthermal emission. The recently reported fast variability of TeV  $\gamma$ -rays from M87 on a timescale of days strongly constrains the range of speculations concerning the possible sites and scenarios of particle acceleration responsible for the observed TeV emission (Aharonian et al. 2003, 2006). A natural production site of this radiation is the immediate vicinity of the central supermassive mass black hole. Because of the low bolometric luminosity, the nucleus of M87 is effectively transparent for  $\gamma$ -rays up to energy of 10 TeV, which makes this source an ideal laboratory for study of particle acceleration processes close to the BH event horizon. Neronov & Aharonian (2007) analysed different possible radiation mechanisms in this region, and argued that the observed very high-energy  $\gamma$ -ray emission can be explained by the inverse Compton emission of ultrarelativistic electron-positron pairs produced through the development of an electromagnetic cascade in the BH magnetosphere. This is the kind of problem that can be simulated with the Fokker-Planck code in order to compare the predictions of various models to the data. Similarly, the modelling of the non-thermal  $\gamma$ -ray emission of jets in blazars or even X-ray binaries could be a source of numerous applications.

In fact, radiation physics in relativistic plasma is universal. The codes we are developing are quite versatile and can be applied to many different problems of high energy astrophysics. Applications to pulsars, different classes of  $\gamma$ -loud AGNs or even  $\gamma$ -ray bursts can be envisioned. I would be happy to help experts in those areas to adapt the codes to their peculiar problems. For instance, Gabriele Ghisellini and Analisa Celotti got me interested in a fundamental problem which has important implications for the observational appearance of  $\gamma$ -ray bursts. This problem is to calculate Comptonisation spectra in an expanding plasma. Indeed, the prompt emission of  $\gamma$ -ray burst is believed to be produced in a fireball which is expanding at the velocity of light. This fast expansion must have profound effects on the radiation processes. But so far, it has not been possible to take it into account. I hope to be able to tackle the problem using the Fokker-Planck code coupled with the NLMC code.

### 3.6.7 Observation of X-ray binaries with Simbol-X

Once Simbol-X is launched in 2013, I plan to work on the interpretation of observations of X-ray binaries with this instrument. Indeed, the phenomenology of accretion discs, coronae and jets in X-ray binaries is rather well established. However, as I have shown in this report, the structure of the accretion flow in the various spectral states is still debated and the connection between the hot flow and compact jet is far from being understood. Simbol-X should address these two important questions in several ways.

It will provide us with the capability of producing high sensitivity, broad band spectra and therefore constrain simultaneously the shape and luminosity of all spectral components (iron line, reflection bump, thermal disc and comptonised emission) which in turn provides information on the geometry of the accretion flow.

<sup>14</sup><http://www.mpi-hd.mpg.de/hfm/HESS/HESS.html>

<sup>15</sup><http://glast.gsfc.nasa.gov/science/>

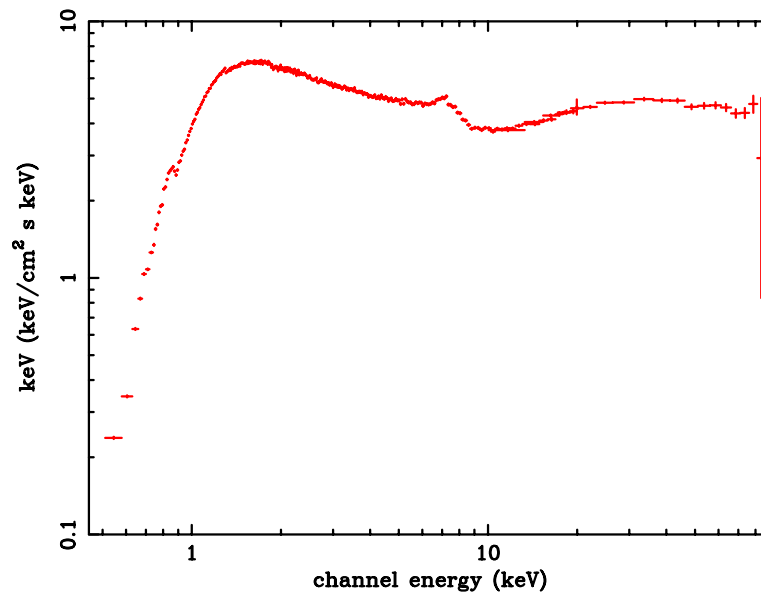


Figure 3.13: Simulated Simbol-X spectrum of a 1 ks observation of Cygnus X-1 with the current response matrices. These data were simulated according to the best fit EQPAIR model to the INTEGRAL spectrum of the 2003 Intermediate State (Malzac et al. 2006) which is displayed on Fig.3.1.

It will shed new lights on the underlying mechanisms triggering spectral state transitions by allowing us to follow in exquisite details the rapid spectral evolution and its correlation with the radio jet emission during these transitions. In particular, in bright sources such as Cyg X-1, it will be extremely interesting to perform time-resolved spectroscopy during spectral transitions. For instance, in my work on the INTEGRAL observations of Cygnus X-1 (see section 3.4.1.2), this technique allowed us to infer that state transitions are associated with a redistribution of the available accretion power between the compact jet and the cold accretion disc. In the standard hot disc scenario described in Sec. 3.1.2, this redistribution of accretion power could occur because the jet shrinks as the inner radius of the outer disc moves closer to the black hole. From this interpretation we also inferred that the bolometric luminosity jumps by a factor of about 2 during the hard to soft transition, suggesting a radiatively inefficient accretion flow in the Low Hard State.

However, this interpretation relies on the assumption that the temperature (or at least the luminosity) of the Shakura-Sunyaev accretion disc changes during the transition. Unfortunately, this cannot be observed directly with INTEGRAL since the thermal disc emission peaks around 1 keV and the INTEGRAL/JEM-X lower energy threshold is only at 3 KeV (see model spectrum and data on Fig. 3.1). Other contemporary instruments, such as XMM would have been able to detect changes in the cold disc luminosity, but their lack of sensitivity above 10 keV would have prevented the identification the pivoting pattern of the Comptonised component. Simbol-X with its high sensitivity over a broad energy range will certainly provide a critical test for state transition models. The rapid evolution of the thermal disc emission, hard comptonised component and reflection features (both line and reflection component) will be followed simultaneously and accurately. Fig. 3.13 shows that 1ks exposure will be enough to have all the features of

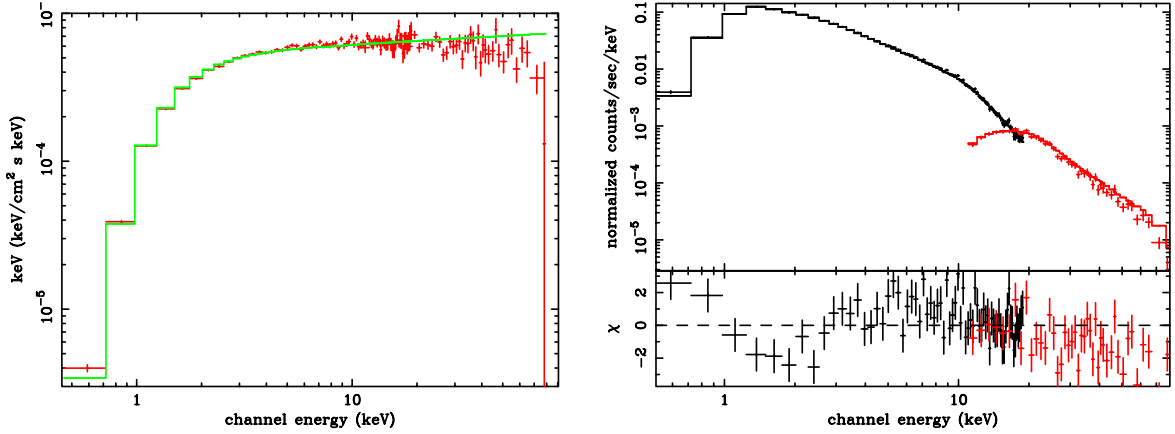


Figure 3.14: Simulation of a 400 ks observation of the quiescent source V404 Cyg with the latest response matrices. The shape of the observed Chandra spectrum (power-law with photon index  $\Gamma = 0.81$  absorbed by a column density  $N_h = 0.7 \cdot 10^{22}$ ; Kong et al. 2002) was extrapolated into the hard X-rays domain assuming a high energy cut-off around 80 keV (cutoffpl model in XSPEC). The simulated data were then fitted with a simple absorbed powerlaw model. The left hand side panel shows the fit in  $\nu F_\nu$  representation while the right hand panel shows the count rates in the CZT and MPD detectors as well as the residuals. The fit is poor (reduced  $\chi^2$  of 1.94 for 136 degrees of freedom, null hypothesis probability  $3 \cdot 10^{-10}$ , F-test probability  $2 \cdot 10^{-21}$ ). The slight curvature introduced by the high energy cut-off is therefore clearly detected. It can be seen in the residuals.

the the high energy spectrum of Cygnus X-1 revealed with a high accuracy. Such broad band, time resolved spectroscopy studies of bright sources will certainly provide extremely valuable information on the evolution of the geometry and energetics of the accretion flow during spectral state transitions.

Simbol-X will also help to determine the exact contribution of jets to the X-ray band in quiescent states. Indeed, as I already mentioned, jet spectral components have recently been added to the ADAF model and make it possible to produce good fits of the whole spectral energy distribution from radio to hard X-rays (Yuan et al 2007 and references therein). In this model, the X-ray emission is almost always dominated by comptonised radiation from the ADAF. However, an interesting prediction of this model is that jet synchrotron emission could have a dominant contribution to the the X-ray emission of very faint sources (of luminosity lower than  $10^{-6} L_{\text{Edd}}$ ). This transition from an ADAF dominated to a jet dominated X-ray emission could be evidenced through a change in the slope of the radio/X-ray flux correlation at low luminosities (Yuan & Cui 2005). This prediction could in principle be used to test this model. Gallo et al. (2006) have performed deep observations with the Very Large Array of A062000, leading to the first detection of radio emission from a black hole binary at X-ray luminosities as low as  $10^{-8.5} L_{\text{Edd}}$ . Combined with simultaneous Chandra data, this observation suggests that the non-linear correlation is maintained without change in slope down to quiescence. Actually, very few sources with luminosities lower than  $10^{-6}$  are accessible to both radio and X-ray investigations. An alternative approach could be to use X-ray spectroscopy alone. Indeed, at such low mass accretion rates an ADAF radiates essentially through Bremsstrahlung or inverse Compton in an optically (very) thin plasma. As a consequence, the resulting ADAF X-ray

spectrum should be very bumpy, while jet synchrotron emission is expected to remain a power-law even at very low accretion rates. The spectroscopy of quiescent sources was performed with Chandra and XMM (Kong et al. 2002; Hameury et al. 2003) and usually, in the limited bandwidth of these instrument they show a powerlaw spectrum of photon index  $\Gamma \sim 2$  (or harder) which is actually compatible with both a jet and ADAF interpretation. The high sensitivity of Simbol-X over a broader energy range should be decisive in establishing the shape of the high energy spectrum of quiescent sources and discriminating between those models. For example, the observation of a pure powerlaw emission extending up to 80 keV would certainly exclude an ADAF as the main source of hard X-rays in quiescent low mass X-ray binaries. A simulation of a Simbol-X observation of the quiescent source V404 Cyg is shown in Fig. 3.14. This source is a close (3.5 kpc) LMXB with quiescent luminosities reaching  $10^{-6} L_{\text{Edd}}$ . This simulation demonstrates that Simbol-X should be sensitive to even a small amount of curvature, if any, in the quiescent spectrum of this source.

### 3.6.8 Conclusion

Since photons are the main vector of information in astronomy, the detailed study of radiation processes is of prime importance. In the context of high energy astrophysics, this radiation is produced in hot plasmas with a significant fraction of the energy carried by relativistic particles. My research activities are centred on the study of high energy radiative processes in these relativistic plasmas. This physics finds applications in all kinds of astrophysical source of high energy radiation such as AGNs, X-ray binaries or gamma-ray bursts.

These sources are of major scientific interest and it is important to understand how they work. They constitute a unique laboratory for the study of fundamental physics associated with black holes and hot plasmas. They are also suspected to play a role in the production the most energetic particles in the universe (cosmic rays). Moreover they are of interest for the understanding of the formation and evolution of the first structures and can also be used as probes of the distant universe (AGNs, GRBs).

My research project is at the interface between observations and theory. It offers to connect increasingly rich and accurate data with the models. This detailed confrontation of a model with data allows us to extract important information on the physical conditions in objects harbouring the most violent phenomena of the universe.



## Chapter 4

# LIST OF PUBLICATIONS AND CONFERENCE CONTRIBUTIONS

### 4.1 Articles in refereed international journals

1. Gandhi P., Fabian A., Suebsuwong T., **Malzac J.**, Miniutti G., Wilman R., 2007, “Constraints on light bending and reflection from the hard X-ray background”, MNRAS, 382, 1005.
2. Petrucci P.O., Ponti G., Matt G., Longinotti A.L., **Malzac J.**, Mouchet M., Boisson C., Maraschi L., Nandra K., Ferrando P., 2007, “Unveiling the X-ray broad band continuum and iron line complex in Mkn 841”, A&A, 470, 889.
3. Joinet A., Jourdain E., **Malzac J.**, Roques J.-P., Corbel S., Rodriguez J., Kalemci E., 2007, “Hard X-ray emission of the microquasar GX339-4 in the low/hard state”, ApJ, 657, 400.
4. Merloni A., **Malzac J.**, Fabian A.C., Ross R.R., 2006, “On the X-ray spectra of luminous, inhomogeneous accretion flows”, MNRAS, 390, 1699.
5. Suebsuwong T., **Malzac J.**, Jourdain E., Marcowith A., 2006, “Gravitational effects on the high energy emission of accreting black holes”, A&A, 453, 773.
6. **Malzac J.**, Petrucci P.O., Jourdain E., Cadolle Bel M., Sizun P., Pooley G., Cabanac C., Chaty S., Belloni T., Rodriguez J., Roques J.P., Durouchoux P., Goldwurm A., Laurent P., 2006, “Bimodal spectral variability of Cygnus X-1 in an intermediate state”, A&A, 448, 1125.
7. Cadolle Bel M., Sizun P., Goldwurm A., Rodriguez J., Laurent P., Zdziarski A.A., Foschini L., Goldoni P., Gouiffes C., **Malzac J.**, Jourdain E., Roques J.P., 2006, “The high-energy spectrum of Cygnus X-1 as measured by INTEGRAL”, A&A, 446, 591.
8. Beckmann V., Gehrels N., Schrader C., Soldi S., Lubinski P., Zdziarski A.A., Petrucci P.O., **Malzac J.**, 2005, “The high energy spectrum of NGC 4151”, ApJ, 634, 939.
9. **Malzac J.**, Dumont A.M., Mouchet M., 2005, “Full radiative coupling in the two-phase models for accreting black holes”, A&A, 430, 761.

10. Teegarden B.J., Watanabe K., Jean P., Knoedlseder J., Lonjou V., Roques J. P., Skinner G.K., von Ballmoos P., Weidenspointner G., Bazzano A., Butt Y. M., Decourchelle A., Fabian A. C., Goldwurm A., Gudel M., Hannikainen D. C., Hartmann D. H., Hornstrup A., Lewin W. H. G., Makishima K., **Malzac J.**, Miller J., Parmar A. N., Reynolds S. P., Rothschild R. E., Schönfelder V., Tomsick J. A., Vink J., 2005, “INTEGRAL/SPI Limits on Electron-Positron Annihilation Radiation from the Galactic Plane”, *ApJ*, 621, 296.
11. Jointet A., Jourdain E., **Malzac J.**, Roques J.P., Schönfelder V., Ubertini P., Capitanio F., 2005, “State transition and flaring activity of IGR J17464-3213/H1743-322 with SPI/INTEGRAL telescope”, *ApJ*, 629, 1008.
12. **Malzac J.**, Merloni A., Fabian A. C., 2004, “Jet-disc coupling through a common energy reservoir in the black hole XTE J1118+480”, *MNRAS*, 351, 253.
13. Beckman V., Gehrels G., Favre P., Courvoisier T., Petrucci P.O., **Malzac J.**, 2004, “INTEGRAL and XMM-Newton spectral studies of NGC 4388”, *ApJ*, 614, 641.
14. **Malzac J.**, Belloni T., Spruit H.G., Kanbach G., 2003, “The optical and X-ray flickering of XTE J1118+480”, *A&A*, 407, 335.
15. Marcowith A., **Malzac J.**, 2003, “Cyclotron-synchrotron: Harmonic fitting functions in the non-relativistic and trans-relativistic regime”, *A&A*, 409, 9.
16. Chaty S., Haswell C.A., **Malzac J.**, Hynes R.I., Shrader C.R., Cui W., 2003, “Multi-wavelength observations revealing the evolution of the outburst of the black hole XTE J1118+480”, *MNRAS*, 346, 689.
17. **Malzac J.**, Petrucci P.O., 2002, “Reflection at large distance from the central engine in Seyferts”, *MNRAS*, 336, 1209.
18. **Malzac J.**, Celotti A., 2002, “X-ray spectra emitted by a hot plasma containing cold clouds”, *MNRAS*, 335, 23.
19. **Malzac J.**, Beloborodov A., Poutanen J., 2001, “X-ray spectra of accretion discs with dynamic coronae”, *MNRAS*, 326, 417.
20. **Malzac J.**, 2001, “A quasi-spherical accretion flow in Seyfert galaxies?”, *MNRAS*, 325, 1625.
21. Petrucci P.O., Haardt F., Maraschi L., Grandi P., **Malzac J.**, Matt G., Nicastro F., Piro L., Perola G.C., De Rosa A., 2001, “Testing Comptonization model using BeppoSAX observations of Seyfert 1 galaxies”, *ApJ*, 556, 716.
22. **Malzac J.**, Jourdain E., 2000, “Temporal properties of flares in accretion disk coronae”, *A&A*, 359, 843.
23. **Malzac J.**, Jourdain E., Petrucci P.O., Henri G., 1998, “Anisotropic Illumination in AGNs. The reflection component. Comparison with high energy spectra from Seyfert galaxies.”, *A&A*, 336, 807.

24. Goldoni P., Vargas M., Goldwurm A., Laurent P., Roques J. -P., Jourdain E., **Malzac J.**, Vedrenne G., Revnivtsev M., Churazov E., Gilfanov M., Sunyaev R., Dyachkov A., Khavenson N., Tserenin I., Kuleshova N., 1998, “SIGMA observations of X-ray Nova Velorum 1993 (GRS 1009-45)”, *A&A*, 329, 186.

## 4.2 Invited talks or reviews at international conferences

The references of the proceedings, if any, are given in Sections 4.3 and 4.4:

1. “Modelling the X-ray spectral states and the disc/jet connection”, Microquasar/AGN Workshop in Crete, Agios Nikolaos, Greece, 4-8 June 2007 (no proceedings).
2. “Accretion discs, coronae and jets in black holes binaries”, invited review at the international conference “Black holes in Krakow”, Kracow, Poland, 16-20 May 2007 (no proceedings).
3. “Accreting black holes: spectral states and the jet disc connection”, international conference “Simbol-X: the hard X-ray universe in focus”, CNR conference centre, Bologna, Italy, 14-16 Mai 2007 (proceedings in press).
4. “Accretion disc coronae in black hole binaries”, invited review at the international conference “Coronae of Stars and Accretion Disks”, Max-Planck -Institut für Radioastronomie, Bonn, Germany, 11-12 December 2006 (proceedings published).
5. “Jet-disc coupling in black hole binaries”, invited review at the “Fifth Stromlo Symposium: Disks, Winds & Jets – From Planets to Quasars”, Mt Stromlo Observatory, ANU, Canberra, Australia, 3-8 December 2006 (proceedings published).
6. “A mini-state transition in Cygnus X-1”, conference “Black Holes: Power behind the Scene”, Kathmandu, Nepal, 23-27 October, 2006 (no proceedings).
7. “Appearance of luminous accreting black holes: light bending effects or inhomogeneous accretion ?”, conference “Black Holes: Power behind the Scene”, Kathmandu, Nepal, 23-27 October, 2006 (no proceedings).
8. “Models for microquasars”, invited review at the VI Microquasar Workshop “Microquasars and Beyond”, Como, Italy, 18-22 September 2006 (proceedings published).
9. “Optical/X-ray correlations as a signature of jet-disc coupling in the accreting black hole XTE J1118+480”, ‘COSPAR Colloquium on Spectra and timing of X-ray binaries’, January 17-21, 2005 (proceedings published)
10. “Jet-Disc coupling in the accreting black hole XTEJ1118+480”, conference “From X-ray binaries to quasars: Black hole accretion on all mass scales”, Amsterdam, July 2004, (proceeding published).
11. “Correlated optical/X-ray variability in XTE J1118+480”, Light from black holes, Kathmandu, 30 September-4 October 2002 (no proceedings).
12. “Reflection at large distances from the central engine in Seyferts”, Light from black holes, Kathmandu, 30 September-4 October 2002 (no proceedings).

### 4.3 Refereed conference proceedings

1. **Malzac, J.**, 2007, “Jet-disc coupling in black hole binaries”, invited review at the “Fifth Stromlo Symposium: Disks, Winds & Jets – From Planets to Quasars”, Proceedings of Mt Stromlo Observatory, ANU, Canberra, Australia, 3-8 December 2006, Astrophysics and Space Science, Volume 311, Issue 1-3, pp. 149-159
2. Petrucci, P. O., Ponti G., Matt G., Maraschi L., **Malzac J.**, Mouchet M., Boisson C., Nandra K., Longinotti A., Ferrando P., Henri G., 2007, “The origin of the strong soft excess and puzzling iron line complex in Mkn 841”, proceedings of the conference ‘The multicolored landscape of compact objects and their explosive origins’, Cefalù, Italy, 11-18 June 2006, AIP Conference Proceedings, Volume 924, pp. 583-588.
3. Joinet A., Jourdain E., **Malzac J.**, Roques J.P., Corbel S., Rodriguez J., Kalemci E., 2006, “Study of GX339-4 and H1743-322 during state transition”, Proceedings of the VI INTEGRAL Workshop ‘The obscured universe’, Moscow, Russia, 2-8 July 2006, ESA SP-622, in press
4. **Malzac J.**, Petrucci P.O., Jourdain E., Cadolle-Bel M., Pooley G., Cabanac C., Chaty S., Belloni T., Rodriguez J., Roques J.P., Durouchoux P., Goldwurm A., Laurent P., 2006, “A mini-state transition in Cyg X-1”, Proceedings of the VI INTEGRAL Workshop ‘The obscured universe’, Moscow, Russia, 2-8 July 2006, ESA SP-622, in press
5. **Malzac J.**, Merloni A., Thitiwat S., 2006, “Models for Luminous accreting black holes”, Variable broad iron lines around black holes, Proceedings of the XMM-Newton Science Operations Centre Workshop “Variable and Broad Iron Lines around Black Holes”, 26 - 28 June 2006, *Astronomische Nachrichten / Astronomical Notes*, Vol.327, Issue 10, p.985.
6. Petrucci P. O., Ponti G., Matt G., Maraschi L., **Malzac J.**, Mouchet M., Boisson C., Longinotti A., Nandra K., Ferrando P., Henri, G., 2006, “The origin of the strong soft excess and puzzling iron line complex in Mkn 841”, *Astronomische Nachrichten / Astronomical Notes*, Vol.327, Issue 10, p.1043
7. **Malzac J.**, 2006, “Optical/X-ray correlations as a signature of jet-disc coupling in the accreting black hole XTE J1118+480”, Proceedings of the COSPAR Colloquium on Spectra and timing of X-ray binaries, January 17-21, 2005, Tata Institute of Fundamental Research, Mumbai, India, *Advance in Space Research*, 38, 2872
8. Cadolle Bel M., Sizun P., Rodriguez J., Goldwurm A., Laurent P., Goldoni P., **Malzac J.**, Jourdain E., Roques J.P., 2006, “The high energy spectrum of cygnus X-1 as measured by INTEGRAL”, in ‘35th COSPAR Scientific Assembly, Held 18 - 25 July 2004, in Paris, France’, *Advances in Space Research*, 38, 1354.
9. **Malzac J.**, Petrucci P.O., Jourdain E., Sizun P., Cadolle Bel M., Pooley G., Cabanac C., Chaty S., Belloni T., Rodriguez J., Roques J.P., Durouchoux P., Goldwurm A., Laurent P., 2004, ‘INTEGRAL observation of Cygnus X-1 in an intermediate State’, Proceedings of the 5th INTEGRAL Workshop on the INTEGRAL Universe (ESA SP-552). 16-20 February 2004, Munich, Germany. Scientific Editors: V. Schönfelder, G. Lichti & C. Winkler, p.341, astro-ph/0411069.

10. Beckmann V., Gehrels G., Favre P., Courvoisier T., Walter R., **Malzac J.**, P.O. Petrucci, 2004, “NGC 4388 - Spectral studies of the first Seyfert 2 seen by INTEGRAL”, Proceedings of the 5th INTEGRAL Workshop on the INTEGRAL Universe (ESA SP-552). 16-20 February 2004, Munich, Germany. Scientific Editors: V. Schönfelder, G. Lichti & C. Winkler, p 535.
11. Beckmann V., Courvoisier T., Favre P., **Malzac J.**, Petrucci P.-O., Walter R., 2004, “INTEGRAL and XMM-Newton spectral studies of NGC 4388” in ‘35th COSPAR Scientific Assembly. Held 18 - 25 July 2004, in Paris, France’, p.2281.
12. **Malzac J.**, Belloni T., Spruit H.C., Kanbach G., 2004, “The optical and X-ray flickering of XTE J1118+480”, Proceedings of the 2nd BeppoSAX Conference: The Restless High-Energy Universe, Nuclear Physics B, Proc. Supp, 132, 400.
13. **Malzac J.**, Beloborov A., Poutanen J., 2001, “X-ray spectra of accretion discs with dynamic coronae”, 2001, Exploring the gamma-ray universe. Proceedings of the Fourth INTEGRAL Workshop, 4-8 September 2000, Alicante, Spain, Scientific editors: A. Gimenez, V. Reglero & C. Winkler. ESA SP-459, Noordwijk: ESA Publications Division, ISBN 92-9092-677-5, p. 325-328.
14. Petrucci P.O., Haardt F., Maraschi L., Grandi P., **Malzac J.**, Matt G., Nicastro F., Piro L., Perola G.C., De Rosa A., 2001, “Testing Comptonization models using BeppoSAX observations of Seyfert 1 galaxies”, Proceedings of “X-ray astronomy 2000”, (Palermo Sep.2000), Eds. R. Giacconi, L. Stella, S. Serio, ASP Conf. Series, 234, 445, astro-ph/0101219.
15. **Malzac J.**, Jourdain E., 2001, “Time dependent Comptonisation”, in “X-ray astronomy: Stellar Endpoints, AGN and the Diffuse X-ray Background”, Bologna, Italy, 1999, Eds. N.E. White, G. Malaguti, G.G.C. Palumbo, AIP conference Proceedings 599, 742.
16. **Malzac J.**, Jourdain E., 1999, “IC emission above a disk”, Proceedings of the Third INTEGRAL Workshop, Astrophys. Letters & Communications, Vol 38, p. 201, Gordon & Breach, astro-ph/9901186.
17. Petrucci P.O., Henri G., **Malzac J.**, Jourdain E., 1999, “The anisotropic illumination Model for the OPT.-UV. to X-ray emission of Seyfert I galaxies”, Proceedings of the Third INTEGRAL Workshop, Astrophys. Letters & Communications, Vol. 39, p 101, Gordon & Breach.
18. Renaud N., Henri G., **Malzac J.**, Jourdain E., 1999, “On the two  $\gamma$ -ray spectral states of Galactic Black Holes”, Proceedings of the Third INTEGRAL Workshop, Astrophys. Letters & Communications, Vol 38, p 221, Gordon & Breach.
19. Petrucci P.O., Henri G., **Malzac J.**, Jourdain E., 1997, “An anisotropic Illumination Model for Seyfert 1 galaxies”, Proceedings of the Fourth Compton Symposium, Ed. C. Dermer, M.S. Strickman & J.D. Kurfess, AIP 410, p. 1403.

#### 4.4 Non-refereed publications

1. **Malzac J.**, 2007, “Models for the spectra and variability of bright AGN”, actes de la Journées de la Société Française d’Astronomie et Astrophysique, Grenoble, July 2-6 2007, in press.
2. **Malzac J.**, 2007, “Accreting black holes: spectral states and the jet disc connection”, revue invitée à la conférence internationale “Simbol-X: the hard X-ray universe in focus”, CNR conference centre, Bologna, Italy, May 14-16 2007, Memorie della Societa Astronomica Italiana, in press.
3. Belmont R., **Malzac J.**, Marcowith A., 2007, “A new code for radiation processes in high energy plasmas”, Proceedings of the international conference “Simbol-X: the hard X-ray universe in focus”, CNR conference centre, Bologna, Italy, May 14-16 2007, Memorie della Societa Astronomica Italiana, in press.
4. **Malzac J.**, 2007, “Accretion disc coronae in black hole binaries”, invited review at the international conference “Coronae of Stars and Accretion Disks”, Max-Planck -Institut für Radioastronomie, Bonn, Germany, December 11-12 2006, Memorie della Societa Astronomica Italiana, v.78, p.382 (2007)
5. **Malzac J.**, 2007, “Models for microquasars”, invited review at the “Sixth Microquasar workshop: Microquasars and Beyond”, Como, Italy 18-22 September 2006, PoS (MQW6) 030 , <http://pos.sissa.it/>
6. Petrucci P.O, Ponti G., Matt G. Longinotti A., Mouchet M., Boisson C., Maraschi L., **Malzac J.**, Nandra K., Ferrando P., 2006, “Unveiling the X-ray broad band continuum and iron line complex in Mkn 841”, proceedings of “Sixth Microquasar workshop: Microquasars and Beyond”, Como, Italy 18-22 September 2006, PoS (MQW6) 089 , <http://pos.sissa.it/>
7. Del Santo M., **Malzac J.**, Ubertini P., Belloni T., 2006, “Spectral variability modes of GX 339-4 in a hard-to-soft state transition”, proceedings of “Sixth Microquasar workshop: Microquasars and Beyond”, Como, Italy 18-22 September 2006, PoS (MQW6) 076, <http://pos.sissa.it/>
8. Cadolle Bel M., Ribo M., Rodriguez J., Chaty S., Corbel S., Goldwurm A., **Malzac J.**, 2006, “Broad-band spectral changes of the microquasars Cygnus X-1 and SWIFT J1753.5-0127”, proceedings of “Sixth Microquasar workshop: Microquasars and Beyond”, Como, Italy 18-22 September 2006, PoS (MQW6) 003, <http://pos.sissa.it/>
9. Cadolle Bel M., Goldwurm A., Rodriguez J., Sizun P., Laurent P., Goldoni P., Malzac J., Jourdain E., Roques J.P., 2006, “Hybrid modelization of the high-energy broad-band spectra of Cygnus X-1 observed by INTEGRAL”, *SF2A-2006: Semaine de l’Astrophysique Francaise*, 119.
10. **Malzac J.**, Petrucci P.O., Jourdain E., Cadolle Bel M., Sizun P., Pooley G., Cabanac C., Chaty S., Belloni T., Rodriguez J., Roques J.P., Durouchoux P., Goldwurm A., Laurent P., 2006, Proceedings of the “The X-ray Universe 2005”, 26-30 September 2005, El Escorial, Madrid, Spain. Ed. by A. Wilson. ESA SP-604, Volume 1, Noordwijk: ESA Publications Division, ISBN 92-9092-915-4, 2006, p. 223 - 228

11. Cabanac V., **Malzac, J.**, Odier J., Petrucci P.-O., Henri G. Rodriguez J., 2006, “Combining rayleigh test and PIF method for timing analysis with coded mask aperture instrument, application to quasi-periodic oscillation detection and modelling”, Proceedings of the “The X-ray Universe 2005”, 26-30 September 2005, El Escorial, Madrid, Spain. Ed. by A. Wilson. ESA SP-604, Volume 1, Noordwijk: ESA Publications Division, ISBN 92-9092-915-4, 2006, p. 251 - 252
12. Joinet A., Jourdain E., **Malzac J.**, Roques J.-P., 2006, “Comparison between two outbursting galactic black holes” , Proceedings of the “The X-ray Universe 2005”, 26-30 September 2005, El Escorial, Madrid, Spain. Ed. by A. Wilson. ESA SP-604, Volume 1, Noordwijk: ESA Publications Division, ISBN 92-9092-915-4, 2006, p. 271 - 272
13. **Malzac J.**, Merloni M., Fabian A.C., 2005, “Jet-Disc coupling in the accreting black hole XTEJ1118+480”, proceedings of “From X-ray binaries to quasars: Black hole accretion on all mass scales, (Amsterdam, July 2004)”, Eds. T. Maccarone, R. Fender, L. Ho, Astrophysics and Space Science, Volume 300, Issue 1-3, pp. 31-38, astro-ph/0411066.
14. **Malzac J.**, Belloni T., Spruit H.C., Kanbach G., 2003, “The optical and X-ray flickering of XTEJ1118+480”, Nuclear Physics B (Proc. Suppl.), 132, 400, Proceedings of the 2nd BeppoSAX conference “The restless High Energy Universe”, Amsterdam, The netherlands, 5-8 May 2003, Ed. E.P.J. Van den Heuvel, R.A.M.J. Wijers, J.J.M. Iin’t Zand.
15. **Malzac J.**, Mouchet M., Dumont A.M., 2003, “Self consistent radiative coupling in the two-phase models for AGNs”, Proceedings of the conference “Active Galactic Nuclei: from Central Engine to Host Galaxy” held in Meudon, France, July 23-27, 2002, Eds.: S. Collin, F. Combes and I. Shlosman. ASP Conference Series, Vol. 290, p.109.
16. Chaty S., Haswell C.A., **Malzac J.**, Hynes R.I., Shrader, C. R., Mauche C.W., Cui W., 2003, “Multiwavelength Observations Revealing the Evolution of the Outburst of the Black Hole XTE J1118+480”, New Views on MICROQUASARS, the Fourth Microquasars Workshop, Institut d’Etudes Scientifiques de Cargèse, Corsica, France, May 27 - June 1, 2002. Edited by Ph. Durouchoux, Y. Fuchs, and J. Rodriguez. Published by the Center for Space Physics: Kolkata (India), p. 23.
17. **Malzac J.**, Belloni T., Spruit H.G., Kanbach G., 2003, “Correlated optical/X-ray variability in XTE J1118+480”, New Views on MICROQUASARS, the Fourth Microquasars Workshop, Institut d’Etudes Scientifiques de Cargèse, Corsica, France, May 27 - June 1 2002. Edited by Ph. Durouchoux, Y. Fuchs, and J. Rodriguez. Published by the Center for Space Physics: Kolkata (India), p. 31.
18. **Malzac J.**, Mouchet M., Dumont A.M., Collin S., 2002, “A detailed treatment of reprocessing and ionisation in the accreting black holes”, Proceedings of the XXXVIIth Rencontres de Moriond, XXIIInd Moriond Astrophysics Meeting, “The Gamma-Ray Universe”, Les Arcs, Savoie, France, March 16-23 2002, Eds: A. Goldwurm, D.N. Neumann, Trân Thanh Vân, p 35.
19. Chaty S., Haswell C.A., **Malzac J.**, Hynes R.I., Shrader, C. R., Mauche C.W., Cui W., 2002, “Multiwavelength Observations Revealing the Evolution of the Outburst of the Black Hole XTE J1118+480”, Proceedings of the XXXVIIth Rencontres de Moriond, XXIIInd

- Moriond Astrophysics Meeting, “The Gamma-Ray Universe”, Les Arcs, Savoie, France, March 16-23 2002, Eds: A. Goldwurm, D.N. Neumann, Tr an Thanh V an, p 47.
20. **Malzac J.**, Dumont A.M., Mouchet M., 2002, “Reflection and reprocessing in black hole binaries and Seyfert galaxies”, in “Inflow, outflow and reprocessing around black holes”, Quinto Congresso Nazionale AGN, villa Olmo, Como, 11-14 Giugno 2002, <http://www.unico.it/ilaria/AGN>
  21. **Malzac J.**, Mouchet M., Dumont A.M., Collin S., 2001, “A full treatment of radiative coupling in the two-phase models for black hole binaries and AGN”, Proceedings of the conference “New Vision of the X-ray Universe in the XMM-Newton and Chandra Era, Nov. 2001, ESTEC, The Netherlands, ESA SP-488, ed. F. Jansen.
  22. **Malzac J.**, Celotti A., 2001, “X-ray spectra emitted by a hot plasma containing cold clouds”, Proceedings of the conference “New Vision of the X-ray Universe in the XMM-Newton and Chandra Era, Nov. 2001, ESTEC, The Netherlands, ESA SP-488, ed. F. Jansen.
  23. **Malzac J.**, Petrucci P.O., 2001, “Reflection at large distance from the central engine in Seyfert galaxies”, Proceedings of the conference “X-ray emission from accretion onto black holes”, held in Baltimore, 20-23 june 2001, publication  electronique disponible   [www.pha.jhu.edu/groups/astro/workshop2001/papers/](http://www.pha.jhu.edu/groups/astro/workshop2001/papers/).
  24. **Malzac J.**, 2001, “Modelling the  $R - \Gamma$  correlation in accreting black hole sources”, Proceedings of the “Gamma-ray Astrophysics 2001” symposium held in Baltimore, April 4-6 2001, Eds S. Ritz, N. Gehrels, C.R. Shrader, AIP conferences proceedings 587, p 375.
  25. **Malzac J.**, Beloborodov A.M., Poutanen J., 2001, “X-ray spectra of accretion discs with dynamic coronae”, Proceedings of the “Gamma-ray Astrophysics 2001” symposium held in Baltimore, April 4-6 2001, Eds S. Ritz, N. Gehrels, C.R. Shrader, AIP conferences proceedings 587, p111.
  26. Petrucci, P. O., Merloni A., Fabian A.C., Haardt F., Gallo E., Malzac J., 2001, “The effects of a comptonizing corona on the appearance of the reflection components in accreting black hole spectra”, Proceedings of the “Gamma-ray Astrophysics 2001” symposium held in Baltimore, April 4-6 2001, Eds S. Ritz, N. Gehrels, C.R. Shrader, AIP conferences proceedings 587, p 121.
  27. **Malzac J.**, 2001, “X-ray spectra emitted by a hot plasma containing cold clouds”, 2001, Proceedings of the “Gamma-ray Astrophysics 2001” symposium held in Baltimore, April 4-6 2001, Eds S. Ritz, N. Gehrels, C.R. Shrader, AIP conferences proceedings 587, p 385.
  28. Petrucci P.O., Haardt F., Maraschi L., Grandi P., **Malzac J.**, Matt G., Nicastro F., Piro L., Perola G.C., De Rosa A., 2001, “Testing Comptonization model using BeppoSAX observations of Seyfert 1 galaxies”, Proceedings of the “Gamma-ray Astrophysics 2001” symposium held in Baltimore, April 4-6 2001, Eds S. Ritz, N. Gehrels, C.R. Shrader, AIP conferences proceedings 587, p 395.
  29. **Malzac J.**, 2001, “A quasi-spherical inner accretion flow in Seyfert galaxies”, Proceedings of the “Gamma-ray Astrophysics 2001” symposium held in Baltimore, April 4-6 2001, Eds S. Ritz, N. Gehrels, C.R. Shrader, AIP conferences proceedings 587, p 404.

30. **Malzac J.**, 2001, “Modeling the high-energy radiative processes in relativistic plasma”, 2001, ”Similarities and Universality in Relativistic Flows”, Proceedings of the Euroconference held in Mykonos, Greece, 1-5 October 2000, Ed. M. Georganopoulos, A. Guthmann, K. Manolakou, A. Marcowith, Logos Verlag, Berlin, p. 33.
31. **Malzac J.**, 2001, “What the  $R$ - $\Gamma$  correlation tells us about geometry and physical processes in accreting black hole sources”, 2001, Atelier d’astronomie X, X-ray Astronomy workshop, Toulouse (France), Sept. 20, 2000, Eds. J. Ballet and D. Barret, p. 69-74.
32. **Malzac J.**, Jourdain E., 1999, “A time dependent model for accretion disk corona”, Proceedings of the 19th Texas Symposium on Relativistic Astrophysics, 01/17, Ed. J. Paul, T. Montmerle & E. Aubourg.
33. Petrucci P.O., Henri G., **Malzac J.**, Jourdain E., 1999, “The anisotropic illumination Model for the OPT.-UV. to X-ray emission of Seyfert I galaxies”, Proceedings of the 19th Texas Symposium on Relativistic Astrophysics, 01/23, Ed. J. Paul, T. Montmerle & E. Aubourg.
34. **Malzac J.**, “Modélisation de l’émission à haute énergie des objets compacts”, 1999, Actes de la réunion du GDR disque-accrétion-jet.

## 4.5 Communications in conferences

When relevant the references of the conference proceedings can be found in sections 4.3 et 4.4:

### 4.5.1 Talks in international conferences

#### 4.5.1.1 Presented by myself

1. “Cygnus X-1: the flare of september 2006”, SPI Scientific Team Meeting, MPE Garching, Germany, 19-21 March 2007, no proceedings.
2. “Models for Luminous accreting black holes”, Variable broad iron lines around black holes, An ESAC/XMM-Newton Science Operations Centre Workshop, 26 - 28 June 2006, l’ European Space Astronomy Centre de l’ESA, Madrid, Spain, published proceedings .
3. “Bi-modal spectral variability of Cygnus X-1 in an intermediate state”, The X-ray 2005 Symposium, El Escorial, Madrid, Spain, 26 au 30 September 2005, published proceedings .
4. “Bi-modal spectral variability of Cygnus X-1 in an intermediate state”, High energies in the Highlands, Fort-William, Scotland, 27 June 1st July 2005, no proceedings .
5. “Bi-modal spectral variability of Cygnus X-1 in an intermediate state”, SPI/IBIS Scientific Teams Meeting CNR Roma March 16 2005, no proceedings .
6. “INTEGRAL observation of Cygnus X-1 in an intermediate state”, SPI Scientific Team Meeting CESR 7-9 June 2004, no proceedings.
7. “INTEGRAL observation of Cygnus X-1 in an intermediate state”, 5th INTEGRAL Workshop, The Integral Universe, Munich, Germany, 16-17 February 2004, published proceedings

8. “Multi-wavelength observations of galactic black holes”, Astroparticle Meeting, Toulouse, 14-16 Avpril 2004, no proceedings.
9. “Correlated optical/X-ray variability in XTE J1118+480”, “Fourth Microquasar Workshop: microquasar and their relation to other jet sources in the Universe”, Cargese, Corse, France, June 2002, published proceedings .
10. “Reprocessing and reflection in accreting black hole sources”, “ The Gamma-ray Universe , XXXVIIth Rencontres de Moriond, XXII Moriond Astrophysics Meetings”, Les Arcs, Savoie, France, March 2002, published proceedings .
11. “The  $R - \Gamma$  correlation in accreting black hole sources”, meeting of the TMR network: Accretion onto Black Holes, Compact Stars and Protostars, Puerto de la Cruz, Tenerife, Spain, January 2002, no proceedings.
12. “Modeling the  $R - \Gamma$  correlation in accreting black hole sources”, “Gamma-ray 2001 Astrophysics” symposium, Baltimore, Maryland, USA, April 2001, published proceedings .
13. “Modeling high energy radiation processes in relativistic plasma”, SURF 2000 conference, Mykonos, Greece, October 2000, published proceedings .

#### 4.5.1.2 Presented by collaborators

1. Cadolle Bel et al., “Broad-band spectral changes of the microquasars Cygnus X-1 and SWIFT J1753.5-0127”, VI Microquasar Workshop “Microquasars and Beyond”, Como, Italy, 18-22 September 2006, published proceedings.
2. Merloni A. et al., “X-ray spectra and variability of luminous inhomogeneous accretion flows”, High energy in the Highlands, Fort William, Scotland, 27 June 1st July 2005, no proceedings.
3. Beckmann V., et al. “INTEGRAL and XMM-Newton spectral studies of NGC 4388”, 35th COSPAR Scientific Assembly, Paris, 18- 25 July 2004, published proceedings .
4. Cadolle Bel M., et al. “The high energy spectrum of Cygnus X-1 as measured by INTEGRAL”, 35th COSPAR Scientific Assembly. Paris, 18 - 25 July 2004, published proceedings .
5. Beckmann V., et al. “NGC 4388 - Spectral studies of the first Seyfert 2 seen by INTEGRAL”, 5th INTEGRAL Workshop on the INTEGRAL Universe., Munich, Germany, 16-20 February 2004, published proceedings .
6. Chaty S. et al., “Multiwavelength Observations Revealing the Evolution of the Outburst of the Black Hole XTE J1118+480”, New Views on MICROQUASARS, the Fourth Microquasars Workshop, Institut d’Etudes Scientifiques de Cargèse, Corse, France, 27 May - 1st June, 2002, published proceedings .
7. Chaty S. et al., “Multiwavelength Observations Revealing the Evolution of the Outburst of the Black Hole XTE J1118+480”, XXXVIIth Rencontres de Moriond, XXIIInd Moriond Astrophysics Meeting, “The Gamma-Ray Universe”, Les Arcs, 6-23 March 2002, published proceedings .

#### 4.5.2 Talks in national conferences

1. “Models for the spectra and variability of bright AGN”, Journées de la Société Française d’Astronomie et Astrophysique, Grenoble 2-6 July 2007, proceedings in press.
2. “Observations des Binaires X avec Simbol-X”, Réunion de l’Equipe Scientifique Française de SIMBOL-X, CEA Saclay, 3 May 2006, no proceedings.
3. “La Comptonisation dans les sursauts gamma”, Rencontre “sursauts gamma” du GDR PCHE, Toulouse, January 2003, no proceedings.
4. “Modélisation des processus de haute énergie dans les plasmas relativistes”, J. Malzac, Forum ASSNA, 15-17 December 2003, IDRIS, Orsay, no proceedings.
5. “La géométrie des sources compactes”, Atelier d’astronomie X de la réunion du GDR PCHE, Toulouse, September 2000, published proceedings .
6. “Modélisation de l’émission des sources de haute énergie”, Atelier AGNs, radiosources, jets et implications pour la cosmologie, Institut d’Astrophysique de Paris, December 1998, no proceedings.
7. “Modélisation de l’émission à haute énergie des Objets Compacts”, Réunion du GDR disque-accrétion-jet, Observatoire de Strasbourg, November 1998, published proceedings .
8. “Modélisation de l’émission X et  $\gamma$  des Seyferts”, Atelier Galaxies de Seyferts, Observatoire de Grenoble, November 1997, no proceedings.

#### 4.5.3 Posters in international conferences

1. Belmont R., **Malzac J.**, Marcowith A., “A new code for radiation processes in high energy plasma”, “INTERNATIONAL WORKSHOP Simbol-X: the hard X-ray Universe in focus, CNR conference centre, Bologna, Italy, 14-16 May 2007, proceedings in press.
2. Gandhi P., Fabian A.C., Suebsuwong T., **Malzac J.**, Miniutti G., “The effect of light bending on the X-ray background spectrum”, Suzaku conference, Kyoto, November 2006, no proceedings.
3. Joinet A., Jourdain E., **Malzac J.**, Roques J.P., Corbel S., Rodriguez, J., Kalemci E., “Study of GX339-4 and H1743-322 during state transition”, VI INTEGRAL Workshop Moscow, Russia, 2-8 July 2006, published proceedings
4. Del Santo M., **Malzac J.**, Ubertini P., Belloni T., “Spectral variability modes of GX 339-4 in a hard-to-soft state transition”, Sixth Microquasar workshop: Microquasars and Beyond, Como, Italy 18-22 September 2006, published proceedings .
5. **Malzac J.**, Petrucci P.O., Jourdain E., Cadolle-Bel M., Pooley G., Cabanac C., Chaty S., Belloni T., Rodriguez J., Roques J.P., Durouchoux P., Goldwurm A., Laurent P. , “A mini-state transition in Cyg X-1”, VI INTEGRAL Workshop Moscow, Russia, 2-8 July 2006, published proceedings

6. Cabanac V., **Malzac J.**, Odier J., Petrucci P.-O., Henri G., Rodriguez J., “Combining rayleigh test and PIF method for timing analysis with coded mask aperture instrument, application to quasi-periodic oscillation detection and modelling”, The X-ray 2005 Symposium, El Escorial, Madrid, Spain, 26-30 September 2005, published proceedings .
7. Joinet A., Jourdain E., **Malzac J.**, Roques J.-P., “Comparison between two outbursting galactic black holes” ,The X-ray 2005 Symposium, El Escorial, Madrid, Spain, 26-30 September 2005, published proceedings .
8. **Malzac J.**, Belloni T., Spruit H.C., Kanbach G, “The optical and X-ray flickering of XTEJ1118+480”, 2nd BeppoSAX conference “The restless High Energy Universe”, Amsterdam, Netherlands, 5-8 May 2003, published proceedings .
9. **Malzac J.**, Mouchet M., Dumont A.M., “Self consistent radiative coupling in the two-phase models for AGNs”, Conference “Active Galactic Nuclei: from Central Engine to Host Galaxy”, Meudon, France, 23-27 July 2002, published proceedings .
10. **Malzac J.**, Dumont A.M., Mouchet M., “Reflection and reprocessing in black hole binaries and Seyfert galaxies”, “Inflow, outflow and reprocessing around black holes”, Quinto Congresso Nazionale AGN, Cme, Italie, 11-14 June, 2002, published proceedings .
11. **Malzac J.**, Mouchet M., Dumont A.M., Collin S., “A full treatment of radiative coupling in the two-phase models for black hole binaries and AGN”, conference ”New Vision of the X-ray Universe in the XMM-Newton and Chandra Era, ESTEC, Netherlands, November 2001, published proceedings .
12. **Malzac J.**, Celotti A., “X-ray spectra emitted by a hot plasma containing cold clouds”, conference ”New Vision of the X-ray Universe in the XMM-Newton and Chandra Era, ESTEC, Netherlands, November 2001, published proceedings .
13. **Malzac J.**, Petrucci P.O., “Reflection at large distance from the central engine in Seyfert galaxies”, conference “X-ray emission from accretion onto black holes”, Baltimore, USA, 20-23 June 2001, published proceedings .
14. **Malzac J.**, Beloborodov A.M., Poutanen J., “X-ray spectra of accretion discs with dynamic coronae”, “Gamma-ray Astrophysics 2001” symposium, Baltimore, USA, 4-6 April 2001, published proceedings .
15. Petrucci, P. O., Merloni A., Fabian A.C., Haardt F., Gallo E., **Malzac J.**, “The effects of a comptonizing corona on the appearance of the reflection components in accreting black hole spectra” “Gamma-ray Astrophysics 2001” symposium, Baltimore, USA, 4-6 April 2001, published proceedings .
16. **Malzac J.**, “X-ray spectra emitted by a hot plasma containing cold clouds”, “Gamma-ray Astrophysics 2001” symposium, Baltimore, USA, 4-6 April 2001, published proceedings .
17. Petrucci P.O., Haardt F., Maraschi L., Grandi P., **Malzac J.**, Matt G., Nicastro F., Piro L., Perola G.C., De Rosa A., “Testing Comptonization model using BeppoSAX observations of Seyfert 1 galaxies”, “Gamma-ray Astrophysics 2001” symposium, Baltimore, USA, 4-6 April 2001, published proceedings .

18. **Malzac J.**, “A quasi-spherical inner accretion flow in Seyfert galaxies”, “Gamma-ray Astrophysics 2001” symposium, Baltimore, USA, 4-6 April 2001, published proceedings .
19. **Malzac J.**, Beloborov A., Poutanen J., “X-ray spectra of accretion discs with dynamic coronae”, 4th INTEGRAL workshop, “Exploring the Gamma-ray Universe”, Alicante, Spain, 4-8 September 2000, published proceedings .
20. Petrucci P.O., Haardt F., Maraschi L., Grandi P., **Malzac J.**, Matt G., Nicastro F., Piro L., Perola G.C., De Rosa A., “Testing Comptonization models using BeppoSAX observations of Seyfert 1 galaxies”, “X-ray astronomy 2000”, Palermo, Italy, September 2000, published proceedings .
21. **Malzac J.**, Jourdain E., “Time dependent Comptonisation”, “X-ray astronomy 1999”: Stellar Endpoints, AGN and the Diffuse X-ray Background”, Bologna, Italy, October 1999, published proceedings .
22. **Malzac J.**, Jourdain E., “A time dependent model for accretion disk corona”, 19th Texas Symposium on Relativistic Astrophysics, Paris, France, 14-18 December 1998, published proceedings .
23. Petrucci P.O., Henri G., **Malzac J.**, Jourdain E., “The anisotropic illumination Model for the OPT.-UV. to X-ray emission of Seyfert I galaxies”, 19th Texas Symposium on Relativistic Astrophysics, Paris, France, 14-18 December 1998, published proceedings .
24. **Malzac J.**, Jourdain E., “IC emission above a disk”, Third INTEGRAL Workshop, “The Extreme Universe”, Taormina, Italy, September 1998, published proceedings .
25. Petrucci P.O., Henri G., **Malzac J.**, Jourdain E., “The anisotropic illumination Model for the OPT.-UV. to X-ray emission of Seyfert I galaxies”, Third INTEGRAL Workshop “The Extreme Universe”, Taormina, Italy, September 1998, published proceedings .
26. Renaud N., Henri G., **Malzac J.**, Jourdain E., “On the two  $\gamma$ -ray spectral states of Galactic Black Holes”, 1999, Third INTEGRAL Workshop, “The Extreme Universe”, Taormina, Italy, September 1998, published proceedings .
27. Petrucci P.O., Henri G., **Malzac J.**, Jourdain E., “An anisotropic Illumination Model for Seyfert 1 galaxies”, Fourth Compton Symposium on Gamma-ray Astronomy and Astrophysics, Williamsburg, Virginia, USA, April 1997, published proceedings .

## 4.6 Seminars

1. “Accretion discs, coronae and jets in accreting black holes”, University of Southampton, England, 9 May 2007
2. “Les couronnes de disque d’accrétion dans les binaires X contenant un trou noir”, CESR, Toulouse, February 2007.
3. “Jet-Disc coupling in black hole X-ray binaries”, Max-Planck Institut für Astrophysik, Garching, Germany, December 2006.

4. “Observing the X-ray and Gamma-ray sky with INTEGRAL”, Observing the X- and Gamma-ray Sky, Astrophysical Spring School, Cargse/Corsica, France, April 2006
5. “Jet-Disc coupling in black hole X-ray binaries”, Istituto di Astrofisica Spaziale e Fisica cosmica - CNR, Rome, Italy, December 2005.
6. “Jet-Disc coupling in black hole X-ray binaries”, Osservatorio Astronomico di Brera, Milan, Italy, November 2005.
7. “Jet-Disc coupling in black hole X-ray binaries”, Centrum Astronomiczne im. M. Kopernika (CAMK), Warsaw, Poland, October 2005.
8. “Jet-Disc coupling in black hole X-ray binaries”, Aspen Center for Physics, Colorado, USA, July 2005, Aspen summer program: ”Revealing black holes”
9. “Couplage accretion-éjection dans les binaires X contenant un trou noir”, Institut d’Astrophysique de Paris, France, June 2005
10. “Interaction Between Disks and Jets in Black Hole Binaries: The Case of KV UMa”, Kavli Institute for Theoretical Physics, Santa-Barbara, California, USA, April 2005, KITP Program: Physics of Astrophysical Outflows and Accretion Disks, <http://online.kitp.ucsb.edu/online/jet+disc>
11. “Variabilité bimodale de Cygnus X-1 dans un état intermédiaire”, Centre d’Étude Spatiale des Rayonnements, Toulouse, France, April 2005
12. “Couplage disque-jet dans le trou noir XTEJ1118+480”, Observatoire de Grenoble, France, November 2004
13. “INTEGRAL observation of Cyg X-1 in an intermediate state”, Institute of Astronomy, Cambridge, England, April 2004
14. “Couplage disque-jet dans le trou noir XTEJ1118+480”, Centre d’Étude Spatiale des Rayonnements, Toulouse, France, March 2004
15. “Jet/Disc coupling through a common energy reservoir in the black hole XTEJ1118+480”, SRON, Utrecht, Netherlands, February 2004
16. “Jet/Disc coupling through a common energy reservoir in the black hole XTEJ1118+480”, Astronomical Institute ‘Anton Pannekoek’, Amsterdam, Netherlands, February 2004
17. “Disc/jet coupling through a common energy reservoir in the black hole XTE J1118+480”, Institute of Astronomy, Cambridge, England, October 2003.
18. ‘Modeling the high energy emission of accreting black holes’, Institute of Astronomy, Cambridge, England, February 2003.
19. “Emission à haute énergie des sources accrétantes contenant un trou noir”, Centre d’Étude Spatiale des rayonnements, Toulouse, France, January 2003.
20. “X-ray and optical flickering of the X-ray nova XTE J1118+480”, Institute of Astronomy, Cambridge, England, November 2002.

21. “The high energy continuum of accreting black hole sources”, Institute of Astronomy, Cambridge, England, August 2001.
22. “The high energy continuum of accreting black hole sources”, Open University, Milton Keynes, England, July 2001.
23. “Modeling the high energy processes in relativistic plasma: the hard X-ray emission of accreting black holes”, Osservatorio Astronomico di Brera, Milan, Italy, June 2001.
24. “Modélisation de l’émission haute énergie des trous noirs accrétants”, Service d’Astrophysique, CEA, Saclay, France, January 2001.
25. “Modélisation de l’émission haute énergie des trous noirs accrétants”, Observatoire de Paris-Meudon, France, January 2001.
26. “Modélisation de l’émission haute énergie des trous noirs accrétants”, Centre d’Étude Spatiale des rayonnements, Toulouse, France, December 2000.
27. “Modélisation de l’émission haute énergie des trous noirs accrétants”, Observatoire de Grenoble, France, December 2000.
28. “Temporal Properties of Flares in Accretion Disk Corona”, Stockholm Observatory, Sweden, February 2000.

## 4.7 Software

1. 1996: Linear Monte-Carlo Code computing thermal Comptonisation spectra
2. 1999: Non Linear Monte-Carlo code (MCNL) simulating high energy radiative processes in relativistic plasmas.

## 4.8 Others

### 4.8.1 Newsletters

1. **Malzac J.**, 2004, “INTEGRAL observation of Cygnus X-1 during an intermediate state”, ISDC-Astrophysics Newsletter, N16, <http://isdc.unige.ch/Newsletter/N16/>

### 4.8.2 Thesis and dissertations

1. 1999: PhD, “Modélisation de l’émission X et  $\gamma$  des Objets Compacts par les méthodes Monte-Carlo”, Université Paul Sabatier Toulouse 3  
available online: <http://tel.ccsd.cnrs.fr/tel-00010420/en/>
2. 1996: DEA, “Calculs de spectres de Comptonisation par les Méthodes de Monte-Carlo”, Université Paul Sabatier Toulouse 3

3. 1995: Maîtrise, “Extraction d’énergie d’un trou noir de Kerr par le mécanisme de Penrose”, Université Bordeaux 1

## Chapter 5

# FIVE SIGNIFICANT PUBLICATIONS

1. **“X-ray spectra of accretion discs with dynamic coronae”**,  
Malzac Julien, Beloborodov Andrei M., Poutanen Juri, Monthly Notices of the Royal Astronomical Society, Volume 326, Issue 2, pp. 417-427 (2001).
2. **“The optical and X-ray flickering of XTE J1118+480”**,  
Malzac J., Belloni T., Spruit H. C., Kanbach G., Astronomy and Astrophysics, v.407, p.335-345 (2003)
3. **“Jet-disc coupling through a common energy reservoir in the black hole XTE J1118+480”**,  
Malzac Julien, Merloni Andrea, Fabian Andrew C., Monthly Notices of the Royal Astronomical Society, Volume 351, Issue 1, pp. 253-264 (2004).
4. **“Full radiative coupling in two-phase models for accreting black holes”**,  
Malzac J., Dumont A.-M., Mouchet M., Astronomy and Astrophysics, v.430, p.761-769 (2005).
5. **“Bimodal spectral variability of Cygnus X-1 in an intermediate state”**,  
Malzac J., Petrucci P.O., Jourdain E., Cadolle Bel M., Sizun P., Pooley G., Cabanac C., Chaty S., Belloni T., Rodriguez J., Roques J.P., Durouchoux P., Goldwurm A., Laurent P. , Astronomy and Astrophysics, Volume 448, pp.1125-1137 (2006).



## **5.1 “X-ray spectra of accretion discs with dynamic coronae”**

Malzac Julien, Beloborodov Andrei M., Poutanen Juri, *Monthly Notices of the Royal Astronomical Society*, Volume 326, Issue 2, pp. 417-427 (2001).



## X-ray spectra of accretion discs with dynamic coronae

Julien Malzac,<sup>1,2★</sup> Andrei M. Beloborodov<sup>3,4★</sup> and Juri Poutanen<sup>3★</sup>

<sup>1</sup>Centre d'Etude Spatiale des Rayonnements (CNRS/UPS) 9, Av. du Colonel Roche, 31028, Toulouse Cedex 4, France

<sup>2</sup>Osservatorio Astronomico di Brera, via Brera, 28, 20121 Milano, Italy

<sup>3</sup>Stockholm Observatory, SE-133 36 Saltsjöbaden, Sweden

<sup>4</sup>Astro Space Centre of Lebedev Physical Institute, 84/32 Profsojuznaja Street, Moscow 117810, Russia

Accepted 2001 February 19. Received 2001 February 13; in original form 2000 October 13

### ABSTRACT

We compute the X-ray spectra produced by *non-static* coronae atop accretion discs around black holes and neutron stars. The hot corona is radiatively coupled to the underlying disc (the reflector) and generates an X-ray spectrum which is sensitive to the bulk velocity of the coronal plasma,  $\beta = v/c$ . We show that an outflowing corona reproduces the hard-state spectrum of Cyg X-1 and similar objects. The dynamic model predicts a correlation between the observed amplitude of reflection  $R$  and the X-ray spectrum slope  $\Gamma$  since both strongly depend on  $\beta$ . A similar correlation was observed and its shape was well fitted by the dynamic model. The scattering of soft radiation in an outflowing corona can also account for the observed optical–UV polarization pattern in active galactic nuclei.

**Key words:** accretion, accretion discs – radiative transfer – stars: individual: Cyg X-1 – galaxies: Seyfert – gamma-rays: theory – X-rays: general.

### 1 INTRODUCTION

The hard X-ray spectra of galactic black holes (GBHs) and active galactic nuclei (AGN) indicate the presence of hot plasmas with temperatures  $kT_e \sim 100$  keV and scattering optical depths  $\tau_T \sim 1$  in the vicinity of accreting black holes (see reviews by Zdziarski et al. 1997; Poutanen 1998). The plasma can be identified with a corona of a black hole accretion disc (e.g. Bisnovatyi-Kogan & Blinnikov 1977; Galeev, Rosner & Vaiana 1979; Liang 1979; see Beloborodov 1999a, hereafter B99a, for a recent review). The corona is likely to form as a result of magnetorotational instabilities in the disc and the buoyancy of the generated magnetic field (Tout & Pringle 1992; Miller & Stone 2000). The corona is probably heated in flare-like events of magnetic dissipation producing the variable X-ray emission.

The dominant cooling mechanism of the flaring plasma is the Compton cooling. The observed hard X-rays are generated by the Comptonization process, i.e. by multiple upscattering of seed soft photons by the hot electrons in the corona. The Comptonization process generally produces power-law X-ray spectra. In addition to the direct power-law radiation from the corona, one also observes the X-rays reflected by the underlying (relatively cold) accretion disc (e.g. George & Fabian 1991). The arising reflection features in the spectrum, in particular the Compton bump and the fluorescent iron line, provide diagnostics for the accretion models.

The cold accretion disc partly re-emits the incident X-rays in the form of soft thermal radiation. This radiation cools the corona, providing the feedback loop which regulates the temperature of the corona (Haardt & Maraschi 1993, hereafter HM93). The geometry of the corona can hardly be derived from first principles. It might be a large cloud covering the whole inner region of the disc. It may also be a number of small-scale blobs with short lifetimes, with the energy release concentrated in space and time. The resulting X-ray spectrum is however not sensitive to the exact shape of the cloud, its density distribution, and other details. The only important parameter is the effective feedback factor (HM93; Stern et al. 1995b; Poutanen & Svensson 1996, hereafter PS96; Svensson 1996), that is the fraction of the X-ray luminosity which re-enters the source after reprocessing.

Previous computations of the disc–corona models all assumed that the corona is static (e.g. HM93; Stern et al. 1995b; PS96; see Svensson 1996, Poutanen 1998 for a review). The model was successfully applied to Seyfert 1 AGN. However, it was found to disagree with the observations of some black hole sources in the hard state, for instance Cyg X-1 (see e.g. Gierliński et al. 1997 and Section 3). Three alternatives have been suggested: (i) the cold disc is disrupted in the inner region (e.g. Poutanen, Krolik & Ryde 1997; Esin et al. 1998), (ii) the disc is highly ionized (Ross, Fabian & Young 1999; Nayakshin, Kazanas & Kallman 2000), and (iii) the coronal plasma is moving away from the disc and emits beamed X-rays (Beloborodov 1999b, hereafter B99b). We study the third scenario here.

B99b showed that the static model is not self-consistent for  $e^\pm$ -dominated flares and argued that the hot plasma should be

★E-mail: malzac@brera.mi.astro.it (JM); andrei@astro.su.se (AMB); juri@astro.su.se (JP)

ejected with a mildly relativistic bulk velocity  $\beta = v/c \lesssim 0.5$ . The bulk acceleration is also efficient in flares dominated by normal e–p plasma if the compactness parameter of the flare exceeds  $\sim 100$  (B99a). The likely pattern of ejection resembles that of solar flares (scaled to higher velocities because of higher compactness). The ejection velocity may be directed away from or towards the disc (and it may change) with the preferential direction being away from the disc.

Mildly relativistic bulk motion causes an aberration of the X-ray emission and strongly affects both the amplitude of reflection  $R$  and the spectrum slope  $\Gamma$ . Using a simple analytical model, B99b estimated the dependence of  $R$  and  $\Gamma$  on  $\beta$  and found that the low amplitude of reflection  $R \sim 0.3$  and the spectrum hardness  $\Gamma \sim 1.6$  observed in the hard state of Cyg X-1 can be explained with  $\beta \sim 0.3$ . The model also explains the observed correlation between  $R$  and  $\Gamma$  (B99a; Zdziarski, Lubiński & Smith 1999; Gilfanov, Churazov & Revnivtsev 2000).

In the present paper, we perform exact computations of the X-ray spectra produced by dynamic coronae. We use a non-linear Monte Carlo code (Malzac & Jourdain 2000) that is based on the large-particle method (Stern 1985; Stern et al. 1995a). The formulation of the problem and details of simulations are described in Section 2. In Section 3, we compute the spectra in the static case which was well studied previously, and highlight the problem of static models. In Section 4, we present spectra from dynamic coronae. The results are compared with the observations in Section 5.

## 2 SETUP

### 2.1 A heated cylinder

Consider a cylinder of radius  $r$  and height  $h$  located atop the accretion disc (Fig. 1). The cylinder may be associated with a hot outflow covering the disc or a heated magnetic tube in a compact flare. In the limit  $r \gg h$  we get a slab geometry of the corona, which has the largest feedback. In the opposite case,  $r \ll h$ , the feedback tends to zero (most of the reprocessed radiation goes away from the cylinder). We study the sequence of geometries parametrized with the ratio  $h/r$ . The plasma in the cylinder is assumed to have a constant density and is heated homogeneously at a constant rate.

The plasma moves through the cylinder with a velocity  $\beta$  directed normally to the disc. We assume that the heated cylindrical volume is static with respect to the disc. The motion of the plasma

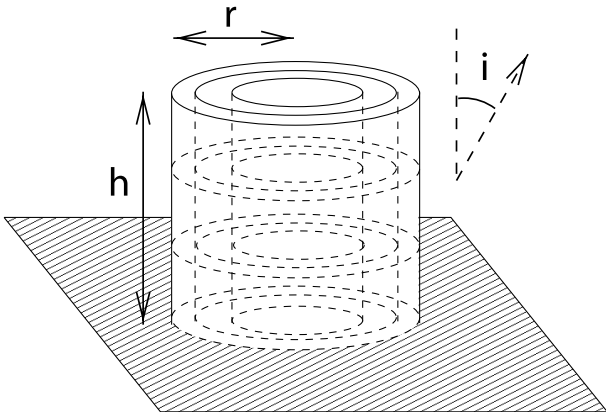


**Figure 1.** A heated cylinder atop the accretion disc. The cylinder is divided into nine computational cells, each of equal volume. The hot plasma moves through the cylinder with a velocity  $\beta$ .

then implies a flux of particles through the cylinder. If  $\beta < 0$  then the particle flux is absorbed by the disc at the bottom. If  $\beta > 0$  then the particles escape through the top of the cylinder. Outside the heated region, the particles are immediately (on a time-scale  $\ll h/c$ ) cooled down to the Compton temperature of the radiation field,  $kT_C \sim 1\text{--}10\text{ keV}$ . In our simulations, we do not take into account the scattering on the escaped cold particles. Their density is likely to be reduced if the plasma flows out along diverging magnetic lines.

In this paper, we restrict our consideration to thermal coronae and assume that the heated electrons have a Maxwellian distribution with a temperature  $T_e$  in the plasma rest frame. The cylinder is divided into nine cells of equal volumes (see Fig. 1) and the temperature  $T_e$  is calculated from the local heating = cooling balance in each of the cells separately. Note that the resulting equilibrium temperature is not homogeneous.

### 2.2 Feedback

The X-rays from the corona strike the underlying disc and get reprocessed. We assume that reprocessed radiation is the main cooler of the coronal plasma and neglect soft radiation generated viscously inside the accretion disc. This should be a good approximation if the corona releases energy in the form of strong concentrated flares; then, locally, the soft flux from inside the disc is much smaller than the reprocessed flux.<sup>1</sup> We also neglect additional photon sources such as bremsstrahlung and cyclotron emission in the corona (see e.g. Wardziński & Zdziarski 2000). An independent argument in favour of the reprocessed radiation as the main cooler comes from the observed  $R$ – $\Gamma$  correlation (Gilfanov, Churazov & Revnivtsev 1999; Zdziarski et al. 1999; see Section 5).

We assume that the reflecting material of the disc is sufficiently dense so that the ionization parameter  $\xi \lesssim 10^3$ , and the ionization effects are weak (e.g. Życki et al. 1994). Then the albedo is small,  $a \sim 0.2$ , and most of the X-rays impinging the disc are reprocessed. We assume that the reprocessed flux has a quasi-blackbody spectrum (possibly diluted) with a constant temperature  $T_{bb}$ . In the simulations, we consider two cases:  $kT_{bb} = 150\text{ eV}$  and  $kT_{bb} = 5\text{ eV}$ , representing typical blackbody temperatures in GBHs and AGN, respectively.

The feedback factor  $D$  is defined as the ratio of the soft blackbody luminosity entering the cylinder,  $L_s$ , to the total luminosity going out from the cylinder,  $L$ . The Comptonization time-scale is quite short,  $t_* \sim (h/c) \log(m_e c^2/3kT_{bb})$ , and we assume the heating rate to be steady on time-scales  $t \gtrsim t_*$ . Then the X-rays are generated in a quasi-stationary regime and the feedback factor determines the Compton amplification factor of the hot plasma  $A = L/L_s$  through the relation

$$DA = 1. \quad (1)$$

The amplification factor, for its part, is the main magnitude controlling the spectral slope  $\Gamma$  of the Comptonized radiation (see B99a and Section 4.3).

### 2.3 Radiative transfer and energy balance

We compute the plasma temperature simultaneously with the

<sup>1</sup> Yet, the total surface-integrated intrinsic luminosity of the cold disc does not need to be much smaller than the coronal luminosity since the covering factor of the corona may be small (Haardt, Maraschi & Ghisellini 1994).

radiative transfer. Our code is based on the non-linear Large Particle Monte Carlo method (Stern 1985; Stern et al. 1995a). In contrast to the standard Monte Carlo technique, this method allows one to follow the path and successive interactions of photons and particles in parallel. The code is described and tested in Malzac & Jourdain (2000).

We start a simulation from an initial (non-equilibrium) state and follow the evolution of the system plasma plus radiation until a steady state is achieved. The time-step is about  $10^{-2} h/c$ . We compute the evolution of the temperature distribution in the cylinder from the local energy balance. The plasma gains energy due to constant heating and loses energy via Compton cooling. The difference between the heating and cooling determines the change of temperature during each time-step.

The radiative transfer (photon tracking) is dealt with in the lab frame in the same way as for static coronae (Malzac & Jourdain 2000). The only difference is that the velocity of the scattering electron is generated from an isotropic Maxwellian distribution in the plasma rest frame and then it is Lorentz transformed to the lab frame.

In all the simulations of this paper, we assume a constant density throughout the cylinder and parametrize our models using the Thomson optical depth  $\tau_T = n_e \sigma_T h$  rather than a dissipation rate  $L_{\text{diss}}$  or compactness  $l_{\text{diss}} \equiv (L_{\text{diss}}/h)(\sigma_T/m_e c^3)$ . Strictly speaking, the model is self-consistent for low temperatures or for low compactness, when pair production is not important. In pair-dominated blobs, the density cannot be assumed homogeneous: the density distribution is then determined by the local pair balance. Yet, models with pair production give similar results if they have same  $\tau_T$ .

The model has four parameters: (i) Thomson optical depth  $\tau_T$  (defined along the height of the cylinder), (ii) height to radius ratio of the cylinder  $h/r$ , (iii) bulk velocity  $\beta$ , and (iv) blackbody temperature  $T_{\text{bb}}$ . Given these parameters the code computes the emitted spectrum as a function of the inclination angle  $i$  (the angle between the disc normal and the line of sight). We consider 10 angular bins of equal width  $\Delta \cos i = 0.1$ . The spectra are averaged within each bin.

## 2.4 The intrinsic and reflected components

For each inclination we compute two components of the observed emission.

(i) The ‘intrinsic’ Comptonized X-rays, i.e. the photons coming to the observer directly after the upscattering in the hot blob. The slope of the intrinsic X-ray spectrum (the photon index  $\Gamma$ ) is evaluated from a least-squares fit in the 2–10 keV range.

(ii) The reflected/reprocessed radiation from the underlying disc. We count only those reflected photons that are not scattered in the blob, thus accounting for the attenuation of reflection by the blob.

We model the reflector as an infinite slab, and compute the reflection component assuming neutral reflecting material with standard abundances (Anders & Ebihara 1982). The amplitude of reflection is defined as the ratio of an observed reflected component to that expected from an isotropic point source illuminating the slab,

$$R(i) = \frac{L_{\text{refl}}(i)}{L_{\text{refl}}^{\text{iso}}(i)}. \quad (2)$$

The simulations yield the intrinsic Comptonized spectrum emitted

at an inclination  $i$  and the reflected luminosity  $L_{\text{refl}}(i)$ . We then compute the reflected luminosity  $L_{\text{refl}}^{\text{iso}}(i)$  for an isotropic point source with the same intrinsic spectrum and find  $R(i)$  from equation (2). We fitted some of our simulated spectra with the PEXRAV model (Magdziarz & Zdziarski 1995) under XSPEC. The best-fitting values we found for  $R$  are very close to those derived using equation (2).

## 3 STATIC CORONAE

We have computed a set of static models ( $\beta = 0$ ) with different  $h/r$ ,  $\tau_T$ , and  $T_{\text{bb}}$ , and have determined  $R$  and  $\Gamma$  in the calculated spectra. The results are shown in Fig. 2. For simplicity, the presented amplitude of reflection is averaged over inclinations,  $R = \int_0^1 R(i) d(\cos i)$ .

### 3.1 Feedback, amplification, and the spectral index

In the static case, the feedback factor  $D_{\text{static}}$  is determined mainly by the geometry of the cloud, i.e. by  $h/r$  in our parametrization. We express the feedback factor as

$$D_{\text{static}} = A_{\text{static}}^{-1} = \frac{1}{2}(1 - a)(1 - \mu_s), \quad (3)$$

where  $a$  is the energy-integrated albedo of the disc. This equation defines the effective geometrical parameter  $\mu_s$  for a static cloud (B99a,b). The difference  $1 - \mu_s$  is the fraction of reprocessed radiation that returns to the hot cloud. To the first approximation,  $\mu_s$  can be associated with  $\mu_0 \equiv h/(4r^2 + h^2)^{1/2}$ , where  $1 - \mu_0$  corresponds to the angular size of the cylinder base measured from its centre. Numerically, we find  $\mu_s \approx (4/5)\mu_0$  (see Fig. 3b).

As one can see from Fig. 3, the effective  $\mu_s$  is not fully determined by  $h/r$  but also depends on  $\tau_T$ . The strongest dependence on  $\tau_T$  is observed for flat geometries ( $h/r \lesssim 1$ ):  $\mu_s$  and  $A$  substantially decrease as  $\tau_T$  increases. This effect can be understood analytically. Consider a slab corona and denote the radiation fluxes outgoing from the slab at the bottom and the top as  $F_-$  and  $F_+$ , respectively. The reprocessed flux entering the slab from below is  $F_s = (1 - a)F_-$ . The amplification factor is, by definition,

$$A = \frac{F_- + F_+}{F_s} = \frac{1 + F_+/F_-}{1 - a}. \quad (4)$$

One can estimate the ratio  $F_+/F_-$  by solving the radiative transfer equation in the Eddington approximation (see Rybicki & Lightman 1979, chapter 1) and by assuming isotropic scattering. Taking into account that the energy sources are homogeneously distributed in the slab, we get

$$\frac{F_+}{F_-} = \frac{1 + 2/\sqrt{3}}{1 + \sqrt{3}\tau_T/2}, \quad \mu_s = \frac{4 - 3\tau_T}{4(1 + \sqrt{3}) + 3\tau_T}. \quad (5)$$

These expressions are in good agreement with the results of the simulations (see Fig. 3,  $h/r = 0$ ). If  $\tau_T$  is large, the radiation is trapped at the bottom, near the reflector. In the limiting case  $\tau_T \gg 1$ , one has  $F_+ \ll F_-$ ,  $A \rightarrow (1 - a)^{-1}$  and  $\mu_s \rightarrow -1$ . Then almost all the X-rays are reprocessed because the source emits most of them towards the reflector. The bottom layers of the slab are cold and emit a soft spectrum for which the disc albedo  $a$  is close to zero (see Fig. 4b) and  $A \rightarrow 1$ . Such a small  $A$  results in the high  $\Gamma$  (see Fig. 2c).

At small  $\tau_T$ , the emitted spectrum hardens (Fig. 2c). This is because of the number of photons scattered in an optically thin blob

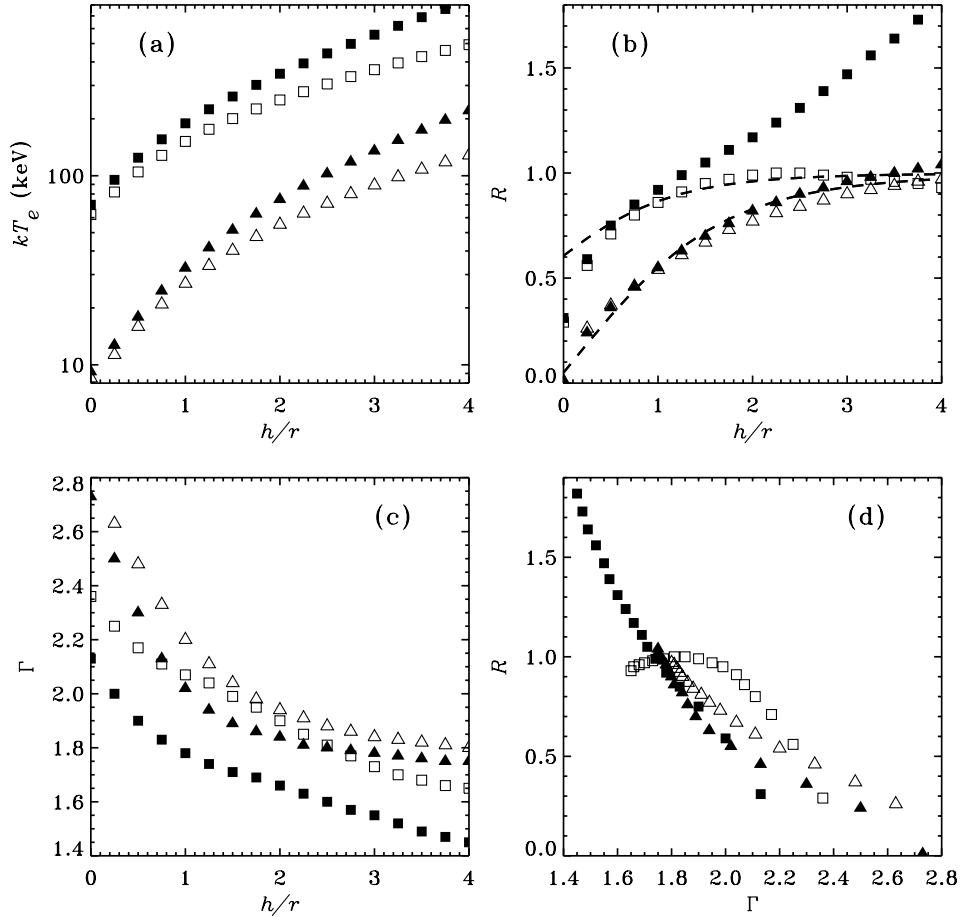


**Figure 2.** Characteristics of the static disc–corona model ( $\beta = 0$ ). The active blob is a cylinder of height  $h$  and radius  $r$ . The model is determined by three parameters:  $h/r$ , the optical depth of the cylinder,  $\tau_T$  (measured in the vertical direction), and the temperature of the soft radiation entering the blob,  $T_{bb}$ . Filled and open symbols correspond to  $kT_{bb} = 150$  eV (GBHs) and  $kT_{bb} = 5$  eV (AGN), respectively. Squares and triangles show the cases  $\tau_T = 0.5$  and  $\tau_T = 3$ , respectively. (a) The average electron temperature in the blob versus  $h/r$ . (b) The inclination-averaged amplitude of reflection  $R$  versus  $h/r$ . The dashed curves represent the analytical formula (6). (c) The inclination-averaged photon index of the intrinsic X-ray spectrum  $\Gamma$  (measured in the 2–10 keV band) versus  $h/r$ . (d)  $R$  versus  $\Gamma$ .

is small. When the Comptonized spectrum is made of fewer photons, the same luminosity can be emitted only if the average photon energy is high. This leads to a hard spectrum (Fig. 2c) with a break at high energies. The optically thin models have high temperatures (Fig. 2a): at a fixed geometry and  $T_{bb}$  the product  $\tau_T T_e$  stays approximately constant (HM93; Stern et al. 1995b; Svensson 1996; see also Fig. 10, later) and hence an optically thin blob must be hotter.

Blobs with high  $h/r$  (‘elongated cylinders’) have a low feedback and the resulting spectrum is hard (Fig. 2c). This behaviour is known from previous simulations (see Svensson 1996 for a review; the previously computed spectra of detached spheres are similar to those of elongated cylinders). The product  $\tau_T T_e$  increases with  $h/r$ ; for fixed  $\tau_T$  it implies an increase in the plasma temperature with  $h/r$  (Fig. 2a).

The emitted spectrum depends on  $T_{bb}$ . For this reason, we perform computations for GBHs ( $kT_{bb} = 150$  eV) and AGN ( $kT_{bb} = 5$  eV) separately. For the same  $h/r$  and  $\tau_T$ , we get a harder spectrum for GBHs than for AGN (despite the fact that the feedback factor and  $A$  are not sensitive to  $T_{bb}$ ). The hardening occurs for two reasons. (i) The energy range in which the Comptonized luminosity is liberated is narrower in GBHs. Therefore, in order to radiate a given amount of luminosity the

spectrum has to harden and cut off at a higher energy. (ii) Low- $\tau_T$  models are hot and have an anisotropy break in the spectrum (Stern et al. 1995b). In GBHs, this break is in the 2–10 keV band and affects the measured  $\Gamma$ .

### 3.2 The amplitude of reflection

The reflection component produced beneath the blob is partly scattered and attenuated while passing through the blob. To a first approximation, the attenuation effect can be described analytically,

$$R = \mu_0 + (1 - \mu_0)e^{-\tau_T(1-\mu_0)}, \quad \mu_0 = \frac{h/2}{\sqrt{r^2 + (h/2)^2}}. \quad (6)$$

Here it is assumed that the fraction  $\mu_0$  of the reflected luminosity goes directly to the observer. The remaining fraction,  $1 - \mu_0$ , is reflected at the base of the cylinder and attenuated when transmitted through the hot plasma. The optical depth of the cylinder seen by soft photons emitted at the base depends on  $\tau_T$  and  $h/r$ ; it equals  $\sim \tau_T$  for  $h/r = 0$  and vanishes at  $h/r \gg 1$ . We interpolate between the two extremes as  $\tau_T(1 - \mu_0)$ , and use this effective optical depth in the exponential of equation (6).

The attenuation formula given by equation (6) assumes that the scattered reflection component is completely destroyed. Indeed,

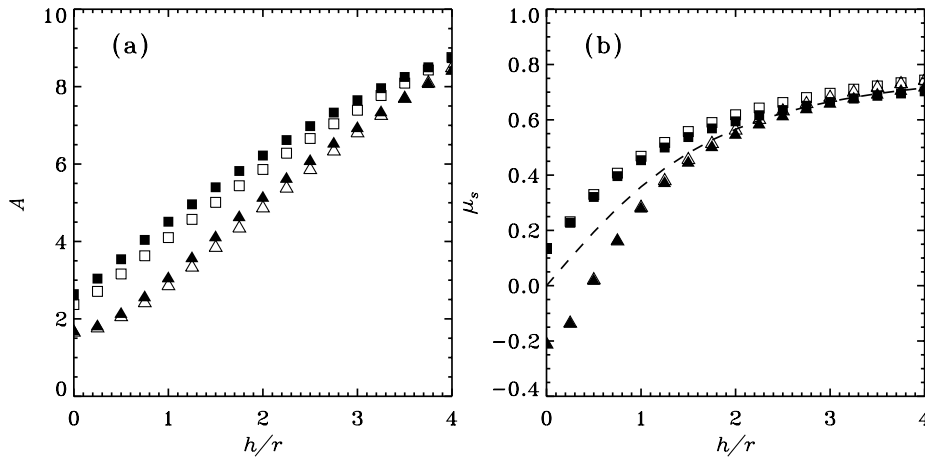


**Figure 3.** (a) Amplification factor,  $A$ , and (b) the effective geometrical factor  $\mu_s$  (see equation 3) for static coronae. The symbols have the same meaning as in Fig. 2. The dashed curve shows  $(4/5)\mu_0$ , where  $\mu_0$  is given in equation (6).

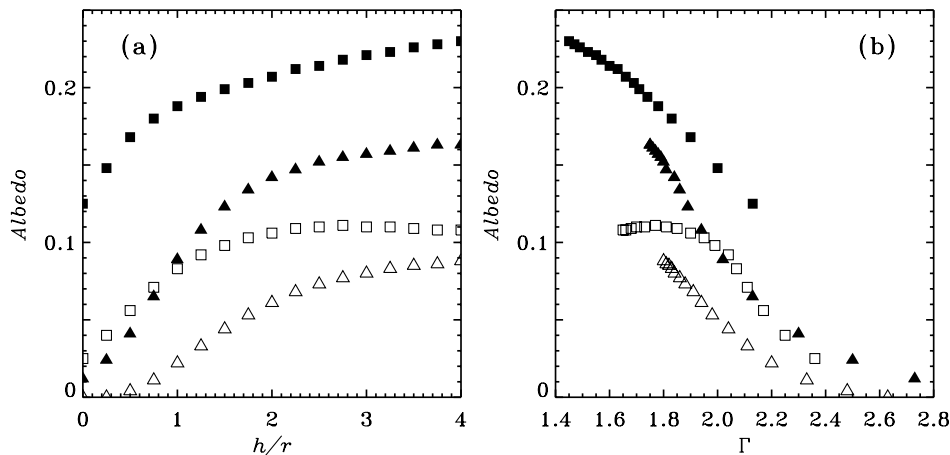


**Figure 4.** Energy-integrated albedo,  $a$ , as a function of (a)  $h/r$  and (b) spectral index  $\Gamma$ . The symbols have the same meaning as in Fig. 2.

the ‘Comptonized reflection’ component has a power-law spectrum where the reflection features (the Fe lines and the edge) disappear.

Equation (6) is in good agreement with the results of the simulation (see Fig. 2b). The attenuation effect is strong if  $h/r$  is small (so that a large fraction of the reflected radiation has to pass through the cylinder) and if  $\tau_T$  is large. In the optically thick regime,  $\tau_T \gtrsim 3$ , almost all reflected photons re-entering the cloud are Compton scattered and the attenuation effect saturates: further increase in  $\tau_T$  does not reduce  $R$ .

For elongated cylinders, the attenuation affects only a small fraction of the reflected luminosity and  $R$  approaches unity at high  $h/r$ . The reflection amplitude is higher in GBHs, especially in the high-temperature models (with small  $\tau_T$  and large  $h/r$ ) where  $R$  substantially exceeds unity (see Fig. 2b). The explanation is as follows. The radiation scattered once is strongly anisotropic and collimated towards the reflector (HM93). In GBHs, because of the relatively large temperature of seed soft photons, the first-order scattering peaks above 1 keV and contributes significantly to the reflected flux. As a result,  $R$  increases. In contrast, in the AGN, the Comptonized emission above 1 keV is made of multiply scattered photons and the anisotropy effects are small.

### 3.3 $R$ – $\Gamma$ anticorrelation

Models with low values of  $h/r$  have soft spectra because of high

feedback. These models also have lower reflection amplitudes because of stronger attenuation (see Section 3.2). Therefore, variations in  $h/r$  produce an anticorrelation between  $R$  and  $\Gamma$  (Fig. 2d). The anticorrelation disagrees with the data (see Section 5). A static model with a neutral reflector never predicts a small  $R$  simultaneously with a hard spectrum. In particular, the parameters  $R \sim 0.3$  and  $\Gamma \sim 1.6$  observed in Cyg X-1 and similar hard-state objects cannot be reproduced.

## 4 DYNAMIC CORONAE

### 4.1 Examples of spectra

In the dynamic case,  $\beta \neq 0$ , the corona spectrum is strongly affected by the bulk motion of the hot plasma. This is illustrated in Fig. 5 where we compare the cases  $\beta = 0.3$  and  $\beta = -0.2$  with the static case. The spectra are computed for the same optical depth,  $\tau_T = 3$ , and geometry,  $h/r = 2$ .

In the case of  $\beta = 0.3$  (plasma moves away from the disc), the observed Comptonized luminosity is enhanced as a result of relativistic aberration. The X-rays are beamed away from the disc, and the reprocessed and reflected luminosities are reduced. The low feedback leads to a hard intrinsic spectrum.

In the case of  $\beta = -0.2$  (plasma moves towards the disc), the Comptonized luminosity is beamed towards the disc, and the

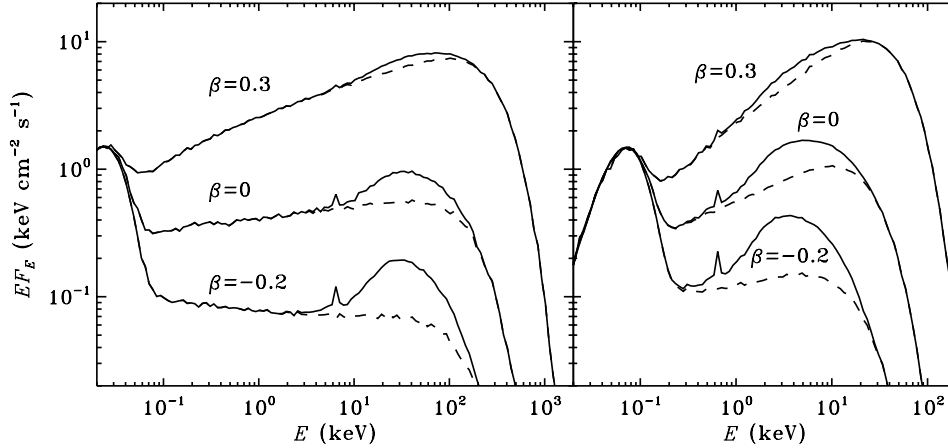


**Figure 5.** The effect of bulk motion on the emitted spectra. Here  $h/r = 2$ ,  $\tau_T = 3$ , and nearly face-on inclination is assumed,  $0.9 < \cos i < 1$ . The spectra are normalized to the blackbody peak. The left-hand panel shows the case of AGN ( $kT_{\text{bb}} = 5$  eV) and the right-hand panel corresponds to GBHs ( $kT_{\text{bb}} = 150$  eV).

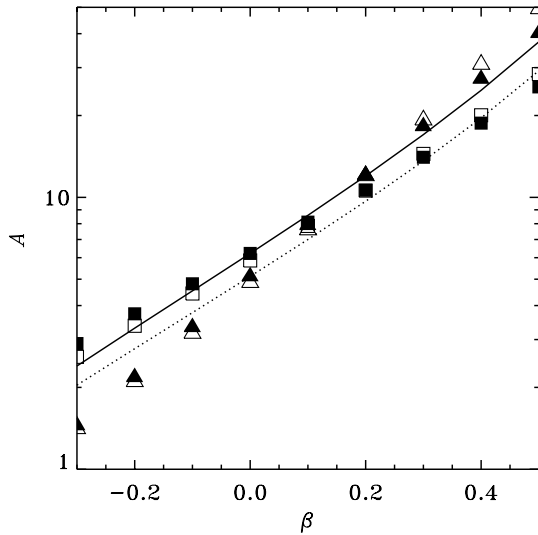


**Figure 6.** Amplification factor  $A$  as a function of  $\beta$ . The simulations are done for a cylinder with  $h/r = 2$ . The results are shown by symbols which have the same meanings as in Fig. 2. The solid and dotted curves display the analytical formula given by equation (7) for GBH models with  $\tau_T = 0.5$  and  $\tau_T = 3$ , respectively.

reprocessed and reflected components are enhanced. The high feedback leads to a soft intrinsic spectrum.

Since  $\tau_T$  is fixed in Fig. 5, a high (low) feedback leads to a low (high) coronal temperature. This causes the shift of the spectral break to lower energies with decreasing  $\beta$ .

The moderate changes in the amplitude and direction of the bulk velocity thus induce crucial changes in the emitted spectra. Note that in most of our simulations, the bulk velocity is smaller than the thermal electron velocity  $\beta_{\text{th}}$  (e.g.  $\beta_{\text{th}} \sim 0.5$  for  $kT_e = 100$  keV).

#### 4.2 The amplification factor

The low feedback at  $\beta > 0$  implies a high Compton amplification-factor of the X-ray source (equation 1). The main effect can be estimated analytically assuming that the source is isotropic in the plasma rest frame (see equation 7 in B99b),

$$A(\beta) = A_{\text{static}} \frac{\gamma^2(1 + \beta)^2(1 + \beta\mu_s)^2}{1 - \beta^2(1 + \mu_s)^2/4}. \quad (7)$$

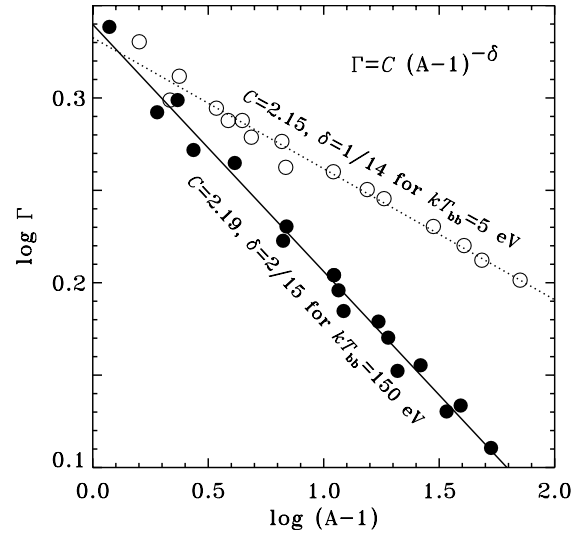


**Figure 7.**  $\Gamma$  versus  $A$ . The results of simulations for GBHs and AGN are shown by filled and open circles, respectively. The source geometry is fixed (a cylinder with  $h/r = 2$ ), while  $\tau_T$  and  $\beta$  vary. Only models with  $50 < kT_e < 300$  keV are shown here. The lines correspond to the approximation given by equation (8).

Here,  $\gamma = 1/\sqrt{1 - \beta^2}$  and  $\mu_s$  is the effective geometrical parameter which we take from the static model (see equation 3 and Fig. 3b); a more exact definition of  $\mu_s$  is given in B99b.  $A = A_{\text{static}}$  at  $\beta = 0$ , and monotonically increases with  $\beta$ ; at  $\beta < 0$  equation (7) gives  $A < A_{\text{static}}$ .

In Fig. 6 we compare the results of simulations with the analytical estimate given by equation (7). In the optically thin models ( $\tau_T = 0.5$ ), we observe the reduction in  $A$  for large positive  $\beta$  compared with equation (7). This is caused by the anisotropy of scattering in the plasma rest frame (optically thin models have very high temperatures, see Fig. 8a later, and scatter preferentially downwards). At  $\beta < 0$ ,  $T_e$  is small and the agreement is good.

In the optically thick models ( $\tau_T = 3$ ), we see that the actual value of  $A$  at  $\beta < 0$  is smaller than that given by equation (7). This is caused by the trapping of radiation and its advection downwards by the moving plasma. The advection enhances the anisotropy of the blob radiation compared with the optically thin case. In the limiting case of large optical depths, the velocity of photon diffusion  $\beta_{\text{diff}} \approx 1/\tau_T$  is smaller than the advection velocity,  $\beta$ , so

that almost no radiation can escape through the upper boundary. When viewed from the plasma rest frame, the effect can be understood by noting that both the bottom and top boundaries of the cylinder move upwards; as a result, the escape probability is larger for photons emitted towards the bottom boundary.

For a similar reason, equation (7) underestimates  $A$  for high- $\tau_T$  models at  $\beta > 0$ . In this case, the radiation is advected towards the upper boundary, and is strongly beamed away from the disc, more than in the optically thin case.

### 4.3 The spectral index

A simple functional shape  $\Gamma(A)$  suggested in B99a fits the results of the simulations,

$$\Gamma = C(A - 1)^{-\delta}. \quad (8)$$

The fitting parameters are  $C = 2.19$ ,  $\delta = 2/15$  for GBHs ( $kT_{\text{bb}} = 150$  eV) and  $C = 2.15$ ,  $\delta = 1/14$  for AGN ( $kT_{\text{bb}} = 5$  eV). These parameters are not far from those found by B99a in the case of a spherical blob:  $C = 2.33$  for both GBHs and AGN and  $\delta = 1/6$  and  $1/10$  for GBHs and AGN, respectively. Equation (8) is a good

approximation for models with  $kT_e$  in the range between 50 and 300 keV (Fig. 7).

Equation (8) combined with equation (7) yields the analytical dependence  $\Gamma(\beta)$ , which is in good agreement with the results of simulations (see Fig. 8c). Only for GBH models with very high electron temperatures ( $kT_e \gtrsim 300$  keV) do the deviations  $\Delta\Gamma$  exceed 0.1. The reasons of these deviations are the same as those in the static case discussed at the end of Section 3.1.

### 4.4 The amplitude of reflection

Following the analysis of B99a,b, but accounting for the attenuation effect (see Section 3.2), we get an analytical formula for the reflection amplitude,

$$R(\mu) = \frac{(1 - \beta\mu)^3}{(1 + \beta\mu_0)^2} \left\{ \mu_0 \left( 1 + \frac{\beta\mu_0}{2} \right) + \frac{(1 - \mu_0)[1 + \beta(1 + \mu_0)/2]}{(1 + \beta)^2} e^{-\tau_T(1 - \mu_0)} \right\}, \quad (9)$$

where  $\mu = \cos i$ , and  $i$  is the disc inclination. Here, the reflected luminosity is represented as a sum of two parts: the first one is

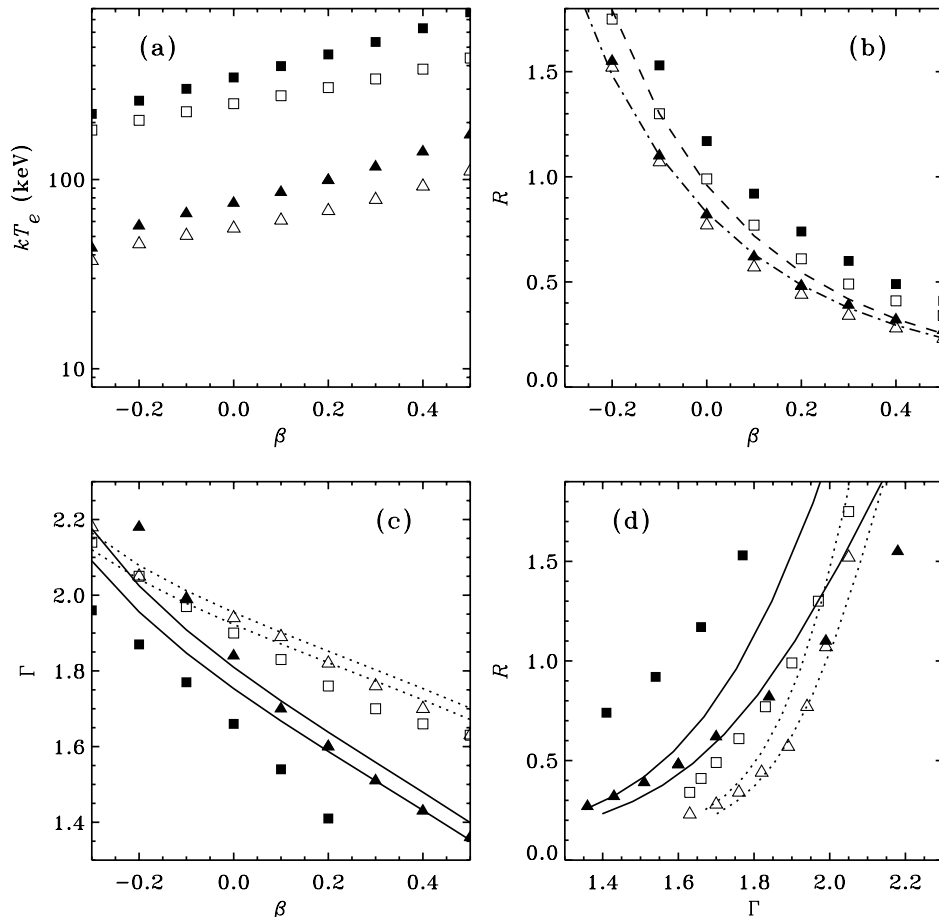


**Figure 8.** Characteristics of the dynamic disc–corona model. The model is determined by four parameters:  $h/r = 2$ , the optical depth of the cylinder,  $\tau_T$  (measured in the vertical direction), the temperature of the soft radiation entering the blob,  $T_{\text{bb}}$ , and the velocity of bulk motion  $\beta$ . The observed characteristics are inclination-averaged. Filled and open symbols correspond to  $kT_{\text{bb}} = 150$  eV (GBHs) and  $kT_{\text{bb}} = 5$  eV (AGN), respectively. Squares and triangles show the cases  $\tau_T = 0.5$  and  $\tau_T = 3$ , respectively. (a) The average temperature in the blob versus  $\beta$ . (b) The amplitude of reflection  $R$  versus  $\beta$ . The curves give analytical  $\mu$ -averaged  $R$  from equation (9) (dashed –  $\tau_T = 0.5$ , dot-dashed –  $\tau_T = 3$ ). (c) The photon index of the intrinsic X-ray spectrum  $\Gamma$  (in the 2–10 keV band) versus  $\beta$ . The analytical approximation (equations 7 and 8) is shown by solid curves for GBHs and dotted curves for AGN. (d) Reflection  $R$  versus spectral slope  $\Gamma$ . The analytical model is shown by solid curves for GBHs and dotted curves for AGN (left curves for  $\tau_T = 0.5$  and right curves for  $\tau_T = 3$ ).

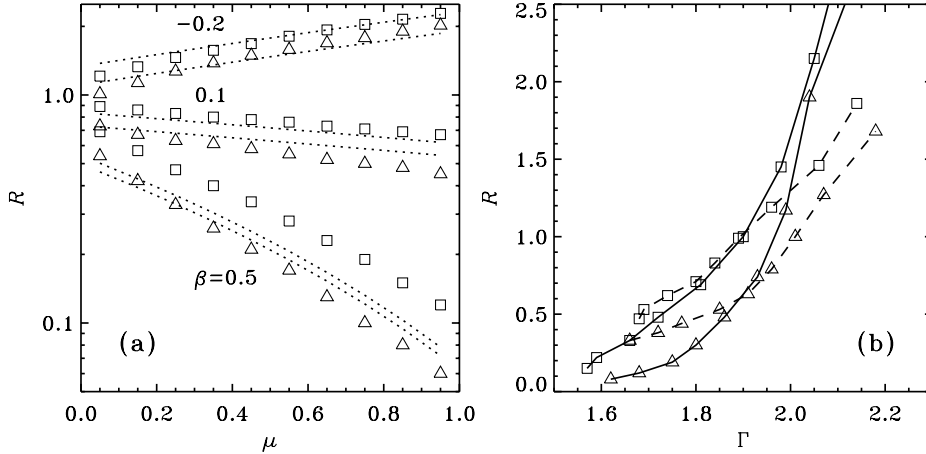


**Figure 9.** (a) Reflection,  $R$ , versus inclination ( $\mu = \cos i$ ). Squares are for  $\tau_T = 0.5$ , triangles for  $\tau_T = 3$ . Here  $h/r = 2$ ,  $kT_{\text{bb}} = 5$  eV, and  $\beta = -0.2, 0.1, 0.5$ . Reflection is larger than unity for negative  $\beta$  (bulk motion directed towards the reflector), and is much smaller than unity for the outflows. The dotted curves are the analytical estimates given by equation (9). (b)  $R$ - $\Gamma$  correlation for two inclinations  $\mu = 0.25$  ( $i = 76^\circ$ , dashed curves), and  $\mu = 0.85$  ( $i = 32^\circ$ , solid curves). Here  $\beta$  varies from  $-0.3$  (upper points) to  $0.5$  (lower points) with a step of  $0.1$ . The curves connecting the points are added for clarity.

reflected outside the cylinder base and does not experience any attenuation and the second one is reflected from the base and is partially attenuated, depending on  $\tau_T$ . When  $\mu_0$  approaches unity (or  $\tau_T \rightarrow 0$ ), the attenuation is not important and equation (9) changes to equation (3) in B99b:

$$R(\mu) = \frac{(1 + \beta/2)(1 - \beta\mu)^3}{(1 + \beta)^2}. \quad (10)$$

Equation (9) is in good agreement with the simulations (see Fig. 8b). Substantial differences appear only in the case of low- $\tau_T$  GBH models. The differences are caused mainly by the anisotropy of scattering in the rest frame of the hot plasma. A similar effect was observed in the static GBH models (Fig. 2b) and was discussed in Section 3.2.

The left panel of Fig. 9 shows the dependence of reflection on the disc inclination. Note that  $R$  is less sensitive to  $\beta$  at large inclinations. The overall angular dependence of  $R$  is well represented by equation (9).

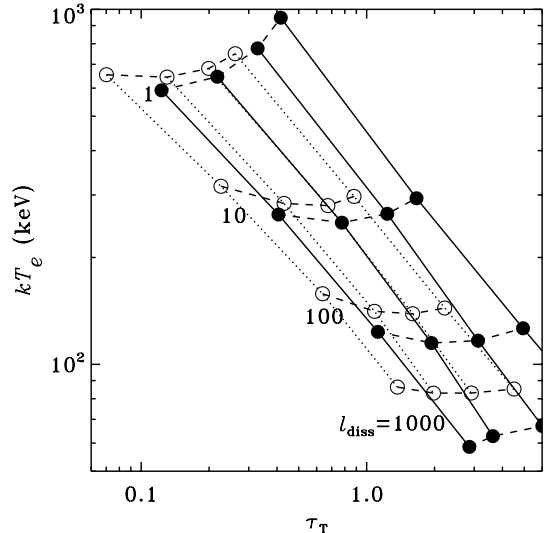
#### 4.5 $R$ - $\Gamma$ correlation

Fig. 8(d) shows  $R$  versus  $\Gamma$ . Again we see that the analytical formulae are in good agreement with the results of the simulations. The  $R$ - $\Gamma$  correlation is steeper in AGN than in GBHs. This is caused by the fact that  $\Gamma(A)$  is a flat function at small  $T_{\text{bb}}$  [see Section 4.3; the index  $\delta$  in equation (8) is smaller for AGN than that for the GBHs].

The shape of the  $R$ - $\Gamma$  correlation also depends on the disc inclination: the reflection amplitude is very sensitive to  $\beta$  at small inclinations and the correlation gets stretched in the vertical direction (see Fig. 9b).

#### 4.6 Pair-dominated coronae

A compact and energetic blob emitting hard X-rays may be mainly composed of  $e^\pm$  pairs produced in  $\gamma$ - $\gamma$  reactions. In this case, the optical depth of the blob and temperature are determined by the compactness parameter  $l_{\text{diss}} = L_{\text{diss}}\sigma_T/hm_e c^3$ , where  $L_{\text{diss}}$  is the power dissipated in the blob (see e.g. Stern et al. 1995a,b). The equilibrium  $\tau_T$  is controlled by the balance between pair production and annihilation and  $T_e$  is controlled by energy balance.



**Figure 10.** The relation between  $T_e$  and  $\tau_T$  for  $\beta = -0.3, 0.0, 0.3, 0.5$  (from left to right). The simulations are done for a cylinder with  $h/r = 2$ ; the open and filled circles show the AGN and GBH models, respectively. The  $T_e$ - $\tau_T$  relation is shown by dotted curves for AGN and solid curves for GBHs. This relation does not depend on the nature of the scattering plasma. The dashed curves, describing the case of pure  $e^\pm$  plasma, connect points of equal dissipation compactness  $l_{\text{diss}}$ .

We have calculated a set of pair-dominated dynamic models with the  $h/r = 2$  geometry. For simplification, we compute a global pair balance assuming a uniform pair distribution in the cylinder. The results are shown in Fig. 10.

At fixed  $\beta$ , the model follows an equilibrium  $T_e$ - $\tau_T$  curve. We emphasize that the  $T_e$ - $\tau_T$  relation for  $e^\pm$  plasma is the same as for normal  $e$ - $p$  plasma, since it is determined by the energy balance only (see HM93; Stern et al. 1995b; PS96) and the annihilation radiation does not contribute much to the total energy budget.

With increasing  $\beta$ , the  $T_e$ - $\tau_T$  curve moves to the right. An increase in  $\beta$  at fixed  $l_{\text{diss}}$  leads to an increase in the  $e^\pm$  optical depth while the temperature does not change much. This is the ‘thermostat’ effect of pairs discussed previously in the static models (see figs 2 and 3 in Svensson 1996). The typical values  $kT_e \sim 100$  keV and  $\tau_T \sim 1$ -2 inferred from observations

(Zdziarski et al. 1997; Poutanen 1998) are obtained for large but possible values of the dissipation compactness,  $l_{\text{diss}} > 100$ .

We now briefly discuss the  $R$ – $\Gamma$  correlation expected at fixed  $l_{\text{diss}}$  and varying  $\beta$ . The correlation will be steeper compared with the  $\tau_{\text{T}} = \text{constant}$  case shown in Fig. 8(d). At large  $\beta$ , the equilibrium  $\tau_{\text{T}}$  is large and here the  $R$ – $\Gamma$  track is close to that of  $\tau_{\text{T}} = 3$ . At  $\beta < 0$ ,  $\tau_{\text{T}}$  drops and the  $R$ – $\Gamma$  track approaches the  $\tau_{\text{T}} = 0.5$  curve.

## 5 COMPARISON WITH OBSERVATIONS

### 5.1 Broad-band spectra of individual sources

Fig. 11 shows the spectra of one GBH source, Cyg X-1, and one bright Seyfert 1 galaxy, IC 4329A, together with model spectra. We did not use a real fitting procedure (since each simulation takes a few hours on a modern workstation). Instead, we used unfolded spectra and searched for similar spectra in our sample of models. We find that the spectrum of Cyg X-1 is well reproduced by the model with a bulk velocity  $\beta = 0.3$ , an optical depth  $\tau_{\text{T}} = 3$ , and

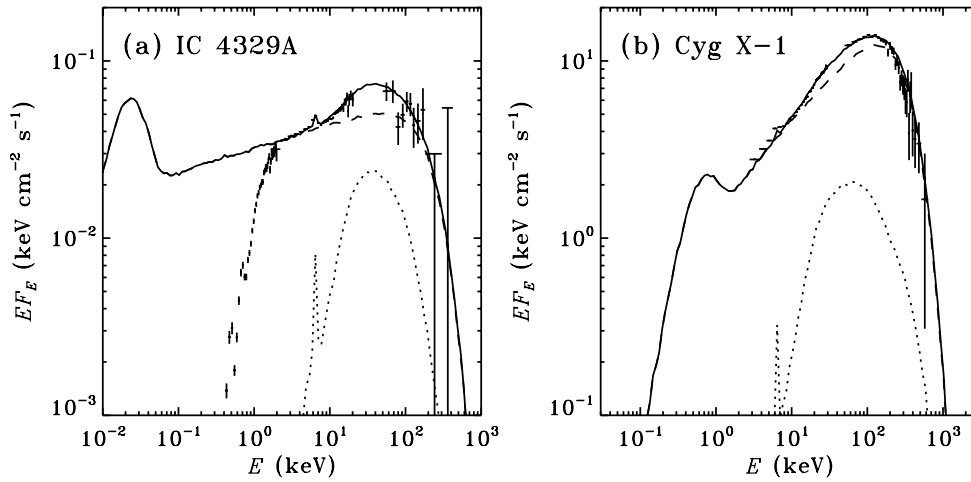
$h/r = 1.25$ . The inclination that gives the best agreement with the data,  $i = 50^\circ$ , is compatible with the current estimates  $25^\circ \leq i \leq 67^\circ$  (see Gierliński et al. 1999 and references therein).

For IC 4329A, we find  $\beta = 0.1$ ,  $\tau_{\text{T}} = 3$ , and  $h/r = 2$ . The inclination,  $i = 40^\circ$ , is consistent with the Seyfert unification scheme stating that Seyfert 1s should be seen face-on (Antonucci 1993). Note that  $h/r$  is smaller in the case of Cyg X-1.

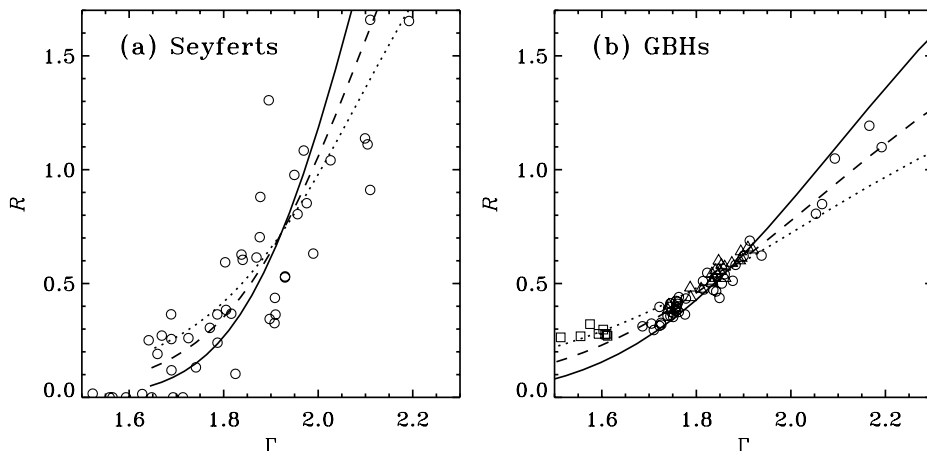
### 5.2 $R$ – $\Gamma$ correlation

Fig. 12 gives the observed  $R$ – $\Gamma$  correlation for Seyferts and GBHs (Gilfanov et al. 1999; Zdziarski et al. 1999). The correlation exists in individual objects observed at different periods as well as in a sample of sources. Such a correlation supports the hypothesis that it is the reprocessed/reflected radiation that cools the X-ray source via Comptonization.

The  $R$ – $\Gamma$  correlation expected in the dynamic corona model is similar in shape to the observed one, and we now try to fit the data



**Figure 11.** (a) Spectrum of the Seyfert 1 galaxy IC 4329A observed by *ROSAT*, *Ginga*, and *CGRO/OSSE* (crosses, data from Madejski et al. 1995). The low-energy cut-off is due to the Galactic absorption. The solid curve shows the model spectrum for  $\tau_{\text{T}} = 3$ ,  $h/r = 2$ ,  $\beta = 0.1$  at an inclination of  $i = 40^\circ$ . (b) Spectrum of Cyg X-1 as observed by *Ginga* and *CGRO/OSSE* in 1991 September (crosses, set 2 from Gierliński et al. 1997). The solid curve shows the model spectrum for  $\tau_{\text{T}} = 3$ ,  $h/r = 1.25$ ,  $\beta = 0.3$  at an inclination of  $i = 50^\circ$ . In both panels, the dotted curves give the reflected components and the dashed curves show the intrinsic Comptonized spectra.



**Figure 12.** (a) The observed  $R$ – $\Gamma$  correlation for Seyfert galaxies (circles). Data from Zdziarski et al. (1999). The curves show the correlation predicted by the model (equations 3, 7–9). Here  $\mu_s = \mu_0 = 0.6$ ,  $\tau_{\text{T}} = 3$ ,  $a = 0.15$ . The solid, dashed, and dotted curves correspond to  $\mu = 0.85, 0.55$ , and  $0.35$  (i.e.  $i = 32^\circ, 57^\circ$ , and  $70^\circ$ ), respectively. (b) The observed  $R$ – $\Gamma$  correlation for GBHs, Cyg X-1 (circles), GX 339-4 (triangles), and GS 1354-644 (squares). Data from Gilfanov et al. (2000). The curves correspond to the same three inclinations as on the left panel. Here  $\mu_s = \mu_0 = 0.45$ ,  $\tau_{\text{T}} = 3$ ,  $a = 0.15$ .

with the model. As we showed in Section 4, the analytical model is a sufficiently good approximation to the results of exact simulations and it is reasonable to use this simple model in a fitting procedure, instead of the exact transfer model (especially taking into account the uncertainties in the validity of assumptions such as homogeneous density and uniform heating of the blob).

The analytical model yields explicit expressions for  $R(\beta)$  (equation 9) and  $\Gamma(\beta)$  (equations 7 and 8) for given parameters  $\mu_s$ ,  $\mu_0$ ,  $a$ , and  $\tau_T$ . For simplicity, we assume  $\mu_s = \mu_0$  and fix the albedo at a reasonable value,  $a = 0.15$ . The fit to the  $R$ – $\Gamma$  correlation is shown in Fig. 12 for AGN and GBHs.

It is interesting to note that the correlations for AGN and GBHs cannot be fitted with the same value of  $\mu_s$ . We find  $\mu_s$  to be lower for GBHs ( $\mu_s = 0.45$ , or equivalently  $h/r = 1$ ) than for the AGN ( $\mu_s = 0.6$  or  $h/r = 1.5$ ). This might indicate different geometries of emission regions in GBHs and AGN.

### 5.3 The beaming effects

The observed flux  $F_h$  of the hard X-rays beamed away from the disc can dominate over the blackbody component  $F_{bb}$  when the disc is observed at small inclinations. The hard X-rays can dominate even if only a modest fraction  $f$  of the accretion energy is dissipated in the corona. In the case of a patchy corona, the model predicts

$$\frac{F_{bb}}{F_h} \approx R(i) 2 \cos i \left( 1 + \frac{1-f}{f} \frac{1+d}{d} \right). \quad (11)$$

Here  $d = L_-/L_+$  is the ratio of the Comptonized luminosities emitted towards and away from the disc,

$$d = \frac{1 + \beta/2 (1 - \beta)^2}{1 - \beta/2 (1 + \beta)^2}. \quad (12)$$

For example, in the case of Cyg X-1, taking  $i = 50^\circ$  and  $\beta = 0.3$ , one gets  $F_{bb}/F_h \approx 0.4$  for  $f = 3/4$  or  $F_{bb}/F_h \approx 0.85$  for  $f = 1/2$ , in agreement with the data (e.g. Di Salvo et al. 2001).

The beaming of the coronal X-rays may be tested in a sample of hard-state objects with known inclinations:  $R$  should increase with  $i$ . Also, the shape of the  $R$ – $\Gamma$  correlation varies with  $i$  (Fig. 9), which may be checked in the data on GBHs. Unfortunately, in the case of AGN, the high-inclination objects are obscured by the large-scale molecular torus which dominates the reflection component.

The ejection model with  $\beta < 0$  predicts very soft spectra and large ratios  $F_{bb}/F_h$ . This situation might take place in some soft objects, e.g. narrow-line Seyfert 1 galaxies (see Brandt 1999 for a review).

## 6 DISCUSSION

### 6.1 Variability

The coronal emission should be variable, with a temporal pattern governed by the complicated processes of the magnetic field buoyancy and its dissipation in the corona. The ejection velocity can vary from flare to flare and the fit parameters of the observed spectrum should be considered with caution since they give only effective/average values.

The main X-ray emitting region probably extends through a decade in radius, and  $\beta$  is likely to be different at different radii. Recent temporal studies (e.g. Gilfanov et al. 2000; Revnivtsev, Gilfanov & Churazov 2000) suggest that harder spectra with lower

reflection come from the inner radii. In the context of the dynamic corona model it would correspond to an increase of  $\beta$  in the innermost region. The analysis of Cyg X-1 and GX 339-4 at different periods of the hard state showed that the typical variability time-scales grow when the spectrum hardens. This behaviour may indicate that the accretion is slower in the hardest periods (Beloborodov 2001).

### 6.2 Pair envelopes in quasars

In this paper, we neglected scattering on the particles that escaped or were created in  $\gamma$ – $\gamma$  collisions outside the heated region. In the brightest sources, with luminosities comparable to the Eddington limit, the hard X-rays from the flares will interact with each other and create an optically thick  $e^\pm$  outflow covering the whole inner region of the accretion disc (Beloborodov 1999c). Such an outflow is relatively cold (at the Compton temperature,  $kT_C \sim 1$ – $10$  keV), and it has an equilibrium bulk velocity such that the radiative pressure from the disc is balanced by the Compton drag. The velocity is mildly relativistic ( $\beta$  increases from 0.3 at the base to 0.7 at the photosphere of the outflow) and the scattering of the disc/corona radiation in the outflow strongly affects the angular distribution of the observed luminosity. The reflection amplitude will then be suppressed, whatever the dynamics that takes place in the compact flares hidden in the  $e^\pm$  outflow.

### 6.3 Optical and UV polarization of Seyferts and quasars

The scattering of soft radiation in a dynamic corona is accompanied by a strong effect that can be tested in optical/UV observations: the polarization of the scattered radiation is sensitive to  $\beta$ . The polarization is perpendicular to the disc if  $0.12 < \beta < 0.78$  and parallel otherwise (Beloborodov 1998). The observed optical polarization in the non-blazar AGN is parallel to the radio jet that is presumably perpendicular to the accretion disc (Stockman, Moore & Angel 1984); it is consistent with the scattering in a mildly relativistic outflow.

In three of the ten quasars with measured UV polarization, a steep rise in polarization was observed blueward of the Lyman limit (see Koratkar & Blaes 1999 for a review). The outflowing corona model may provide a natural explanation for this mysterious rise (Beloborodov & Poutanen 1999).

## 7 CONCLUSIONS

We performed detailed Monte Carlo simulations of the X-ray production by hot coronae atop accretion discs, and tested the model against the data. The main results are as follows.

(i) A static corona atop a neutral reflector is not able to produce the observed hard spectra with low reflection. Furthermore, changes in the coronal geometry produce an anticorrelation between the hard X-ray spectral slope  $\Gamma$  and the amplitude of reflection  $R$ . This anticorrelation is opposite to what is observed.

(ii) The disc–corona model becomes consistent with the data if the hot plasma is dynamic, i.e. if it moves with a mildly relativistic bulk velocity,  $\beta = v/c$ , with respect to the accretion disc. In particular, the spectrum of Cyg X-1 is reproduced by the model with  $\beta = 0.3$ , confirming the estimate of B99b.

(iii) The observed  $R$ – $\Gamma$  correlation is well explained by varying  $\beta$ . It suggests that  $\beta$  may be the main parameter controlling the X-ray spectrum.

(iv) The results of the simulations are in good agreement with the analytical description of B99a,b. We improved the analytical model by accounting for the attenuation of the reflection component by the hot plasma atop the disc (equation 9).

(v) The optical and UV polarization properties of the AGN are sensitive to the dynamics of the corona. The polarization data provide an independent indication for the mildly relativistic bulk motion.

## ACKNOWLEDGMENTS

This work was supported by the Italian MURST grant COFIN98-02-15-41 (JM), the Swedish Natural Science Research Council (AMB, JP), the Anna-Greta and Holger Crafoord Fund (JP), and RFBR grant 00-02-16135 (AMB). We thank Andrzej Zdziarski and Marat Gilfanov for providing the  $R$ – $\Gamma$  correlation data, and Andrei F. Illarionov for comments on the manuscript.

## REFERENCES

- Anders E., Ebihara M., 1982, *Geochim. Cosmochim. Acta*, 46, 2363  
 Antonucci R., 1993, *ARA&A*, 31, 473  
 Beloborodov A. M., 1998, *ApJ*, 496, L105  
 Beloborodov A. M., 1999a, in Poutanen J., Svensson R., eds, *ASP Conf. Ser. Vol. 161, High Energy Processes in Accreting Black Holes*. Astron. Soc. Pac., San Francisco, p. 295 (B99a)  
 Beloborodov A. M., 1999b, *ApJ*, 510, L123 (B99b)  
 Beloborodov A. M., 1999c, *MNRAS*, 305, 181  
 Beloborodov A. M., 2001, *Adv. Space Res.*, in press  
 Beloborodov A. M., Poutanen J., 1999, *ApJ*, 517, L77  
 Bisnovatyĭ-Kogan G. S., Blinnikov S. I., 1977, *A&A*, 59, 111  
 Brandt W. N., 1999, in Poutanen J., Svensson R., eds, *ASP Conf. Ser. Vol. 161, High Energy Processes in Accreting Black Holes*. Astron. Soc. Pac., San Francisco, p. 166  
 Di Salvo T., Done C., Życki P. T., Burderi L., Robba N. R., 2001, *ApJ*, 547, 1024  
 Esin A. A., Narayan R., Cui W., Grove J. E., Zhang S.-N., 1998, *ApJ*, 505, 854  
 Galeev A. A., Rosner R., Vaiana G. S., 1979, *ApJ*, 229, 318  
 George I. M., Fabian A. C., 1991, *MNRAS*, 249, 352  
 Gierliński M., Zdziarski A. A., Done C., Johnson W. N., Ebisawa K., Ueda Y., Haardt F., Philips B. F., 1997, *MNRAS*, 288, 958  
 Gierliński M., Zdziarski A. A., Poutanen J., Coppi P. S., Ebisawa K., Johnson W. N., 1999, *MNRAS*, 309, 496  
 Gilfanov M., Churazov E., Revnivtsev M., 1999, *A&A*, 352, 182  
 Gilfanov M., Churazov E., Revnivtsev M., 2000, *Proc. 5th CAS/MPG Workshop on High Energy Astrophysics*, in press (astro-ph/0002415)  
 Haardt F., Maraschi L., 1993, *ApJ*, 413 507 (HM93)  
 Haardt F., Maraschi L., Ghisellini G., 1994, *ApJ*, 432, L95  
 Koratkar A., Blaes O., 1999, *PASP*, 111, 1  
 Liang E. P. T., 1979, *ApJ*, 231, L111  
 Madejski G. M. et al., 1995, *ApJ*, 438, 672  
 Magdziarz P., Zdziarski A. A., 1995, *MNRAS*, 273, 837  
 Malzac J., Jourdain E., 2000, *A&A*, 359, 843  
 Miller K. A., Stone J. M., 2000, *ApJ*, 534, 398  
 Nayakshin S., Kazanas D., Kallman T. R., 2000, *ApJ*, 537, 833  
 Poutanen J., 1998, in Abramowicz M. A., Björnsson G., Pringle J., eds, *Theory of Black Hole Accretion Disks*. Cambridge Univ. Press, Cambridge, p. 100  
 Poutanen J., Svensson R., 1996, *ApJ*, 470, 249 (PS96)  
 Poutanen J., Krolik J. H., Ryde F., 1997, *MNRAS*, 292, L21  
 Revnivtsev M., Gilfanov M., Churazov E., 2000, *A&A*, submitted (astro-ph/9910423)  
 Ross R. R., Fabian A. C., Young A. J., 1999, *MNRAS*, 306, 461  
 Rybicki G. B., Lightman A. P., 1979, *Radiative Processes in Astrophysics*. Wiley, New York  
 Stern B. E., 1985, *SvA*, 29, 306  
 Stern B. E., Begelman M. C., Sikora M., Svensson R., 1995a, *MNRAS*, 272, 291  
 Stern B. E., Poutanen J., Svensson R., Sikora M., Begelman M. C., 1995b, *ApJ*, 449, L13  
 Stockman H. S., Moore R. L., Angel J. R. P., 1984, *ApJ*, 279, 485  
 Svensson R., 1996, *A&AS*, 120, 475  
 Tout C. A., Pringle J. E., 1992, *MNRAS*, 259, 604  
 Wardziński G., Zdziarski A. A., 2000, *MNRAS*, 314, 183  
 Zdziarski A. A., Johnson W. N., Poutanen J., Magdziarz P., Gierliński M., 1997, in Winkler C., Courvoisier T. J.-L., Durouchoux Ph., eds, *ESA SP-382, Proc. 2nd INTEGRAL Workshop, The Transparent Universe*. ESA, Noordwijk, p. 373  
 Zdziarski A. A., Lubiński P., Smith D. A., 1999, *MNRAS*, 303, L11  
 Życki P. T., Krolik J. H., Zdziarski A. A., Kallman T. R., 1994, *ApJ*, 437, 597

This paper has been typeset from a  $\text{\TeX}/\text{\LaTeX}$  file prepared by the author.



## **5.2 “The optical and X-ray flickering of XTE J1118+480”**

Malzac J., Belloni T., Spruit H. C., Kanbach G., *Astronomy and Astrophysics*, v.407, p.335-345 (2003)



## The optical and X-ray flickering of XTE J1118+480

J. Malzac<sup>1,2</sup>, T. Belloni<sup>2</sup>, H. C. Spruit<sup>3</sup>, and G. Kanbach<sup>4</sup>

<sup>1</sup> Institute of Astronomy, Madingley Road, Cambridge, CB3 0HA, UK

<sup>2</sup> Osservatorio Astronomico di Brera, Via Brera 28, 20121 Milano, Italy

<sup>3</sup> Max-Planck-Institut für Astrophysik, Postfach 1317, 85741 Garching, Germany

<sup>4</sup> Max-Planck-Institut für Extraterrestrische Physik, Postfach 1317, 85741 Garching, Germany

Received 21 January 2003 / Accepted 27 May 2003

**Abstract.** We use both time-domain and Fourier techniques to study the correlated optical/X-rays variability in the black hole X-ray nova XTE J1118+480. Its X-ray timing properties such as the shape of the X-ray power spectrum and cross-correlation functions (CCFs) between X-ray energy bands, the slight decrease of rms variability from 30% in the 2–5.9 keV to 19% in the 15.5–44.4 keV band, as well as the X-ray hardness/flux anti-correlation are very similar to what is found in other black hole binaries in the hard state. The optical/X-ray CCF is virtually independent of the X-ray energies. The optical flux appears to be correlated not only with the X-ray flux but also with the X-ray spectral variability. Both the coherence function and the lags between optical and the X-rays are Fourier frequency dependent. The optical/X-ray coherence function reaches its maximum ( $\sim 0.3$ ) in the 0.1–1 Hz range and the time-lags decrease with frequency approximatively like  $f^{-0.8}$ . The correlation between X-ray and optical light curves appears to have time-scale-invariant properties. The X-ray/optical CCF maintains a similar but rescaled shape on time-scales ranging at least from 0.1 s to few 10 s. Using the event superposition method we show that the correlation is not triggered by a single type of event (dip or flare) in the light curves. Instead, optical and X-ray fluctuations of very different shapes, amplitudes and time-scales are correlated in a similar mode where the optical light curve is seemingly related to the time derivative of the X-rays.

**Key words.** black hole physics – stars: individual: V\*KV UMa – X-rays: binaries – X-rays: individuals: XTE J1118+480

### 1. Introduction

The X-ray nova XTE J1118+480 (=V\* KV UMa), was discovered by the Rossi X-Ray Timing Explorer (*RXTE*) All-Sky Monitor (*ASM*) on March 29 2000 (Remillard et al. 2000) as a slowly rising source. The outburst lasted a few months with a plateau-like X-ray light-curve that rapidly fell down around mid-July. A post-analysis revealed an earlier outburst in January 2000. The optical spectrophotometry proved a low mass X-ray binary system containing a black hole of at least  $6 M_{\odot}$  (Mc Clintock et al. 2001a; Dubus et al. 2001; Wagner et al. 2001). The interstellar extinction towards the source is exceptionally low (Garcia et al. 2000). This fact allowed an unprecedented wavelength coverage (Mauche et al. 2000; Hynes et al. 2000; McClintock et al. 2001b; Hynes et al. 2003; Chaty et al. 2003 and reference therein). In the radio to optical bands, a strong non-thermal component was associated with synchrotron emission from a powerful jet or outflow (Fender et al. 2001). In the optical to EUV bands the spectral energy distribution is dominated by a thermal component from the accretion disc. The X-ray emission consists in a typical powerlaw spectrum with photon index  $\Gamma \sim 1.8$ . Such a spectrum is generally associated with Comptonisation in

the hot inner part of the disc or corona. In the case of XTE J1118+480, alternative interpretations in terms of jet emission through inverse Compton (Georganopoulos et al. 2002) or synchrotron (Markoff et al. 2001) were also put forward.

The X-ray variability is characterized by a flaring activity on time-scales of a few seconds typical of accreting black hole sources (Revnivtsev et al. 2000). A  $\sim 0.1$  Hz quasi-periodic oscillation (QPO) was reported by the same authors and subsequently confirmed by the *ASCA* data (Yamaoka et al. 2000) as well as other *RXTE* observations where it appeared to be variable (Wood et al. 2000). The simultaneous *RXTE/HST* observations showed that a similar QPO is also present in the *HST* data and that the X-rays and optical/UV bands are correlated on time-scales of seconds (Haswell et al. 2000; Hynes et al. 2003).

Kanbach et al. (2001, hereafter K01) performed 4 observations on the nights of 4, 5, 6, and 7 July 2000, shortly before the end of the outburst. They combined simultaneous observations with *RXTE* and the rapid optical photo-meter *OPTIMA* (Straubmeier et al. 2001) attached to the 1.3 m telescope on Mt Skinakas, Crete. They studied the X-ray and optical auto-correlation functions (ACFs) and X-ray/optical cross-correlation (CCFs). They found the optical ACF to be significantly narrower than the X-ray ACF. The full width at

mid height (FWMH) of the two ACFs differs by a factor  $>2$ . They found the correlation between the optical and X-ray light curves to be surprisingly complex. The CCF rises very quickly at positive optical lags, peaks around 0.5 s and then declines slowly at larger lags. Therefore, the optical light curve tends to be delayed relatively to the X-rays by a relatively long time (of order of 1 s). Strikingly, the two bands appear to be anti-correlated at negative optical lags indicating a systematic optical dip 1–2 s before the X-rays reach their maximum. As this feature suggests that the optical band “knows” about what will happen in the X-rays about 1 s later, it was named “precognition dip” by K01. K01 further showed that the detailed shape of the CCF is variable on time-scales as short as 30 s. Spruit & Kanbach (2002, hereafter SK02) analyzed this variability of the CCF in terms of a principal component analysis. They found that there are two systematic components which vary statistically independently. Both have the shape of a broad dip followed by a sharper peak, but their duration differs by a factor of about 3.

K01 argued that those characteristics rule out reprocessing as the origin of the optical variability and favors synchrotron emission. Merloni et al. (2000) had previously interpreted the correlated X-ray/optical variability in terms of thermal Comptonisation of synchrotron radiation in an accretion disc corona. It is not clear however how such a model could reproduce the complicated shape of the cross-correlation function. K01 proposed a somewhat different scenario where the X-rays are produced within a few hundred Schwarzschild radii from the black hole and the optical is produced by synchrotron effect at much larger distance, in a magnetic outflow. In this framework the optical lags would be due to the travel-time of a perturbation from the disc to the optical photo-sphere of the outflow. This scenario however (as well as reprocessing models) does not explain the “precognition dip”.

The only other source for which simultaneous X-optical observations at millisecond time resolution have been reported is GX 339-4, where an anti-correlation between the X-rays and optical, similar to the “precognition” dip, was observed (Motch et al. 1982). Fabian et al. (1982) interpreted the optical emission as cyclo-synchrotron radiation produced in the inner parts of the accretion flow.

In this paper we use the data of K01 to investigate further the optical X-ray correlation in XTE J1118+480. The optical observations and data processing are described in K01 and SK02. The PCA X-ray light curves used in these previous analyses were decomposed into 3 energy bands: 2–5.9 keV (referred hereafter as b1), 5.9–15.5 keV (b2) and 15.5–44.4 keV (b3). In order to study a range of time-scales, we used only the data for which we had a sufficiently long continuous exposure. The analysis was performed over 11 light curves segments of 590 s duration and 3 ms resolution taken during the four observation nights. Most of the results shown in this paper are averaged over all these data segments. The paper is divided into three sections presenting successively the results from the time-domain, Fourier domain and superposition analysis. These results are then summarized and briefly discussed in Sect. 5.

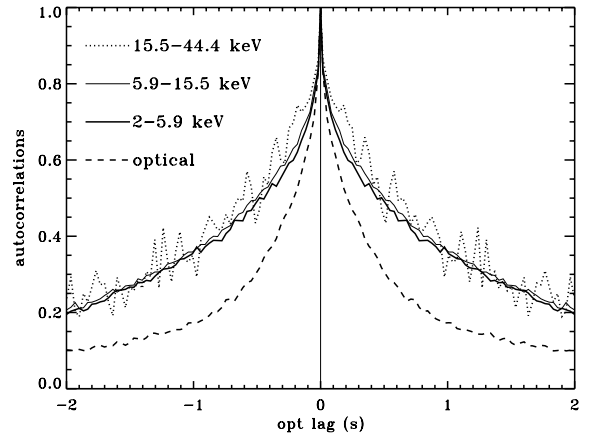


**Fig. 1.** Optical and X-ray ACFs of the photon flux in the X-ray bands b1, b2, b3 and optical. In this figure as well as in Figs. 2 and 3, the low frequency noise on time-scales longer than 100 s was removed by dividing the light curves by the piecewise linear trend. This piecewise linear trend is defined as the linear interpolation between the 100 s average count rate computed at time bins separated by 50 s. The presence of noise due to the optical telescope oscillations (see SK02 and Sect. 3.2) significantly affects the shape of the ACF. Therefore, only the 2 segments in which these oscillations are minimal were used to estimate the optical ACF. For clarity, the ACFs were rebinned with 30 ms resolution.

## 2. Time domain analysis

### 2.1. X-ray properties

We first examine the properties of the X-ray light curves in the time domain. The X-ray ACFs in the three energy bands are, within the uncertainties, indistinguishable from the total X-ray ACF and broader than the optical ACF (as shown in Fig. 1). The FWHM of the X-ray CCFs is  $\sim 1$  s while that of the optical is only of 0.4 s. The X-ray CCFs of the different energy bands, shown in the panels (a) and (b) of Fig. 2, are all strongly peaked at lags  $<30$  ms with a shape very similar to that of the ACFs. The different energy bands are thus strongly correlated at (nearly) 0 lag. These results are very similar to that of Maccarone et al. (2000) for Cygnus X-1.

We then searched for correlations between variations of the X-ray hardness and the X-ray flux. We computed the ratio of the two light curves in two energy bands b3 and b1. The resulting time series represents the time dependent hardness b3/b1. Then we computed its CCF with the third energy band b2. In practice, the hardness ratio b3/b1 cannot be computed for the b1 time bins containing 0 counts. We thus rebinned the light curves with a 90 ms resolution before estimating b3/b1, so that zero count bins are reduced to a negligible fraction of the total number of bins. For the few remaining bins with zero count, b3/b1 was arbitrarily set to the time averaged hardness ratio.

Panel of (c) of Fig. 2 displays the resulting hardness vs. flux CCF. Clearly the count rate in the b2 band is strongly anti-correlated with hardness at (almost) zero lags. The source is thus softer when brighter for fluctuations of time-scale of seconds. We note also that this CCF shape is similar to the shape of the X-ray ACFs, suggesting that spectral variations map very closely the flux. We also computed the hardness-flux

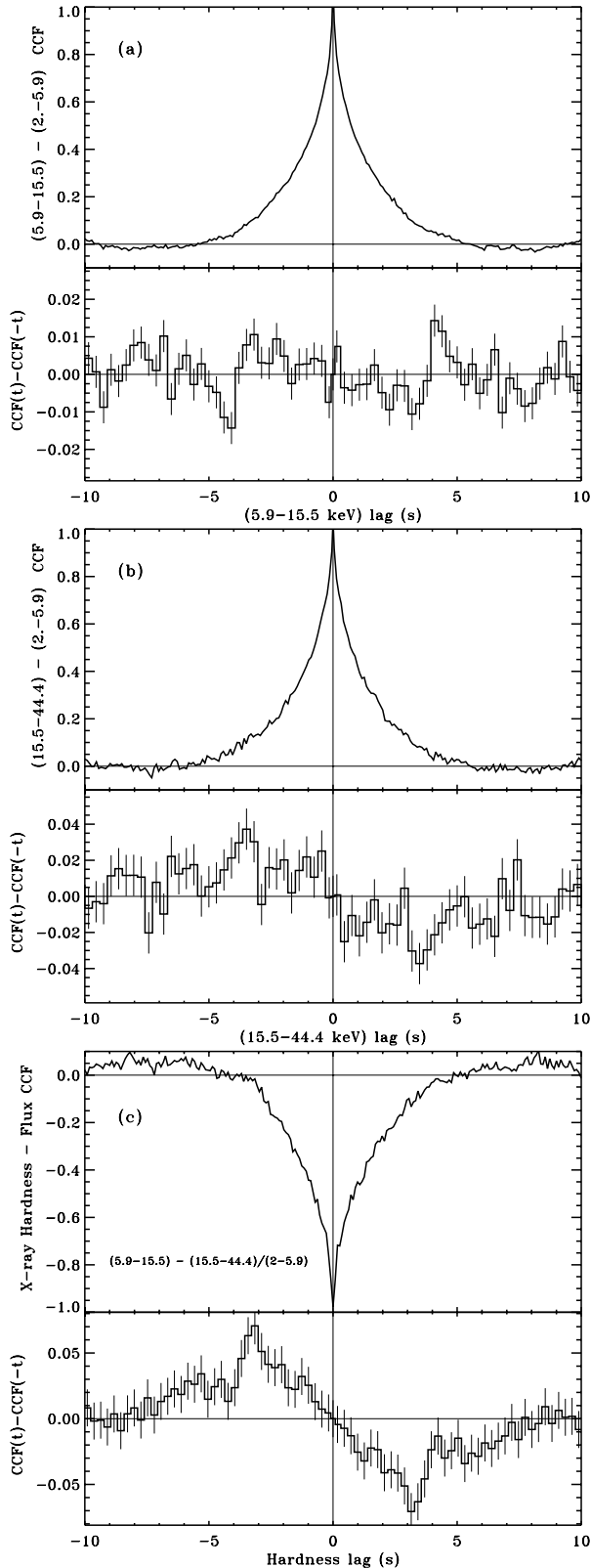


**Fig. 2.** X-ray CCFs and their anti-symmetric parts  $CCF(t) - CCF(-t)$ . **a)** flux in band b2 vs. flux in band b1. **b)** flux in band b3 vs. flux in band b1. **c)** hardness ratio b3/b1 vs. flux in band b2. The one sigma uncertainties on the anti-symmetrized CCFs were estimated from the photon noise in the original data using the standard statistical error propagation method. The CCFs and anti-symmetrized CCFs were rebinned with 90 ms and 300 ms resolution respectively.

correlation for the different combinations between our three energy bands and found very similar results. The b2/b1-b3 CCF appeared noisier indicating that the amplitude of the fluctuations of the b2/b1 hardness is lower than that of b3/b1 or b3/b2. Such a hardness/flux anti-correlation looks similar to what found in Cygnus X-1 in the hard state (see e.g. Li et al. 1999; Feng et al. 1999)

The antisymmetrized CCFs (i.e.  $CCF(t) - CCF(-t)$ ), also shown in Fig. 2, indicate that the X-ray CCFs as well as the hardness flux CCF are asymmetric for lags in the approximate range 1–5 s (outside this range the poor statistics in the XTE J1118+480 data did not enable us to firmly establish any asymmetry). The shape of the asymmetries suggests that the spectrum is relatively harder during the rising phase of a flare than its decay. In term of lags between X-ray bands this implies that the soft band is delayed with respect to the hard one. This kind of asymmetry is thus opposite to that found by Maccaronne et al. (2000) in the X-ray CCFs of Cygnus X-1, and more generally to the hard lags often reported in hard-state sources.

## 2.2. Optical/X-ray correlations

We then investigated the dependence of the optical/X-ray correlation on the X-ray energies. We found that the optical/X-ray CCF does not depend significantly on the X-ray band considered. Actually, our 3 optical/X-ray CCF are identical within the uncertainties, as shown in Fig. 3a.

The optical/X-ray *hardness* CCF (shown in Fig. 3b) is qualitatively similar to the optical/X-ray *flux* CCFs modulo a mirror symmetry around the X-ray axis. The optical flux and X-ray hardness are indeed anti-correlated at positive optical lags and positively correlated at negative lags. This feature derives naturally from the X-ray flux hardness anti-correlation demonstrated in the previous section. It follows that the optical flux is correlated not only with the X-rays count rate but also with the X-ray spectral variability. Similar results were found for the hardness ratios computed with the different combinations of the 3 bands.

The time-domain analysis presented above provides only information (such as time lags) that is averaged over all time-scales present in the signal. However, in general, the properties of time-series or the correlation between two time-series does depend on the time-scale considered. In order to study the dependence of the optical/ X-ray CCF on the time-scale of the fluctuations we thus filtered the light curves before computing the CCF keeping only a small range of time-scales in both signals.

The results are displayed in Fig. 4. For all of the different time-scales considered, both the anti-correlation at negative lags and positive correlation at positive lags is present. The characteristics lags appears to depend on the time scale of the fluctuations. The lag of the optical peak increases from  $\sim 30$  ms for time-scales shorter than 0.1 s to  $\sim 3$  s for the 10–100 s fluctuations. Similarly the optical dip ranges from  $\sim -6$  ms to  $\sim -30$  s, so that, in the rescaled plot, we see both the optical peak and dip shifting toward negative lags as the time-scale of the

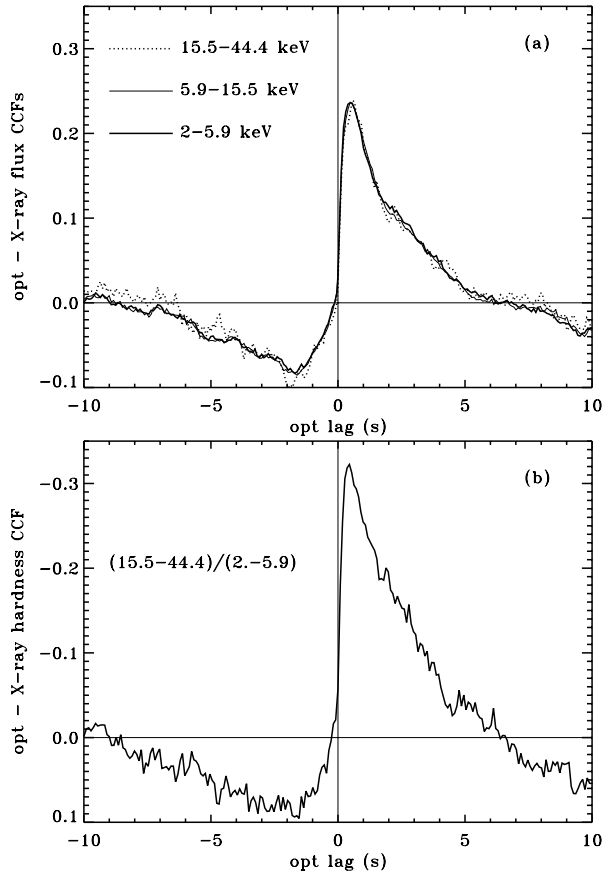


**Fig. 3.** Correlations between X-ray and the optical. and X-ray flux. **a)** X-ray flux vs. optical flux CCF for the 3 X-ray bands. **b)** X-ray hardness vs. optical flux CCF. For clarity the CCFs were rebinned with a 90 ms resolution.

fluctuations increases. Still in the rescaled plot, the optical flare appears narrower at longer fluctuations.

Despite these significant differences, the overall shape of the CCF appears similar but rescaled over a range covering more than three decades of time-scales.

### 3. Fourier analysis

In the following, we will use a Fourier analysis to explore more quantitatively the dependence of the optical/X-ray correlation in XTE J1118+480 on the time-scale of the fluctuations.

#### 3.1. Power density spectra

Figure 5a shows the X-ray and optical power density spectra (PDS). The PDS were computed, averaged, rebinned and normalized to the total rms variability as described in Nowak et al. (1999). The counting noise was approximated by a white noise component that was then subtracted from the total PDS.

The fractional rms variability amplitude integrated over the frequency range  $10^{-3}$ – $10^2$  Hz is about 26% in the X-rays and 13% in the optical. The optical and total X-ray power spectra were already shown and discussed in SK02. Here we will just note the similarities of the X-ray PDS with that of other black hole candidates in the hard state such as the plateau like

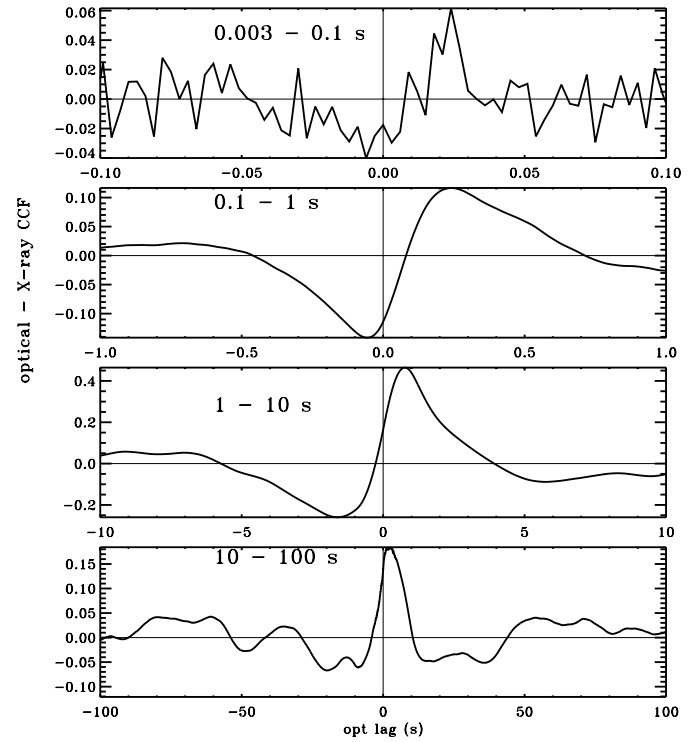


**Fig. 4.** Optical vs. X-ray CCFs for different time-scales of the fluctuations. The CCFs were computed after both light curve have been filtered keeping only the time-scales in the range indicated. High frequency noise was removed applying a box car filter, the low frequency trend was removed by dividing the light curve by the piecewise linear trend.

shape up to  $\sim 0.1$  Hz and then a power law component. We note also that in our July observation the X-ray PDS is slightly different from that found in the earlier observation of Revnivtsev et al. (2000) with a break at higher frequencies (0.1 Hz instead of 0.03 Hz) a flatter power-law component with slope  $\sim 1.4$  as compared to the 1.6 slope reported by Revnivtsev et al. 2000. This evolution of the power spectrum was accompanied by a significant reduction of the total rms amplitude that was 40% during the observation of Revnivtsev et al. More strikingly, the power spectra of Fig. 5a show little to no evidence for the QPO reported in previous observations both in the X-ray and optical (see e.g. for comparison Fig. 1 of Revnivtsev et al. 2000). This is however consistent with the previously reported trend in the evolution of the timing properties of the source during the outburst. Indeed the *RXTE* monitoring campaign showed that all the characteristics frequencies increased with time and the QPO became much weaker (Wood et al. 2000; Hynes et al. in prep.).

As shown in Fig. 6, the X-ray PDS depends only slightly on energy. We find that the PDS in the two lower energy bands (b1 and b2) are extremely similar. On the other hand, at higher energy (b3) the shape of the PDS differs significantly at low frequency and the integrated rms amplitude is lower (19% instead of  $\sim 30\%$  in b1 and b2). A similar energy dependence of the rms variability amplitude is reported in Cygnus X-1 in the hard state (e.g. Nowak et al. 1999).

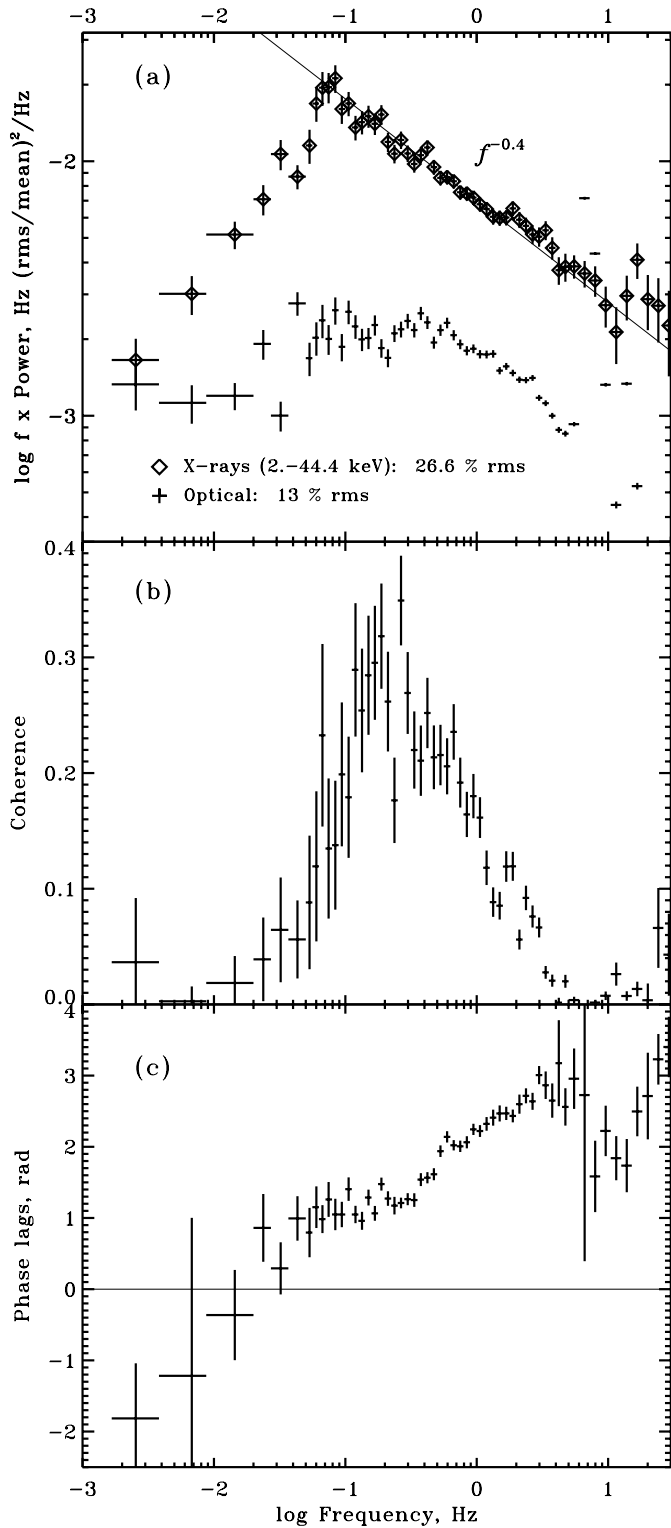


**Fig. 5.** The optical/X-ray correlation in the Fourier domain. **a)** X-ray and optical power spectra. The counting noise was subtracted (see Sect. 3.1). **b)** X-ray/optical coherence. **c)** phase-lags as function of Fourier frequency. A positive lag implies that the optical is delayed with respect to the X-rays. Uncertainties were computed according to Eq. (8) of Vaughan & Nowak (1997) for the coherence, and Eq. (16) of Nowak et al. (1999) for the phase-lags. All error bars are at the 1 sigma level.

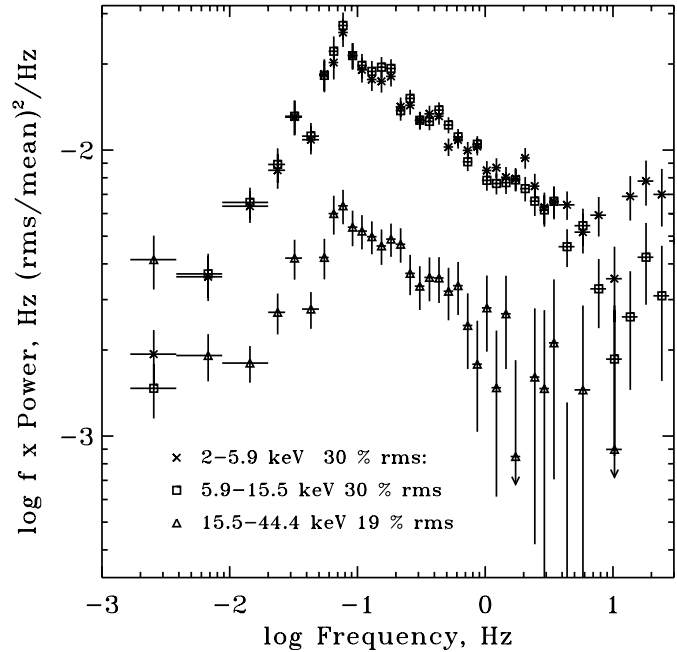


**Fig. 6.** X-ray power spectra in bands b1, b2 and b3. The counting noise was subtracted (see Sect. 3.1).

### 3.2. Coherence and lags

The coherence function represents the degree of linear correlation between two time series as a function of Fourier frequency (Vaughan & Nowak 1997). The coherence function between different X-ray bands appears to be unity over a wide range of frequencies in black hole candidates (Nowak et al. 1999). We found a similar behaviour in XTE J1118+480 as shown in Fig. 7a.

The X-ray phase lags between energy bands are shown in Fig. 7b. Due to the poor statistics of the data, the phase lags are very difficult to measure. In order to improve the statistic we averaged the frequency bins over a broad range of frequencies (nearly a decade). Even so, we get essentially upper limits that are above the typical amplitude of the hard lags reported in Cyg X-1 or GX 339-4 in the hard state. There is however an indication that the lags are increasing with frequency, and surprisingly, the lags tend to be negative at low frequency. In particular in the frequency range  $2 \times 10^{-3}$ – $2 \times 10^{-2}$  Hz, the phase lag between b3 and b1, is detected at the 3 sigma level and is negative. This implies that the soft band leads the hard band by 2 to 20 s in this frequency range. This is qualitatively consistent with the asymmetry found in the X-ray CCFs (see Sect. 2.1). This result should however be regarded with caution since it involves frequencies that correspond to time scales approaching the duration of the light-curve segments. In an attempt to improve the statistics, we used public *RXTE* archive data to compute the phase-lag spectra with a longer exposure time. These additional data consisted in a set of observations made between April 15 and May 23, 2000 with a total exposure time of 33 ks. Unfortunately, although we found a similar trend for negative lags at low frequencies, the results were still inconclusive.

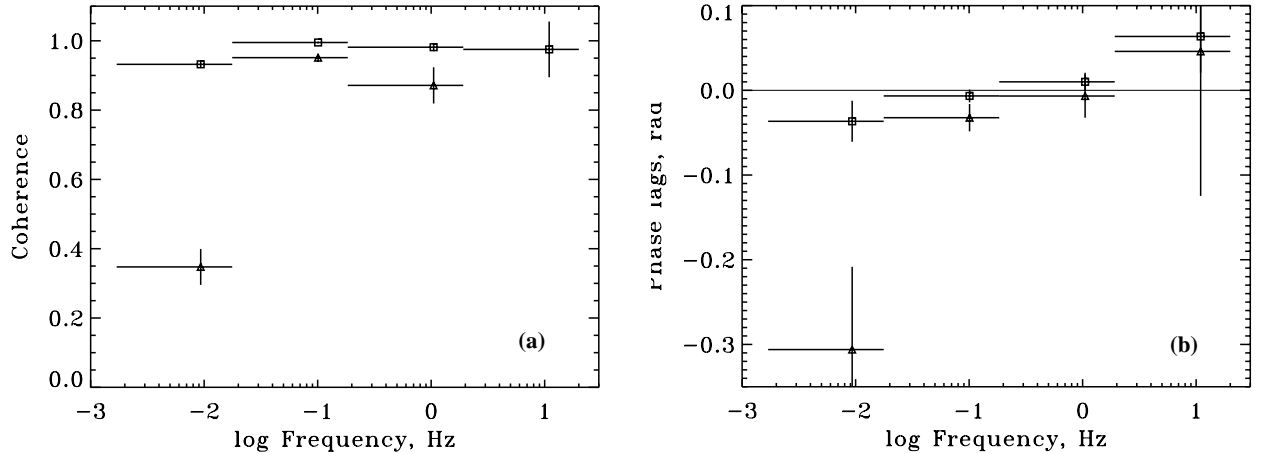


**Fig. 7.** a) X-ray coherence and b) phase lags. Squares stand for b2 versus b1, triangles for b3 vs. b1. Due to the high noise level it has not been possible to estimate conveniently the b3 vs. b1 coherence in the higher frequency bin.

On the other hand, the data enable us to clearly detect the optical light curve lagging the X-ray one. The optical phase lags as a function of Fourier frequency are displayed in Fig. 5c. These phase-lags increase significantly with the Fourier frequency covering a broad range of angles centered around  $\pi/2$ . This leads to time lags (shown in Fig. 8) decreasing with frequency approximately like  $f^{-0.8}$  in the range  $10^{-2}$ – $10$  Hz and spanning roughly  $10^{-2}$ – $10$  s over this frequency range. The frequency dependence of the lags is not exactly a power law as additional structures are apparent, in particular around 0.5 Hz. Such structures are even more apparent in the phase lag diagram. Interestingly, as in the case of X-ray lags the data suggest the presence of negative lags at low frequencies. The significance of these negative lags is however very low.

The optical vs. X-ray coherence function (shown in Fig. 5b) is frequency dependent as well. It reaches a maximum in the 0.1–1 Hz range and decreases rapidly both at lower and higher frequency. The overall coherence is not very high ( $<0.3$ ) indicating that only a relatively small fraction of the optical and X-ray variability are actually correlated. As the coherence gives only the *relative* importance of correlated variability, it is not clear whether the observed frequency dependence is a property of the physical process producing the correlation, or if it is driven mainly by changes in the amplitude of the uncorrelated fraction of the variability. We note that part of the loss of coherence around 10 Hz is due to the artifact QPO visible in the optical power spectrum that is due to telescope oscillations (see Spruit & Kanbach 2002).

This Fourier analysis is consistent with the CCF shape. Basically the CCF plots the coherence as a function of time-lags weighted with the fractional amplitudes of variability at the frequencies producing such lags. The CCF indeed appears to peak at values  $\sim 0.3$  at lags  $\sim 0.5$  s i.e. roughly corresponding to the frequency range where coherence is maximum.

In addition, the reduction of the optical time-lags with frequency while the phase-lags increase is qualitatively consistent with the changes of the optical peak lag in the CCF at different time-scales of the fluctuations (shown in Fig. 4 and discussed in Sect. 2.2). On the other hand the Fourier time-lag diagram does not show any evidence for the optical dip at negative lags

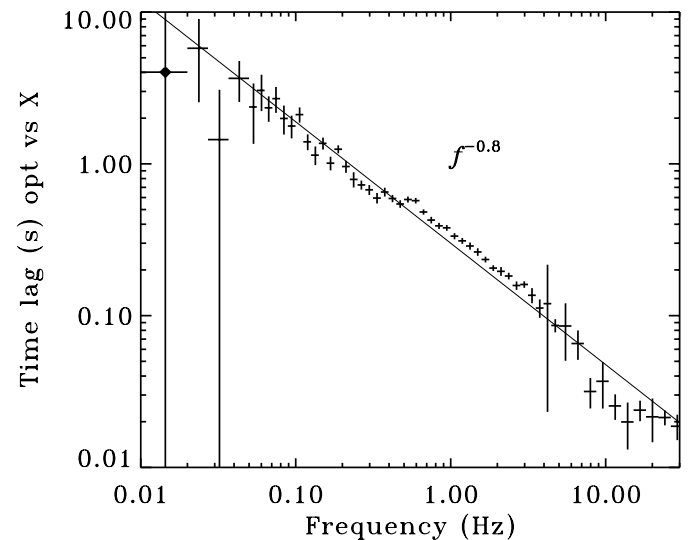


**Fig. 8.** Frequency dependent optical time-lags. Filled diamonds stand for negative lags.

apparent in the optical X-ray CCF. Indeed, since in the Fourier method, the light curves are decomposed over cosine functions, an anti-correlation at negative optical lags appears exactly in the same way as a positive correlation at positive lags. Thus, the optical dip and peak information are all mixed together in the Fourier representation.

#### 4. Superposed shot and dip analysis

Besides Fourier and time domain analysis, there is a third method occasionally used to study the variability of X-ray binaries. It is based on the selection and averaging of flares events in the light curves.

In the following we will apply a method similar to that used by Negoro et al. (2001) to study the average shot profile in Cyg X-1. We select flare events in the lower energy light curve (b1, 2–5.9 keV). These shots are selected according to the same criteria as those used by Negoro et al. (2001): the peak count rate of the shot is greater than  $f$  times the local count rate as

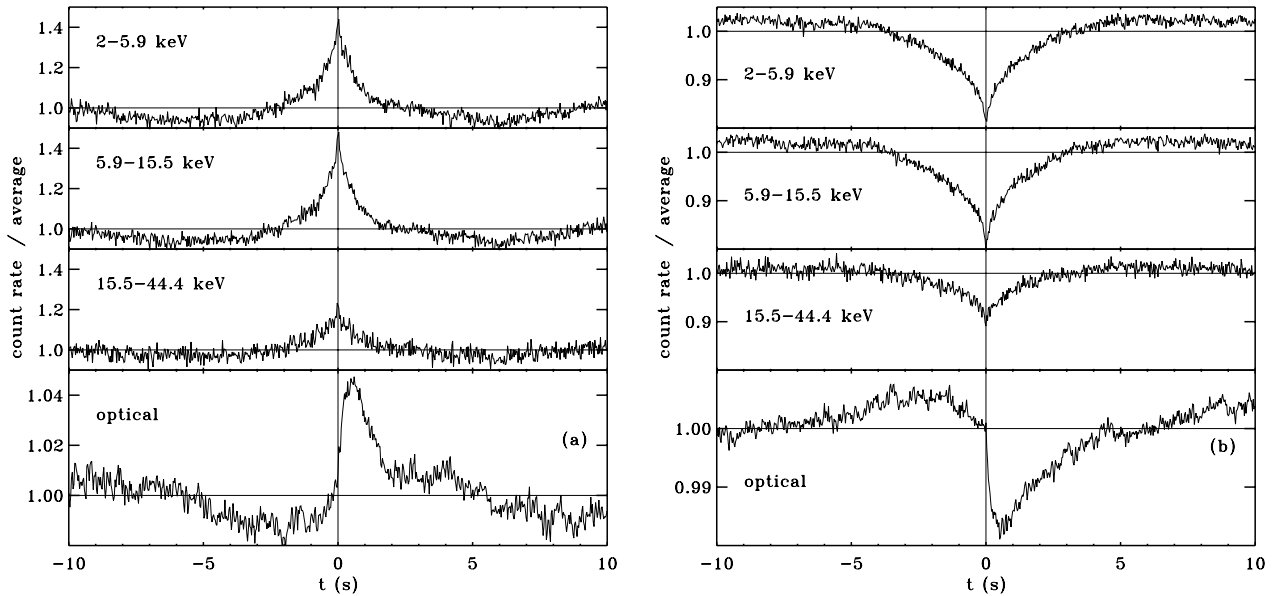


**Fig. 9.** Results from the shot (panel a) and dip (panel b)) superposition technique when the flares or dips are selected in band b1. The selection parameters (see Sect. 4) are  $f = 2$ ,  $t_p = 8$  s,  $t_m = 32$  s in both panels.

obtained from an average over time  $t_m$ . The peak bin is further required to have the maximum count-rate over bins within  $t_p$  before and after the peak bin. The selected shots are then peak aligned and averaged. The corresponding pieces of light curves in the b2, b3 and optical band are centered on the time bin corresponding to the b1 peak and averaged in the same way.

Figure 9a shows the results for  $f = 2$ ,  $t_p = 8$  s and  $t_m = 32$  s. The light curves were rebinned on 30 ms time bins before applying the shot selection. For such parameters the resulting average X-ray shot is slightly asymmetric, with a duration of  $\sim 10$  s. The b2 and b3 bands appears to present shots that are similar to that in the b1 band. This illustrates the high degree of coherence between the different energy bands.

The shot in the b3 band has a lower amplitude than the b1 and b2 shots. This is consistent with the energy dependent power spectrum indicating a lower amplitude of variability in the higher energy band. In addition, this enables us to see in a more direct way the spectral evolution leading to the anti-correlation between X-ray hardness and flux discussed in Sect. 2. The average optical light curve corresponding to the shots is similar in shape to that of the optical/ X-ray CCF. This suggests, as previously noted by Spruit & Kanbach (2002), that the shape of the CCF is representative of the shape of the optical light curve as a response to a shot event.

Then it is interesting to see whether the optical light curve responds only to X-ray flares or is also correlated to other types of events occurring in the X-ray light curve. We thus performed a similar analysis but instead of flares, we selected dips in the b1 band. The selecting criteria were that the minimum count rate of the dip is lower than  $1/f$  times the local count rate as obtained from an average over  $t_m$ . The minimum bin is further required to have the minimum count-rate over the bins within  $t_p$  on either side.

The results are shown in Fig. 9b. Surprisingly, the answer is that the optical responds to X-ray dips in a similar but inverted

way as it responds to the X-ray flares. The optical flux rises a few seconds before the minimum in the X-ray light curve, at  $t = 0$  it decays abruptly with a minimum half a second after the X-ray dip. The panels (a) and (b) of Fig. 9 are actually very similar but with inverted count-rate axis.

To learn about the response of the X-rays to optical fluctuations we performed a similar shot and dip analysis using the optical band as the selecting light curve. The results are shown in Fig. 10. The X-ray shots and dips are not simply the same as in Fig. 9 shifted by  $\sim 0.5$  s as one would expect if the correlation was linked only to the X-ray dips and shots. The X-ray response to optical shots and dips is very asymmetric. The optical shots are associated with an X-ray flux that rises slowly during a few seconds and decays sharply in  $\sim 0.5$  s. There is an indication for the presence of an X-ray dip after the peak in the optical. A similar asymmetry is apparent in the dip analysis. Thus from Figs. 9 and 10, it appears that the correlated optical and X-ray shots and dips all have a profile resembling that of the optical/X-ray CCF (modulo the relevant symmetries).

The superposition method is far less rigorous than usual time-domain and Fourier techniques. In particular the results are affected by strong biases. It tends to favor a certain range of time-scales and amplitude depending on the selection criteria. In general, the selected events are not representative of the whole variability of the source. It could be also, that the light curves are not made of a superposition of shots at all. Moreover a description of the variability of accreting black hole sources in terms of shots models (e.g. Poutanen & Fabian 1999 and reference therein) requires, in general, events with a broad range of time-scales and amplitude. The superposed events are not representative of a clearly defined scale, rather, they represent an average over a range of scales that is poorly controlled.

The drawbacks of the method can be taken into our advantage. By changing the selection criteria one can select (in a very qualitative way) the time-scale and amplitude of the

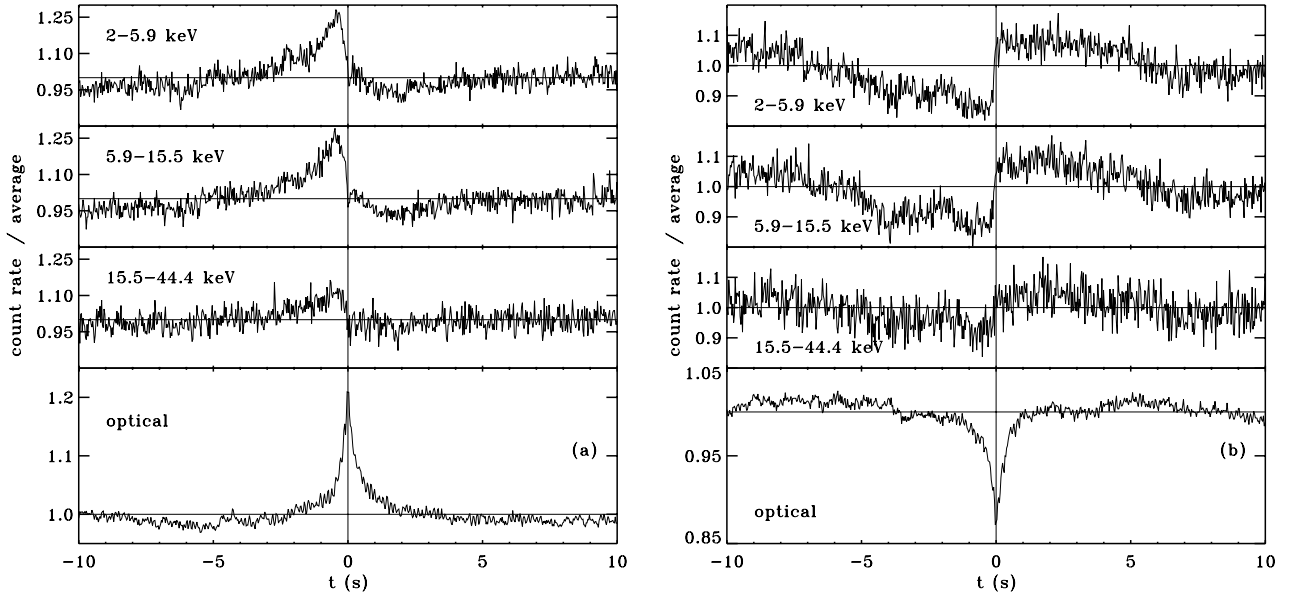


**Fig. 10.** Results from the shot (panel a) and dip (panel b) superposition technique when the flares or dips are selected in the optical band. The selection parameters (see Sect. 4) are  $f = 1.2$ ,  $t_p = 8$  s  $t_m = 32$  s in both panels.

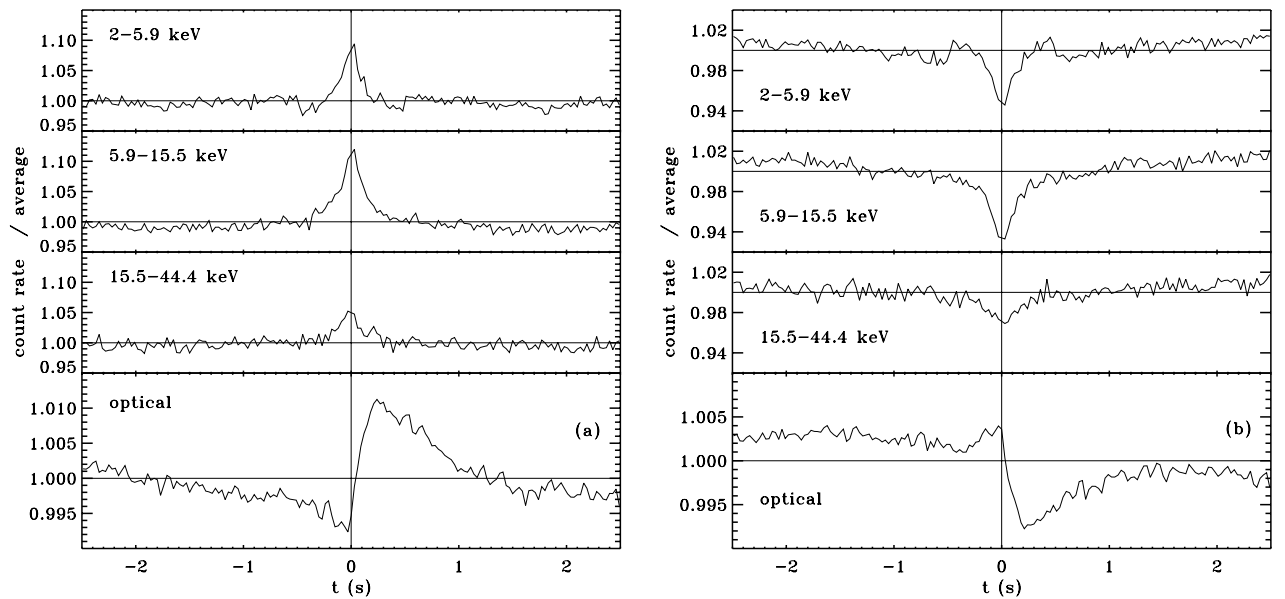


**Fig. 11.** Results from the shot (panel a) and dip (panel b) superposition technique using band b1 as the selecting band. The selection parameters (see Sect. 4) are  $f = 1.8$ ,  $t_p = 0.5$  s and  $t_m = 5$  s.

typical selected events. For instance, Fig. 11 shows the results of the shot and dip superposition for  $t_p = 0.5$  s and  $t_m = 5$  s and  $f = 1.8$  selected in the b1 band. The resulting average profiles have clearly a lower amplitude and shorter duration ( $< 1$ ) s. The interesting thing is that the both the X-ray and optical light curves look like a rescaled version of Fig. 9. In particular, the softening of the spectrum with the enhanced count rate, and the presence of an optical dip and flare respectively before and after the X-ray peak. The superposition analysis thus confirms that both the optical pre-dip and post-peak are present over a wide range of time-scales.

More importantly, the superposition method, despite all its biases, reveals that the optical/X-ray correlation is not triggered by a single type of event (flare or dip) in the light curves. The correlation is thus a global property of the light curves. Flares and dips of different shapes and time-scales appear to contribute to the shape of the total optical X-ray CCF. Strikingly, they all contribute in a similar way to the formation of the pre-dip and post-peak features.

Also, when comparing the superposed light curves we see that the changes occur on similar time-scales, and almost at the same time in the different bands. The general impression is that high (low) optical fluxes are associated with a sharp

decay (rise) in the X-rays. In other words the optical appears to be proportional to the opposite of the time derivative of the X-rays. If such a relation was to hold strictly, we would expect a constant optical phase-lag of value  $\pi/2$  (due to the fact that a derivation in the time domain translates into a constant phase factor in the Fourier domain). In contrast, we found (see Fig. 5) that the phase-lags do depend on Fourier frequency and approximatively cover the range  $0-\pi$ . Nevertheless, we see that the phase lags are close to  $\pi/2$  in the frequency range 0.1–1 Hz where the coherence is significant. Therefore, in the frequency range where most of the correlation occurs, the optical is indeed related to the time derivative of the correlated X-ray flux. Equivalently, the  $\sim\pi/2$  lags can be interpreted as the X-ray light curve scaling like the time derivative of its correlated optical counterpart. Due to the remarkable symmetry of the correlation, this interpretation would be also roughly consistent with the general trend observed in the superposition analysis (Figs. 9–11). There is thus a “differential” relation between the optical and the X-rays: the variability of a light curve appears related to the time derivative of the correlated fraction of the other.

With this regard, rather than using concepts like “precognition” dip and delays, the shape of the superposed light curves and CCF could be interpreted as the signature of a process affecting at the same time, both the X-ray and optical emitting region. In this context, it is not clear whether the “differential” relation reflects an intrinsic “differential” property of the underlying physical process, or on the contrary, emerges casually from the fact that the phase-lags are close to  $\pi/2$  in the frequency range where coherence is important.

## 5. Discussion

Several studies already emphasized the similarity of the X-ray power spectrum in XTE J1118+480 with that of typical black hole candidates in the hard state. Here we find that the similarity extends to other X-ray timing features, namely:

- The weak energy dependence of the power spectrum.
- The reduction of the integrated rms amplitude at high energy.
- The shape of the X-ray ACF and CCFs.
- The presence of an anti-correlation between the X-ray flux and hardness.
- The unity coherence between X-ray bands over a wide range of frequencies.

Together with the presence of striking spectral similarities (Frontera et al. 2001, 2003), this probably makes XTE J1118+480 a typical hard state source. On the other hand our study suggests that XTE J1118+480 might differ from typical hard states sources by the presence of soft lags at frequencies below 0.1 Hz apparent both in the Fourier analysis and through the asymmetry found in the X-ray CCFs.

Our study of the correlated optical/X-ray flickering reveals that:

- The optical X-ray CCF is independent of the X-ray band.

- The optical band is correlated not only to the X-ray flux but also, and in a similar way, to the rapid X-ray spectral fluctuations. This is shown by the computation of the optical flux vs. X-ray hardness CCF and the superposition analysis.
- The optical phase-lags increase significantly with Fourier frequency covering the range  $0-\pi$ . This leads to time-lags decreasing roughly like  $f^{-0.8}$ .
- The optical/X-ray coherence is maximum ( $\sim 0.3$ ) for fluctuations in the range 1–10 s and decreases sharply both at shorter and longer time-scales.
- The shape of the X-ray CCFs asymmetry (Fig. 2) is reminiscent of the asymmetry of the optical/X-ray CCF (Fig. 3a). This may indicate a connection between the X-ray and optical lags. This suggestion is strengthened by the dependence of the optical time-lags at higher frequency  $\sim f^{-0.8}$  that is comparable to the dependence of the X-ray lags in hard state black holes.
- The filtered CCF analysis as well as the superposition technique shows that the underlying process, giving rise to the correlated variability, acts in a similar but rescaled way at different time- and amplitude-scales of the fluctuations.
- The superposition technique shows that the optical response is not triggered by a specific type of event in the X-ray light curve (shot or dip). Rather, events of very different shapes and time-scales contribute in a similar way to the shape of the optical/X CCF. In the range of frequencies where the optical/X-ray coherence is maximum, the light curve in one band is related to the time derivative of its correlated counterpart.

One of the main result of this work is that the optical/X-ray correlation can be described as self-similar. We note that this scaling in time is consistent with what SK02 find by the completely independent method of principal component analysis (PCA). With this analysis, the X-ray/optical cross correlation is computed on short segments of data (25s long), yielding a large number of samples (300) of the cross correlation, which turn out to be somewhat variable in shape. With the PCA (e.g. Kendall 1980), the similarities and difference between samples are analyzed by finding linear combinations of the samples which are statistically uncorrelated. If the variability of the signal comes about as a mixture of a few signals of fixed shape but independently varying amplitudes, the PCA will extract these shapes as the “principal components”. In SK02, two significant components were found, both of which were of the dip-plus-spike shape but on time scales differing by a factor 3. This is similar to the results presented here (compare Fig. 9 lower left with Fig. 11 lower left panel). The “scaling” of the components suggests that there is just one underlying process, but that it can take place on different time scales, possibly in a continuous fashion. The filtered CCF analysis (see Fig. 4) and the power-law dependence of optical time-lag on Fourier frequency (Fig. 8), suggest that indeed, this underlying process is continuously self-similar. Actually, the PCA is not well suited to study such a continuous variations. If the signal shape varies in a continuous way, the PCA will represent this continuum by a number of discrete components. These components will be representative of the range of variation through this continuum.

Moreover, the PCA is sensitive to the coherence and amplitude of variability of the two signals at a given time-scale. Only the time-scales where both the coherence and the amplitude of variability is high will contribute significantly to the variability of the CCF. The finding of SK02 that there are only two significant components simply reflects the fact that the coherence is high only in a relatively narrow range of Fourier frequencies. In other words, the *shape* of CCF at different time-scales appears to be continuously self-similar, but the *amplitude* of the average CCF is dominated by the two time-scales evidenced by the PCA of SK02 and our shot selection analysis.

This scaling is not readily explained by the current accretion models. The ideas that were proposed so far to explain the long optical lags were based on the propagation time between two distinct X-ray and optical emitting regions that are causally connected. In the reprocessing models the lags are interpreted as the light travel-time between the corona and the disc. In the Kanbach et al. (2001) scenario a perturbation propagates from the X-ray corona to the optical outflow photosphere. In such propagation models, the nearly scale-invariant correlation then requires that the small-scale fluctuations have a large propagation speed (outflow model) or alternatively that there are numerous pairs of X-ray/optical emitting regions at different distances from each other, the small-scale perturbation being produced in the closest pairs. Propagation models thus appear strongly constrained and require some complications to fit the scale-invariance. Also as discussed in K01 the propagations models encounter important difficulties in producing features such as a precognition dip that occurs together with a post-peak.

Although the lags indicate a form of causal connection between the X-rays and optical emitting regions they do not necessarily involve a propagation process. Rather, the event superposition analysis suggests that the complicated correlation could be the signature for a self-similar process acting *simultaneously* in both emitting regions with different manifestations in both bands.

The apparent advances/delays of the optical signal with respect to the X-rays could then be a consequence of a (somewhat complex) evolution of the spectral shape of the emitted radiation during an X-ray event. Such an explanation has already been proposed for the lags observed between hard and soft X-rays in Cyg X-1 (e.g. Poutanen & Fabian 1999). In this case the hard and soft X-rays are produced by a single emission mechanism and in the same physical volume. In our case however the situation is more complex. The optical/X CCF is much more complex than the X-ray CCFs and the emission process in the two band is probably different. It is also not clear whether the X-ray and optical emission are produced in the same physical region. Finding a consistent physical scenario that would make such a model predictive and testable is very challenging.

In the jet model of Markoff et al. (2001), the X-rays and optical are both formed through synchrotron emission in the jet. The X-ray CCF could be, in principle due to a characteristic time-evolution of the distributions of the emitting particles in the jet. The difficulty, here, is that no obvious physical mechanism can produce such a spectral evolution.

In other models, such as the ADAF model of Esin et al. (2001) or the coronal model of Merloni et al. (2000) both the optical and X-rays are emitted in the hot inner part of the accretion disc. For instance, if we assume that the optical is self-absorbed synchrotron radiation produced by the Comptonising cloud itself (with a temperature  $kT_e \sim 100$  keV as estimated by Frontera et al. 2001, 2003). Then, the observed optical flux implies a size of the emitting region of a few hundred Schwarzschild radii. Incidentally, this dimension is of the same order as the cold disc inner radius estimated in XTE J1118+480 from fits of the optical to EUV spectra (see Chaty et al. 2003). Then the correlated variability could be caused, for instance, by temporal fluctuations of the magnetic field and/or optical depth of the comptonising plasma. The details are however to be precised and physically motivated. This scenario also encounter a problem to reproduce the observed optical spectrum. This spectrum indeed appears much flatter than that produced through self-absorbed synchrotron. Thus, again, some complications (e.g. strong gradients of magnetic field and/or plasma temperature of the Comptonising plasma) would be required to fit the spectral data.

It could be also that, contrary to what is assumed in the above mentioned models, the X-ray and optical are produced in two distinct regions (e.g. disc+jet). In this case a spectral evolution scenario could also, in principle, account for the correlated X-ray optical variability. Then, the two regions should be physically connected on a time-scale shorter than  $\sim 0.1$  s, that is the shortest time-scale on which we have been able to observe the typical spectral evolution. The complication with such a model is that it should provide a physical description of the connection between the two regions that is well beyond the simple radiation physics. In the case where the X-rays come from the disc and the optical from the jet, the optical X-ray CCFs, their self-similarity and the apparent “differential” relation between the two light curves would constitute important signatures of the underlying accretion-ejection process.

*Acknowledgements.* This work was partly supported by the European Commission (contract number ERBFMRX-CT98-0195, TMR network “Accretion onto black holes, compact stars and protostars”). JM also acknowledges fundings from the MURST (COFIN98-02-15-41) and PPARC. We thank Andrea Merloni for valuable discussion.

## References

- Chaty, S., Haswell, C. A., Malzac, J., et al. 2003, MNRAS, submitted  
 Dubus, G., Kim, R., Menous, K., Szkody, P., & Bowen, D. 2001, ApJ, 553, 307  
 Esin, A. A., McClintock, J. E., Drake, J. J., et al. 2001, ApJ, 555, 483  
 Fabian, A. C., Guilbert, P. W., Motch, C., et al. 1982, A&A, 111, L9  
 Fender, R. P., Hjellming, R. M., Tilanus, R. P. J., et al. 2001, MNRAS, 322, L23  
 Frontera, F., Zdziarski, A. A., Amati, L., et al. 2001, ApJ, 561, 1006  
 Frontera, F., Amati, L., Zdziarski, A. A., et al. 2003, ApJ, in press [astro-ph/0304261]  
 Feng, Y. X., Li, T. P., & Chen, L. 1999, ApJ, 514, 373  
 Garcia, M., Brown, W., Pahre, M., et al. 2000, IAU Circ., 7392, 2  
 Georganopoulos, M., Aharonian, F. A., & Kirk, J. G. 2002, A&A, 388, L25

- Haswell, C. A., Skillman, D., Patterson, J., Hynes, R. I., & Cui, W. 2000, IAU Circ., 7427, 1
- Hynes, R. I., Mauche, C. W., Haswell, C. A., et al. 2000, ApJ, 539, L37
- Hynes, R. I., Haswell, C. A., Cui, W., et al. 2003, MNRAS, in press [astro-ph/0306626]
- Kendall, M. S. 1980, Multivariate analysis, 2nd edition (London: Griffin)
- Kanbach, G., Straubmeier, C., Spruit, H. C., & Belloni, T. 2001, Nature, 414, 180
- Li, T. P., Feng, Y. X., & Chen, L. 1999, ApJ, 521, 789
- Maccarone, T. J., Coppi, P. S., & Poutanen, J. 2000, ApJ, 537, L107
- Markoff, S., Falcke, H., & Fender, R. 2001, A&A, 372, L25
- Mauche, C., Hynes, R., Charles, P., & Haswell, C. 2000, IAU Circ., 7401, 2
- McClintock, J. E., Garcia, M. R., Caldwell, N., et al. 2001, ApJ, 551, L147
- McClintock, J. E., Haswell, C. A., Garcia, M. R., et al. 2001, ApJ, 555, 447
- Merloni, A., Di Matteo, T., & Fabian, A. C. 2000, MNRAS, 318, L15
- Motch, C., Ilovaisky, S. A., & Chevalier, C. 1982, A&A, 109, L1
- Negoro, H., Kitamoto, S., & Mineshige, S. 2001, ApJ, 554, 528
- Nowak, M. A., Vaughan, B. A., Wilms, J., Dove, J. B., & Begelman, M. C. 1999, ApJ, 510, 874
- Poutanen, J., & Fabian, A. C. 1999, MNRAS, 306, L31
- Remillard, R., Morgan, E., Smith, D., & Smith, E. 2000, IAU Circ., 7389, 2
- Revnivtsev, M., Sunyaev, R., & Borozdin, K. 2000, A&A, 361, L37
- Spruit, H. C., & Kanbach, G. 2002, A&A, 391, 225
- Straubmeier, C., Kanbach, G., & Schrey, F. 2001, Exp. Astron., 11, 157
- Vaughan, B. A., & Nowak, M. A. 1997, ApJ, 474, L43
- Wagner, R. M., Foltz, C. B., Shahbaz, T., et al. 2001, ApJ, 556, 42
- Wood, K. S., Ray, P. S., Bandyopadhyay, R. M., et al. 2000, ApJ, 544, L45
- Yamaoka, K., Ueda, Y., Dotani, T., Durouchoux, P., & Rodriguez, J. 2000, IAU Circ., 7427, 2



### **5.3 “Jet–disc coupling through a common energy reservoir in the black hole XTE J1118+480”**

Malzac Julien, Merloni Andrea, Fabian Andrew C., *Monthly Notices of the Royal Astronomical Society*, Volume 351, Issue 1, p. 253-264 (2004).



# Jet–disc coupling through a common energy reservoir in the black hole XTE J1118+480

Julien Malzac,<sup>1,2★</sup> Andrea Merloni<sup>3</sup> and Andrew C. Fabian<sup>1</sup>

<sup>1</sup>*Institute of Astronomy, Madingley Road, Cambridge CB3 0HA*

<sup>2</sup>*Centre d'Etude Spatiale des Rayonnements, CNRS-UPS, 9 Avenue du Colonel Roche, 31028 Toulouse Cedex 4, France*

<sup>3</sup>*Max-Planck-Institut für Astrophysik, Karl-Schwarzschild-Strasse 1, D-85741 Garching, Germany*

Accepted 2004 February 26. Received 2004 February 23; in original form 2003 November 20

## ABSTRACT

We interpret the rapid correlated ultraviolet/optical/X-ray variability of XTE J1118+480 as a signature of the coupling between the X-ray corona and a jet emitting synchrotron radiation in the optical band. We propose a scenario in which the jet and the X-ray corona are fed by the same energy reservoir where large amounts of accretion power are stored before being channelled into either the jet or the high-energy radiation. This time-dependent model reproduces the main features of the rapid multiwavelength variability of XTE J1118+480. Assuming that the energy is stored in the form of a magnetic field, we find that the required values of the model parameters are compatible with both a patchy corona atop a cold accretion disc and a hot thick inner disc geometry. The range of variability time-scales for the X-ray emitting plasma is consistent with the dynamical times of an accretion flow between 10 and 100 Schwarzschild radii. On the other hand, the derived range of time-scales associated with the dissipation in the jet extends to time-scales more than 10 times larger, confirming the suggestion that the generation of a powerful outflow requires large-scale coherent poloidal field structures. A strong requirement of the model is that the total jet power should be at least a few times larger than the observed X-ray luminosity, implying a radiative efficiency for the jet  $\epsilon_j \lesssim 3 \times 10^{-3}$ . This would be consistent with the overall low radiative efficiency of the source. We present independent arguments showing that the jet probably dominates the energetic output of all accreting black holes in the low/hard state.

**Key words:** accretion, accretion discs – black hole physics – magnetic fields – radiation mechanisms: non-thermal – stars: individual: XTE J1118+480 – X-rays: binaries.

## 1 INTRODUCTION

The high-energy spectrum ( $>1$  keV) of accreting stellar mass black holes in the low/hard state can be roughly described by a power law with photon index  $\Gamma \sim 1.4$ – $2$ , and a nearly exponential cut-off at a characteristic energy  $E_c$  of a few hundred keV (see, for example, Tanaka & Lewin 1995; Gierlinski et al. 1997; McClintock & Remillard 2004). Such a spectrum is generally interpreted as due to thermal Comptonization in a plasma with electron temperature  $kT_e \sim 100$  keV and Thomson optical depth  $\tau \sim 1$  (see, for example, Poutanen 1998). There are two possible explanations for the presence of this very hot plasma (often called ‘corona’). It could be either a geometrically thick, optically thin innermost part of the accretion flow (Shapiro, Lightman & Eardley 1976; Narayan & Yi 1994) or a collection of small-scale active regions located atop a cold, geo-

metrically thin and optically thick accretion disc (Haardt, Maraschi & Ghisellini 1994), possibly powered by magnetic reconnection.

When the X-ray luminosity increases above a few per cent of the Eddington luminosity ( $L_{\text{Edd}}$ ), accreting black holes are observed to switch from the low/hard state to the so-called high/soft state (see, for example, McClintock & Remillard 2004). Then the X-ray luminosity is dominated by a strong thermal component originating from a geometrically thin, optically thick disc. Current observations show that the power-law component is steeper ( $\Gamma \sim 2.5$ – $3$ ) and much less luminous than in the hard state, suggesting the disappearance of the Comptonizing plasma in this state.

Recent multiwavelength observations of accreting black holes in the hard state have shown the presence of a ubiquitous flat-spectrum radio emission (see, for example, Fender 2004), which may extend up to infrared and optical wavelengths. The properties of the radio emission indicate it is likely produced by synchrotron emission from relativistic electrons in compact, self-absorbed jets (Blandford & Königl 1979; Hjellming & Johnston 1988). This idea was confirmed

★E-mail: malzac@ast.cam.ac.uk

by the discovery of a continuous and steady millisecond compact jet around Cygnus X-1 (Stirling et al. 2001). Moreover, in hard state sources a tight correlation has been found between the hard X-ray and radio luminosities, holding over more than three decades in luminosity (Corbel et al. 2003; Gallo, Fender & Pooley 2003). In contrast, during high/soft state episodes the sources appear to be radio weak (Tananbaum et al. 1972; Fender et al. 1999; Corbel et al. 2000), suggesting that the Comptonizing medium of the low/hard state is closely linked to the continuous ejection of matter in the form of a small-scale jet.

Merloni & Fabian (2001) have pointed out that the energy content of the electrons in the Comptonizing medium is too low to account for the observed X-ray luminosities. The Comptonizing electrons have to be tightly connected to an energy reservoir where a large amount of accretion power is stored before being transferred to them, and ultimately radiated. Independently, the rapid X-ray variability in Cyg X-1 also suggests the presence of energy reservoirs (Negoro et al. 1995; Maccarone & Coppi 2002). Because angular momentum transport in accretion flow is most likely due to magneto-rotational instability (MRI; see Balbus & Hawley 1998), a natural candidate for the energy repository is the magnetic field amplified in the disc by the MRI-turbulent flow. However, if the dissipation of the tangled field (via magnetic reconnection) and non-adiabatic turbulent heating preferentially energize the protons, rather than the electrons, the hot Comptonizing plasma could become two-temperature, and the protons themselves act as the main energy reservoir (Di Matteo, Blackman & Fabian 1997).

Models and simulations of jet production (Blandford & Znajek 1977; Blandford & Payne 1982; Meier 2001) indicate that jets are driven by the poloidal component of the magnetic field. Therefore, storage of energy into magnetic structures driving the jet and powering the Comptonizing electrons is the most straightforward explanation for the observed corona–jet association.<sup>1</sup> In this context, the corona would constitute the location where the jet is launched. These ideas were developed by several authors in the context of geometrically thin and/or thick accretion flows (Meier 2001; Livio, Pringle & King 2003) as well as accretion disc coronae (Merloni & Fabian 2002).

Besides the radio/X-ray correlation observed on long ( $> 1$  d) time-scales, there are indications that the corona–jet coupling operates on time-scales as short as a few seconds or less. The best example is provided by the X-ray nova XTE J1118+480 (Remillard et al. 2000; McClintock et al. 2001a). During its outburst in 2000, this black hole showed all the X-ray properties of hard state sources. Fast optical and ultraviolet (UV) photometry has shown rapid optical/UV flickering presenting complex correlations with the X-ray variability (Kanbach et al. 2001; Hynes et al. 2003, hereafter K01 and H03, respectively). This correlated variability cannot be caused by reprocessing of the X-rays in the external parts of the disc. Indeed, the optical flickering occurs, on average, on shorter time-scales than the X-ray one (K01), and reprocessing models fail to fit the complicated shape of the X-ray/optical cross-correlation function (H03). Spectrally, the jet emission seems to extend at least up to the optical band (McClintock et al. 2001b; Chaty et al. 2003, hereafter C03), although the external parts of the disc may provide an important contribution to the observed flux at such wavelengths. The jet activity is thus the most likely explanation for the rapid observed optical

flickering. For this reason, the properties of the optical/X-ray correlation in XTE J1118+480 might be of primary importance for the understanding of the jet–corona coupling and the ejection process.

The simultaneous optical/X-ray observations are described at length in a number of papers (K01; Spruit & Kanbach 2002; H03; Malzac et al. 2003, hereafter M03). As discussed in these works, the observations are very challenging for any accretion model. The most puzzling pieces of evidence are the following.

(i) The optical/X-ray cross-correlation function (CCF) shows the optical band lagging the X-ray by 0.5 s, but with a dip 2–5 s in advance of the X-rays (K01).

(ii) The correlation between X-ray and optical light curves appears to have time-scale-invariant properties; the X-ray/optical CCF maintains a similar, but rescaled, shape on time-scales ranging at least from 0.1 s to a few tens of seconds (M03).

(iii) The correlation does not appear to be triggered by a single type of event (dip or flare) in the light curves; instead, as was shown by M03, optical and X-ray fluctuations of very different shapes, amplitudes and time-scales are correlated in a similar way, such that the optical light curve is related to the time derivative of the X-ray one.

Indeed, in the range of time-scales where the coherence is maximum, the optical/X-ray phase lag is close to  $\pi/2$ , indicating that the two light curves are related through a differential relation. Namely, if the optical variability is representative of fluctuations in the jet power output  $P_j$ , the data suggest that the jet power scales roughly as  $P_j \propto -dP_x/dt$ , where  $P_x$  is the X-ray power.

Here we will show that, if indeed there is a common energy reservoir feeding both the jet and the corona, this differential relation is naturally satisfied, provided that the jet power dominates over the X-ray luminosity.

We first present the energy reservoir model and suggest a simple physical scenario for the energy reservoir and jet disc/coupling (Section 2). We then present a time-dependent model that captures the main features of the multiwavelength variability observed in XTE J1118+480, and we discuss our main results obtained by comparing the properties of the simulated light curves with the observations (Section 3). Section 4 is devoted to a discussion of the constraints on the nature of the accretion flow in XTE J1118+480 derived from both spectral and temporal analysis while, in Section 5, we make an attempt to generalize these results to other accreting black hole sources. Finally, we summarize our conclusions in Section 6.

## 2 ENERGY RESERVOIR MODEL

### 2.1 A simple analogue

The time-dependent model that we have developed is complicated in operation and behaviour. In order to gain some insight into its operation, we consider a simple model consisting of a tall water tank with an input pipe and two output pipes, one of which is much smaller than the other. The larger output pipe has a tap on it. The flow in the input pipe represents the power injected in the reservoir  $P_i$ , that in the small output pipe the X-ray power  $P_x$  and in the large output pipe the jet power  $P_j$ .

If the system is left alone, the water level rises until the pressure causes  $P_i = P_j + P_x$ . Now consider what happens when the tap is opened more, causing  $P_j$  to rise. The water level and pressure (proportional to  $E$ ) drop causing  $P_x$  to reduce. If the tap is then partly closed, the water level rises,  $P_j$  decreases and  $P_x$  increases. The rate  $P_x$  depends upon the past history, or integral of  $P_j$ . Identifying the

<sup>1</sup> See, however, Markoff, Falcke & Fender (2001) and Georganopoulos, Aharonian & Kirk (2002) for alternative interpretations involving dominant X-ray emission from the jet.

optical flux as a marker of  $P_j$  and the X-ray flux as a marker of  $P_x$  we obtain the basic behaviour seen in XTE J1118+480.

In the real situation we envisage that the variations in the tap are stochastically controlled by a shot noise process. There are also stochastically-controlled taps on the input and other output pipes as well. The overall behaviour is therefore complex. The model shows, however, that the observed complex behaviour of XTE J1118+480 can be explained by a relatively simple basic model involving several energy flows and an energy reservoir.

## 2.2 A magnetic energy reservoir?

This simple model is largely independent of the physical nature of the energy reservoir. In a real accretion flow, the reservoir could take the form of either electromagnetic energy stored in the X-ray emitting region, or thermal (hot protons) or turbulent motions. The material in the disc could also constitute a reservoir of gravitational or rotational energy behaving as described above.

In order to be more specific, let us outline the possibility of jet–disc coupling through a magnetic energy reservoir. For the sake of simplicity, we assume that the main energy reservoir for the radiating electrons is indeed the magnetic field. This would correspond to a system in which the heating of the protons by the magnetohydrodynamics (MHD) turbulence is negligible. Quataert (1998) and Quataert & Gruzinov (1999) have shown that this is the case if magnetic pressure is not much smaller than gas pressure (low plasma  $\beta$  parameter), and we will therefore assume this is indeed the case here. Then, the power channelled into the particle heating (through magnetic reconnection) and escaping the corona as X-ray radiation can be written as

$$P_x = (v_d/R_x)E, \quad (1)$$

where  $v_d$  is the field dissipation speed, which depends on the details of the dissipation process,  $R_x$  is the typical size of an X-ray emitting region and  $E = (B^2/8\pi)V$  is the total magnetic energy contained in the hot phase ( $V$  is its volume).

The jet power is instead related to the poloidal field component. For the purpose of simple estimates, the MHD jet power can be written as (Livio, Ogilvie & Pringle 1999):

$$P_j = (B_p^2/8\pi)AR_c\Omega, \quad (2)$$

where  $A$  is the area of the disc threaded by the poloidal field and  $R_c\Omega$  is the typical rotational velocity of the field lines. If the field in the disc is amplified by MRI turbulence and dissipates mainly in the hot coronal phase (i.e. it does not possess a large-scale external component), then its poloidal component can be expressed as  $B_p \simeq hB$ , where  $h = H/R_c$  is the scaleheight of the hot phase (Livio et al. 1999; Meier 2001; Merloni & Fabian 2001). The jet power can then be rewritten:

$$P_j = \frac{A}{V}h^2R_c\Omega E. \quad (3)$$

For the sake of simplicity, we assume that the jet power is taken mainly from the tangled magnetic field. This implies that the outflow is accelerated by magnetic dissipation processes and/or that the magnetic energy of the corona is carried away by an essentially electromagnetic outflow. In fact, it is possible that the jet is powered directly by the disc rotational energy without significant field dissipation. This would be the case whenever the poloidal field is coherent on large enough scales to exert a significant torque on the disc (see, for example, the model of King et al. 2004). However, such a mechanism for angular momentum transport in the disc competes

with MRI, so that when large-scale fields extract energy and angular momentum from the disc, the MRI dynamo switches off, also draining the magnetic energy reservoir.

Summarizing, we will make the assumption that both the jet and X-ray power are tapped from the same magnetic energy reservoir. Note that from equations (1) and (3) both jet and X-ray powers scale linearly with the total reservoir energy. The total power extracted from the magnetic field in the hot phase is then

$$P_x + P_j = \frac{B^2}{8\pi} \left( \frac{Vv_d}{R_x} + Ah^2R_c\Omega \right). \quad (4)$$

If we define the relative fractional power of the jet  $\eta = P_j/(P_x + P_j)$ , we then find that (see also Merloni & Fabian 2002)

$$\eta = \left( 1 + \frac{V}{AR_x} \frac{v_d}{R_c\Omega} h^{-2} \right)^{-1}. \quad (5)$$

The discussion so far makes no distinction between a corona made of a collection of active phases atop a cold disc and a continuous hot inner flow. Indeed the differences show up in the geometrical factors in the above equations. In the case of a structured corona, we consider  $N$  cylindrical active regions (magnetic tubes) located atop the disc at distances ranging from  $3R_S$  to  $R_c$ . The typical radius  $R_a$  and height  $H_a$  of the active regions scale linearly with their distance  $R$  from the black hole, we note  $a = R_a(R)/R$  and  $h = H_a(R)/R$ . We assume that their radial distribution scales as  $1/R$  so that the covering factor of the corona is independent of distance. Then the average radius of an active region is  $R_x = aR_c/\ln(R_c/3R_S)$ ,  $A = (\pi/2)Na^2R_c^2/\ln(R_c/3R_S)$ , and  $V = (\pi/3)Na^2hR_c^3/\ln(R_c/3R_S)$ .

On the other hand, in the thick disc case, we have  $R_x = R_c$ ,  $A = \pi R_c^2$  and  $V = (2/3)\pi hR_c^3$ , where here  $R_c$  is taken to coincide with the outer radius of the thick disc and a constant  $H/R$  (wedge-like geometry) is assumed.

## 2.3 Time-dependent model

In a stationary flow, the extracted power  $P_j + P_x$  would be perfectly balanced by the power injected into the magnetic field, which is, in the most general case, given by the difference between the accretion power and the power advected into the hole and/or stored in convective motions:<sup>2</sup>  $P_i \simeq \dot{M}c^2 - P_{\text{adv,conv}}$ . However, observations of strong variability on short time-scales clearly indicate that the heating and cooling of the X-ray (and optical) emitting plasma are highly transient phenomena, and the corona is unlikely to be in complete energy balance on short time-scales. We therefore introduce a time-dependent equation governing the evolution of its total energy  $E$

$$\dot{E} = P_i - P_j - P_x, \quad (6)$$

and we assume that all the three terms on the right-hand side are time-dependent.

Furthermore, we assume that the optical light comes mainly from synchrotron emission in the inner part of the jet. A contribution

<sup>2</sup> In fact, the secular evolution of convection dominated accretion flow leads to accumulation of mass at the outer disc boundary, and thus to a non-stationary flow. However, if we limit ourselves to observations which are shorter than a typical outburst duration, we can regard convection as an alternative escape route for the gravitational energy dissipated by the accreting matter out of the region of interest (where X-ray and optical emission are produced).

256 *J. Malzac, A. Merloni and A. C. Fabian*

from X-ray light reprocessed in the external part of the disc could be present in the optical emission. However, this component is likely to be weak (cf. K01; H03).

The (time-averaged) total observed optical flux is

$$O_{\text{pt}} \propto P_j + f_r P_x \quad (7)$$

where the normalization factor  $f_r$  depends on the geometry of the system and on the optical wavelength, with  $f_r$  increasing towards shorter wavelengths.<sup>3</sup>

We introduce the instantaneous dissipation rates  $K_j$  and  $K_x$

$$P_j(t) = K_j(t)E(t) \quad (8)$$

$$P_x(t) = K_x(t)E(t), \quad (9)$$

and we consistently denote  $\langle K_j \rangle$ ,  $\langle K_x \rangle$ ,  $\langle P_i \rangle$  and  $\langle E \rangle$  as the time-averaged values. We define the average dissipation time

$$T_{\text{dis}} = (\langle K_j \rangle + \langle K_x \rangle)^{-1}, \quad (10)$$

such that if the energy reservoir is not fed (i.e.  $P_i = 0$ ) its level decays with an e-folding time  $T_{\text{dis}}$ . Also, it is convenient to define

$$f_x = 1 - \eta = \langle K_x \rangle T_{\text{dis}}, \quad (11)$$

which is the average fraction of the total power that goes into the X-ray emission. In the framework of the magnetic reservoir of Section 2.2, the average values of the dissipation rates are related by equations (1) and (2) to the (time-averaged) values of the physical parameter of the system: namely,  $\langle K_j \rangle = (Ah^2/V)R_c\Omega$  and  $\langle K_x \rangle = v_d/R_x$ .

Obviously, the detailed physical modelling of the time evolution of such a jet corona system is an extremely complex problem that is beyond the present computer capabilities. Instead we will adopt a more phenomenological approach. We will model the variability of the source by assuming random fluctuations of  $K_j$ ,  $K_x$  and  $P_i$ , then compare the results with the observations and constrain the properties of these fluctuations.

In general, both the instantaneous injected power  $P_i$  and the dissipation rates  $K_j$  and  $K_x$  may depend on the amount of energy  $E$  stored in the reservoir. However, the fact that  $P_i$  and  $K_x$  are required to vary on time-scales different from those of  $P_x$  (see below) suggests that they are rather independent of  $E$ . Moreover, observations show that in black hole binaries and Seyfert galaxies the X-ray amplitude of variability is linearly related to the X-ray flux level (Uttley & McHardy 2001). In general, if  $P_i$ ,  $K_x$  and  $K_j$  are either strongly dependent on  $E$ , or correlated with each other, this would introduce a non-linear relation between rms amplitude and observed flux. The observations thus suggest that the values of  $P_i$  and the dissipation rates  $K_j$  and  $K_x$  at a given time are nearly independent of the level of the reservoir energy (although  $E$  does depend on the history of  $K_j$  and  $K_x$ ). For these reasons, as well as for the sake of simplicity, we will then assume that  $K_j$ ,  $K_x$  and  $P_i$  fluctuate randomly and independently, driving the fluctuations of the energy reservoir.

<sup>3</sup> In the fully time-dependent model we will consider, additional effects on the properties of the optical emission should be considered. First of all, there is a time delay  $\Delta$  between matter ejection and dissipation in the form of optical photons. As the jet is relativistic and the optical light is produced at short distance ( $\lesssim 1000GM/c^2$ ) from the hole, the delay should be  $\Delta \lesssim 0.1$  s. Similarly, reprocessing will also introduce a time delay of the order of 0.1 s and any variability of  $P_x$  on time-scales shorter than a few seconds will not be apparent in the reprocessed light.

For the specific form of the fluctuation, we use exponentially rising shot profiles:

$$s(t) = A \frac{\exp(t/\tau) - 1}{\exp(1) - 1} \quad \text{for } t < \tau. \quad (12)$$

This profile was chosen for its simplicity. Our results regarding the optical/X-ray correlation are not sensitive to the shape of the individual flares. On the other hand, they will strongly depend on the amplitude, time-scales and occurrence rate of the shots. The amplitude  $A$  and the occurrence rate  $\lambda$  of the random shots are taken constant. These quantities are related to the average dissipation rate. The shot duration  $\tau$  is distributed within  $\tau_{\text{min}}$  and  $\tau_{\text{max}}$  with a power-law distribution  $\rho(\tau) \propto \tau^{-p}$ . These parameters constrain the fractional amplitude of variability and the shape of the power spectrum of the fluctuations that are imposed on the system. The fractional rms scales as  $1/\sqrt{\lambda}$ , and the power spectrum is a power law ranging from frequencies  $1/\tau_{\text{max}}$  to  $1/\tau_{\text{min}}$  with a slope  $\alpha = 3 - p$  (see, for example, Poutanen & Fabian 1999). For  $K_x$ ,  $K_j$  and  $P_i$ , the parameters  $\lambda$ ,  $p$ ,  $\tau_{\text{min}}$  and  $\tau_{\text{max}}$  are, in general, not identical. In presenting our results, the subscripts ‘x’, ‘j’ and ‘i’ will refer to  $K_x$ ,  $K_j$  and  $P_i$ , respectively.

For a specific set of parameters we first generate time series for  $K_x$ ,  $K_j$  and  $P_i$ , solve the time evolution of the energy reservoir  $E$  and then use it to derive the resulting optical and X-ray light curves. The ejected material travels from the corona to the shock region or photosphere where the optical photons are produced. As discussed above, this introduces a time delay of  $\Delta < 0.1$  s in the optical emission. To model this delay, we simply shift the optical light curve by  $\Delta$ . We then compute the X-ray and optical power density spectrum (PDS), autocorrelation function (ACF), their CCF, coherence and phase lag spectrum for comparison with the observed ones, in order to obtain the largest possible number of different observational tests for our variability model.

## 2.4 Main observational constraints

Before we proceed and illustrate the results of our simulations, a remark is in place with respect to the requirement any specific realization of our model will have to fulfil in order to reproduce the main observational characteristics. This will guide us in the exploration of the vast parameter space of the model, as well as provide us with useful insight on the physical interpretation of the results.

We first note that combining equations (6) and (9) we obtain for the total instantaneous jet power the following relation:

$$P_j = P_i - \left(1 + \frac{\dot{K}_x}{K_x^2}\right) P_x - \dot{P}_x/K_x. \quad (13)$$

We can see from this equation that the differential scaling  $P_j \propto -\dot{P}_x$ , observed in XTE J1118+480, will be rigorously reproduced provided that:

- (i)  $K_x$  is a constant;
- (ii)  $P_i - P_x$  is a constant.<sup>4</sup>

It is physically unlikely that these conditions will be exactly verified. In particular,  $P_x$  is observed to have a large rms amplitude of variability of about 30 per cent. However, the observed differential relation holds only roughly and only for fluctuations within

<sup>4</sup> This constant can differ from 0 because the differential scaling is observationally demonstrated only for the varying fraction of the optical and X-ray fluxes.

a relatively narrow range of time-scales, 1–10 s. Therefore, the above conditions need only to be fulfilled approximately and for low-frequency fluctuations ( $>1$  s). In practice, the following requirements will be enough to make sure that the low-frequency fluctuations of the right-hand side of equation (13) are dominated by  $\dot{P}_x$ :

- (i)  $P_x \ll P_i$ , implying that the jet power, on average, dominates over the X-ray luminosity;
- (ii) the amplitude of variability of  $K_x$  and  $P_i$  in the 1–10 s range is low compared to that of  $P_j$ . In other words the 1–10 s fluctuations of the system are mainly driven by the jet activity.

The first condition is crucial, and will be discussed in more detail in Section 4. The second condition requires that the mechanisms for energy reservoir filling and dissipation in the corona and in the jet are occurring on quite different time-scales, and this will also provide us with additional constraints on the global dynamical properties of the system.

### 3 RESULTS

In Fig. 1, we show the results of a simulation with  $T_{\text{dis}} = 0.5$  s and  $f_x = 0.1$  (see Table 1 for the values of the other parameters). The model produces an X-ray power spectrum with a plateau up to  $\sim 0.1$  Hz and a power-law component with slope  $\sim 1.4$  above that frequency, with most of the X-ray variability occurring around 0.1 Hz. The optical PDS power law has a flatter slope ( $\sim 1$ ) up to 1 Hz and then softens to a slope similar to that of the X-ray PDS. The resulting optical ACF is significantly narrower than the X-ray one. The full width at half-maximum (FWHM) of the two ACFs differs by a factor of  $>2$ . The overall coherence is low ( $<0.4$ ), reaching a maximum in the 0.1–1 Hz range and decreasing rapidly both at lower and higher frequency. The phase lags are close to  $\pi/2$  in the 0.1–1 Hz range and increase from 0 at low frequencies up to  $\pi$  at around 6 Hz. At higher frequencies the phase-lag spectrum is characterized by large oscillations. Finally, the resulting CCF rises very quickly at positive optical lags, peaks around 0.5 s (this is the post-peak) and then declines slowly at larger lags. The two bands appear to be anticorrelated at negative optical lags indicating a systematic optical dip 1–2 s before the X-rays reach their maximum (pre-dip).

All these characteristics are observed in XTE J1118+480. Moreover, the integrated X-ray rms is 25 per cent as observed. The optical variability is 20 per cent, slightly larger than the 16 per cent reported by M03, but this could be reduced if the expected constant disc component is added.

Obviously the model parameter values were carefully selected in order to reproduce these characteristics. Given the complexity of the model, a full investigation of the parameter space is premature. However, it may be useful to illustrate the main effects of the different parameters by considering several simple situations.

#### 3.1 Variability dominated by the jet dissipation rate $K_j$

##### 3.1.1 Jet dominated models ( $f_x \ll 1$ )

We first consider the case where the X-ray emission is energetically negligible. The jet fully drives the variability of the system in the limit of large  $\lambda_i$  and  $\lambda_x$ , and low  $f_x$ . In this limit, both conditions for the applicability of the model discussed in the previous section are exactly verified. We thus expect the scaling  $P_j \propto -\dot{P}_x$  to be realized. Indeed, we obtain phase lags that are close to  $\pi/2$  independent of frequency. In this limit, the resulting CCF is purely antisymmetric

with pre-dip and post-peak of identical amplitude and lag (contrary to what is observed). The optical lag of the post-peak is controlled by  $T_{\text{dis}}$ , which sets the time-scale on which the energy reservoir responds to the imposed fluctuations. At frequencies larger than  $1/T_{\text{dis}}$  the X-ray variability decreases because there cannot be any variability of the reservoir energy  $E$  on time-scales larger than  $T_{\text{dis}}$ . The coherence function also decreases at frequencies above  $1/T_{\text{dis}}$ . On the other hand, at frequencies lower than  $1/T_{\text{dis}}$  the optical variability decreases because at such low frequencies the system evolves in a quasi-static way. Because  $P_i$  is constant and  $P_x$  is energetically negligible, the variability of  $K_j$  is compensated by the variability of  $E$  so that  $P_j$  also remains almost constant.

##### 3.1.2 X-ray dominated models ( $f_x \sim 1$ )

If  $f_x$  is large but the amplitudes of variability of  $K_x$  and  $P_i$  are kept negligible by increasing  $\lambda_x$  and  $\lambda_i$ , then the power output can be dominated by the X-rays but the variability is still driven by the jet.

In this case, we still have  $\pi/2$  phase lags but only at frequencies  $>1/T_{\text{dis}}$ . The effect of a large X-ray dissipation is the appearance of phase lags  $\pi$  at frequencies  $<1/T_{\text{dis}}$  indicating an anticorrelation. This anticorrelation is also apparent in the CCF, which tends to be negative and symmetric around zero lag. The anticorrelation at low frequencies is due to the fact that on long time-scales the system is always in equilibrium, but, contrary to the jet dominated case, X-ray losses are not negligible in this case. The reservoir energy  $E$  changes in order to keep the total output constant (and equal to  $P_i$ ), but  $P_j$  does change. For this reason the fluctuations of the jet output are strictly anticorrelated to that of the X-ray power. Such an anticorrelation is in clear conflict with the data, the observed phase lags indicating rather a correlation at low frequencies. Thus, even if the jet drives the variability as in the previous example, we definitely need  $f_x \ll 1$  in order to reproduce the data. In practice, exploring a large volume of the parameter space we could not find a reasonable agreement with the data for  $f_x$  larger than  $\sim 0.2$ . This is a very robust result of our time-dependent modelling, and we examine its consequences in Section 4.

#### 3.2 Variability dominated by the coronal dissipation rate $K_x$ and/or by the power input $P_i$

The situation where the variability is dominated by the X-ray dissipation rate in the corona is perfectly symmetric to the case where the variability is dominated by the jet, studied above, with however an inversion of the sign of phase lags and time-axis in the CCF plot.

On the other hand, fluctuations of  $P_i$  introduce perfectly positively correlated fluctuations of  $P_j$  and  $P_x$ . If the fluctuations of  $P_i$  dominate we obtain X-ray and optical light curves that are perfectly correlated on all time-scales with identical power spectrum and unity coherence, in contrast with the observations.

In general, when in a given range of time-scales more than one component (i.e.  $P_i$ ,  $K_j$  or  $K_x$ ) drives the variability, the main effect is a strong reduction of the coherence function in the corresponding range of frequencies.

#### 3.3 A realistic case

Now that we understand the basic effects of the different parameters, we return to our ‘realistic’ model and explain how we were guided toward this solution and how it reproduces qualitatively all the timing features observed in XTE J1118+480.

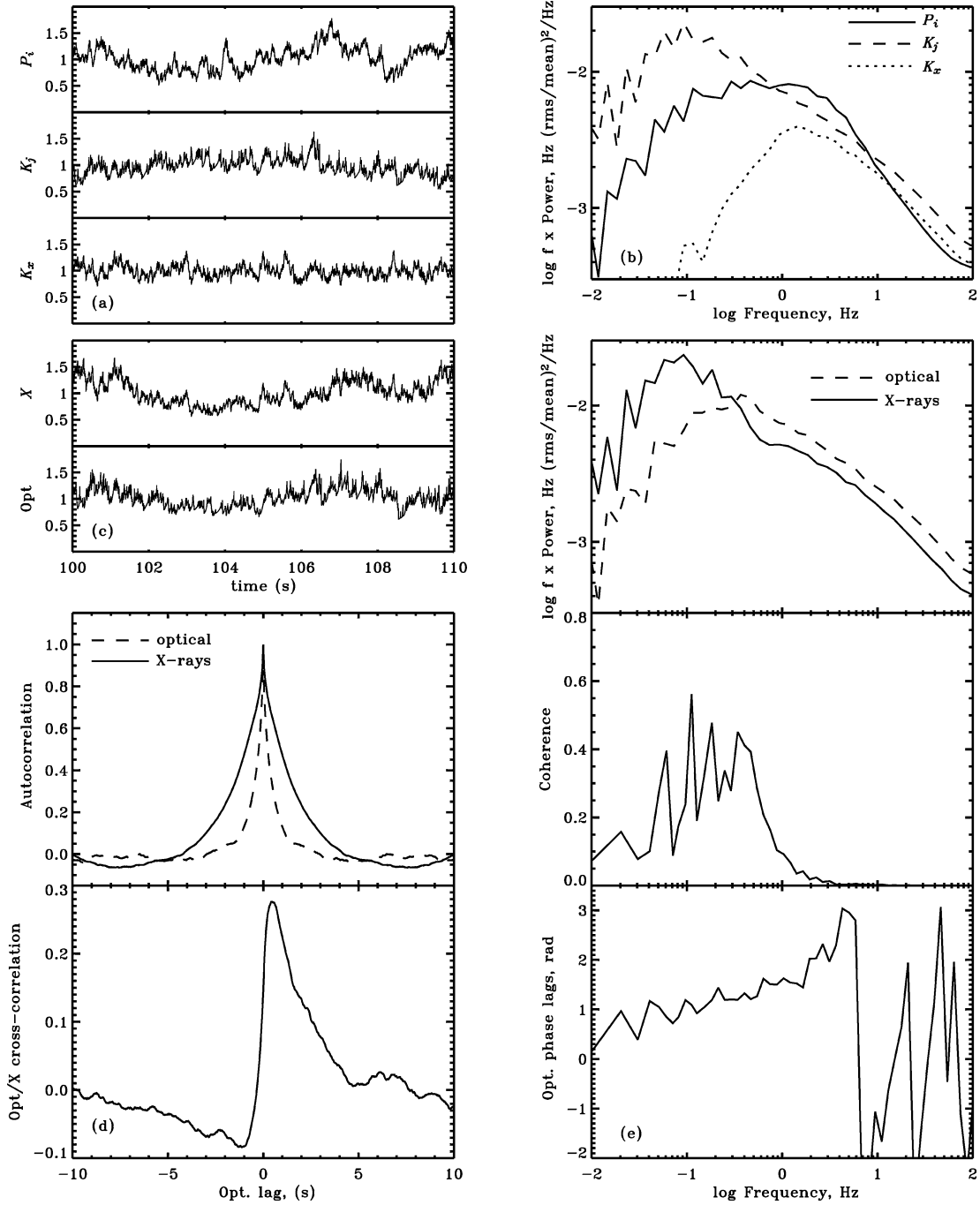


**Figure 1.** Results of simulations for parameters given in Table 1. Sample time series (a) and power spectra (b) of  $P_i$ ,  $K_j$  and  $K_x$ , resulting X-ray and optical fluxes light curves (c), X-ray/optical autocorrelation and cross-correlation functions (d), power spectra, coherence and phase lags (e). In panels (a) and (c), the time series are renormalized so that their time average is unity.

As discussed above, reproducing the data requires the jet to dominate the energy budget and be the main driver of the variability (at least for the 1–10 s fluctuations). Therefore, we set  $f_x = 0.1$  and the parameters  $\lambda_j$ ,  $p_j$ ,  $\tau_{\min j}$  and  $\tau_{\max j}$  were adjusted in order to have large enough 1–10 s fluctuations of the jet power. These parameters also control the shape of the optical power spectrum. In particular, the slope of the shot distribution  $p_j$  is chosen so that it leads to the observed slope of the optical power spectrum above 1 Hz. The dissipation time is set to  $T_{\text{dis}} = 0.5$  in order to match the observed optical lag in the CCF reported by K01.

The values of  $\lambda_i$ ,  $p_i$ ,  $\tau_{\min i}$  and  $\tau_{\max i}$  were fixed so that the variability of  $P_i$  introduces some correlated variability at low frequencies, enabling us to reproduce the asymmetry of the CCF and the small phase lags observed at low frequency. The loss of coherence below 10 Hz is due to the simultaneous large variability of  $P_i$  and  $K_j$  at low frequencies.

Finally, we also introduce fluctuations of the X-ray dissipation rate at high frequencies. This enables us to reproduce the loss of coherence observed above 1 Hz. Also,  $\lambda_x$ ,  $p_x$ ,  $\tau_{\min x}$  and  $\tau_{\max x}$  were chosen in order to reproduce the X-ray power spectrum at high frequencies, which is otherwise too steep.

**Table 1.** The model parameters used in the simulations of Fig. 1. The last two rows show the resulting fractional amplitude of the dissipation rates, energy reservoir, optical and X-ray fluxes. In model 2 some reprocessing was added and the optical fractional rms is then reduced to 0.16.

$T_{\text{dis}} = 0.5 \text{ s}$	$f_x = 0.1$	
$\lambda_i = 100 \text{ s}^{-1}$	$\lambda_j = 50 \text{ s}^{-1}$	$\lambda_x = 1000 \text{ s}^{-1}$
$p_i = 2.1$	$p_j = 1.4$	$p_x = 1.1$
$\tau_{\text{min } i} = 0.1 \text{ s}$	$\tau_{\text{min } j} = 0.01 \text{ s}$	$\tau_{\text{min } x} = 0.01 \text{ s}$
$\tau_{\text{max } i} = 7 \text{ s}$	$\tau_{\text{max } j} = 10 \text{ s}$	$\tau_{\text{max } x} = 0.5 \text{ s}$
rms $P_i = 0.20$	$K_j = 0.27$	$K_x = 0.11$
rms $E = 0.23$	Opt = 0.21	$X = 0.26$

A propagation lag of  $\Delta = 0.05 \text{ s}$  then provides the observed high-frequency behaviour of the phase lags. If the propagation lag is neglected, the phase-lag spectrum is flat at high frequencies with phase lag at a constant value  $\sim \pi/2$ . The constant time delay introduces an additional phase lag  $\psi = 2\pi f \Delta$ . As the time-scale of the fluctuations approaches that of the time delay, this additional phase lag becomes dominant. The overall phase lag thus increases and reaches  $\pi$  at  $\sim 6 \text{ Hz}$ . The phase lags are defined only in the range  $[-\pi, \pi]$  and can only be measured modulo  $2\pi$ . Thus, at higher frequencies the phase lag shifts to  $-\pi$  then increases linearly to  $\pi$  and so on, producing large ‘oscillations’ in the phase-lag spectrum. A similar behaviour of the phase lags above 1 Hz is observed in XTE J1118+480 (see M03, fig. 5), indeed suggesting a propagation lag of  $\Delta \sim 0.05 \text{ s}$ . On the other hand, the overall effects of propagation delays on the CCF and coherence function are negligible.

### 3.4 Effects of reprocessing

We now consider the effects of a possible reprocessing component from the disc. We model this component by convolving the X-ray light curve with a transfer function  $T_r$  describing the time delay and variability smearing due to reprocessing. We use the following transfer function

$$T_r(t) \propto \frac{t}{\delta} \exp(-t) \exp\left[\left(\frac{t}{\delta}\right)^{0.01} - \frac{t}{\delta}\right] + 0.28 \left[1 - \exp\left(-10\frac{t}{\delta}\right)\right] \exp\left[-(t/5)^{20}\right] \quad (14)$$

where  $t$  is measured in seconds and the reprocessing time delay  $\delta = 0.1 \text{ s}$ .

This function is a rough analytical approximation to the theoretical transfer functions shown in H03.

The reprocessed component is added to the optical light curve. Its normalization is parametrized by the ratio of the average flux of the reprocessed component to that of the jet component. In the simulation shown in Fig. 2, we take this ratio to be 0.5, keeping all other parameter values identical to those of the previous simulation. The main effect is to add a low-frequency component to the optical light curves highly correlated to the X-ray one. By comparison with Fig. 1, the optical ACF is broader, the coherence is higher at low frequency and the optical pre-dip tends to disappear; the optical lags are shorter in particular at low frequency.

The increase of the reprocessed component is associated with an increase in the coherence function, and the X-ray and optical ACF and PDS becoming similar and shorter optical lags. We expect to observe this evolution if we look at shorter and shorter wavelengths where the disc emission increasingly dominates the total optical/UV flux. Indeed, H03 report similar trends in the dependence of the correlation upon wavelength. We also note that at low frequencies

( $< 0.1 \text{ Hz}$ ), H03 observe a large coherence in the far-UV domain, while M03 report almost zero coherence. This could be interpreted as the effects of reprocessing in the far-UV that would become negligible at optical wavelengths.

## 4 NATURE OF THE LOW-LUMINOSITY ACCRETION FLOW IN XTE J1118+480

### 4.1 Constraints from the time variability study

The detailed analysis of the complicated structure of the multiwavelength variability of the source have allowed us to select a region of parameter space for which our model successfully reproduces all the main observational pieces of evidence. The parameters are summarized in Table 1. In principle, these parameters can constrain the dynamics and geometry of the accretion flow. However, this would require a detailed physical model for the jet–disc coupling. Here we assume that, as suggested in Section 2.2, the magnetic field constitutes the main energy reservoir and we investigate the consequences for the accretion flow.

Let us start by examining the two parameters that reflect the time-averaged global energetics of the system:  $T_{\text{dis}}$  and  $f_x$ . From equations (1), (3), (10) and (11), we see that they are related to the physical parameters of the system:

$$\frac{v_d}{R_x} = \frac{f_x}{T_{\text{dis}}} \quad (15)$$

$$\frac{A}{V} h^2 v_K(R_c) = \frac{1 - f_x}{T_{\text{dis}}}. \quad (16)$$

Here, we have assumed that the disc rotation law is Keplerian and we denote by  $v_K(R_c)$  the Keplerian speed at the radius  $R_c$ .

In the estimates below, we assume, as we do throughout the paper, a black hole mass of  $10 M_\odot$  for XTE J1118+480. Equation (15) is a constraint on the magnetic field dissipation speed in the hot phase. For  $f_x = 0.1$  and  $T_{\text{dis}} = 0.5 \text{ s}$  it can be rewritten as

$$\frac{v_d}{c} \simeq 2 \times 10^{-5} r_x, \quad (17)$$

where  $r_x = R_x/R_s$ .

On the other hand, equation (16) constrains the corona/hot flow scaleheight, which should be defined by selecting one of the two possibilities for the hot phase geometry. It turns out that for both geometries we obtain the same relation

$$h \simeq 1.7 \times 10^{-1} \frac{0.5}{T_{\text{dis}}} \frac{\eta}{0.9} \left(\frac{r_c}{100}\right)^{3/2}, \quad (18)$$

where  $r_c = R_c/R_s$ .

In the case of the thick inner flow, self-consistency would require a substantial scaleheight of the hot flow. If, for example, we require  $h \gtrsim 0.1$ , we obtain a constraint on the radial extent of the inner hot flow  $r_c \gtrsim 70$ , which, incidentally, appears to be consistent with the spectroscopically-inferred inner radius of the truncated cold disc (Esin et al. 2001; C03).

The same spectroscopic constraints also apply to the patchy corona case (see next section) and the radial extension of the corona above the disc should also be at least  $r_c \sim 100$ . Then for typical inferred values of the size of the active regions ( $r_x \sim$  a few; see, for example, Haardt et al. 1994; Di Matteo, Celotti & Fabian 1999), the aspect ratio of the cylindrical regions is written

$$\frac{h}{a} \simeq 1.6 \frac{0.5}{T_{\text{dis}}} \frac{\eta}{0.9} \frac{3}{r_x} \left(\frac{r_c}{100}\right)^{5/2} \frac{\ln(r_c/3)}{\ln(100/3)}. \quad (19)$$

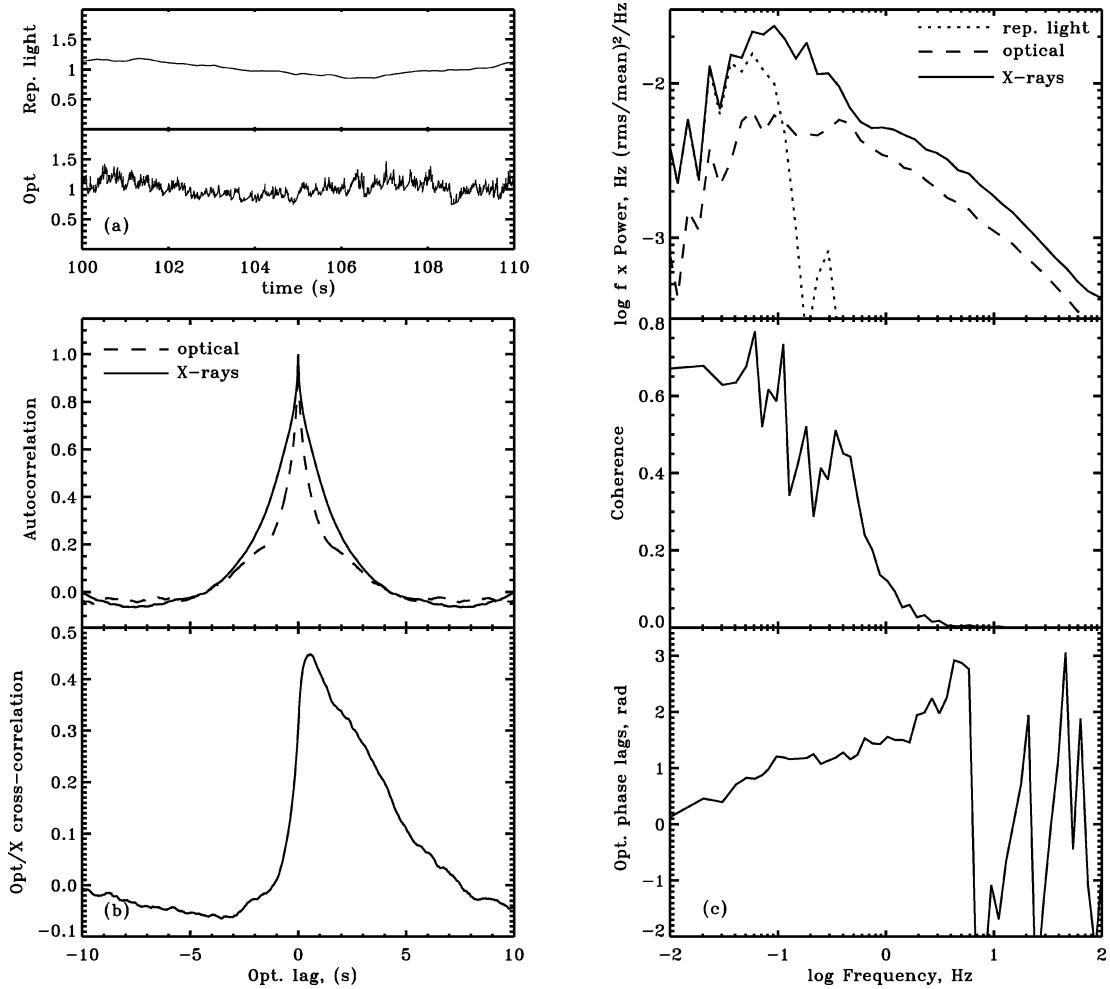


**Figure 2.** Same simulation as in Fig. 1 but adding a disc reprocessing component accounting for 30 per cent of the optical flux on average (see Section 3.4). (a) Sample light curves of the reprocessed component and total optical. (b) X-ray/optical autocorrelation and cross-correlation functions. (c) Power spectra of the reprocessed component, total optical and X-rays (top), X-ray/optical coherence and phase lags (middle and bottom).

It appears to be slightly larger than unity, as required to reproduce the hard X-ray spectrum (see, for example, Malzac, Beloborodov & Poutanen 2001). Note that the aspect ratio is very sensitive to the coronal radius. If  $r_c$  is as large as 350, as inferred by C03 we obtain quite a large ratio  $h/a \simeq 27$ , then internally generated cyclotron radiation should dominate over reprocessing as a source of seed photons for the Comptonization process.

Moreover, combining the expression that relates the observed X-ray luminosity (equation 1) with the constraints obtained above on the field dissipation speed, we can estimate the value of the magnetic field. In the case of the thick inner flow we obtain

$$B \simeq 3.2 \times 10^6 \left[ \frac{f_x}{0.1} \frac{\eta}{0.9} \right]^{-1/2} \frac{T_{\text{dis}}}{0.5s} \left( \frac{r_c}{100} \right)^{-9/4} \text{ G.} \quad (20)$$

From the lower limit on the inner disc radius derived above, we conclude that  $B \lesssim 7 \times 10^6$  G. In the case of the patchy corona

$$B \simeq 2.5 \times 10^7 \left[ \frac{f_x}{0.1} \frac{\eta}{0.9} \frac{\ln(r_c/3)}{\ln(100/3)} \frac{N}{10} \right]^{-1/2} \times \frac{T_{\text{dis}}}{0.5s} \frac{3}{r_x} \left( \frac{r_c}{100} \right)^{-5/4} \text{ G.} \quad (21)$$

We note that the rms variability amplitude should scale as  $N^{-1/2}$ , so that the magnetic field intensity is directly proportional to the observed variability level.

Finally, let us discuss the different variability time-scales of the dissipation rates, as fixed in our fiducial model. On the one hand, the range of time-scales on which the variability of  $K_x$  is maximal is between 50 and 1 Hz, corresponding to the Keplerian frequencies between 10 and 100  $R_S$  (for a 10- $M_\odot$  black hole). This is consistent with the X-rays being produced in the hot phase of the accretion flow (either in a geometrically thick disc or in the corona). In general, the dissipation of the tangled magnetic field into particle heating is essentially a local process acting on time-scales comparable to the local dynamical time. Therefore, the minimum and maximum variability time-scales of  $K_x$  reflect the smallest and largest radii where we have substantial energy in the hot phase/corona.

On the other hand, we see from Fig. 1 that the variability of  $K_j$  is high on a much wider range of time-scales than  $K_x$ , from 0.01 to 10 s. As discussed in Sections 2.4 and 3, the data require that at low frequencies the fluctuations of  $K_j$  dominate over the other sources of variability. The physical interpretation is that generating a powerful outflow requires large-scale coherent poloidal field structures threading a significant fraction of the inner disc surface and extending also in the vertical direction. Such structures may take more time

to build and destroy. So, locally, the time-scale of variation of  $K_j$  can go from the dynamical time itself to larger time-scales (in the rare cases where the field builds up its poloidal component to a larger scale). Based on simple arguments, Livio et al. (2003) estimate that the time-scale for establishing a change in the scale of the poloidal component of the magnetic field through dynamo processes is larger than the dynamical time-scale by a factor  $t_{\text{jet}}/t_{\text{dyn}} \sim 2^{1/h}$ . Because our model indicates  $t_{\text{jet}}/t_{\text{dyn}} \sim 10$ , this would imply  $h \sim 0.3$ , which appears to be in agreement with the independent estimate provided by equation (18).

We also note that the variability of  $K_j$  induces large amplitude fluctuations of the energy reservoir, which in turn lead to an important X-ray variability on time-scales much larger than the dynamical time. In fact, most of the observed X-ray variability is caused by the jet activity, providing an explanation for the long observed time-scales. Recently, King et al. (2004) have proposed a detailed physical model for the X-ray variability of accreting black holes that considers a similar situation where large-scale ejection events modulate the strong X-ray emission from the inner disc.

#### 4.2 Constraints from time-averaged spectroscopy

We have shown in Section 3 that there is an important condition for our model to work, namely that the jet power should dominate over the X-ray luminosity. We will now discuss how realistic this assumption is.

First, let us examine the observed energetic output of XTE J1118+480. We stress that this is the best source available for such a study, given its unsurpassed spectral coverage. In the following we express all the luminosities in units of the Eddington luminosity ( $L_{\text{Edd}} = 1.3 \times 10^{38} (M/M_{\odot}) \text{ erg s}^{-1}$ , with  $M = 10 M_{\odot}$ ). The numbers given below are taken from the results of the multi-wavelength spectral analysis of C03. These authors decomposed the overall spectral energy distribution (SED) into three components, as follows.

(i) The jet component has a total observed radiative luminosity of  $L_j = 3.8 \times 10^{-5}$ , assuming isotropy and integrating the power-law emission from the radio to the optical band. In the optical/UV, the emission should start to be dominated by the cold accretion disc, but the possibility that the jet spectrum extends up into the UV domain cannot be ruled out. Indeed, the fact that H03 observe similar correlated variability in the UV and optical lends support to this hypothesis. If this is the case, the estimated jet luminosity can increase by up to a factor of 8.

(ii) For the standard cold accretion disc we have  $L_d = 1.7 \times 10^{-3}$ . This estimate was obtained by C03 with a fit of the optical to extreme ultraviolet (EUV) spectrum with a multicolour blackbody model. The inner disc temperature was found to be very low  $kT \sim 20 \text{ eV}$ , suggesting that either the inner disc is truncated at  $\sim 350 R_S$ , or that the bulk of the accretion power is driven away in a coronal outflow and the disc is left very cold.

(iii) Finally, for the luminosity of the X-ray emitting plasma, or corona, we have  $L_x = 1.2 \times 10^{-3}$ , assuming isotropy.

Summing up all three spectral components above, we find that the bolometric luminosity of the source is

$$L_{\text{bol}} = L_j + L_d + L_x \simeq 3 \times 10^{-3}. \quad (22)$$

The total mass accretion rate on to the black hole can be estimated from the observed luminosity of the cold disc component. We define the Eddington-scaled accretion rate  $\dot{m} = \epsilon \dot{M} c^2 / L_{\text{Edd}}$  where  $\epsilon$  is the Newtonian accretion efficiency  $\epsilon = 1/12$ . If the cold, geometrically

thin and optically thick disc is indeed truncated at  $R_{\text{in}} = 350 R_S$ , as the spectral analysis of C03 suggests, then standard accretion formulae (Frank, King & Raine 2002) give

$$\dot{m} = 4\epsilon \frac{R_{\text{in}}}{R_S} L_d \sim 0.2. \quad (23)$$

On the other hand, if the accretion disc extends down to the innermost stable orbit ( $R_{\text{in}} = 3 R_S$ ), but is sandwiched by a powerful corona, where a fraction  $f_H$  of the power is dissipated, then we can estimate that

$$f_H = \left( 1 + \frac{L_d(1-\eta)}{L_x} \right)^{-1}. \quad (24)$$

The  $\eta$  parameter is only poorly constrained, but in any case  $f_H$  should be very large in order to explain the low inner disc temperature (Merloni, Di Matteo & Fabian 2000). Taking  $\eta \simeq 0.9$  as indicated by the time-dependent model, we obtain  $f_H = 0.88$ , and, for the total mass accretion rate

$$\dot{m} = 4\epsilon \frac{R_{\text{in}}}{R_S} \frac{L_d}{(1-f_H)} \sim 0.015. \quad (25)$$

In both cases, the estimated accretion rate is much larger than the observed bolometric luminosity. Thus, most of the accretion power is not radiated and the source appears to be radiatively inefficient.

The important issue, however, would be to determine whether the missing accretion power escapes the system in the (low radiative efficiency) jet or in other forms of non-radiative losses, such as a slow wind, or large-scale convective motions, or advection into the black hole. The answer to this question resides in the exact determination of the jet kinetic power. Unfortunately, there are major uncertainties in this determination, mainly because the jet radiative efficiency is not known. The jet is expected to be a poor radiator because most of the energy is lost in adiabatic expansion, thus, although the radiation from the jet represents a small fraction of the bolometric luminosity the jet could dominate the energetics. Both theory and observations indicate that the efficiency can be extremely low (as low as  $\epsilon_j \sim 10^{-4}$ ; see Celotti & Fabian 1993), but all present estimates are model-dependent. In general, they indicate radiative efficiencies of the order of  $\epsilon_j \sim 0.01$ . For the case of XTE J1118+480 this would already imply that the total jet power dominates over the X-ray luminosity. Obviously, if the jet efficiency is lower, or the jet spectrum extends to shorter wavelength, or beaming effects are important, the jet dominance can easily be much larger. As discussed above, the analysis of our time-dependent modelling strongly requires  $f_x \lesssim 0.1$ , corresponding to a jet efficiency  $\epsilon_j \lesssim 3 \times 10^{-3}$ .

In the case of the truncated disc plus hot inner flow model, the derived  $\dot{m}$  sets an upper limit to the jet power, in the case where all the accretion power is lost in the jet:  $P_j/L_x \sim \dot{m}/L_x \sim 200$ . On the other hand, if the jet power is comparatively modest, e.g.  $P_j/L_x \sim 10$  as assumed in the simulation of Fig. 1, this would imply that, although the jet dominates over the X-ray emission, it does not dominate as a power sink. If the dominant power sink is, for example, advection on to the black hole, the mass accretion rate we derive appears somewhat large to be consistent with advection dominated accretion flow (ADAF) models (Narayan & Yi 1994). However, it is important to notice that the observed accretion rate is very sensitive to the value of the inner disc radius (see equation 23), which is actually poorly constrained. Moreover, the critical accretion rate for ADAF models above which the ADAF solution breaks down scales as  $\alpha^2$  (Rees et al. 1982; Narayan & Yi 1995), and the unknown standard  $\alpha$  parameter could be larger than usually considered leading to the existence of solutions at higher  $\dot{m}$  than previously thought. Finally, we note that the dynamics of the ADAF solutions coupled

with jets have not been worked out yet. The structure of the accretion flow as well as the (in)stability of the solution at high  $\dot{m}$  are likely to be strongly affected by the presence of the jet. Although an ADAF is in many aspects consistent with our analysis, it should certainly differ considerably from the standard solution.

In the case of the accretion disc plus patchy corona (or coronal outflow) model the  $\dot{m}$  derived assuming  $\eta = 0.9$  is consistent with all of the non-radiated power driving the jet. However, when we attempted to fit the optical/UV spectrum of XTE J1118+480 with the disc corona solution of Merloni & Fabian (2002), we found that it was not possible to produce inner disc temperatures as low as observed ( $\sim 20$  eV). The coronal outflow model could be reconciled with the EUV spectral data only if an even larger fraction of the power was extracted from the disc into the corona/jet, requiring  $f_H$  to be very close to 1. However, in the framework of magnetic coronae powered by an MHD turbulent disc, having  $f \sim 1$  also requires a very large (magnetic) viscosity (Merloni 2003), and implies an even stronger jet dominance of the total energy budget of the source.

An alternative way to obtain a low inner disc temperature together with a reasonable value of  $f_H$  would be that the cold disc does not extend down to the last stable orbit. Instead, below a few tens of  $R_S$  the disc is truncated and the flow becomes very inefficient. However, such a picture would be very similar to the truncated disc plus hot inner flow scenario discussed above, except that the jet would be launched from the external accretion disc corona.

## 5 SOME WIDER IMPLICATIONS OF THE MODEL

### 5.1 Comparison with other sources

The behaviour of XTE J1118+480 demonstrates that the accretion flow on to a black hole can lead to a strong jet with little disc emission. A similar situation occurs in the massive elliptical galaxy M87 where powerful jets are associated with an otherwise weak galactic nucleus. The Bondi accretion rate on to the supermassive black hole in M87, deduced from the properties of the surrounding gas with *Chandra* observations (Di Matteo et al. 2003), can give the observed jet power, deduced from the cavities made by them in the surrounding intracluster medium, provided that accretion efficiency is 0.1 or more. Assuming that the flow is in a steady state, such a high efficiency argues that most of the accreting gas flows to within a few gravitational radii of the black hole. Because thick hot flows are unstable to mass loss over a wide range of radii (Blandford & Begelman 1999; Stone et al. 1999; Quataert & Gruzinov 2000), this favours a magnetically dominated cold disc flow in the case of M87. By similarity it argues for a magnetically dominated cold disc in XTE J1118+480 as well. The reservoir and presumably the base of the jet must also lie within a few gravitational radii of the black hole in both cases.

As mentioned in the introduction, the low state of many Galactic black hole systems appears to contain a powerful jet. When systems drop below about 1 per cent of the Eddington accretion rate, the disc may be magnetically dominated (Merloni & Fabian 2002; Livio et al. 2003), with a fast jet taking most of the gravitational energy released. This may also apply to massive black holes, as illustrated above with M87. The issue of how apparently well-fed massive black holes in galactic nuclei are feeble sources of electromagnetic radiation has been a puzzle for some years (Fabian & Canizares 1988; Fabian & Rees 1995; Di Matteo et al. 2001, 2003; Loewenstein et al. 2001; Pellegrini et al. 2003). Most of these objects do however have jetted radio emission (Franceschini et al. 1998) and a solution in which

the accretion power is principally carried away by jets is a strong possibility. Unless the energy contained in black hole spin is a key factor, then magnetically dominated discs should be part of that solution.

Further time-dependent studies of the multiwavelength behaviour in other stellar-mass and massive black hole systems may show similar behaviour to that of XTE J1118+480. Some examples which already offer tantalizing behaviour are the Galactic microquasar GRS1915+105 (Mirabel et al. 1998; Klein-Wolt et al. 2002), the Galactic binary GX339–4, which has also displayed rapid optical flickering (Motch, Ilovaisky & Chevalier 1982), and the blazar 3C 120, which shows X-ray dips before radio jet events are seen (Marscher et al. 2002).

### 5.2 Jet dominated sources in the low/hard state

Whatever the actual structure of the accretion flow, we have shown that, during the outburst of XTE J1118+480, the total kinetic jet power should dominate over the X-ray luminosity, and could possibly be the dominant repository of the accretion power. There are additional independent arguments in favour of jet dominance in low/hard state sources and in XTE J1118+480 in particular. Based on the observed radio flux ( $L_R$ ) and X-ray correlation observed in hard state sources (Falcke & Biermann 1996; Gallo et al. 2003), as well as on standard synchrotron formulae (Heinz & Sunyaev 2003), Fender, Gallo & Jonker (2003, hereafter FGJ03) have shown that, provided that advection into the black hole horizon and/or convective motions do not store a large fraction of the accretion power, there should exist a critical accretion rate,  $\dot{m}_{cr}$ , below which an accreting black hole is jet dominated.

The exact value for the critical accretion rate could be inferred from the observations, if we knew the total jet power at a certain X-ray luminosity, and is given by  $\dot{m}_{cr} = 2P_j^2/L_x$ , corresponding to a critical X-ray luminosity  $L_{x,cr} = \dot{m}_{cr}/2$ . Fender et al. (2001) derived a lower limit for the jet to X-ray power ratio in XTE J1118+480 ( $P_j/L_x = 0.2$ ) and FGJ03 used this conservative estimate to determine the value of the critical rate  $\dot{m}_{cr} \simeq 7 \times 10^{-5}$ . However, such a low value of the critical luminosity leads to several problems.

First, as shown in FGJ03, during the transition from a disc to a jet dominated state, the dependence of the X-ray luminosity on the accretion rate changes from being  $L_x \propto \dot{m}^2$ , the right scaling for radiatively inefficient flows, to  $L_x \propto \dot{m}$ , the scaling for radiatively efficient flows (see fig. 1 of FGJ03). This would imply that with  $L_x \sim 10^{-3}$ , XTE J1118+480 should be a radiatively efficient system. As discussed above, there is however strong observational evidence of the contrary.

Secondly, during the transition from jet to disc dominated state, the jet power changes from  $P_j \propto \dot{m}$ , which is the natural scaling expected in most jet models, to the seemingly unphysical  $P_j \propto \dot{m}^{1/2}$ .

Furthermore, black holes in the hard state should show some kind of spectral transition in the X-ray band at the critical luminosity  $L_{x,cr} \sim 3 \times 10^{-5}$ , due to the drastic changes in emission mechanisms that are needed to account for the different scalings of  $L_x$  with the accretion rate. The observations of low/hard state sources at such low luminosities are few and hard to perform, however no indication of any dramatic spectral change in any hard state source down to quiescent level has ever been reported (Kong et al. 2002; Hameury et al. 2003)

In fact, the only physical transition that we do actually observe is the transition between the hard and the soft state that occurs at luminosities of at least a few per cent of Eddington luminosity (Maccarone 2003). We believe that, if the above-mentioned

difficulties are to be solved, then  $\dot{m}_{\text{cr}}$  has to correspond to luminosities that are comparable to, or larger than, hard-to-soft state transition luminosities.

For the case of XTE J1118+480, instead of using the lower limit for the jet to X-ray power ( $P_j/L_x = 0.2$ ), we can adopt the much larger value  $P_j/L_x \sim 10$  required by our variability model. Then we find  $\dot{m}_{\text{cr}} \sim 0.2$ , involving a transition at  $L_{x,\text{cr}} = \dot{m}_{\text{cr}}/2 \sim 0.1$ . This is in agreement with the idea that the transition from jet dominated to X-ray dominated states occurs at luminosities similar or slightly higher than the hard-to-soft state transition. We stress that the argument of FGJ03 holds only as long as the  $L_R-L_x$  correlation is valid, i.e. not in the soft state. There is thus no reason to associate the disc dominated state of FGJ03 with the soft state.

If, as we suggest, the critical luminosity  $L_{x,\text{cr}}$  is at or above the hard-to-soft state transition luminosity, then the disc dominated state of FGJ03 does not exist. Moreover, although one can speculate that the transition to soft state may be triggered by the loss of the jet dominance, there is a priori no reason for the critical luminosity  $L_{x,\text{cr}}$  to be coincident with the hard-to-soft state transition luminosity. In other words, the observed presence of a hard-to-soft state transition does not provide an upper limit to the jet power, but only a lower limit.

We also note that the above discussion was made neglecting any contribution from advection and other possible non-radiative losses. However, in jet dominated sources the jet power scales proportionally to the accretion rate, as is the case for any adiabatic loss. Therefore, the effects of advection (and/or convection) would not change the scalings of jet and X-ray powers provided that we replace the accretion rate  $\dot{m}$  with  $\dot{m}_{\text{eff}} = \dot{m}(1 - f_{\text{ad}})$ , where  $f_{\text{ad}}$  is the fraction of accretion power that is advected into the black hole. In particular, the critical X-ray luminosity  $L_{x,\text{cr}}$ , although corresponding to a larger ‘real’  $\dot{m}$ , would remain unchanged.

To conclude, the central requirement of our model, i.e. that in XTE J1118+480 the jet power dominates over the X-ray luminosity, appears to be supported by the observations of hard state black holes. Then, if the arguments of FGJ03 are correct, an important consequence of the jet dominance in XTE J1118+480 is that all hard state sources are jet dominated (in the sense that the jet power dominates over the X-ray power). This jet dominance also implies that all hard state sources should be radiatively inefficient.

It is not clear whether most of the accretion energy is channelled into the jet or across the black hole event horizon. The  $L_x \propto \dot{m}_{\text{eff}}^2$  dependence of the X-ray luminosity (also observed in low-luminosity active galactic nuclei, as inferred from the multivariate radio-X-rays–mass correlation; Merloni et al. 2003; Falcke et al. 2004) is similar to what is predicted by the radiatively inefficient accretion model. The reason for this inefficiency could be advection into the jet as well as advection into the black hole.

## 6 CONCLUSIONS

We have shown that the puzzling optical/X-ray correlations of XTE J1118+480 can be understood in terms of a common energy reservoir for both the jet and the Comptonizing electrons. For illustration purposes, we have presented a specific shot noise variability model that reproduces all the main observed features of the multiwavelength correlated variability.

Our time-dependent model is fairly general, and our main conclusions hold regardless of the specific geometrical and dynamical properties of the system. The main results can be summarized as follows.

(i) Any energy reservoir model for XTE J1118+480 requires that the total jet power dominates over the X-ray luminosity. In particular, assuming that the compact jet synchrotron emission extends up to the optical band, this implies a radiative efficiency for the jet  $\epsilon_j \lesssim 3 \times 10^{-3}$ . Following the same line of argument as FGJ03, we have shown that this situation is likely and probably represents a common feature of all black holes in the low/hard state.

(ii) The range of typical variability time-scales of dissipation rate of the X-ray emitting plasma is consistent with the dynamical times of an accretion disc between  $\sim 10$  and 100 Schwarzschild radii (for a  $10\text{-}M_{\odot}$  black hole). As expected, the X-ray variability can be associated with either a hot, thick inner accretion flow or with a patchy corona.

(iii) As jet launching requires large-scale coherent magnetic structures, the energy dissipation in the jet should vary on longer time-scales. Indeed, the derived range of time-scales associated with the dissipation in the jet extends to time-scales more than 10 times larger than the X-ray emitting one.

(iv) By combining the information obtained from our time variability model with (time-averaged) spectral analysis we conclude that, whatever the accretion geometry, the whole disc–corona–jet system must be radiatively inefficient. It is therefore possible, in principle, that the system is energetically dominated by the jet, as suggested by FGJ03, although whether the bulk of the accretion power is advected into the black hole or into the jet remains at present an open question.

(v) In terms of specific dynamical models, we conclude that the observed properties of XTE J1118+480 during its low/hard state outburst are consistent with either an inner hot, quasi-spherical, radiatively inefficient flow, from which the jet originates (Meier 2001), surrounded by a geometrically thin, optically thick cold disc, or with a powerful patchy, outflowing corona on top of an extremely cold standard thin disc. In the first case, multicolour disc fits to the UV/EUV spectrum indicate a very large inner disc radius, implying a large total accretion rate ( $\dot{m} \simeq 0.2$ ), which might be in conflict with the hypothesis of standard advection dominated flow theory. In the second case, in order to reproduce the very low inner disc temperature, an (uncomfortably) extreme coronal power is needed, together with substantial relativistic bulk motion of the coronal plasma, both possibly associated with very high magnetic viscosity.

## ACKNOWLEDGMENTS

JM acknowledges financial support from the Particle Physics and Astronomy Research Council (PPARC). We are grateful to Annalisa Celotti and Jim Pringle for useful discussions.

## REFERENCES

- Balbus S. A., Hawley J. F., 1998, *Rev. Mod. Phys.*, 70, 1
- Blandford R. D., Begelman M. C., 1999, *MNRAS*, 303, L1
- Blandford R. D., Königl A., 1979, *ApJ*, 232, 34
- Blandford R. D., Payne D. G., 1982, *MNRAS*, 199, 883
- Blandford R. D., Znajek R. L., 1977, *MNRAS*, 179, 433
- Celotti A., Fabian A. C., 1993, *MNRAS*, 264, 228
- Chaty S., Haswell C. A., Malzac J., Hynes R. I., Shrader C. R., Cui W., 2003, *MNRAS*, 346, 689 (C03)
- Corbel S., Fender R. P., Tzioumis A. K., Nowak M., McIntyre V., Durouchoux P., Sood R., 2000, *A&A*, 359, 251
- Corbel S., Nowak M. A., Fender R. P., Tzioumis A. K., Markoff S., 2003, *A&A*, 400, 1007
- Di Matteo T., Blackman E. G., Fabian A. C., 1997, *MNRAS*, 291, L23

264 *J. Malzac, A. Merloni and A. C. Fabian*

- Di Matteo T., Celotti A., Fabian A. C., 1999, *MNRAS*, 304, 809
- Di Matteo T., Johnstone R. M., Allen S. W., Fabian A. C., 2001, *ApJ*, 550, L19
- Di Matteo T., Allen S. W., Fabian A. C., Wilson A. S., Young A. J., 2003, *ApJ*, 582, 133
- Esin A. A., McClintock J. E., Drake J. J., Garcia M. R., Haswell C. A., Hynes R. I., Munro M. P., 2001, *ApJ*, 555, 483
- Fabian A. C., Canizares C. R., 1988, *Nat*, 333, 829
- Fabian A. C., Rees M. J., 1995, *MNRAS*, 277, L55
- Falcke H., Biermann P. L., 1996, *A&A*, 308, 321
- Falcke H., K rding E., Markoff S., 2004, *A&A*, 414, 895
- Fender R., 2004, in Lewin W. H. G., van der Klis M., eds, *Compact Stellar X-Ray Sources*. Cambridge Univ. Press, Cambridge, in press (astro-ph/0303339)
- Fender R. et al., 1999, *ApJ*, 519, L165
- Fender R. P., Hjellming R. M., Tilanus R. P. J., Pooley G. G., Deane J. R., Ogle R. N., Spencer R. E., 2001, *MNRAS*, 322, L23
- Fender R. P., Gallo E., Jonker P. G., 2003, *MNRAS*, 343, L99 (FGJ03)
- Franceschini A., Vercellone S., Fabian A. C., 1998, *MNRAS*, 297, 817
- Frank J., King A., Raine D. J., 2002, *Accretion Power in Astrophysics*, 3rd edn. Cambridge Univ. Press, Cambridge
- Gallo E., Fender R. P., Pooley G. G., 2003, *MNRAS*, 344, 60
- Georganopoulos M., Aharonian F. A., Kirk J. G., 2002, *A&A*, 388, L25
- Gierlinski M., Zdziarski A. A., Done C., Johnson W. N., Ebisawa K., Ueda Y., Haardt F., Philips B. F., 1997, *MNRAS*, 288, 958
- Haardt F., Maraschi L., Ghisellini G., 1994, *ApJ*, 432, L95
- Hameury J.-M., Barret D., Lasota J.-P., McClintock J. E., Menou K., Motch C., Olive J.-F., Webb N., 2003, *A&A*, 399, 631
- Heinz S., Sunyaev R. A., 2003, *MNRAS*, 343, L59
- Hjellming R. M., Johnston K. J., 1988, *ApJ*, 328, 600
- Hynes R. I. et al., 2003, *MNRAS*, 345, 292 (H03)
- Kanbach G., Straubmeier C., Spruit H. C., Belloni T., 2001, *Nat*, 414, 180 (K01)
- King A. R., Pringle J. E., West R. G., Livio M., 2004, *MNRAS*, 348, 111
- Klein-Wolt M., Fender R. P., Pooley G. G., Belloni T., Migliari S., Morgan E. H., van der Klis M., 2002, *MNRAS*, 331, 745
- Kong A. K. H., McClintock J. E., Garcia M. R., Murray S. S., Barret D., 2002, *ApJ*, 570, 277
- Livio M., Ogilvie G. I., Pringle J. E., 1999, *ApJ*, 512, 100
- Livio M., Pringle J. E., King A. R., 2003, *ApJ*, 593, 184
- Loewenstein M., Mushotzky R. F., Angelini L., Arnaud K. A., Quataert E., 2001, *ApJ*, 555, L21
- Maccarone T. J., 2003, *A&A*, 409, 697
- Maccarone T. J., Coppi P. S., 2002, *MNRAS*, 336, 817
- McClintock, J. E., Remillard, R. A., 2004, in Lewin W. H. G., van der M., eds, *Compact Stellar X-ray Sources*. Cambridge Univ. Press, Cambridge, in press (astro-ph/0306213)
- McClintock J. E., Garcia M. R., Caldwell N., Falco E. E., Garnavich P. M., Zhao P., 2001a, *ApJ*, 551, L147
- McClintock J. E. et al., 2001b, *ApJ*, 555, 477
- Malzac J., Beloborodov A. M., Poutanen J., 2001, *MNRAS*, 326, 417
- Malzac J., Belloni T., Spruit H. C., Kanbach G., 2003, *A&A*, 407, 335 (M03)
- Markoff S., Falcke H., Fender R., 2001, *A&A*, 372, L25
- Marscher A. P., Jorstad S. G., McHardy I. M., Aller M. F., Balonek T. J., Sokolov A. S., 2002, *A&AS*, 34, 1246
- Meier D. L., 2001, *ApJ*, 548, L9
- Merloni A., 2003, *MNRAS*, 341, 1051
- Merloni A., Fabian A. C., 2001, *MNRAS*, 321, 549
- Merloni A., Fabian A. C., 2002, *MNRAS*, 332, 165
- Merloni A., Di Matteo T., Fabian A. C., 2000, *MNRAS*, 318, L15
- Merloni A., Heinz S., Di Matteo T., 2003, *MNRAS*, 345, 1057
- Mirabel I. F., Dhawan V., Chaty S., Rodriguez L. F., Marti J., Robinson C. R., Swank J., Geballe T., 1998, *A&A*, 330, L9
- Motch C., Ilovaisky S. A., Chevalier C., 1982, *A&A*, 109, L1
- Narayan R., Yi I., 1994, *ApJ*, 428, L13
- Narayan R., Yi I., 1995, *ApJ*, 452, 710
- Negoro H., Kitamoto S., Takeuchi M., Mineshige S., 1995, *ApJ*, 452, L49
- Pellegrini S., Baldi A., Fabbiano G., Kim D.-W., 2003, *ApJ*, 597, 175
- Poutanen J., 1998, in Abramowicz M. A., Bj rnsson G., Pringle J., eds, *Theory of Black hole Accretion Disc*. Cambridge Univ. Press, Cambridge, p. 100
- Poutanen J., Fabian A. C., 1999, *MNRAS*, 306, L31
- Quataert E., 1998, *ApJ*, 500, 978
- Quataert E., Gruzinov A., 1999, *ApJ*, 520, 248
- Quataert E., Gruzinov A., 2000, *ApJ*, 539, 809
- Rees, M. J., Phynney, E. S., Begelman, M. C., Blandford, R. D., 1982, *Nat*, 295, 17
- Remillard R., Morgan E., Smith D., Smith, E., 2000, *IAU Circ.*, 7389, 2
- Shapiro S. L., Lightman A. P., Eardley D. M., 1976, *ApJ*, 204, 187
- Spruit H. C., Kanbach G., 2002, *A&A*, 391, 225
- Stirling A. M., Spencer R. E., de la Force C. J., Garrett M. A., Fender R. P., Ogle R. N., 2001, *MNRAS*, 327, 1273
- Stone J. M., Pringle J. E., Begelman M. C., 1999, *MNRAS*, 310, 1002
- Tanaka Y., Lewin W. H. G., 1995, in Lewin W. H. G., van Paradjis J., van den Heuvel E., eds, *X-ray Binaries*. Cambridge Univ. Press, Cambridge
- Tananbaum H., Gursky H., Kellogg E., Giacconi R., Jones C., 1972, *ApJ*, 177, L5
- Uttley P., McHardy I. M., 2001, *MNRAS*, 323, L26

This paper has been typeset from a  $\text{\TeX}/\text{\LaTeX}$  file prepared by the author.

#### **5.4 “Full radiative coupling in two-phase models for accreting black holes”**

Malzac J., Dumont A.-M., Mouchet M., *Astronomy and Astrophysics*, v.430, p.761-769 (2005).



## Full radiative coupling in two-phase models for accreting black holes

J. Malzac<sup>1,2</sup>, A. M. Dumont<sup>3</sup>, and M. Mouchet<sup>3</sup>

<sup>1</sup> Centre d'Étude Spatiale des Rayonnements, CNRS-UPS, 9 avenue du Colonel Roche, 31028 Toulouse Cedex 4, France  
 e-mail: malzac@cesr.fr

<sup>2</sup> Institute of Astronomy, Madingley Road, Cambridge, CB3 0HA, UK

<sup>3</sup> LUTH, UMR 8102 (CNRS/Université Paris 7), Observatoire de Paris, Section de Meudon, 92195 Meudon Cedex, France

Received 21 January 2003 / Accepted 21 July 2004

**Abstract.** The emission from galactic black holes and Seyfert galaxies is generally understood in term of two-phase models (Haardt & Maraschi 1991, 1993). Such models postulate that a hot plasma ( $\sim 10^9$  K) coexists with relatively colder material ( $\sim 10^6$  K) in the inner part of the accretion flow. We present the first simulated broad-band spectra produced by such a system and accounting simultaneously for energy balance and Comptonisation in the hot phase, together with reflection, reprocessing, ionization and thermal balance in the cold phase. This was made possible by coupling three radiative transfer codes: a non-linear Monte-Carlo code (NLMC), a photo-ionization code TITAN and a linear Monte-Carlo code NOAR. The equilibrium comptonisation spectrum appears to be sensitive to the shape of the reprocessed spectrum that, in turn, depends on the ionization parameter, but also on the structure of the irradiated cold material. This is illustrated by a comparison of simulations assuming constant density or a constant pressure in the cold phase. We also compare our results with simplified models where reprocessing is approximated by a blackbody spectrum. Our detailed treatment leads to noticeably different spectral energy distributions (SEDs) characterised by harder X-ray spectra. Even at low ionization parameters ( $\xi \sim 300$  erg s<sup>-1</sup> cm) the commonly used blackbody approximation is poor, leading to X-ray spectra that are too soft. The effect, however, seems not to be strong enough to reconcile the slab corona model with the hardest observed spectra, unless the reflector has a constant density and the ionization parameter is large, of the order of  $10^4$  erg s<sup>-1</sup> cm.

**Key words.** accretion, accretion disks – black hole physics – radiative transfer – method: numerical – galaxies: Seyfert – X-ray: binaries

### 1. Introduction

At least two distinct mediums are required to produce the main features observed in the broad band spectra of radio quiet active galactic nuclei (AGN) and black hole binaries (BHBs) in the low/hard state. Their hard X-ray emission exhibits a power-law spectrum cutting-off at a few hundred keV, which is generally interpreted as thermal Comptonisation spectra in a very hot ( $\sim 10^9$  K) optically thin plasma with Thomson depth  $\tau_T \sim 1$  (Sunyaev & Titarchuk 1980; Haardt & Maraschi 1991; Stern et al. 1995b; Poutanen & Svensson 1996; Zdziarski et al. 1998). The big blue bump observed in the UV spectra of Seyfert galaxies (Walter & Fink 1993), as well as the soft X-ray excess in BHBs (e.g. Balucinska-Church et al. 1995) are indicative of thermal emission from optically thick and much colder material with a temperature in the range  $10^5$ – $10^7$  K. The presence of relatively cold material in the innermost part of the accretion flow is corroborated by the existence of reflection features in the X-rays such as the Fe fluorescence line around 6.4 keV and a reflection bump peaking at about 30 keV (George & Fabian 1991; Nandra & Pounds 1994).

The nature and geometry of these two phases are uncertain. The cold medium is generally believed to form an accretion disc (Shakura & Sunyaev 1973), alternatively it could consist of cold dense clouds located inside or around the hot plasma (Rees 1987; Collin-Souffrin et al. 1996; Malzac 2001; Malzac & Celotti 2002). The hot phase could constitute the accretion disc corona (Svensson & Zdziarski 1994; Życki et al. 1995; Sincell & Krolik 1997; Różańska & Czerny 2000, and Ref. therein) or the hot inner part of the accretion disc itself (Shapiro & Lightman 1976).

It was soon realized that, if close to each other, the hot and the cold phases should be strongly radiatively coupled. This led to the development of two-phase models (Haardt & Maraschi 1991, 1993), where the cold phase constitutes the main source of seed photons for the Comptonisation process. The temperature in the hot phase, and thus the detailed shape of the high energy spectrum, is controlled mainly by the flux of soft cooling photons. On the other hand, the thermal reprocessing of the high energy radiation impinging on the cold phase provides a dominant contribution to soft emission from the cold phase.

Due to the complexity of the Comptonisation process, the importance of geometric effects, and the requirement of taking accurately into account the coupling between the two phases, it was necessary to develop sophisticated numerical codes in order to compute the detailed spectrum produced by the two-phase system in different configurations (Stern et al. 1995a; Poutanen & Svensson 1996).

The methods developed in this context, such as the non-linear Monte-Carlo method (Stern et al. 1995a), provide an accurate treatment of the hot phase emission in energy balance. On the other hand, the emission from the cold phase is not detailed: a pure blackbody spectrum with a fixed temperature and reflection on neutral material are generally assumed.

Actually the emission due to X-ray reprocessing in the cold phase differs widely from a simple blackbody, in particular there is a complex line emission. Moreover, due to the hard X-ray irradiation, a ionised skin is likely to form on the surface layers of the cold material (Ross & Fabian 1993; Collin-Souffrin et al. 1996; Nayakshin et al. 2000; Ballantyne et al. 2001). This ionised material affects the line emission as well as the shape and amplitude of the reflection component (Życki et al. 1994; Dumont et al. 2000; Nayakshin et al. 2000; Nayakshin & Kallman 2001). Ionization is also likely to affect the equilibrium in the hot phase. Indeed the hard X-ray albedo for ionised material is larger and, as a consequence, the flux of thermal reprocessed soft photons is lower, affecting the temperature in the hot plasma.

The first attempts to include these effects in the two-phase model calculations used a very simplified approach to the computation of the reprocessed spectrum (e.g. Nayakshin & Dove 2001). Indeed, a detailed self-consistent computation of the emission from irradiated material is an heavy task. It requires one to solve the radiative transfer equations in the cold medium taking into account the energy and ionization balance including all the atomic processes. Another difficulty comes from the fact that the cold material is optically thick and its temperature and ionization structure at equilibrium is strongly inhomogeneous.

The detailed computation of the structure and spectrum of irradiated optically thick material was performed by coupling the photo-ionization code TITAN and the Monte-Carlo code NOAR (accounting for Compton scattering) (Dumont et al. 2000). It enabled one to show the importance of an accurate radiative transfer treatment for the irradiated cold material emission.

However, in these calculations the feedback from the cold radiation on the hot phase equilibrium was not considered. As irradiating spectrum, a simple power-law with a fixed slope was assumed.

Here we add a self-consistent treatment of the hot phase emission by coupling the TITAN/NOAR codes with a third code based on the Non-Linear Monte-Carlo method (Malzac & Jourdain 2000).

This enables us to propose the first full treatment of the radiative coupling, accounting accurately and self-consistently for both the hot and cold phase emission.

## 2. The numerical model

### 2.1. The NOAR/TITAN and NLMC codes

TITAN is a code designed for warm media ( $T >$  a few  $10^4$  K) optically thick to Compton scattering. It computes the structure of a plane-parallel slab of gas in thermal and ionization equilibrium, illuminated by a given spectrum on one or two sides of the slab (Dumont et al. 2000). It takes into account the returning flux using a two-stream approximation to solve the transfer in the lines (instead of the escape probability formalism). This code is coupled with a Monte Carlo code, NOAR, which takes into account Compton and inverse Compton diffusions in any geometry (Abrassart 2000). NOAR uses the local fractional ion abundances and the temperature provided by TITAN, while NOAR provides TITAN with the local Compton gains and losses in each layer. The Compton heating-cooling rate is indeed dominated by energy losses of photons at high energies ( $>25$  keV), not considered by TITAN. The coupling thus allows one to solve consistently both the global and the local energy balance. NOAR also allows computing the fluorescence line profiles which are significantly Compton-broadened in the case of strong illumination, and the Comptonised reflection spectrum above 25 keV.

In parallel, we use the NLMC code described and tested in Malzac & Jourdain (2000) based on the Non-Linear Monte-Carlo method proposed by Stern et al. (1995a). This code computes the Comptonised spectrum and energy balance in the hot phase. The radiation field is represented using about  $10^4$  pseudo-particles called Large Particles (LP). Each LP represents a number of photons with identical characteristics (energy, position, direction of propagation, ...). These LPs are tracked all together in a synchronized way. They may interact by the Compton effect with a Maxwellian electron distribution. These interactions are simulated using standard Monte-Carlo methods. For a fixed heating rate in the hot phase, the temperature of the electron distribution is modified according to the Compton energy losses due to the interactions with the LP photons. Starting from an arbitrary radiation field and temperature the system evolves naturally toward equilibrium. Then, the escaping LP characteristics are used to build up the angle dependent spectrum from the hot phase until satisfying photon statistics are achieved.

### 2.2. Geometry and model parameters

The proposed method can apply to a variety of geometries of the two-phase system. However as the coupled TITAN/NOAR/NLMC simulations are very time-consuming, we will limit this first attempt of full radiative coupling to simple situations. We will consider both the slab and spherical geometry illustrated in Fig. 1. The slab geometry, used e.g. by Malzac & Jourdain (2000), corresponds to the standard infinite slab accretion disc corona model (Haardt & Maraschi 1993). The spherical geometry corresponds to the model of Collin-Souffrin et al. (1996) where the hot phase constitutes a sphere at the center of the accretion flow surrounded by cold material possibly in the form of dense clouds or filaments. For simplicity,

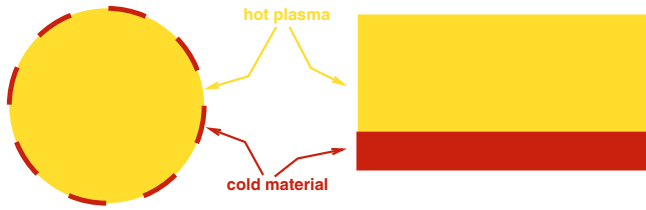


**Fig. 1.** The infinite slab accretion disc corona and spherical cloud geometry. The hot slab is divided into 10 horizontal layers with homogeneous temperatures. The sphere is divided into 5 concentric shells.

we assume that the material is homogeneously distributed at the sphere. For both models, the hot plasma is assumed to have an homogeneous density. It is however divided into a number of zones to account for temperature gradients that are computed according to the local energy balance.

Our model is then fully determined when the following parameters are given:

- Thomson optical depth  $\tau_T$  of the hot phase, defined along the radius of the sphere or the height of the hot slab.
- Density of the cold (homogeneous) material  $n$  ( $\text{cm}^{-3}$ ).
- Hydrogen column density of the cold material  $N_H$  ( $\text{cm}^{-2}$ ), or equivalently its Thomson optical depth  $\tau_c$ .
- Ionization parameter of the cold material  $\xi$ , defined as  $\xi = 4\pi F_{\text{bol}}/n$ , where  $F_{\text{bol}}$  is the integrated flux incident on the cold material surface. In the following  $\xi$  is expressed in  $\text{erg s}^{-1} \text{cm}$ .
- Covering factor  $C$  of the cold material, in the case of the spherical geometry.  $C$  is the surface ratio covered by the cold clouds to that of the sphere. For a photon escaping from the hot sphere,  $C$  represents the probability of entering into the cold medium.

### 2.3. Numerical method

We compute the escaping spectrum as follows. First, we use the non-linear Monte-Carlo code in order to get a first estimate of the high energy spectrum. When a LP photon escapes the hot plasma and enters the cold material, its energy is then reemitted at its surface in the form of reprocessed/reflected LP photons. Their energy and direction are drawn from the assumed angle dependent spectrum of the cold material. Note that the reprocessed photons may be either directed toward the hot plasma (i.e. reflected) or directed outward and escape the system (i.e. transmitted through the cold phase).

In the spherical model, we use a statistical method to model the homogeneous distribution of cold material around the sphere. When a photon LP escapes the hot sphere, a random number  $\eta$  is drawn:

- if  $\eta > C$ , the LP photon truly escapes and its energy is used to build up the escaping spectrum;
- if  $\eta < C$ , the LP photon enters the cold material and its energy is either reflected toward the sphere or transmitted as described above.

At this stage the cold medium spectrum is arbitrary (although it is better if it is similar to a real reprocessed spectrum). We then inject the resulting equilibrium hot-phase spectrum as input in the TITAN/NOAR codes. This provides an estimate of the ionization and temperature structure of the cold phase as well as the reprocessed spectrum. Then we use the TITAN/NOAR spectrum as the local spectrum of the cold material in the NLMC code to get a better estimate of the hot-phase spectrum, and so on. In general, convergence is achieved after 3–4 iterations.

## 3. Results

### 3.1. Spherical model

Figure 2 shows the resulting spectra for  $C = 0.3$  and  $C = 0.5$  and two values of the ionization parameter  $\xi = 300$  and  $\xi = 3000$  assuming a constant density in the cold phase.

For comparison we also show spectra that were obtained with the usual treatment of reprocessing (i.e. blackbody spectrum + neutral reflection). If all the radiation impinging on the cold material is absorbed and reemitted as a blackbody, its temperature is related to the incident flux through the Stefan-Boltzmann law. Therefore the temperature  $kT_r$  of the cold phase is related to the ionization parameter and density of the cold phase as follows:

$$T_r = \left( \frac{\xi n}{4\pi\sigma} \right)^{1/4}, \quad (1)$$

where  $\sigma$  is the Stefan's constant. As a result, this equivalent blackbody temperature is not very sensitive to the incident flux. For our assumed density,  $kT_r$  is 7 and 12 eV for  $\xi = 300$  and 3000 respectively. In accordance, in the blackbody spectrum + neutral reflection simulations, the blackbody temperature was fixed at  $kT_r = 10$  eV in both cases, all the other relevant parameters being kept at the same values. Indeed, one can see from Fig. 2 that the blackbody spectrum peaks at nearly the same energy as the TITAN/NOAR spectrum.

Globally, for larger  $C$ , the X-ray spectra are always softer, i.e. the photon index of the primary emission  $\Gamma$  (estimated with a least square fit of the 2–10 keV primary spectrum) is larger. This is due to the increase of reprocessed cooling flux from the cold material at larger  $C$  which leads to a lower temperature in the hot-phase.

There are however noticeable differences between spectra obtained with the usual treatment (i.e. blackbody spectrum + neutral reflection) and the detailed treatment. The shape of the reprocessed spectrum obviously differs. But the Comptonised emission differs as well. In particular, the spectrum is much harder in the calculations using TITAN/NOAR. Indeed the reprocessed spectrum then is much broader than a simple blackbody, more photons being reprocessed at higher energy. This affects the Compton cooling in the hot phase (which is lower) together with the shape of the Comptonised spectrum which is harder also due to the relatively high energy of the seed photons. This effect is then amplified by the fact that the hard X-ray albedo is larger for a harder spectrum thus enhancing the fraction of the reflected/reprocessed photons at high energy. We

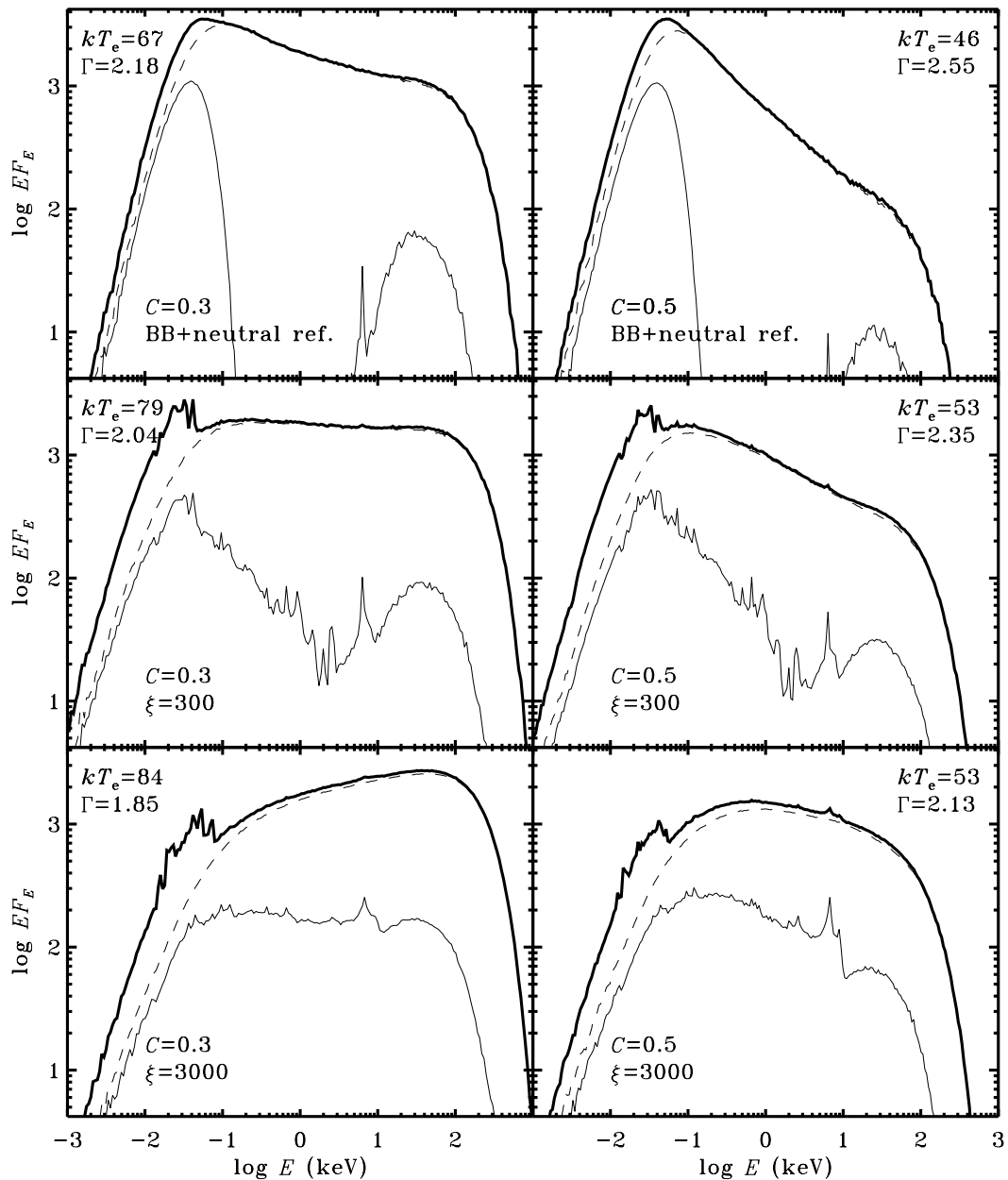


**Fig. 2.** Angle averaged escaping spectra for covering fractions  $C = 0.3$  (left-hand side) and  $C = 0.5$  (right-hand side). Thin curves: reprocessed/reflected spectrum. Dashes: comptonised spectrum. Thick curves: total observed spectrum (including the transmitted component). The upper panels show the results from NLMC calculations with the cold phase emission approximated by a blackbody + neutral reflection. The blackbody temperature is  $kT_r = 10$  eV. The other panels are the results from the TITAN/NOAR/NLMC calculations for the following parameters of the cold medium:  $n = 3 \times 10^{14} \text{ cm}^{-3}$ ,  $N_H = 3 \times 10^{25} \text{ cm}^{-2}$  ( $\tau_c = 24$ ). In all of the simulations the Thomson optical depth of the hot plasma was fixed to  $\tau_T = 1$ . The assumed ionization parameter  $\xi$  is indicated in each panel together with the resulting 2–10 keV photon index of the comptonised emission  $\Gamma$  and the volume averaged temperature of the hot phase  $kT_e$  (in keV).

note that in the “blackbody” simulations, the total flux impinging on the cold material is reemitted toward the hot sphere (i.e. transmission through the cold medium is neglected). In contrast, in the TITAN/NOAR simulations, the transmitted flux<sup>1</sup> represents about 15% of the impinging luminosity, despite our

<sup>1</sup> By “transmission” or “transmitted flux” we refer to the net energy flux across the cloud. This includes the radiation crossing the cloud without interaction, but also the reprocessed radiation that is outwardly reemitted. The latter is largely dominant.

choice of a relatively large hydrogen column density of the cold medium (corresponding to a Thomson optical depth  $\tau_c = 24$ ).

This modest “loss” of soft photons leads to an increase of the temperature of a few percent and a hardening of the spectrum by  $\Delta\Gamma \approx 0.03$ . Therefore, this effect does not contribute much to the resulting higher temperatures and harder spectra in the TITAN/NOAR case.

The hardening of the spectrum increases with  $\xi$  (compare the spectra for  $\xi = 3000$  and  $\xi = 300$ ). The strongly ionised material has indeed a larger X-ray albedo, and more photons

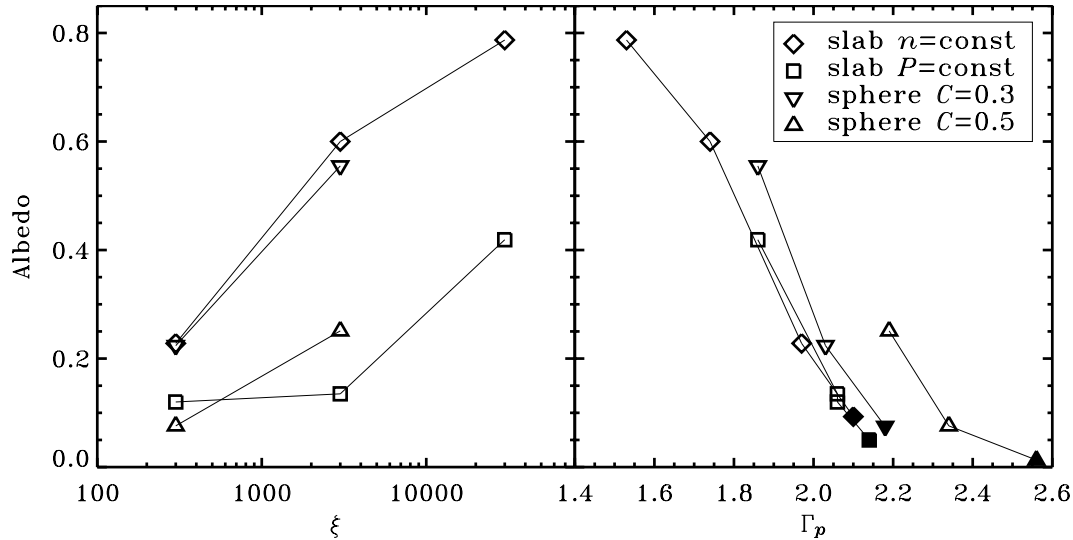


**Fig. 3.** X-ray albedo (i.e. fraction of the reflected/reprocessed luminosity emitted above 1 keV) as a function of the ionization parameter  $\xi$  (left) and spectral index,  $\Gamma_p$  (right), of the simulated spectra obtained from fits with the PEXRAV model (see text and Table 1). The results are plotted using a different symbol for each model, as shown on the figure. Filled symbols correspond to the blackbody and neutral reflection models.

**Table 1.** Spectral parameters obtained when fitting our simulated spectra in the 2–30 keV range under XSPEC with the PEXRAV model plus a Gaussian line.  $\Gamma_p$  and  $R$  are the PEXRAV photon index and reflection amplitude.  $E_\alpha$  is the line centroid energy in keV, and  $EW$  is its equivalent width in eV. During the fit the high energy cut-off energy  $E_c$  and the inclination angle were fixed at 400 keV and 30 degrees respectively, and the abundances were fixed to standard.

simulation		$\Gamma_p$	$R$	$E_\alpha$	$EW$
$C = 0.3$	$T_r = 10$ eV	2.18	0.21	6.40	3.12
$C = 0.3$	$\xi = 300$	2.03	0.12	6.32	29.8
$C = 0.3$	$\xi = 3000$	1.86	0.01	6.61	126
$C = 0.5$	$T_r = 10$ eV	2.56	0.36	6.40	8.66
$C = 0.5$	$\xi = 300$	2.34	0.21	6.31	35.6
$C = 0.5$	$\xi = 3000$	2.19	0.00	6.41	451
Slab	$T_r = 10$ eV	2.10	0.18	6.40	8.0
Slab $n = \text{const.}$	$\xi = 300$	1.97	0.10	6.56	53.5
Slab $n = \text{const.}$	$\xi = 3000$	1.74	$9.5 \times 10^{-2}$	6.1	307
Slab $n = \text{const.}$	$\xi = 30000$	1.53	$2.1 \times 10^{-4}$	1.32	32
Slab	$T_r = 1$ eV	2.14	0.13	6.40	9.53
Slab $P = \text{const.}$	$\xi = 300$	2.06	0.16	6.4	12.9
Slab $P = \text{const.}$	$\xi = 3000$	2.06	0.11	6.4	18.8
Slab $P = \text{const.}$	$\xi = 30000$	1.86	$8.7 \times 10^{-2}$	6.4	7.45

are reprocessed at high energies. We note that the differences between the blackbody + neutral reflection model and the realistic one appear to be important even at moderate  $\xi \sim 300$ . The left panel of Fig. 3 shows the dependence of the X-ray albedo (defined as the fraction of the reflected/reprocessed luminosity emitted above 1 keV) on  $\xi$ . As the X-ray albedo also strongly depends on the shape of the incident spectrum (see Malzac et al. 2001), for a given  $\xi$  the albedo can vary significantly with the geometry considered. The models with  $C = 0.3$  and  $C = 0.5$  have albedos differing by more than a factor of 2, that is as important as the change in albedo when  $\xi$  is increased by a factor of 10. The right panel of Fig. 3 shows the

resulting relation between albedo and spectral index. It is interesting to note that the difference of the albedos for the neutral and the low ionisation models ( $\xi = 300$ ) is too low to account for the important changes in  $\Gamma$  that we obtain. Indeed, the albedo changes by about 0.1, implying an increase in the soft cooling flux of about 10%, which, as noted above, is not sufficient to increase  $\Gamma$  by  $\Delta\Gamma \approx 0.2$ . This shows that the important difference in spectral slope between neutral and weakly ionised cases is essentially due to the different shape of the reprocessed spectrum below 1 keV (as explained above) and not much to changes in the X-ray albedo.

Besides the spectral index, there are other parameters, such as the amplitude of the reflection features, that may be relevant to the observations. To derive those parameters from the simulated spectra in a way similar to those from observed spectra, we fitted our simulated spectra using the X-ray spectral fitting package XSPEC (Arnaud 1996). The fitting model was an e-folded power law plus neutral reflection (PEXRAV, Magdziarz & Zdziarski 1995) and a Gaussian to model the iron line. The results are summarised in Table 1 and Fig. 4. In all cases we found that the spectral index obtained with PEXRAV  $\Gamma_p$ , is very close to that derived through the 2–10 keV least square fit.  $\Gamma$ . They show that the reflection amplitude  $R$ , measured with PEXRAV, strongly depends on the ionization parameter. It decreases by almost a factor of two between the neutral and  $\xi = 300$  case and for the highest ionization parameter  $R$  is almost 0. This is a well known effect due to the fact that the more ionised the reflector is, the more the reflected X-ray spectrum is similar to the incident one due to the predominance of Compton reflection over photoabsorption. As a consequence, the reflection bump appears relatively weaker in the overall spectrum. A further reduction of  $R$  is due the destruction of the reflection component by Comptonisation in the hot phase (Malzac et al. 2001; Petrucci et al. 2001) depending on the Thomson optical depth of the hot sphere.

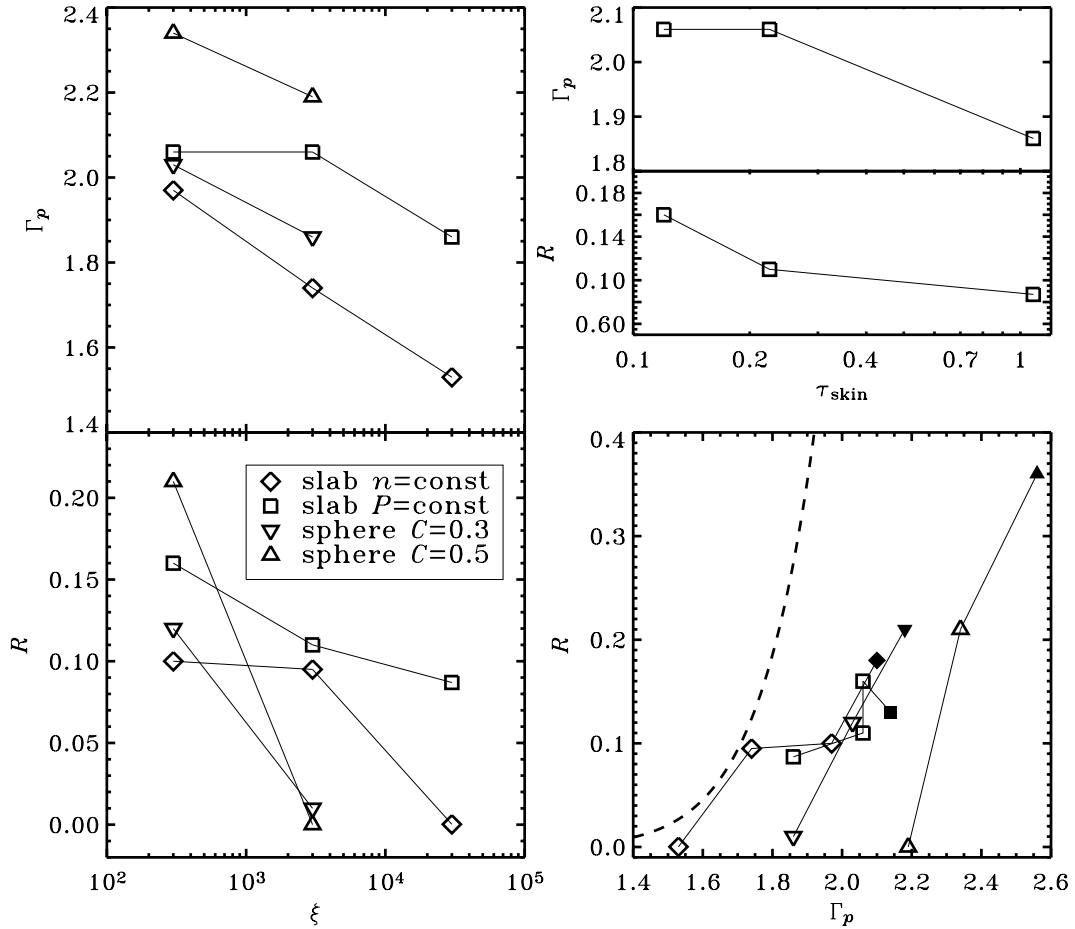


**Fig. 4.** Reflection amplitude  $R$  and spectral index  $\Gamma_p$  of the simulated spectra obtained from fits with the PEXRAV model (see text and Table 1). The results are plotted using a different symbol for each model, as shown in the figure. Filled symbols correspond to the blackbody and neutral reflection models. *Left panels:*  $R$  and  $\Gamma$  as a function of  $\xi$ . *Upper right panel:* in the constant pressure case,  $R$  and  $\Gamma_p$  as a function of the hot skin Thomson optical depth  $\tau_{\text{skin}}$ . *Bottom right panel:*  $R$  versus  $\Gamma_p$ , the dashed curve shows the best fit power law approximation to the observed  $R$ - $\Gamma$  correlation in AGN as given by Zdziarski et al. (1999).

Contrary to the reflection component, the equivalent width of the iron line increases with the ionization parameter. Indeed in our simulations the line intensity increases with  $\xi$  (by a factor of 10 between  $\xi = 300$  and  $\xi = 3000$ ). This is in agreement with previous studies showing that the line intensity increases between these two values of  $\xi$  we considered (Matt et al. 1993, 1996). We note that in our fits the line energy is very weakly constrained. This is due to the low resolution of the fitted simulated spectra and also probably to the inadequacy of the Gaussian approximation to represent the much more complex profile of the actual line. This may explain the few unphysical red-shifted lines we obtain. Indeed, if estimated directly from the simulation, the line peak is always above 6.4 keV and blue shifted at large  $\xi$ .

How do these results compare with the observations? The photon indices  $\Gamma_p > 2$  obtained with PEXRAV for most of our simulations correspond to the softest observed sources (see e.g. Zdziarski et al. 2003). In the context of the spherical model this suggests that either the cold material is usually strongly ionised, or that in most sources, the covering fraction is lower than 0.3. On the other hand, the resulting  $R$  is rather low compared to the average  $R \sim 0.7$  in Seyfert galaxies, suggesting

on the contrary that in most sources the covering fraction is larger. These problems can be easily overcome by considering a slightly different geometry where the cold material, instead of being at the sphere surface would be at some distance. This would decrease both the cooling of the hot phase and the fraction of reflected photons that are Comptonised. Then, as shown by Malzac (2001), for the same covering fraction the spectrum is harder and the reflection component is stronger. We also note that, in Seyfert galaxies, a distant molecular torus could provide a strong additional contribution to the observed reflection component (Malzac & Petrucci 2002).

### 3.2. Slab corona model

In the spherical model, changes in the covering fraction of cold material may produce a range of X-ray photon indices that includes the observed range. On the other hand the slab corona model, in its simplest version, does not allow such freedom; the photon index is tightly constrained (Haardt & Maraschi 1993). Detailed simulations using the blackbody + neutral reflection approximation (Stern et al. 1995b) have shown that the range of  $\Gamma$  expected in this geometry tends to be larger than  $\sim 2$ ,

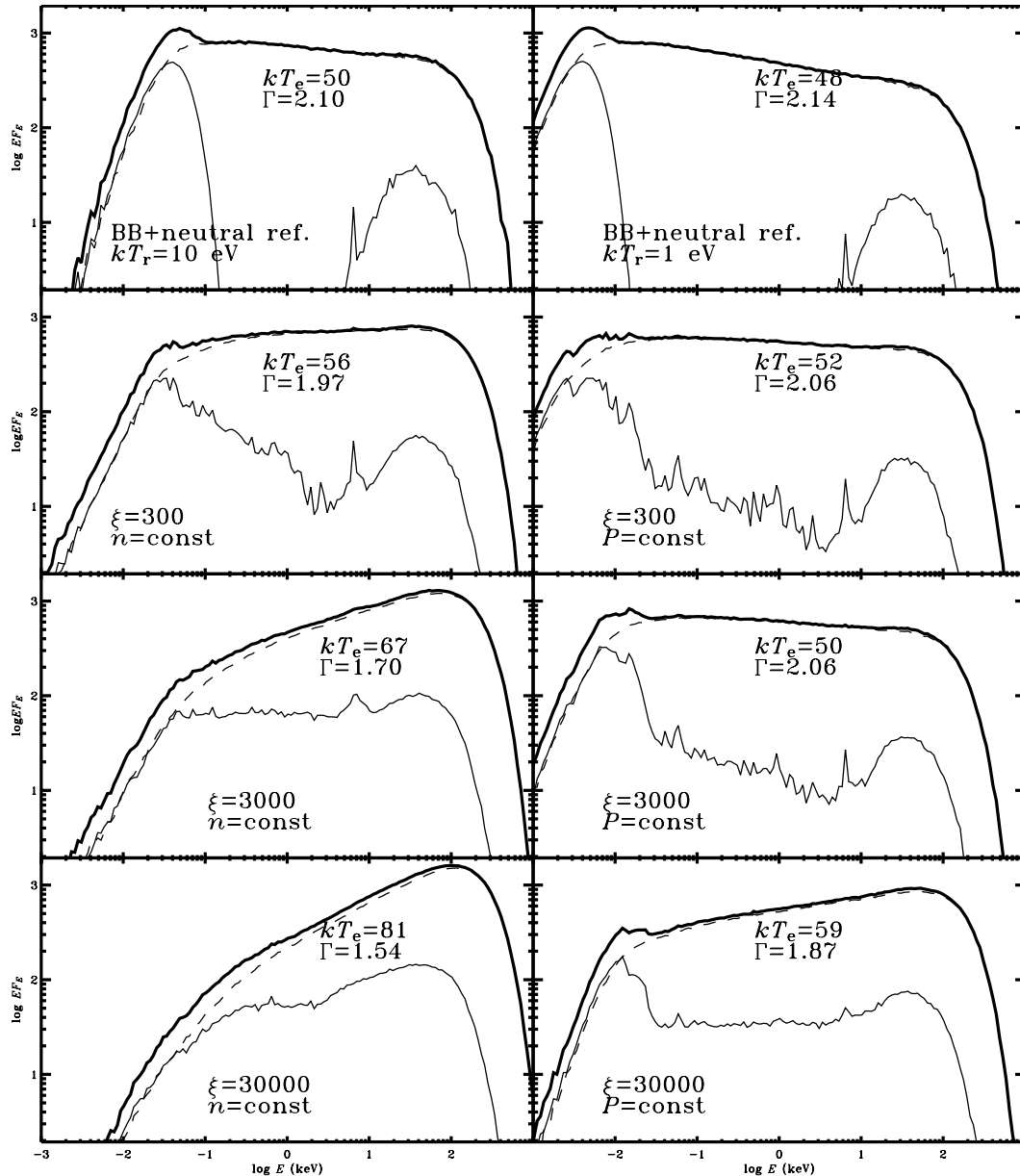


**Fig. 5.** Angle averaged escaping spectra for a plane-parallel geometry. *The bottom panels* are the results from the TITAN/NOAR/NLMC calculations for the same parameters of the cold medium as in Fig. 2, and assuming a constant density (*left hand side*) and a constant pressure (*right hand side*) in the cold phase. *The upper panels* show the results from NLMC calculations with the cold phase emission approximated by a blackbody + neutral reflection for two different blackbody temperatures  $kT_r = 10$  eV (*left hand side*)  $kT_r = 1$  eV (*right hand side*). Thin curves: reprocessed/reflected spectrum. Dashes: comptonised spectrum. Thick curves: total observed spectrum. In all panels, the Thomson optical depth of the hot plasma is  $\tau_T = 1$ . The assumed ionization parameter  $\xi$  is indicated in each panel together with the resulting 2–10 keV photon index of the Comptonised emission  $\Gamma$  and the volume averaged temperature of the hot phase  $kT_e$  (in keV).

while the average  $\Gamma$  in Seyfert 1 galaxies is  $\sim 1.8$ . Observed spectra of Seyfert galaxies and galactic black hole sources can be much harder with photon indices as low as  $\Gamma \sim 1.4$ . Overcoming this problem requires some complications, such as considering the effects of an out-flowing corona (Beloborodov 1999; Malzac et al. 2001) or the presence of holes in the disc (Zdziarski et al. 1998). As a consequence, the simple slab coronal model considered here was often considered as ruled out on this basis.

As our more realistic treatment of reprocessing and ionization tends to produce harder spectra, it is interesting to see

whether this would be sufficient to reconcile the model with the observations. The left panels of Fig. 5 compare spectra for a slab geometry and both the blackbody approximation and realistic reprocessing for  $\xi = 3 \times 10^2$ ,  $\xi = 3 \times 10^3$  and  $\xi = 3 \times 10^4$ , assuming a constant density in the cold phase. Unlike those of the spherical model, these slab spectra are angle dependent. However the weak angular dependence obtained in our detailed reprocessing simulations does not differ qualitatively from what is found in the standard “blackbody” + neutral reflection treatment that was already studied in several papers (see e.g. Malzac et al. 2001). For the sake of simplicity,

we will consider the properties of the angle-averaged spectra only, since the aim of this work is to evaluate the main effects of a detailed treatment of reprocessing and ionization.

The spectral indices from the 2–10 keV least square fit are  $\Gamma = 2.10$  for the “blackbody” simulation and  $\Gamma = 1.97, 1.70$  and  $1.54$  respectively for the ionised cases. Thus although the hardening of the spectrum is significant, the model will be able to reproduce the spectra of the hardest sources only if the disc is strongly ionised.

Since, in our calculation, we neglect the contribution of internal viscous dissipation to the disc emission, our spectra are the hardest possible for the slab corona geometry. Any intrinsic disc emission would make the spectra softer and strengthen the requirements for extreme ionization.

In the TITAN/NOAR simulations shown in Fig. 2 and the left panels of Fig. 5 we assumed a constant density in the cold material. This assumption might be a reasonable approximation in the case of the small-scale magnetically confined clouds of the model of Collin-Souffrin et al. (1996). In the case of the accretion disc corona however, there are certainly strong density gradients driven by the pressure equilibrium. In general, due to the ionization thermal instability, it breaks into two well defined layers: a low density skin at Compton temperature that is almost completely ionised, atop the cooler, high density, low ionization material of the internal disc. The sharp transition between the two layers contrasts with the smooth ionization gradients obtained in the constant density case. This characteristics was studied in a number of papers (Raymond 1993; Ko & Kallman 1994; Róžańska & Czerny 1996; Nayakshin et al. 2000; Dumont et al. 2002) that showed it has strong impact on the reprocessed spectrum. The reprocessed spectrum can then be described as formed by two components associated with two layers. The hot skin component is essentially dominated by Compton reflection with a spectral shape almost indistinguishable from the irradiating spectrum, while the deeper component corresponds to almost neutral reprocessing (Done & Nayakshin 2001; Ballantyne et al. 2001).

Our results indicate that the primary spectrum is sensitive to the shape of the reprocessed spectrum. Therefore, one may wonder what effect different assumptions made about the structure of the cold material (constant density, constant pressure or hydrostatic equilibrium) may have on the shape of the overall equilibrium spectral energy distribution.

In the right panels of Fig. 5, we show the resulting spectra for the slab geometry and a constant pressure in the cold phase. For the 3 simulations with constant pressure the resulting Thomson depth of the ionised skin  $\tau_{\text{skin}}$  is 0.120, 0.225, and 1.08 respectively for  $\xi = 3 \times 10^2, 3 \times 10^3, \text{ and } 3 \times 10^4$ . As compared to the constant density case, and in agreement with previous studies, the reprocessed spectrum is much softer in the X-ray range due to the strong fraction of photons that are Compton reflected in the hot skin and the low ionization state of the deeper layers. For the same reasons, the UV spectrum formed in the colder deeper regions is sharper and peaks at lower frequency. The soft seed photons are thus softer on average and as a consequence the primary X-ray spectrum is slightly steeper than its constant density counterpart.

Despite the reprocessed spectrum, in its lowest energy part, is now closer to a blackbody spectrum, the primary X-ray emission still differs from that obtained in the blackbody approximation.

To facilitate the comparison, the “blackbody” case shown in upper right panel of Fig. 5 is for  $kT_r = 1$  eV, so that the blackbody peaks nearly at the same energy as the realistic reprocessed UV spectrum. For both  $kT_r = 1$  eV and  $kT_r = 10$  eV the primary X-ray spectrum is steeper than in the TITAN/NOAR simulation.

The results of the XSPEC fitting procedure are shown in Table 1. For a very thick reflector subtending a solid angle  $2\pi$ , we expect  $R = 1$ . On the other hand, the reflection coefficient we derive are relatively low,  $\sim 0.1$ – $0.2$  even in the case of neutral reflection. This is a known effect resulting from the destruction of the reflection component by Comptonisation in the hot phase (Malzac et al. 2001; Petrucci et al. 2001). In general, this effect is important for all geometries where the reflector is seen through the hot plasma, such as the slab or spherical geometry considered in Sect. 3.1.

Contrary to the case of a constant density, in the constant pressure models, the spectral index is quite insensitive to the ionization parameter. The spectrum hardens by less than  $\Delta\Gamma \approx 0.2$  when  $\xi$  is increased by 2 orders of magnitude. In this case the ionization effects are not sufficient, to reconcile the slab corona model with the observations. This latter result confirms a similar conclusion reached by Nayakshin & Dove (2001), on the basis of a simplified treatment of the hot skin model. On the other hand, if the reflector has a constant density, we find that the different ionization parameters could explain the whole range of observed spectral indices. This however would require a very wide range of ionization parameters, with an extremely ionised reflector in the hardest sources. Moreover, although the constant density is plausible in the context of the cloud model of Sect. 3.1, an accretion disc with a constant density seems quite unrealistic.

Finally, both for constant density and constant pressure a detailed treatment of reprocessing appears to be important. The usual blackbody + neutral reflection approximation appears inappropriate for an accurate determination of the equilibrium spectra, even at low ionization.

#### 4. Conclusions

We calculated the equilibrium spectra in the context of the two-phase models for the emission from Seyfert galaxies and black hole binaries. For the first time, we included a detailed treatment of reprocessing and ionization and thermal balance in the cold phase.

The resulting broad band spectrum differs significantly from what obtained using the usual “blackbody + neutral reflection” approximation. In particular, our realistic treatment of reprocessing leads to higher hot-phase temperatures associated with harder X-ray spectra. Surprisingly the effect is strong even at low ionization parameters. This is because even if the X-ray albedo is not significantly affected by the weak ionizing illumination, the shape of the reprocessed spectrum below 1 keV is much broader than a simple blackbody.

For the slab model, we performed simulations with two different prescriptions for the cold phase, namely a constant density and a constant pressure. The comparisons between the two cases indicate that the overall spectral shape is also quite sensitive to the physical structure of the cold phase. A slab model at constant density can account for the hardest observed spectra for large values of the ionization parameters. In the case of constant pressure disc however, the hardening is not strong enough to reconcile the model with the even harder spectra observed in Seyfert galaxies and Galactic black holes.

The equilibrium spectra of a two-phase system thus appear to be significantly affected by the shape of the reprocessed spectrum, even at low ionization parameters. A detailed treatment of reprocessing appears to be required for most observationally relevant cases.

*Acknowledgements.* This work was partly supported by the European Commission (contract number ERBFMRX-CT98-0195, TMR network “Accretion onto black holes, compact stars and protostars”). J.M. also acknowledges fundings from the MURST (COFIN98-02-15-41) and PPARC. J.M. acknowledges a travel grant from the GDR PCHE. We are grateful to Suzy Collin and Pierre-Olivier Petrucci for enlightening discussions.

## References

- Abrassart, A. 2000, *Adv. Sp. Res.*, 25, 465
- Arnaud, K. A. 1996, *Astronomical Data Analysis Software and Systems V*, ed. Jacoby G., & Barnes J., ASP Conf. Ser., 101, 17
- Ballantyne, D. R., Ross, R. R., & Fabian, A. C. 2001, *MNRAS*, 327, 10
- Balucinska-Church, M., Belloni, T., Church, M. J., & Hasinger, G. 1995, *A&A*, 302, L5
- Beloborodov, A. M. 1999, *ApJ*, 510, L123
- Collin-Souffrin, S., Czerny, B., Dumont, A.-M., & Życki, P. 1996, *A&A*, 314, 393
- Done, C., & Nayakshin, S. 2001, *MNRAS*, 328, 616
- Dumont, A.-M., Abrassart, A., & Collin, S. 2000, *A&A*, 357, 823
- Dumont, A.-M., Czerny, B., Collin, S., & Życki, P. T. 2002, *A&A*, 387, 63
- George, I. M., & Fabian, A. C. 1991, *MNRAS*, 249, 352
- Haardt, F., & Maraschi, L. 1991, *ApJ*, 380, L51
- Haardt, F., & Maraschi, L. 1993, *ApJ*, 413, 507
- Ko, Y.-K., & Kallman, T. R. 1994, *ApJ*, 431, 273
- Magdziarz, P., & Zdziarski, A. A. 1995, *MNRAS*, 273, 837
- Malzac, J. 2001, *MNRAS*, 325, 1625
- Malzac, J., & Jourdain, E. 2000, *A&A*, 359, 843
- Malzac, J., & Celotti, A. 2002, *MNRAS*, 335, 23
- Malzac, J., & Petrucci, P. O. 2002, *MNRAS*, 336, 1209
- Malzac, J., Beloborodov, A. M., & Poutanen J. 2001, *MNRAS*, 326, 417
- Matt, G., Fabian, A. C., & Ross, R. R. 1993, *MNRAS*, 262, 179
- Matt, G., Fabian, A. C., & Ross, R. R. 1996, *MNRAS*, 278, 1111
- Nandra, K., & Pounds, K. A. 1994, *MNRAS*, 268, 405
- Nayakshin, S., & Dove, J. B. 2001, *ApJ*, 560, 885
- Nayakshin, S., & Kallman, T. R. 2001, *ApJ*, 546, 406
- Nayakshin, S., Kazanas, D., & Kallman T. R. 2000, *ApJ*, 537, 833
- Petrucci, P. O., Merloni, A., Fabian, A., Haardt, F., & Gallo, E. 2001, *MNRAS*, 328, 501
- Poutanen, J., & Svensson, R. 1996, *ApJ*, 470, 249
- Raymond, J. C. 1993, *ApJ*, 412, 267
- Rees, M. J. 1987, *MNRAS*, 228, 47
- Ross, R. R., & Fabian, A. C. 1993, *MNRAS*, 261, 74
- Różańska, A., & Czerny, B. 1996, *AcA*, 46, 233
- Różańska, A., & Czerny, B. 2000, *A&A*, 360, 1170
- Shapiro, S. L., & Lightman, A. P. 1976, *ApJ*, 204, 555
- Sincell, M. W., & Krolik, J. H. 1997, *ApJ*, 476, 605
- Stern, B. E., Begelman, M. C., Sikora, M., & Svensson, R. 1995a, *MNRAS*, 272, 291
- Stern, B. E., Poutanen, J., Svensson, R., Sikora, M., & Begelman, M. C. 1995b, *ApJ*, 449, L13
- Svensson, R., & Zdziarski, A. A. 1994, *ApJ*, 436, 599
- Shakura, N. I., & Sunyaev, R. A. 1973, *A&A*, 24, 337
- Sunyaev, R. A., & Titarchuk, L. G. 1980, *A&A*, 86, 121
- Walter, R., & Fink, H. H. 1993, *A&A*, 274, 105
- Zdziarski, A. A., Poutanen, J., Mikolajewska, J., et al. 1998, *MNRAS*, 301, 435
- Zdziarski, A. A., Lubiński, P., & Smith, D. A. 1999, *MNRAS*, 303, L11
- Zdziarski, A. A., Lubiński, P., Gilfanov, M., & Revnivtsev, M. 2003, *MNRAS*, 342, 355
- Życki, P. T., Collin-Souffrin, S., & Czerny, B. 1995, *MNRAS*, 277, 70
- Życki, P. T., Krolik, J. H., Zdziarski, A. A., & Kallman, T. R. 1994, *ApJ*, 437, 597



## 5.5 “Bimodal spectral variability of Cygnus X-1 in an intermediate state”

Malzac J., Petrucci P.O., Jourdain E., Cadolle Bel M., Sizun P., Pooley G., Cabanac C., Chaty S., Belloni T., Rodriguez J., Roques J.P., Durouchoux P., Goldwurm A., Laurent P., *Astronomy and Astrophysics*, Volume 448, p.1125-1137 (2006).



## Bimodal spectral variability of Cygnus X-1 in an intermediate state

J. Malzac<sup>1</sup>, P. O. Petrucci<sup>2</sup>, E. Jourdain<sup>1</sup>, M. Cadolle Bel<sup>3,4</sup>, P. Sizon<sup>3</sup>, G. Pooley<sup>5</sup>, C. Cabanac<sup>2</sup>, S. Chaty<sup>6</sup>,  
 T. Belloni<sup>7</sup>, J. Rodriguez<sup>3,6,8</sup>, J. P. Roques<sup>1</sup>, P. Durouchoux<sup>3</sup>, A. Goldwurm<sup>3,4</sup>, and P. Laurent<sup>3,4</sup>

<sup>1</sup> Centre d'Étude Spatiale des Rayonnements (CNRS/UPS/OMP), 31028 Toulouse, France  
 e-mail: Julien.Malzac@cesr.fr

<sup>2</sup> Laboratoire d'Astrophysique Observatoire de Grenoble, BP 53, 38041 Grenoble Cedex 9, France

<sup>3</sup> Service d'Astrophysique, CEA-Saclay, Bat. 709, L'Orme des Merisiers, 91191 Gif-sur-Yvette, Cedex, France

<sup>4</sup> APC-UMR 7164, 11 place M. Berthelot, 75231 Paris, France

<sup>5</sup> Cavendish Laboratory, University of Cambridge, Madingley Road, Cambridge CB3 0HE, UK

<sup>6</sup> AIM - Astrophysique Interactions Multi-échelles (Unité Mixte de Recherche 7158 CEA/CNRS/Université Paris 7 Denis Diderot), CEA-Saclay, Bât. 709, L'Orme des Merisiers, 91191 Gif-sur-Yvette Cedex, France

<sup>7</sup> INAF - Osservatorio Astronomico di Brera, via E. Bianchi 46, 23807 Merate, Italy

<sup>8</sup> INTEGRAL Science Data Center, Chemin d'Écogia 16, 1290 Versoix, Switzerland

Received 10 June 2005 / Accepted 16 November 2005

### ABSTRACT

We report the results of an observation of Cygnus X-1 performed on June 7–11, 2003 with *INTEGRAL* that we combine with simultaneous radio observations with the Ryle telescope. Both spectral and variability properties of the source indicate that Cygnus X-1 was in an Intermediate State. The *INTEGRAL* spectrum shows a high-energy cut-off or break around 100 keV. The shape of this cut-off differs from pure thermal Comptonisation, suggesting the presence of a non-thermal component at higher energies. The average broad band spectrum is well represented by hybrid thermal/non-thermal Comptonisation models. However, models with mono-energetic injection, or models with an additional soft component are favoured over standard power-law acceleration models. During the 4 day long observation the broad band (3–200 keV) luminosity varied by up to a factor of 2.6 and the source showed an important spectral variability. A principal component analysis demonstrates that most of this variability occurs through 2 independent modes. The first mode consists in changes in the overall luminosity on time scale of hours with almost constant spectra (responsible for 68% of the variance) that are strikingly uncorrelated with the variable radio flux. We interpret this variability mode as variations of the dissipation rate in the corona, possibly associated with magnetic flares. The second variability mode consists in a pivoting of the spectrum around  $\sim 10$  keV (27% of the variance). It acts on a longer time-scale: initially soft, the spectrum hardens in the first part of the observation and then softens again. This pivoting pattern is strongly correlated with the radio (15 GHz) emission: radio fluxes are stronger when the *INTEGRAL* spectrum is harder. We propose that the pivoting mode represents a “mini” state transition from a nearly High Soft State to a nearly Low Hard State, and back. This mini-transition would be caused by changes in the soft cooling photons flux in the hot Comptonising plasma associated with an increase of the temperature of the accretion disc. The jet power then appears to be anti-correlated with the disc luminosity and unrelated to the coronal power. This is in sharp contrast with previous results obtained for the Low Hard State, suggesting a different mode of coupling between the jet, the cold disc, and the corona in Intermediate States. From this interpretation we also infer that the bolometric luminosity jumps by a factor of about 2 during the transition hard to soft, suggesting a radiatively inefficient accretion flow in the Low Hard State.

**Key words.** gamma-rays: observations – black hole physics – radiation mechanisms: non-thermal – X-rays: binaries – radio continuum: stars – X-rays: individuals: Cygnus X-1

### 1. Introduction

Cygnus X-1 is the prototype of black hole candidates. Since its discovery in 1964 (Bowyer et al. 1965), it has been intensively observed by all the high-energy instruments, from soft X-rays to  $\gamma$ -rays. It is a persistent source most often observed in the so-called Low Hard State (hereafter LHS), characterised by a relatively low flux in the soft X-rays ( $\sim 1$  keV) and a high flux in the hard X-rays ( $\sim 100$  keV). In the LHS, the high-energy

spectrum can be roughly described by a power-law with spectral index  $\Gamma$  varying in the range 1.4–2.2, and a nearly exponential cut-off at a characteristic energy  $E_c$  of a few hundred keV (see e.g. Gierlinski et al. 1997). Occasionally, the source switches to the High Soft State (HSS). The high-energy power-law is then much softer ( $\Gamma > 2.4$ ) and the bolometric luminosity is dominated by a thermal component peaking at a few keV. Finally, there are also Intermediate States (hereafter IMS) in which the source exhibits a relatively soft hard X-ray

spectrum ( $\Gamma \sim 2.1\text{--}2.3$ ) and a moderately strong soft thermal component (Belloni et al. 1996; Mendez & van der Klis 1997). The IMS often, but not always, appears when the source is about to switch from one state to the other. When it is not associated with a state transition, it is interpreted as a “failed state transition”. Until 1998, the source used to spend nearly 90% of its time in the LHS. In the recent years however there have been more IMSs and soft states (see Zdziarski et al. 2002; Pottschmidt et al. 2003; Gleissner et al. 2004).

Simultaneous radio/X-ray and high-energy observations of Cygnus X-1 and other sources have shown that the X-ray LHS is correlated with a strong radio emission which is consistent with arising from a jet (Fender 2001). In contrast, during HSS episodes the source appears to be radio weak (Brocksopp et al. 1999). The presence of a compact jet in the LHS was confirmed by Stirling et al. (2001) who presented evidence for an extended and collimated radio structure on milliarcsecond scales.

State transitions are generally interpreted as being associated with changes in the geometry of the accretion flow. In the HSS the geometrically thin optically thick disk (Shakura & Sunyaev 1973) extends down to the last stable orbit. The spectrum is dominated by the thermal disc component and peaks at a few keV. The hard X-ray emission is then believed to be produced in a non-thermal corona above and below the disc (Gierliński et al. 1999, hereafter G99). In the LHS the geometrically thin disc is truncated at a few hundred Schwarzschild radii, the innermost part of the accretion flow forms a geometrically thick optically thin and hot disc (Shapiro et al. 1976; Narayan & Yi 1994) where high-energy radiation is produced through thermal Comptonisation. During spectral transitions to the HSS the inner radius of the cold accretion disk decreases. This reduction of the inner disc radius is associated with either the cold disk penetrating inside the hot inner flow, or the later collapsing into an optically thick accretion disk with small active regions of hot plasma on top of it (Zdziarski et al. 2002). In both cases the enhanced soft photon flux from the disk tends to cool down the hot phase, leading to softer spectra. An alternative possibility would be that in both LHS and HSS, the geometry is that of a corona above a cold standard accretion disc (Bisnovaty-Kogan & Blinnikov 1976; Haard & Maraschi 1993). In the LHS the coronal plasma is essentially thermal and the cold disc faint because most of the power is transported away and dissipated in the corona and a strong outflow (Beloborodov 1999; Malzac et al. 2001; Merloni & Fabian 2002; Ferreira et al. 2006), while in the HSS most of the power is dissipated into the cold disc and the corona is non-thermal.

In the LHS, the radio flux is then positively correlated with the soft X-ray emission (3–25 keV, Corbel et al. 2000, 2003; Gallo et al. 2003). The X-ray emitting region and the jet seems to be intrinsically associated. This led to the now widely accepted idea that the corona (or hot thick disc) of the LHS constitutes the base of the jet (Fender et al. 1999; Merloni & Fabian 2002; Markoff et al. 2005).

Cygnus X-1 represents a prime target for the *INTEGRAL* mission (Winkler et al. 2003) launched in 2002 October 17, whose instruments offer an unprecedented spectral coverage at high-energy, ranging from 3 keV to several MeV. Cygnus X-1 was extensively observed (1 Ms) during the calibration phase

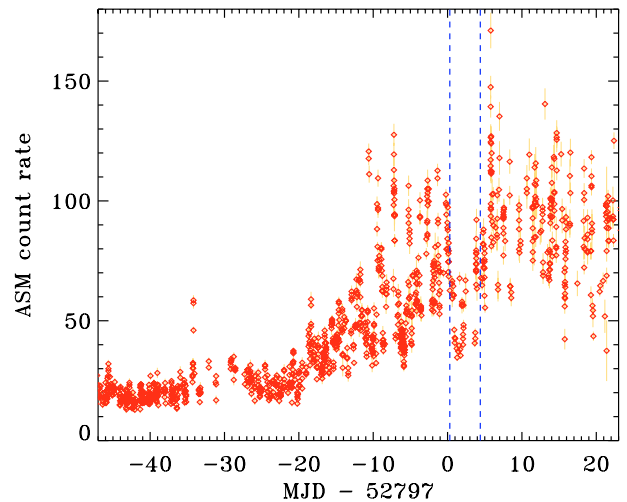


**Fig. 1.** *RXTE/ASM* light curve of Cygnus X-1. The time of the *INTEGRAL* observation is delimited by the vertical dashed lines.

of the mission (Bouchet et al. 2003; Pottschmidt et al. 2003; Bazzano et al. 2003). At that time, the source presented all the characteristics of the LHS. The source was later observed again during the galactic plane survey and open-time programme, and occasionally found in IMSs (Cadolle Bel et al. 2006, hereafter CB05). In this paper we focus on the results of the first observation of Cygnus X-1 in the open time programme. This 300 ks observation was performed on 2003 June 7–11 (rev 79/80) with a  $5 \times 5$  dithering pattern<sup>1</sup> (the effective exposure time was 275 ks for *JEM-X2*, 292 ks for *IBIS/ISGRI*, and 296 ks for *SPI*). At this epoch, the *RXTE* All Sky Monitor count rate of Cygnus X-1 was higher than in typical LHS by up to a factor of 4, and the light curve showed strong X-ray activity characteristic of state (or failed state) transitions (see Fig. 1). We also combine the *INTEGRAL* data with the results of coordinated radio observations (15 GHz) performed with the Ryle telescope. In Sect. 2, we present a spectral analysis of the *JEM-X*, *IBIS/ISGRI* and *SPI* spectra averaged over the whole duration of the observation, in Sect. 3 we study the strong broad band variability of the source during the observation.

## 2. Average spectrum

### 2.1. Data processing

We reduced the *IBIS/ISGRI* and *JEM-X* data with the standard analysis procedure of the Off-Line Scientific Analysis OSA 4.2, released by the ISDC, whose algorithms are described in Goldwurm et al. (2003) and Westergaard et al. (2003) for *IBIS* and *JEM-X* respectively. A basic selection was performed to exclude those pointings too close to radiation belt entry or exit or spoiled by too large noise. The *SPI* data were preprocessed with OSA 4.2 using the standard energy calibration gain coefficients per orbit and excluding bad quality pointings which have anomalous exposure and dead time values,

<sup>1</sup> *INTEGRAL* observations are made of a succession of exposures of about 30 min duration with varied pointed directions to enable *SPI* image deconvolution. Such a 30 min pointing is called a science window.

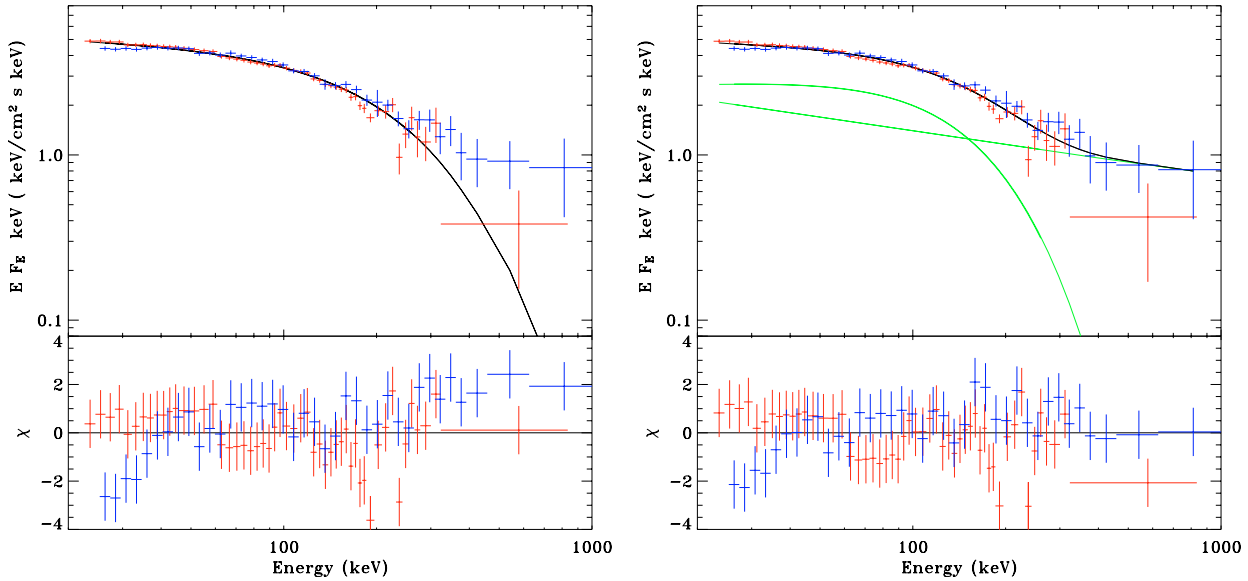


**Fig. 2.** Best fits of the *IBIS/ISGRI* (red) and *SPI* (blue) data with a pure comptonization model (COMPPS, *left*) and Comptonisation plus power-law (*right*).

or with a high final chi-squared during imaging. *SPIROS* 9.2 (Skinner & Connell 2003) was used to extract the spectra of Cygnus X-1, Cygnus X-3 and EXO 20390+375, with background model proportional to the saturating event count rates in the Ge detector. Concerning the instrumental response, version 15 of the IRF (Image Response Files) and version 2 of the RMF (Redistribution Matrix Files) were used.

We produced *JEM-X* (3–25 keV), *ISGRI* (20–800 keV) and *SPI* (25–1000 keV) spectra averaged over revolution 79 and 80. Uncertainties of 3% were added in quadrature to all three spectra to account for systematic errors. The resulting spectra were fitted using *XSPEC* v11.3.1.

## 2.2. *JEM-X* spectrum

The best power-law fit to the 3–20 keV *JEM-X* spectrum has a spectral index  $\Gamma = 2.16$  which is intermediate between LHS and HSS spectral indices. The fit is however not statistically acceptable ( $\chi^2/\nu = 611/131$ ) with strong residuals indicating the presence of strong reflection and broad iron line features and a soft component (see below in Sect. 2.4 and Fig. 3).

## 2.3. *SPI* and *IBIS/ISGRI* spectra

The spectra show a highly significant evidence for a cut-off (or at least a break) around 100 keV (see Fig. 2). We first fit the *ISGRI* and *SPI* spectra independently with the Comptonisation model COMPPS (Poutanen & Svensson 1996) The COMPPS model provides a reasonable fit with reduced  $\chi^2$  values 0.82 and 1.12 for *ISGRI* and *SPI* respectively. The best-fit parameters obtained for both instruments (shown in Table 1) are compatible within the error bars.

However the residuals show an excess emission with respect to the Comptonisation model above the thermal cut-off in the *SPI* spectrum, which is not detected in the *ISGRI*

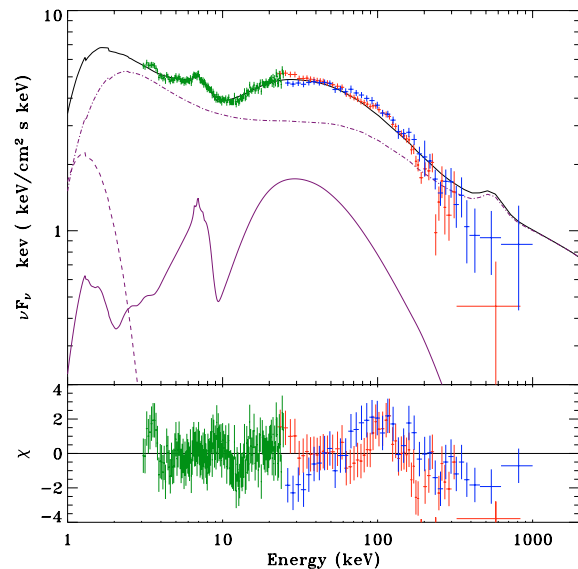


**Fig. 3.** Joint *JEM-X/SPI/ISGRI* spectrum of Cygnus X-1 averaged over revolutions 79 and 80. The data are fitted with the thermal/non-thermal hybrid Comptonisation model EQPAIR with power-law injection of relativistic electrons (see text and Table 2). The lighter curves show the reflection component (solid), the disc thermal emission (dashed) and the Comptonised emission (dot-dash). The green, red and blue crosses show the *JEM-X*, *IBIS/ISGRI* and *SPI* data respectively.

spectrum. This prompted us to reprocess the *SPI* data using different background models based on an empty field observation to model the uniformity map of the detection plan. We also tested using the instrument team processing software instead of OSA. This did not affect the presence of a high energy excess in the *SPI* spectrum. We concluded that the non detection of this excess by *ISGRI* was attributable to its poorer sensitivity above 200 keV. This is also the reason why the *ISGRI* fit appears statistically better. Within the errors bars the highest energy *IBIS* and *SPI* data points are not too far and still compatible.

**Table 1.** Best-fit parameters of the *SPI* and *IBIS* spectra fitted with thermal-Comptonisation and thermal-Comptonisation plus power-law models. For each instrument the first line gives the results of the COMPPS model alone (Comptonisation temperature  $kT$  and Thomson depth  $\tau$ ) while the second line gives the results of the fit with COMPPS plus a power-law (photon index  $\Gamma$ ). In the COMPPS model the black body temperature of the soft seed photons was fixed at 0.1 keV in all fits.

data	$kT$ (keV)	$\tau$	$\Gamma$	$\chi^2/\nu$
<i>ISGRI</i>	$79^{+7.5}_{-7.3}$	$1.06^{+0.17}_{-0.14}$		46/56
<i>ISGRI</i>	$51^{+12}_{-12}$	$2.01^{+0.59}_{-0.81}$	$2.39^{+0.14}_{-1.57}$	43/54
<i>SPI</i>	$90^{+18}_{-8}$	$0.98^{+0.15}_{-0.24}$		50/44
<i>SPI</i>	$45^{+15}_{-12}$	$2.38^{+1.1}_{-0.49}$	$2.06^{+0.24}_{-0.70}$	23/42
<i>SPI+ISGRI</i>	$84^{+6.3}_{-6.8}$	$1.00^{+0.14}_{-0.10}$		142/102
<i>SPI+ISGRI</i>	$42^{+15}_{-4}$	$2.64^{+0.50}_{-0.33}$	$2.27^{+0.66}_{-0.77}$	106/100

To obtain better constraints on the parameters we then fit simultaneously the *SPI* and *ISGRI* data. The results are shown in Fig. 2. In all fits we allow for a free normalisation constant of the model for each instrument to correct for inter-calibration errors. The resulting difference in normalisation between the instruments never exceeds 20%. The simple COMPPS model leads to best-fit parameters that are intermediate between those obtained for the individual *ISGRI* and *SPI* spectra, but the statistical quality of the fit is not as good ( $\chi^2/\nu = 1.4$ ). As a further test for the presence of a high-energy excess, we refit both spectra with COMPPS adding a power law component. When we allowed for this additional component the reduced  $\chi^2$  decreased to 1.05. This improvement is highly significant, a F-test ( $\Delta\chi^2 = 36$  for 2 additional parameters) shows that the probability that this improvement occurred by chance is  $5 \times 10^{-7}$ . We conclude that either the high-energy cut-off is not due to thermal Comptonisation (e.g. associated to a cut-off in a non-thermal lepton distribution) or there is an additional non-thermal component at high-energy. We stress that the presence of the high energy excess is not in conflict with the *ISGRI* data although this instrument was not able to detect it.

#### 2.4. Joint spectrum

We now consider the joint *JEM-X/ISGRI/SPI* spectrum. The simple models considered in the previous section do not provide an acceptable description of the broad band spectrum: strong reflection features and a soft-excess are required by the *JEM-X* data. CB05 present spectral fits of the same data with various thermal and non-thermal Comptonisation models. In these models the soft excess in the *JEM-X* spectrum is accounted for by thermal emission of the accretion disc. However, although, these fits are statistically acceptable, they require high temperatures of the accretion disc ( $1.21 \pm 0.29$  keV). As mentioned in CB05 such a high temperature of the accretion disc is not realistic. Since the distance and scale of the accretion disc (i.e. mass of the black hole) are quite well known for this source, the intrinsic luminosity of the accretion disc is constrained: if the accretion disc in Cygnus X-1 had an

inner temperature of 1 keV, it would produce a flux at least one order of magnitude larger than what is observed.

In order to get a more physically motivated representation of the data, we investigate in more details thermal/non-thermal hybrid Comptonisation models and attempt to fit the data using different variants of the EQPAIR model (Coppi 1999; G99; Frontera et al. 2001 (hereafter F01); Zdziarski et al. 2002, 2004) where the accretion disc temperature is arbitrarily fixed to a reasonable value. This model was shown to be successful in accounting for the high energy spectra of Cygnus X-1 and other black holes candidates in different spectral states and over a very broad energy band ranging from soft X-rays to gamma-rays (see e.g. McConnell et al. 2000, 2002). The wide use of this model in the literature will allow us to compare our observation with previously published results.

#### 2.4.1. The hybrid thermal/non-thermal comptonisation model (EQPAIR)

A detailed description of the EQPAIR model can be found in G99. Its main ingredient is a spherical hot plasma cloud with continuous acceleration of electrons intended to model the emission of the hot disc/corona. The high-energy electrons lose energy because of Compton, Coulomb, and bremsstrahlung processes and thus establish a steady-state distribution. At high energies, the distribution is non-thermal (power-law like), but at low energies a Maxwellian distribution is established. The temperature of the Maxwellian population,  $kT_e$  is determined by balance between Compton gains and losses, Coulomb heating by high energy electrons, bremsstrahlung losses, and direct heating (e.g., Coulomb heating by energetic ions). The total number of electrons (not including  $e^+ - e^-$  pairs, the production of which is also taken into account) is determined by the corresponding Thomson optical depth  $\tau_p$ , which is a free parameter. The cloud is illuminated by soft thermal photons emitted by an accretion disk. These photons serve as seed for Compton scattering by both thermal and nonthermal electrons. The system is characterised by the power  $L_i$  supplied to its different components. We express each of them dimensionlessly as a compactness,  $l_i = L_i \sigma_T / (R m_e c^3)$ .  $R$  is the characteristic dimension of the plasma,  $\sigma_T$  is the Thomson cross-section.  $l_s$ ,  $l_{th}$ ,  $l_{nth}$ , and  $l_h = l_{th} + l_{nth}$  correspond to the power in soft disk photons entering the plasma, thermal electron heating, electron acceleration and the total power supplied to the plasma. We follow G99 and set  $l_s = 10$ .

The disc spectrum incident on the plasma is modelled as coming from a pseudo-Newtonian accretion disk extending from  $R_{out} = 10^3 R_g$  down to the minimum stable orbit,  $R_{in} = 6 R_g$ . Its spectral shape is then characterised by the maximum colour temperature of the disk,  $kT_{max}$ . Previous observations of Cygnus X-1 with X-rays telescopes indicate temperatures ranging from 0.1 keV in the LHS to up to 0.6 keV in the HSS (G99; F01). For such temperatures the peak of the thermal disk emission is below the energy range covered by *INTEGRAL*, and the disk temperature cannot be constrained by our observations, we therefore fixed  $kT_{max} = 0.3$  keV. The covering factor of the corona is unity.

The spectrum from both reflection and the Fe  $K_\alpha$  is calculated, taking into account relativistic smearing with the emissivity dependence  $\propto R^{-2}$ . The reflecting material is allowed to be ionised, with the degree of ionisation characterised by the ionisation parameter  $\xi$ . We follow G99 and fix the column density of absorbing material along the line of sight to  $N_H = 5 \times 10^{21} \text{ cm}^{-2}$  and the inclination angle of the system at 45 degrees.

#### 2.4.2. Fit results

We first performed a fit similar to those of G99 and F01 with the non-thermal electrons injected with a power-law distribution of Lorentz factors ranging from  $\gamma_{\min} = 1.3$  to  $\gamma_{\max} = 1000$ . The upper and lower limits  $\gamma_{\min}$  and  $\gamma_{\max}$  were kept fixed while fitting for the power-law index  $\Gamma_p$ . This results in an acceptable fit with a reduced  $\chi^2$  of 1.29. The unfolded broadband spectrum and residuals are shown in Fig. 3. The best-fit parameters are presented in Table 2.  $l_h/l_s$  is about unity i.e. intermediate between what is generally found in the LHS (4–10, see Ibragimov et al. 2005) and the HSS ( $\leq 0.4$ ), the heating of the plasma is dominated by the non-thermal acceleration ( $l_{\text{nth}}/l_h = 1$ ). Overall the parameters are similar to those obtained by G99 for the IMS of 1996 May 23. However an inspection of the residuals (Fig. 3) shows that the high energy part of the *ISGR*/*SPI* spectrum is not well represented by this model. The model does not provide a good description of the shape of the high-energy cut-off and overestimates the measured flux above 200 keV. As an alternative we attempted to fit the spectrum assuming that the electrons are injected at a single Lorentz factor  $\gamma_{\text{inj}}$  instead of a power-law distribution. Such a mono-energetic injection is not expected in the case of shock acceleration but could be achieved in reconnection events that are expected to power the corona. The resulting fit is displayed in Fig. 4 and the unabsorbed best fit model spectrum is shown in Fig. 13. The best-fit parameters are shown in Table 2. Note that the fraction of non-thermal power is now only  $l_{\text{nth}}/l_h = 0.51$ . This model gives a good description of the *INTEGRAL* spectrum. The best-fit value for the maximum Lorentz factor of the electrons  $\gamma_{\text{inj}} = 8.6$  implies that the once scattered soft photons reach a maximum energy of about  $4\gamma_{\text{inj}}^2 kT_{\text{max}} \sim 90 \text{ keV}$ . In other words, in this model the high-energy cut-off observed in the spectrum is non-thermal and corresponds to the upper end of the non-thermal electron distribution.

So far we have shown that the soft excess in the JEM-X data does not require an unphysical high accretion disc temperature and can be accounted for by an hybrid particle distribution. In this context, our data favour mono-energetic injection over power-law acceleration. However, this is not the only possible interpretation. Indeed, such a soft excess is not uncommon in IMSs and the softest LHSs. It is often interpreted as a hot spot on the accretion disc or alternatively as a component due Comptonisation in the warm upper layers of the disc. It can be accounted for by adding a second Comptonisation component with a temperature of a few keV (Di Salvo et al. 2001; F01; Zicky et al. 2001). Alternatively, Markoff et al. (2005),

**Table 2.** Best-fit parameters of the joint *JEM-X*, *SPI* and *IBIS/ISGR* spectra with hybrid thermal/non-thermal Comptonisation models (EQPAIR, see Sect. 2.4). The temperature of the inner disk (DISKPN) was fixed to  $kT_{\text{max}} = 0.3 \text{ keV}$  in all fits. The soft photon compactness is fixed at  $l_s = 10$ . The absorbing column density is  $N_H = 5 \times 10^{21}$  and the inclination angle 45 degrees. The fit parameter  $\tau_p$  refers to the Thomson optical depth of the electrons associated with ions. The table also gives the resulting total optical depth  $\tau_T$ , including electron-positron pairs whose production is calculated self-consistently, and the temperature  $kT_e$  of the thermalised particles, computed according to energy balance. The extrapolated 0.1–1000 keV model flux,  $F_{\text{bol}}$ , and thermal disc component flux,  $F_{\text{disc}}$ , are given in units of  $10^{-8} \text{ erg s}^{-1} \text{ cm}^{-2}$ . The first column shows the results of the fit with a power law injection of non-thermal electrons with Lorentz factors ranging from  $\gamma_{\min} = 1.3$  to  $\gamma_{\max} = 1000$ . The data are then fitted for the index of the distribution of injected electrons  $\Gamma_p$ . The second column shows the best fit parameters for a mono-energetic injection of electrons, the fit parameter  $\gamma_{\text{inj}}$  represents the Lorentz factor of the injected particles. Finally, the third column gives the results for a power-law injection plus an additional warm Comptonisation component (COMPTT). Its best fit temperature  $kT_{\text{compt}}$ , Thomson depth  $\tau_{\text{compt}}$  and flux  $F_{\text{compt}}$  are also shown. In this fit  $\Gamma_p$  pegged to its minimum allowed boundary (2).

Model	EQPAIR pow.	EQPAIR mono.	EQPAIR+COMPTT
$l_h/l_s$	$1.19^{+0.07}_{-0.06}$	$0.85^{+0.02}_{-0.03}$	$3.06^{+0.41}_{-0.16}$
$l_{\text{nth}}/l_h$	$1^{+0}_{-0.04}$	$0.51^{+0.04}_{-0.04}$	$0.23^{+0.37}_{-0.02}$
$\tau_p$	$1.31^{+0.02}_{-0.04}$	$0.55^{+0.01}_{-0.06}$	$0.79^{+0.13}_{-0.07}$
$\Gamma_p$ or $\gamma_{\text{inj}}$	$2.68^{+0.02}_{-0.01}$	$8.41^{+0.62}_{-0.92}$	$2^{+0.21}_{-0}$
$\Omega/2\pi$	$0.67^{+0.09}_{-0.02}$	$0.71^{+0.09}_{-0.03}$	$0.62^{+0.09}_{-0.06}$
$\xi$ (erg cm s $^{-1}$ )	$2063^{+463}_{-367}$	$525^{+143}_{-84}$	$991^{+297}_{-176}$
$E_{\text{line}}$ (keV)	$6.76^{+0.36}_{-0.33}$	$7.02^{+0.32}_{-0.23}$	$6.67^{+0.25}_{-0.25}$
EW (eV)	$55^{+33}_{-34}$	$90^{+38}_{-24}$	$76.3^{+34}_{-29}$
$kT_{\text{compt}}$ (keV)			$2.53^{+0.20}_{-0.99}$
$\tau_{\text{compt}}$			$2.73^{+0.34}_{-0.27}$
$F_{\text{compt}}$			1.52
$F_{\text{disc}}$	1.9	3.0	0.63
$F_{\text{bol}}$	7.5	7.9	5.9
$kT_e$ (keV)	20.3	50	65
$\tau_T$	1.36	0.55	1.01
$\chi^2/\text{d.o.f.}$	316/245	244/245	216/242

suggest that this soft component originates from optically thin synchrotron emission in the jet.

To check the effect of such an additional soft component on the derived parameters of the EQPAIR model, we fit the spectrum with a model consisting in the power-law injection EQPAIR model, including the same 0.3 keV thermal component, relativistically smeared iron line and ionised reflection component as in our previous models (see Sect. 2.4.1) plus an additional Comptonisation component (COMPTT model in XSPEC) in a warm medium.

This led to an excellent fit of the *INTEGRAL* data, with  $\chi^2/\nu = 0.89$ , that is shown in Fig. 5 and Table 2. The additional Comptonisation component has a best-fit temperature of 2.5 keV and a Thomson optical depth of 2.7. The fit is much

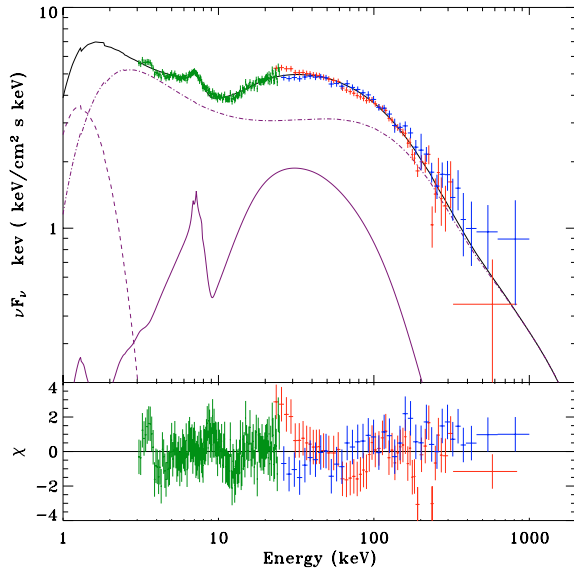


**Fig. 4.** Same as in Fig. 3 except that the fitting model is now EQPAIR with *mono-energetic* injection of relativistic electrons with Lorentz factor  $\gamma_{\text{inj}} = 8.6$  (see text and Table 2).

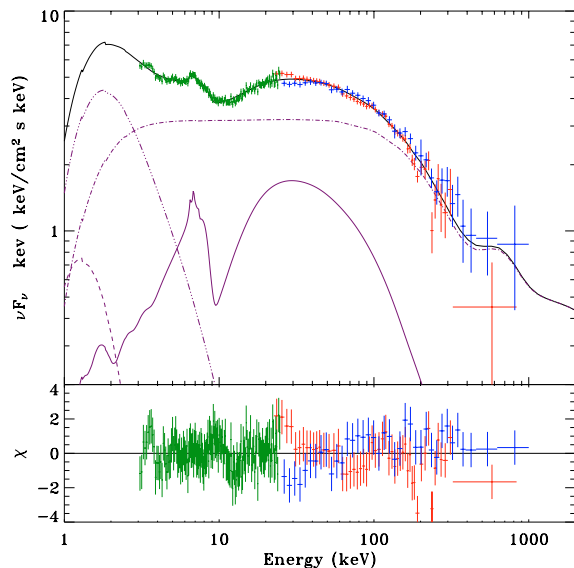


**Fig. 5.** Same as in Fig. 3 except that the fitting model is now EQPAIR with a power-law injection relativistic electrons *plus* an additional warm Comptonisation soft component (COMPTT, see text and Table 2). The COMPTT component is shown by the 3-dot-dashed curve.

better than what obtained with the powerlaw injection EQPAIR model. The probability that the improvement obtained when the soft COMPTT component is added to the powerlaw injection EQPAIR model occurred by chance is  $7 \times 10^{-20}$  according to F-test ( $\Delta\chi^2 = 100$  for 3 additional parameters). This fit is statistically comparable to that obtained with mono-energetic injection. It demonstrates that mono-energetic injection is far from inevitable.

We also note an interesting difference between power-law and mono-energetic injection models: the presence of a broad  $e^+ - e^-$  pair annihilation line around 511 keV that is clearly visible in Figs. 3 and 5 (power-law injection) but absent

from Fig. 4 (mono-energetic injection). In the power-law model some electrons are injected at very high Lorentz factors ( $\lesssim 1000$ ) these electrons efficiently up-scatter soft-photons at energies above the pair production threshold, leading to a pair cascade and subsequent annihilation, whereas in the mono-energetic case the pair content of the plasma is negligible due to the much lower energy of the electrons ( $\lesssim 8.41$ ). Unfortunately the poor statistics of the data does not allow us to discriminate between these models on the basis of the annihilation line.

In the EQPAIR+COMPTT spectral model the fraction of non-thermal power ( $l_{\text{nth}}/l_{\text{h}}$ ) is reduced to about 20% (to be compared to 100% and 50% obtained respectively for the simple power-law and mono-energetic injection models). This shows that the measured non-thermal fraction is sensitive to the assumptions of the spectral model. In the latter fit the hot plasma is essentially thermal, in agreement with the conclusions of CB05. Indeed, the equilibrium temperature and optical depth we obtain are similar to what obtained by these authors fitting the same data with a simple thermal Comptonisation model plus a multicolour disc spectrum. We also note that in the EQPAIR+COMPTT fit, the hard to soft compactness ratio is larger ( $l_{\text{h}}/l_{\text{s}} \approx 3$  instead of  $\approx 1$  in the previous fits). Overall the parameters are closer to what is usually obtained in the LHS.

In short, our spectral analysis does not favour the simple power-law injection EQPAIR model. Rather, models including an additional soft component (and a weak non-thermal fraction), or alternatively, models with an important thermal fraction but mono-energetic injection are preferred. There are however some caveats in our spectral analysis that might affect any conclusion drawn from our fits: First, there are still open calibration issues, in particular regarding the X-ray monitor *JEM-X* specially below 5 keV. It is in this energy range that the soft component shows up and it is very important to constrain the parameters of the hybrid model. Second, our model assumes a unique emitting zone although it is likely that in an IMS the situation is more complex. Indeed, the thermal hot flow of the LHS probably coexists with the non-thermal corona of the HSS in distinct regions of the accretion flow. If various emitting regions, with very different spectra and physical parameters, contribute to the observed spectrum, then the derived best-fit parameters have a poor physical significance. Similarly, and perhaps more importantly, the parameters determining the shape of the spectrum vary not only within the accretion flow but also with time. As we will show below, the source exhibited a strong spectral variability during the observation with the appearance of spectra ranging from quasi-LHS to quasi-HSS. Under such circumstances, the precise value of the best-fit parameters of the average spectrum may be physically irrelevant.

### 3. Spectral variability

#### 3.1. Set up

In order to study the spectral variability of the source during the observation, we produced light curves in 16 energy bands ranging from 3 to 200 keV<sup>2</sup> with a time resolution of the duration

<sup>2</sup> Namely: 3–4, 4–5, 5–6, 6–7, 7–9, 9–11, 11–13, 13–15, 15–20, 20–30, 30–40, 40–50, 50–80, 80–100, 100–140 and 140–200 keV.

of a science window (i.e.  $\sim 30$  min). Above 200 keV, the variability is dominated by statistical noise. The count rate in each band was then renormalised so that its time average matches the energy flux calculated from the best-fit model of the joint average *JEM-X/ISGRI/SPI* spectrum shown in Fig. 5. Namely, for each energy band we compute the quantity

$$F(t) = \frac{C(t)}{\bar{C}} \bar{F}, \quad (1)$$

where  $C(t)$  is the mean count rate during pointing  $t$ ,  $\bar{C}$  is the count rate averaged over the whole observation,  $\bar{F}$  is the observation average energy flux in this band given by the best fit model. We use  $F(t)$  as a proxy for the instantaneous energy flux, therefore neglecting the effects of the spectral variations on the instrumental response. This simple deconvolution method provides us with a convenient approximate of the broadband energy spectrum for each pointing that will be useful for a physical interpretation of the variability. This method is much more convenient than fitting the spectra for each science window, in particular if one considers the large number of parameters required to fit the data and the poor statistic in the short exposure spectra. On the other hand our method for estimating the spectra from the light curves also enables us to improve the photon statistics by combining the *IBIS/ISGRI* and *SPI* instruments in the energy range where they overlap. The time dependent flux  $F(t)$  in an overlapping band is estimated as follows:

$$F(t) = \frac{\sigma_S^2 F_1(t) + \sigma_I^2 F_S(t)}{\sigma_S^2 + \sigma_I^2}. \quad (2)$$

Where  $F_1$  and  $F_S$  are the measured *ISGRI* and *SPI* fluxes in that band;  $\sigma_1$  and  $\sigma_S$  are their time averaged uncertainties. This combination minimises the average uncertainty on  $F$ .

The resulting light curves are shown in Fig. 6. The time averaged 3–200 keV model flux is  $\bar{F}_{3-200} = 2.87 \times 10^{-8} \text{ erg cm}^{-2} \text{ s}^{-1}$ . The energy flux has a rms amplitude of 16%, and the ratio of the maximum to the minimum luminosity is 2.6.

### 3.2. Principal Component Analysis (PCA)

The light curves shown in Fig. 6 exhibit a complex and strong broad band variability of the spectra as well as the overall flux. We use a principal component analysis (PCA) to seek for variability patterns in our sample. PCA is a powerful tool for multivariate data analysis used for a broad range of applications in natural as well as social sciences (see e.g. Kendall 1980). It has also been used in astronomy. For instance, Francis & Wills (1999) provide a brief introduction to PCA as applied to quasar spectra. Previous application of PCA to spectral variability include Mittaz et al. (1990) who discussed the UV variability of NGC 4151 and Vaughan & Fabian (2004) for the X-ray variability of MCG6-30-15.

The main use of PCA is to reduce the dimensionality of a data set while retaining as much information as possible. It transforms a number of (possibly) correlated variables into a (smaller) number of uncorrelated variables called principal components. These principal components may define patterns

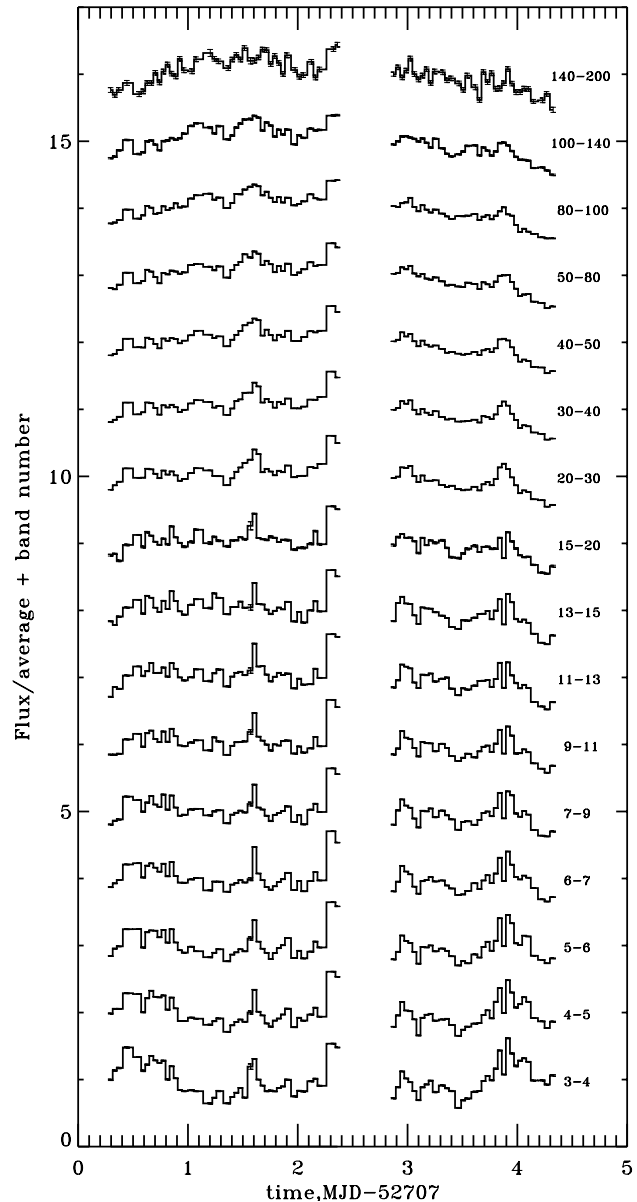


**Fig. 6.** Light curves in different *JEM-X* an *ISGRI/SPI* bands with increasing photon energy from bottom to top, as labelled in keV. Each light curve was re-scaled to the average flux and then incremented according to its energy range for clarity.

or correlations in the data set that can often be interpreted more easily than the original (large) data sets.

In our specific application we have  $p = 79$  spectra measured at times  $t_1, t_2, \dots, t_p$  and binned into  $n = 16$  bins corresponding to energies  $E_1, E_2, \dots, E_n$ . Each spectrum can be thought of as a point in a  $n$ -dimensional space, so that the coordinate of the point  $j$  along the  $E_i$  axis is given by the corresponding energy flux  $F(t_j, E_i)$ . The shape and extension of the cluster of points formed by the whole set of spectra characterises the source variability. The idea behind PCA is to determine a new coordinate system in which the description of this cluster will be simpler.

For this purpose, the data can be viewed as the  $p \times n$  matrix which coefficients are given by the energy fluxes  $F(t_j, E_i)$ . Then

one can compute the  $n \times n$  covariance matrix of the data. In practice, PCA consists in diagonalizing this covariance matrix to obtain its eigenvalues and eigenvectors. This procedure gives the coordinates of each eigen vector i.e. the  $C_k(E_i)$  coefficients denoting the coordinate of the  $k$ th eigenvector along  $E_i$  axis.

These eigenvectors define a new coordinate system, in this  $n$ -dimensional parameter space, which best describes the variance in the data. The first principal component, or PC 1 (the eigenvector with the highest eigenvalue), marks the direction through the parameter space with the largest variance. The next Principal Component (PC 2) marks the direction with the second largest amount of variance, etc.

Let  $\alpha_k(t_j)$  be the new coordinate of the spectrum  $j$  along the  $k$ th eigen vector, then the relation between the two coordinate systems can be written as follows:

$$F(t_j, E_i) = \bar{F}(E_i) + \sum_{k=1}^n \alpha_k(t_j) C_k(E_i), \quad (3)$$

where  $\bar{F}(E_i)$  is the time averaged flux at energy  $E_i$  (the time averaged spectrum is used as the origin for the eigenvector coordinate system).

Equation (3) amounts to a linear decomposition into  $n$  independent components of the variability (the eigenvectors  $C_1, C_2, \dots, C_n$ ). The normalisation coefficients of each PCA component (respectively  $\alpha_1, \alpha_2, \dots, \alpha_n$ ) vary in time. Their fluctuations account for the sample variance. On the other hand the eigenvectors  $C_k$  are constant, they define the variability mode of each PCA component. Since the eigenvectors describe fluctuations around the time-average flux, both the  $\alpha_k$  and  $C_k$  coefficients can take negative as well as positive values. If the  $C_k$  coefficients are positive at all energies, the variability mode associated to component  $k$  can be understood as due to an additive spectral component with a fixed shape and a variable normalisation. When the sign of  $C_k$  depends on energy, this corresponds to more complex spectral variability modes (e.g. pivoting).

As mentioned above, the PCA components are ordered according to the amount of sample variance they account for (i.e. the observed fluctuations of  $\alpha_1$  cause more variance than those of  $\alpha_2$  which produce more variance than  $\alpha_3$  etc.). The first few Principal Components (those representing most of the variance in the data) should reveal the shape of the relevant spectral components or variability modes. The weaker Principal Components might be expected to be dominated by the statistical and systematic noise in the spectra. To summarise, PCA finds the decomposition that maximises the variability due to lower order components, so that most of the variability can be described using a small number of components.

### 3.3. Results of the PCA analysis

The results of our PCA analysis of the spectral variability of Cygnus X-1 are illustrated in Fig. 7, which shows how the 2 first principal components affect the flux and spectrum and their respective contribution to the total observed variance as a function of energy. As can be seen in this figure, the first principal component (PC 1) consists in a variability mode

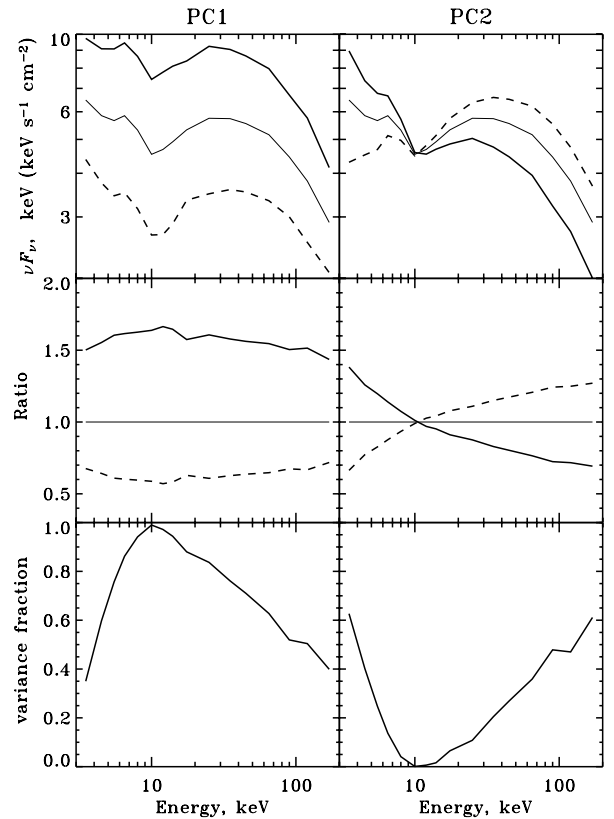


**Fig. 7.** The 2 first principal components of variability. The upper panels illustrate the effects of the each component on the shape and normalisation of the spectrum: time average spectrum (light line) and spectra obtained for the maximum (thick solid line) and minimum (dashed line) observed values of the normalisation parameter. The middle panels show the ratio of spectra obtained of the maximum and minimum spectra to the average one. The bottom panels show the contribution of each component to the total variance as a function of energy.

dominated by variations in the luminosity (normalisation) with little change in the spectral shape. For this reason, in the following, we will refer to PC 1 as the “flaring mode”. This component accounts for 68% of the sample variance. Let us now consider the small spectral fluctuations induced by PC 1. An increase in luminosity is associated with spectral hardening in the 3–10 keV band, and a slight softening at higher energies which is particularly marked in the 10–30 keV band. This spectral variability suggests a variable power-law spectrum with fixed spectral index moving on top of a constant thermal emission disc emission plus reflection component. Despite these small spectral variations, PC1 correlates very well with the high-energy flux. A least square fit shows that the 3–200 keV flux relates to  $\alpha_1$  through:

$$F_{3-200} = \bar{F}_{3-200}(1 + 7.64\alpha_1), \quad (4)$$

with a linear correlation coefficient of 0.98. So that  $\alpha_1$  can be viewed as a tracer of the hard X-ray luminosity of the source.

As shown in Fig. 7, the second PCA component (PC 2) can be described roughly as a pivoting of the spectrum around 10 keV. The two spectra obtained for the minimum and maximum values of the  $\alpha_2$  parameter controlling the strength of

PC 2 are reminiscent of the canonical LHS and HSS spectra. This component is responsible for 27% of the sample variance, and will be referred as the “pivoting mode”.  $\alpha_2$  can thus be seen as a tracer of the hardness of the high-energy spectrum.

The third PCA component (PC 3) accounts for only 2% of the sample variance. It is dominated by fluctuations of the relative normalisation of the spectrum in the *JEM-X* band and *ISGRI/SPI* energy range. This component is most likely an instrumental artefact due to known calibration issues related to the dithering observation mode. Indeed, since the pointed direction changes between successive science windows and as the effects of vignetting and background non-uniformity are not perfectly corrected in the present release of the data analysis software, this results in spurious variability that affects mainly the relative flux normalisation between instruments. This effect is particularly strong in *JEM-X* for which systematic errors as large as 30% are expected for a source 5 degrees off axis. PCA enables us to disentangle such instrumental effects from the intrinsic variability. Because they are independent of the intrinsic source variations and as long as they are not dominant, they are filtered and isolated into higher order PCA components.

Similarly variability due to statistical noise is filtered out into higher order components. From the statistical uncertainties on the measured count rates we expect 3% of the observed variance to be due to statistical noise. As the first 3 PCA components already account for 97% of the sample variance, the higher order components are most likely due to noise. Figure 8 shows the contribution of PC 1, PC 2, PC 3 and statistical noise to the observed variance spectrum (i.e. the measured variance as a function of photon energy). These 4 components are enough to account for the observed variance within a few percents at all energies.

Since PC 3 is likely to be an instrumental artefact and higher order components are probably noise, we conclude that the intrinsic source variability is largely dominated by PC 1 (flaring mode) and PC 2 (pivoting mode). Figure 9 shows the time evolution of the PCA parameters  $\alpha_1$  and  $\alpha_2$ .  $\alpha_1$ , which traces the changes in bolometric luminosity at nearly constant spectra shows important variability on time scales of order of a few hours or less, but no clear systematic trend during the 4 days of observation. In contrast,  $\alpha_2$ , which roughly traces the hardness of the spectrum, seems to vary on longer time scales: it jumps during the first 2 days then decreases in the second part of the observation. This suggests that the physical mechanisms responsible for PC 1 and PC 2 are distinct (which is also expected from the fact that, by construction, PC 1 and PC 2 are linearly independent) and apparently acting on different time scales.

### 3.4. Radio/high-energy correlation

In order to study the possible correlations between the radio and hard X-ray emission, we selected the science windows for which we had simultaneous radio pointings. When there were several radio pointings falling within a given science window we use the mean radio flux. The resulting light curve is shown in the bottom panel of Fig. 9. A comparison with the time

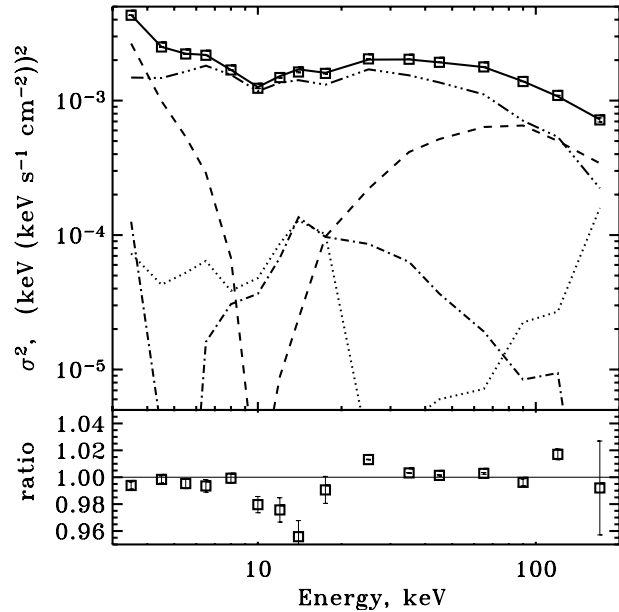


**Fig. 8.** Observed variance spectrum (squares). The curves show the contribution of PC 1 (3 dots-dash), PC 2 (dashes), PC 3 (dot-dash), estimated statistical noise (dots) and their sum (solid). The bottom panel shows ratio of the contribution of PC 1+PC 2+PC 3+noise to the total observed variance (values exceeding unity might be due to overestimated statistical noise).

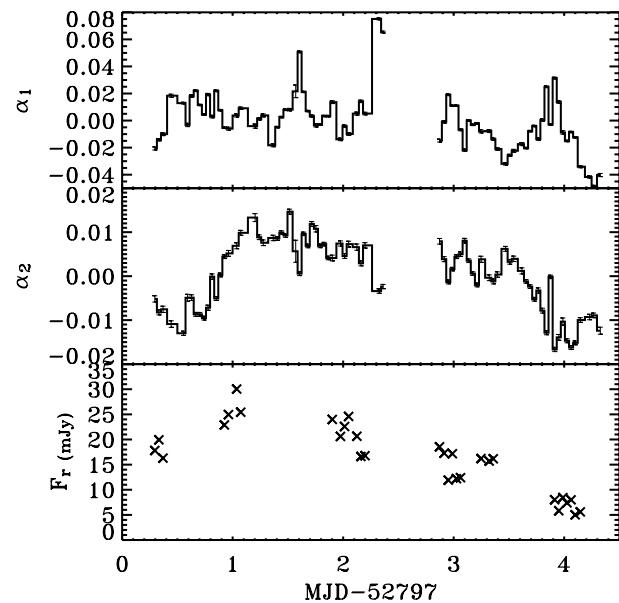


**Fig. 9.** Evolution of the parameters associated to PC 1 (top), PC 2 (middle) and radio light curve (bottom) during the observation.

evolution of  $\alpha_1$  and  $\alpha_2$  indicates that the radio flux tends to follow the evolution of the pivoting mode. In other words, the radio flux tends to be stronger when the hard X-ray spectrum is harder. This is clearly seen in Fig. 10 which shows that the radio emission is strongly correlated to  $\alpha_2$ . The correlation is highly significant. The Spearman rank test correlation coefficient is 0.78 corresponding to a probability that the correlation is by chance of  $2 \times 10^{-7}$ . On the other hand, there is no hint

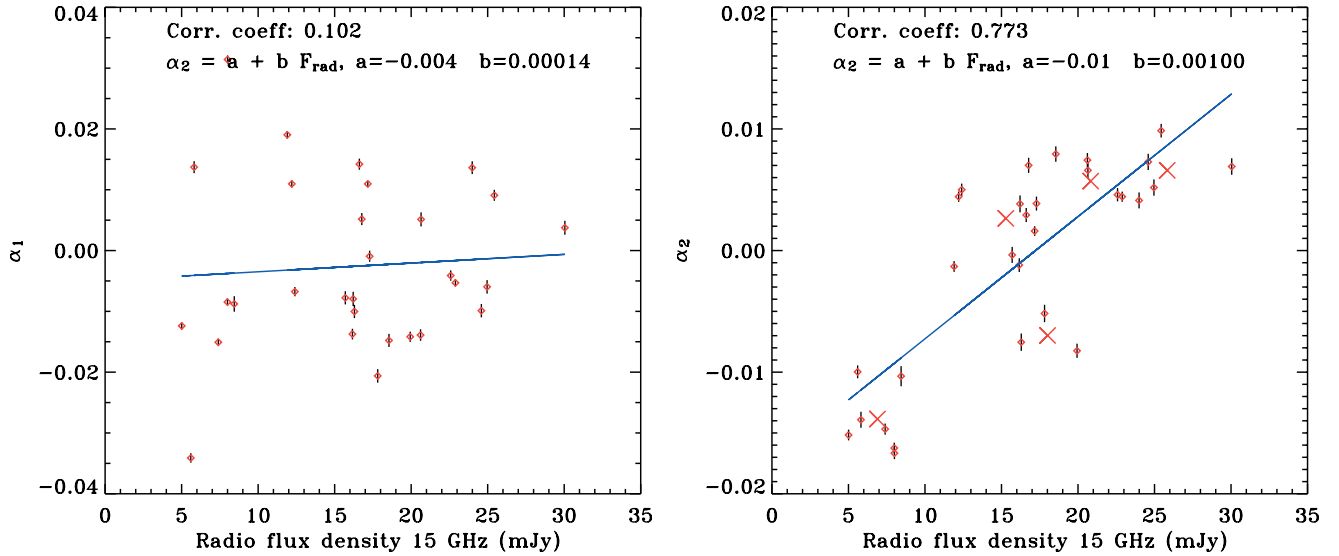


**Fig. 10.** PCA parameters  $\alpha_1$  (left panel) and  $\alpha_2$  (right panel) as a function of the radio flux (diamonds). In both panels, the best linear fits are shown by the solid lines. The crosses indicate the time average over each of the five periods of nearly continuous radio coverage (see Fig. 9). While there is no convincing correlation between the radio flux and  $\alpha_1$ , the radio flux is correlated to  $\alpha_2$  at highly significant level.

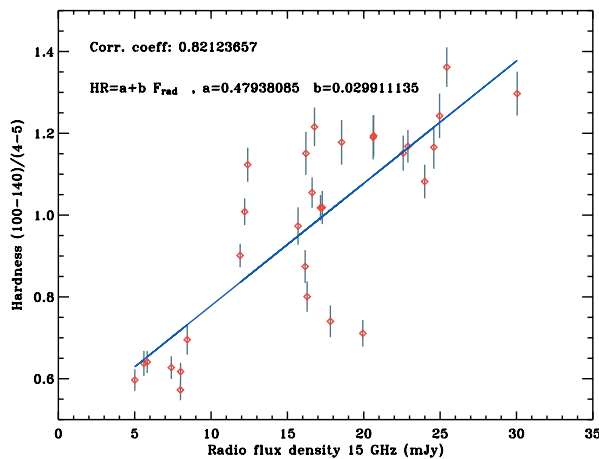


**Fig. 11.** Correlation between radio flux density and  $(100-140 \text{ keV})/(4-5 \text{ keV})$  hardness.

of a correlation with the flaring mode as can be seen in the left panel of Fig. 10.

It is also worth noting that the correlation between the pivoting mode and the radio flux is valid only when we consider the data over more than one day, we find no evidence for a correlation on shorter time-scales. Therefore, our PCA analysis shows that on time scales of days, the radio jet activity is correlated with hardness of the high-energy spectrum rather than hard X-ray luminosity.

Obviously this can be seen directly from the light curves, although less comprehensively. For instance Fig. 11 shows a strong correlation between the  $(100-140 \text{ keV})/(4-5 \text{ keV})$  hardness and the radio flux. Figure 12 shows that the radio flux tends to be anti-correlated with the X-ray flux (3–7 keV) and correlated with the soft gamma-rays ( $>15 \text{ keV}$ ). This dependence of the *INTEGRAL*/radio flux correlation confirms both the presence of a pivot point located around 10 keV and the correlation of the radio luminosity with the pivoting of the

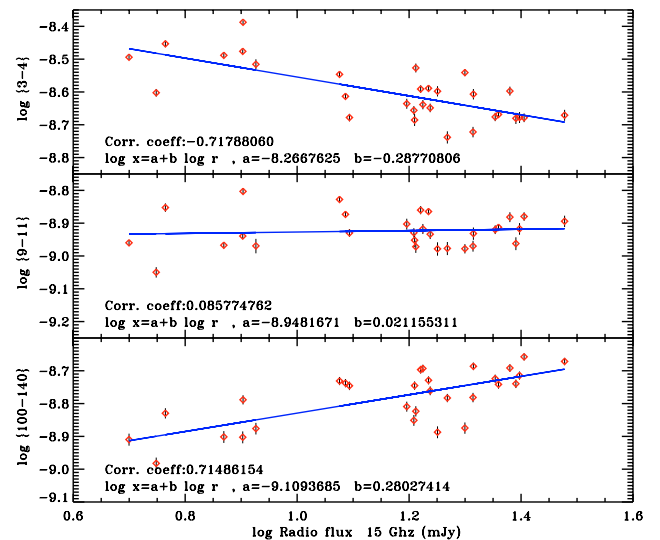


**Fig. 12.** Flux ( $\text{erg cm}^{-2} \text{ s}^{-1}$ ) in different energy bands (as indicated in keV), versus 15 GHz radio flux density.

spectrum. However, without PCA it would have been very difficult to demonstrate the presence of the 2 independent variability modes. PCA also brings a much clearer information on the spectral variability due to each mode, and, on top of that, enables one to filter out systematic and statistical errors.

#### 4. Discussion

We have shown that, during our IMS observation, the variability of Cygnus X-1 can be described by two independent variability modes:

- On time-scales of a few hours or less there are important changes in luminosity with little spectral variations (flaring mode).

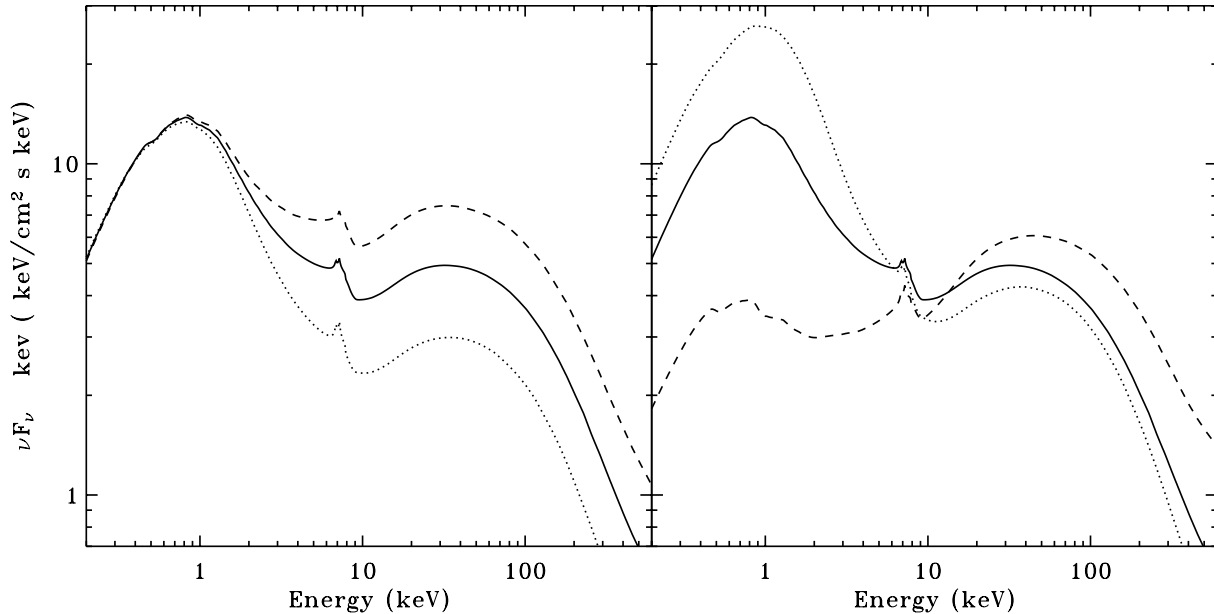


**Fig. 13.** *Left panel:* effect of varying  $l_h$  by a factor of 2 on the EQPAIR model with monoenergetic injection (see Sect. 2.4). Solid curve: unabsorbed best-fit model ( $l_h = 8.5$ ); Dotted curve  $l_h = 5.7$ ; Dashed curve:  $l_h = 11.9$ . *Right panel:* effect of varying the soft photons flux by a factor of 8. Solid curve: unabsorbed best-fit model ( $T_{\text{disc}} = 0.3$  keV;  $l_h/l_s = 0.85$ ). Dotted curve:  $T_{\text{disc}} = 0.357$  keV and  $l_h/l_s = 0.42$ . Dashed curve:  $T_{\text{disc}} = 0.212$  keV and  $l_h/l_s = 3.4$ .

- On longer time scales there is a spectral evolution with the the spectrum pivoting around 10 keV.

We further showed that while there is no hint for a correlation between the radio flux and the flaring mode, the radio is strongly correlated with the pivoting of the spectrum, in the sense that the radio flux is stronger when the hard X-ray spectrum is harder. This result strongly differs from what is usually reported in the LHS. Indeed, the radio flux is then positively correlated with the soft X-ray emission (3–25 keV, Corbel et al. 2000, 2003; Gallo et al. 2003).

However, our results are not in conflict with these observations since Cygnus X-1 was not in a typical LHS but in an IMS, or rather was switching between different IMSs. Indeed, compilations of LHS and HSS spectra suggest that the spectral transition between LHS and HSS occurs through a pivoting around 10 keV (see e.g. Fig. 9 of McConnell et al. 2002). The evolution of the  $\alpha_2$  parameter shown in Fig. 9 indicates that the source, initially in a “soft” IMS, switched to a harder state during the first 2 days of observation and then transited back toward a “soft” state.

Actually, the transition from LHS to HSS is known to be associated with a quenching of the radio emission (Corbel et al. 2000; Gallo et al. 2003). As the transition to the HSS also corresponds to a strong softening of the spectrum, this is consistent with the correlation between hardness and radio flux: when, during the observation, the source gets closer to the HSS the spectrum softens and simultaneously the radio flux decreases. We also note that a recent analysis of Ryle and *RXTE* data of Cygnus X-1 (Gleissner et al. 2004) interestingly shows the same correlation tendencies during failed state transitions (Ryle/ *RXTE/PCA*: moderate anti-correlation,

Ryle/ *RXTE/HEXTE*: correlation) as reported here, albeit on timescales from weeks to years.

It is interesting to speculate on the cause of the two variability modes. We tried to reproduce such variability modes by varying the parameters of the hybrid thermal/non-thermal Comptonisation models considered in Sect. 2.4. We used the best-fit model obtained with EQPAIR and mono-energetic particle injection. We choose this model because it gives a better fit of the average *INTEGRAL* spectrum than the power-law injection model, still avoiding the complication of an additional component that cannot be computed self consistently. Actually, similar results are obtained for all of the 3 models we used to fit the broad band spectrum.

As shown in the left panel of Fig. 13 it is possible to produce variations in luminosity by a factor comparable to what is observed and little spectral changes in the *INTEGRAL* band by varying the coronal compactness  $l_h$  by a factor of 2. In this context the flaring mode would correspond to variations of the dissipation rate in the corona possibly due to magnetic reconnection. This variability mode seems to be a characteristic of the HSS (Zdziarski et al. 2002). As we show here, it also provides a major contribution to the variability of the IMS.

Regarding the pivoting mode, it can be produced by changes in the flux of soft cooling photons at constant dissipation in the hot phase. We performed simulations assuming that the accretion disc radiates like a blackbody i.e. its flux  $F_{\text{disc}} \propto l_s \propto T_{\text{max}}^4$  and constant  $l_h$ . For an increase of the disc temperature by a factor of 1.7, the disc luminosity grows by a factor of 8. As in this model, the disc flux also corresponds to the soft cooling photon input in the corona and the heating ( $\propto l_h$ ) is kept constant, this leads to a steepening of the spectrum with a pivot around 10 keV of similar amplitude as in PC 2 (see Fig. 13). For the 1996 HSS, G99 found a ratio  $l_h/l_s \sim 0.3$  while

in the LHS  $l_h/l_s$  ranges between 3.5 to 15 (Ibragimov et al. 2005). The range of  $l_h/l_s$  (0.4–3.4) required to reproduce the observed amplitude of the pivoting mode matches almost exactly the intermediate range between the HSS and the lower limit of the LHS. The source initially in a (quasi) HSS evolved toward the LHS but as soon as it was reached, it went back toward the HSS.

Since, in the *INTEGRAL* band, the constraints on disc thermal emission are loose we did not attempt to model the data with a varying inner disc radius which is, moreover, difficult to disentangle from fluctuations of the disc temperature. In the fitted models as well as the models shown in Fig. 13, the inner disc radius is fixed at  $6 R_g$ . Nonetheless our result would also be consistent with the disc moving inward and outward of the hot phase during the state transitions. Indeed, when the inner disc radius is approaching the black hole, its maximum temperature and luminosity increases<sup>3</sup> leading to a more efficient cooling of the hot flow/corona. The anti-correlation between radio flux and disc luminosity would be due to the jet expanding when the cold accretion disc recedes and then shrinking in the second phase of the observation when the disc moves back inward. It is interesting to note that the change in disc flux required (a factor of  $\sim 8$ ) to explain the spectral evolution is comparable to the amplitude of the variations of the radio flux (a factor of  $\sim 6$ ). This suggests a direct relation between the disc flux and jet power. The overall change in bolometric luminosity occurring during the PC2 transition estimated from the fiducial “hard” and “soft” state models shown on the left panel of Fig. 13, is about a factor of 2. Because of the relatively short time scale ( $\sim$ a day) on which the variation in luminosity occurs, it is unlikely to be driven by changes in the mass accretion rate. Most probably, it is due to a change in the radiative efficiency of the flow. The accretion flow could be less efficient in the LHS, because about half of the accretion power is either swallowed by the black hole or pumped into the jet, while, in the HSS, the cold disc is expected to be radiatively efficient.

The contribution of the jet power to the total energetic output of black hole candidates in the LHS is a matter of debate. It has been argued that the jet could be strong and even dominant (Fender et al. 2003; Malzac et al. 2004). The jump in luminosity by a factor of 2 that we infer during our mini state transition sets an upper limit to the jet power, namely, the jet power at a luminosity just below the transition is at most comparable to the X-ray luminosity. This upper limit is in agreement with a recent study of the jet interaction with the surrounding interstellar medium by Gallo et al. (2005). According to these authors, the jet power in Cygnus X-1 represents between 6 to 100% of the X-ray luminosity at the peak of the LHS. In our model, the upper limit is reached if there is no advection into the black hole. In this case the mini-transition pivoting mode would correspond to a redistribution of the accretion power between the jet and the cold accretion disc. In this case all LHS sources would be jet dominated, since, according to the jet and X-ray power scaling laws of Fender et al. (2003), the jet share

of the energy budget is increasingly larger at lower luminosities. However, the amplitude of the luminosity changes we infer during the mini-transition (i.e. the factor of 2) is model dependent and also depends on the strength of the thermal disc contribution to the time-averaged spectrum, which is poorly constrained with the *INTEGRAL* data. Similar observations with and even broader spectral coverage (including soft X-rays) are required to consolidate this result.

Moreover, although our data point toward an inefficient accretion flow in the LHS, it does not tell us about the cause of this inefficiency: pure advection as well as jet dominated accretion flows are both viable possibilities. We note that a similar conclusion was reached by Chaty et al. (2003), on the basis of the analysis of the multi-wavelength spectrum of the transient black hole binary XTE J1118+480.

The evolution of the hard X-ray corona luminosity during our IMS observation is very puzzling. Indeed, if, as commonly believed for the LHS, the corona constitutes the base of the jet, it is difficult to conceive that changes in the jet power and/or extension is not associated to changes in the energetics of the corona. The apparent lack of response of the radio jet to the (short time-scale) X-ray fluctuations could well be due to the time delays required to propagate the information from the corona to the distant radio emitting region, which moreover have very different sizes. However, one would still expect the corona/hot accretion flow to track the longer time-scale evolution of the radio jet and also respond to changes in the disc power and/or distance of the truncation radius. Instead, we infer dramatic changes in the jet and disc power that are anti-correlated with each other, but *completely unrelated* to the fluctuations of the coronal power. On the one hand, the spectral pivoting described by PC 2 is understood in terms of changes in the disc luminosity at *constant* coronal luminosity. And, on the other hand, the rapid fluctuations of the coronal power that we do observe through PC 1 are apparently not associated to fluctuations of the cold disc or jet emission. The nature of the instabilities responsible for a coronal activity that is so uncoupled to the jet and disc emission remains to be clarified. In any case, these results indicate that, in the IMS, the corona does not play the same role as in the LHS, and the whole disc-corona-jet interaction seem to work differently.

## 5. Conclusion

The *INTEGRAL* IMS spectrum of Cygnus X-1 shows a high-energy cut-off or break around 100 keV. The shape of this cut-off differs from pure thermal Comptonisation, suggesting the presence of a non-thermal component at higher energies. The average broad band spectrum is well fitted with hybrid thermal/non-thermal Comptonisation models, although some important parameters such as the fraction of non-thermal power are not well constrained because they depend on the assumptions of the model (mono-energetic versus power-law injection, presence or absence of an additional soft component). Models with mono-energetic injection, or models with an additional soft component seem to be favoured over standard power-law acceleration models.

<sup>3</sup> Unless the mass accretion rate is reduced by a larger amount, which seems very unlikely, the evidence being rather that the accretion rate is often (but not always) larger in the soft than in the LHS.

During our observation, the source presented a strong flux spectral variability occurring through 2 independent variability modes:

- i) changes in the dissipation rate in the corona, due to local instabilities or flares, producing a variability of the hard X-ray luminosity on time-scales of hours and no strong spectral alterations. Strikingly, this coronal activity seems to be unrelated to the evolution of the jet and cold disc luminosity.
- ii) A slower 4-day evolution starting from a spectrum close to the canonical HSS toward an almost LHS and back. This spectral evolution was characterized by a pivoting of the spectrum around 10 keV. It was correlated with the radio emission which was stronger when the hard X-ray spectrum was harder. It is interpreted in terms of a variable soft cooling photon flux in the corona associated with changes in the thermal disc luminosity and radio-jet power. This interpretation suggests a jump in bolometric luminosity of about a factor of 2 during the transition from LHS to HSS, which indicates that the LHS accretion flow is radiatively inefficient, half of the accretion power being possibly advected into the black hole and/or the radio jet.

In the IMS, the jet power appears to be anti-correlated with the cold accretion disc luminosity, while the coronal power fluctuates independently. Apparently, the coupling between accretion and ejection processes differs from that of the LHS where the radio jet and the X-ray corona appear intrinsically linked.

*Acknowledgements.* This paper is based on observations with *INTEGRAL*, an ESA project with instruments and science data centre funded by ESA member states (especially the PI countries: Denmark, France, Germany, Italy, Switzerland, Spain), Czech Republic and Poland, and with the participation of Russia and the USA. The Ryle Telescope is supported by PPARC. JM acknowledges financial support from the MURST (COFIN98-02-15-41), PPARC, CNRS and European Union (contract number ERBFMRX-CT98-0195, TMR network “Accretion onto black holes, compact stars and protostars”). This research was also supported in part by the National Science Foundation under Grant No. PHY99-07949.

## References

- Bazzano, A., Bird, A. J., Capitanio, F., et al. 2003, *A&A*, 411, L389
- Bisnovatyi-Kogan, G. S., & Blinnikov, S. I. 1976, *Soviet Astronomy Letters*, 2, 191
- Belloni, T., Mendez, M., van der Klis, M., et al. 1996, *ApJ*, 472, L107
- Beloborodov, A. M. 1999, *ApJ*, 510, L123
- Bouchet, L., Jourdain, E., Roques, J. P., et al. 2003, *A&A*, 411, L377
- Bowyer, S., Byram, E. T., Chubb, T. A., & Friedman, M. 1965, *Sci.*, 147, 394
- Brocksopp, C., Fender, R. P., Larionov, V., et al. 1999, *MNRAS*, 309, 1063
- Cadolle Bel, M., Sizun, P., Goldwurm, A., et al. 2006, *A&A*, 446, 591 (CB05)
- Chaty, S., Haswell, C. A., Malzac, J., et al. 2003, *MNRAS*, 346, 689
- Coppi, P. S. 1999, *High Energy Processes in Accreting Black Holes*, ASP Conf. Ser., 161, 375
- Corbel, S., Fender, R. P., Tzioumis, A. K., et al. 2000, *A&A*, 359, 251
- Corbel, S., Nowak, M. A., Fender, R. P., Tzioumis, A. K., & Markoff, S. 2003, *A&A*, 400, 1007
- Di Salvo, T., Done, C., Życki, P. T., Burderi, L., & Robba, N. R. 2001, *ApJ*, 547, 1024
- Fender, R., Corbel, S., Tzioumis, T., et al. 1999, *ApJ*, 519, L165
- Fender, R. P. 2001, *MNRAS*, 322, 31
- Fender, R. P., Gallo, E., & Jonker, P. G. 2003, *MNRAS*, 343, L99
- Ferreira, J., Petrucci, P. O., Henri, G., Saugé, L., & Pelletier, G. 2006, *A&A*, 447, 813
- Francis P. J., & Wills B. J. 1999, in *Quasars and Cosmology*, ed. G. Ferland, & J. Baldwin, ASP Conf. Ser., 162, 363 [arXiv:astro-ph/9905079]
- Frontera, F., Palazzi, E., Zdziarski, A. A., et al. 2001, *ApJ*, 546, 1027 (F01)
- Gallo, E., Fender, R. P., & Pooley, G. G. 2003, *MNRAS*, 344, 60
- Gallo, E., Fender, R., Kaiser, C., et al. 2005, *Nature*, 436, 819
- Gierliński, M., Zdziarski, A. A., Done, C., et al. 1997, *MNRAS*, 288, 958
- Gierliński, M., Zdziarski, A. A., Poutanen, J., et al. 1999, *MNRAS*, 309, 496 (G99)
- Gleissner, T., Wilms, J., Pottschmidt, K., et al. 2004, *A&A*, 414, 1091
- Goldwurm, A., David, P., Foschini, L., et al. 2003, *A&A*, 411, L223
- Haardt, F., & Maraschi, L. 1993, *ApJ*, 413, 507
- Ibragimov, A., Poutanen, J., Gilfanov, M., Zdziarski, A. A., & Shrader, C. R. 2005, *MNRAS*, 362, 1435
- Kendall, M. G. 1980, *Multivariate Analysis*, Second Edition (Charles Griffin and Co. London)
- Malzac, J., Beloborodov, A. M., & Poutanen, J. 2001, *MNRAS*, 326, 417
- Malzac, J., Merloni, A., & Fabian, A. C. 2004, *MNRAS*, 351, 253
- Markoff, S., Nowak, M. A., & Wilms, J. 2005, *ApJ*, 635, 1203
- Mittaz, J. P. D., Penston, M. V., & Sijnders, M. A. J. 1990, *MNRAS*, 242, 370
- McConnell, M. L., Ryan, J. M., Collmar, W., et al. 2000, *ApJ*, 543, 928
- McConnell, M. L., Zdziarski, A. A., Bennett, K., et al. 2002, *ApJ*, 572, 984
- Mendez, M., & van der Klis, M. 1997, *ApJ*, 479, 926
- Merloni, A., & Fabian, A. C. 2002, *MNRAS*, 332, 165
- Narayan, R., & Yi, I. 1994, *ApJ*, 428, L13
- Pottschmidt, K., Wilms, J., Chernyakova, M., et al. 2003, *A&A*, 411, L383
- Poutanen, J., & Svensson, R. 1996, *ApJ*, 470, 249
- Shakura, N. I., & Sunyaev, R. A. 1973, *A&A*, 24, 337
- Shapiro, S. L., Lightman, A. P., & Eardley, D. M. 1976, *ApJ*, 204, 187
- Skinner, G., & Connell, P. 2003, *A&A*, 411, L123
- Stirling, A. M., Spencer, R. E., de la Force, C. J., et al. 2001, *MNRAS*, 327, 1273
- Vaughan, S., & Fabian, A. C. 2004, *MNRAS*, 348, 1415
- Westergaard, N. J., Kretschmar, P., Oxborrow, C. A., et al. 2003, *A&A*, 411, L257
- Winkler, C., Courvoisier, T. J.-L., Di Cocco, G., et al. 2003, *A&A*, 411, L1
- Zdziarski, A. A., Poutanen, J., Paciesas, W. S., & Wen, L. 2002, *ApJ*, 578, 357
- Zdziarski, A. A., Gierliński, M., Mikołajewska, J., et al. 2004, *MNRAS*, 351, 791
- Życki, P. T., Done, C., & Smith, D. A. 2001, *MNRAS*, 326, 1367



# Bibliography

- Antonucci R., 1993, *ARA&A*, 31, 473
- Abramowicz M. A., Chen X.-M., Granath M., Lasota J.-P., 1996, *ApJ*, 471, 762
- Abrassart A., Czerny B., 2000, *A&A*, 356, 475
- Aharonian F., et al., 2003, *A&A*, 403, L1
- Aharonian F., Akhperjanian A. G., Bazer-Bachi A. R., et al., 2006, *Sci*, 314, 1424
- Ballantyne D.R., Turner N.J., Blaes O., 2004, *ApJ*, 603, 436
- Balucinska-Church M., Belloni T., Church M. J., Hasinger G., 1995, *A&A*, 302, L5
- Beckmann V., Gehrels N., Favre P., Walter R., Courvoisier T. J.-L., Petrucci P.-O., Malzac J., 2004, *ApJ*, 614, 641
- Beckmann V., Shrader C. R., Gehrels N., Soldi S., Lubiński P., Zdziarski A. A., Petrucci P.-O., Malzac J., 2005, *ApJ*, 634, 939
- Begelman M.C., 2001, *ApJ*, 551, 897
- Begelman M.C., 2002, *ApJL*, 568, L97
- Belmont R., Malzac J., Marcowith A., 2007, proceedings of the ‘International Workshop Symbol-X: the hard X-ray Universe in focus, 14-16 May 2007’, *Memorie della Società Astronomica Italiana*, in press.
- Belloni T., Mendez M., van der Klis M., et al., 1996, *ApJ*, 472, L107
- Belloni T., Homan J., Casella P., van der Klis M., Nespoli E., Lewin W.H.G., Miller J. M., Méndez M., 2005, *A&A*, 440, 207
- Beloborodov, A.M., 1999, *ApJL*, 510, L123
- Beloborodov A.M., 2001, *AdSpR*, 28, 411
- Bisnovatyi-Kogan G.S., Blinnikov S.I., 1976, *Soviet Astronomy Letters*, 2, 191
- Blaes O., Socrates A., 2001, *ApJ*, 553, 987
- Blaes O., Socrates A., 2003, *ApJ*, 596, 509
- Blandford R.D., Znajek R.L., 1977, *MNRAS*, 179, 433
- Blandford R.D., Konigl A., 1979, *ApJ*, 232, 34
- Blandford R.D., Payne D.G., 1982, *MNRAS*, 199, 883
- Blandford R.D., Begelman M.C., 1999, *MNRAS*, 303, L1
- Böttcher M., 2001, *ApJ*, 553, 960
- Böttcher M., Jackson D.R., Liang E.P., 2003, *ApJ*, 586, 389
- Bowyer S., Byram E.T., Chubb T.A., Friedman M., 1965, *Sci*, 147, 394
- Cadolle Bel M., et al., 2006, *A&A*, 446, 591
- Celotti A., Fabian A.C., Rees M.J., 1992, *MNRAS*, 255, 419
- Chang J. S., Cooper G., 1970, *JCP*, 6, 1
- Chaty S., Haswell C.A., Malzac J., Hynes R.I., Shrader C.R., Cui W., 2003, *MNRAS*, 346, 689.
- Collin-Souffrin S., Czerny B., Dumont A.-M., Zycki P. T., 1996, *A&A*, 314, 393
- Collin S., Abrassart A., Czerny B., Dumont A.-M., Mouchet M., 2001, *EAS*, 1, 35

- Coppi P.S., 1992, MNRAS, 258, 657
- Coppi P. S. 1999, ASP Conf. Ser. 161: High Energy Processes in Accreting Black Holes, 161, 375
- Corbel S., Fender R.P., Tzioumis A.K., Nowak M., McIntyre V., Durouchoux P., Sood R., 2000, A&A, 359, 251
- Corbel S., Nowak M.A., Fender R.P., Tzioumis A.K., Markoff S., 2003, A&A, 400, 1007
- Crummy J., Fabian A.C., Gallo L., Ross R.R., 2006, MNRAS, 365, 1067
- Czerny B., Dumont A.M., 1998, A&A, 338, 386
- Del Santo M., Malzac J., Ubertini P., Belloni T., 2006, PoS(MQW6)076, <http://pos.sissa.it/>
- Done C., Nayakshin S., 2001, MNRAS, 328, 616
- Done C., Nayakshin S., 2007, MNRAS, 377, L59
- Done C., Gierliński M., Kubota A., 2007, A&AR, in press, [arXiv:0708.0148](http://arxiv.org/abs/0708.0148)
- Dumont A.-M., Abrassart A., Collin S., 2000, A&A, 357, 823
- Esin A.A., McClintock J.E., Narayan R., 1997, ApJ, 489, 865
- Fabian A. C., Ballantyne D. R., Merloni A., Vaughan S., Iwasawa K., Boller T., 2002, MNRAS, 331, L35
- Fabian A.C., Miniutti G., Gallo L., Boller Th., Tanaka Y., Vaughan S., Ross R.R., 2004, 353, 1071
- Fabian A.C., Miniutti G., Iwasawa K. and Ross R.R., 2005, MNRAS, 361, 795
- Fender R., et al., 1999, ApJl, 519, L165
- Fender R.P., 2001, MNRAS, 322, 31
- Fender R. P., Gallo E., Jonker P. G., 2003, MNRAS, 343, L99
- Fender R.P., 2006, in Compact Stellar X-ray Sources, ed. W.H.G. Lewin & M. van der Klis (Cambridge: Cambridge University Press), p 381, [astro-ph/0303339](http://arxiv.org/abs/astro-ph/0303339).
- Ferland G. J., Rees M. J., 1988, ApJ, 332, 141
- Ferreira J. 1997, A&A, 319, 340
- Ferreira J., Petrucci P.-O., Henri G., Saugé L., Pelletier G., 2006, A&A, 447, 813
- Galeev A. A., Rosner R., Vaiana G. S., 1979, ApJ, 229, 318
- Gallo E., Fender R. P., Pooley G. G., 2003, MNRAS, 344, 60
- Gammie C., 1998, MNRAS, 297, 929
- Gandhi P., Fabian A., Suebsuwong T., Malzac J., Miniutti G., Wilman R., 2007, MNRAS, in press, [arXiv:0709.1984](http://arxiv.org/abs/0709.1984)
- Garcia M., Brown W., Pahre M., McClintock J., Callanan P., Garnavich P., 2000, IAUCirc, 7392, 2
- Ghisellini G., Guilbert P. W., Svensson R., 1988, ApJ, 334, L5
- Ghisellini G., Haardt F., Svensson R., 1998, MNRAS, 297, 348
- Ghisellini G., Haardt F., Matt G., 2004, A&A, 413, 535
- Gierliński M., et al., 1999, MNRAS, 309, 496
- Gierliński M., Done C., 2004, MNRAS, 349, L7
- Gilfanov M., Churazov E., Revnivtsev M., 2000, [sgwa.work](http://arxiv.org/abs/sgwa/work), 114, [astro-ph/0002415](http://arxiv.org/abs/astro-ph/0002415)
- Guilbert P.W., Rees M.J., 1988, MNRAS, 233, 475
- Haardt F., Maraschi L., 1991, ApJl, 380, L51
- Haardt F., Maraschi L., 1993, ApJ, 413, 507
- Haardt F., Maraschi L., Ghisellini G., 1994, ApJl, 432, L95
- Haswell C. A., Skillman D., Patterson J., Hynes R. I., Cui W., 2000, IAUC, 7427, 1
- Henri G., Pelletier G., 1991, ApJ, 383, L7
- Henri G., Petrucci P.O., 1997, A&A, 326, 87

- Hjellming R. M., Johnston K. J. 1988, *ApJ*, 328, 600  
Hynes R. I., et al., 2003, *MNRAS*, 345, 292  
Ibragimov A., Poutanen J., Gilfanov M., Zdziarski A. A., Shrader C. R., 2005, *MNRAS*, 362, 1435  
Ichimaru S., 1977, *ApJ*, 214, 840  
Joinet A., Jourdain E., Malzac J., Roques J. P., Schönfelder V., Ubertini P., Capitanio F., 2005, *ApJ*, 629, 1008  
Joinet A., Jourdain E., Malzac J., Roques J. P., Corbel S., Rodriguez J., Kalemci E., 2007, *ApJ*, 657, 400  
Jourdain E., Bassani L., Bouchet L. et al., 1992, *A&A*, 256, L38  
Jourdain E., Roques J. P., 1995, *ApJ*, 440, 128  
Kanbach G., Straubmeier C., Spruit H. C., Belloni T., 2001, *Nature*, 414, 180  
Katarzyński K., Ghisellini G., Svensson R., Gracia J., 2006, *A&A*, 451, 739  
Kazanas D., Hua X.M., Titarchuk L., 1999, *ApJ*, 480, 735.  
Körding E. G., Fender R. P., Migliari S., 2006, *MNRAS*, 369, 1451  
Krolik J.H., 1998, *MNRAS*, 498, L13  
Kuncic Z., Blackman E.G., Rees M.J., 1996, *MNRAS*, 283, 1322  
Kuncic Z., Celotti A., Rees M.J., 1997, *MNRAS*, 284, 717  
Liang E. P. T., Price R. H., 1977, *ApJ*, 218, 247  
Lightman A. P., Eardley D. M., 1974, *ApJ*, 187, L1  
Ling J.C., Wheaton W.A., Wallyn P. et al., 1997, *ApJ*, 484, 375  
Livio, M., Ogilvie G. I., Pringle J. E., 1999, *ApJ*, 512, 100  
Maccarone T. J., Gallo E., Fender R., 2003, *MNRAS*, 345, L19  
Malzac J., Jourdain E., Petrucci P.O., Henri G., 1998, *A&A*, 336, 807  
Malzac J., Jourdain E., 1999, *ApL&C*, 38, 201  
Malzac J., Jourdain E., 2000, *A&A*, 359, 843.  
Malzac J., 2001a, in “Similarities and Universality in Relativistic Flows”, Proceedings of the Euroconference held in Mykonos, Greece, 1-5 October 2000, Ed. M. Georganopoulos, A. Guthmann, K. Manolakou, A. Markowith, Logos Verlag, Berlin, p. 33.  
Malzac J., 2001b, *AIPC*, 587, 385  
Malzac J., 2001c, *MNRAS*, 325, 1625  
Malzac J., Beloborodov A. M., Poutanen J., 2001, *MNRAS*, 326, 417  
Malzac J., Celotti A., 2002, *MNRAS*, 335, 23  
Malzac J., Petrucci P.-O., 2002, *MNRAS*, 336, 1209  
Malzac J., Belloni T., Spruit H. C., Kanbach G., 2003, *A&A*, 407, 335  
Malzac J., Merloni A., Fabian A. C., 2004, *MNRAS*, 351, 253  
Malzac J., Dumont A. M., Mouchet M., 2005, *A&A*, 430, 761  
Malzac J., et al., 2006, *A&A*, 448, 1125  
Marcowith A., Malzac J., 2003, *A&A*, 409, 9  
Markoff S., Falcke H., Fender R., 2001, *A&A*, 372, L25  
Markoff S., Nowak M., Corbel S., Fender R., Falcke H., 2003, *New Astronomy Review*, 47, 491  
Markoff S., Nowak M. A., Wilms J., 2005, *ApJ*, 635, 1203  
McClintock J. E., et al., 2001, *ApJ*, 555, 477  
McClintock J.E., Remillard R.A., 2006, in *Compact Stellar X-ray Sources*, ed. W.H.G. Lewin & M. van der Klis (Cambridge: Cambridge University Press), p157, astro-ph/0306213.  
McConnell M.L., Zdziarski A.A., Bennett K. et al., 2002, *ApJ*, 572, 984  
Merloni A., Di Matteo T., Fabian A. C., 2000, *MNRAS*, 318, L15

- Merloni A., Fabian, A. C., 2002, MNRAS, 332, 165
- Merloni A., Malzac J., Fabian A. C., Ross R. R., 2006, MNRAS, 370, 1699
- Meier D. L., 2001, ApJl, 548, L9
- Middleton M. J., Done C., Gierliński M., 2007, MNRAS in press, arXiv:0704.2970
- Miller K. A., Stone J. M., 2000, ApJ, 534, 398
- Miller J. M., Homan J., Steeghs D., Rupen M., Hunstead R. W., Wijnands R., Charles P. A., Fabian, A. C., 2006, ApJ, 653, 525
- Miller J. M., 2007, ARAA in press, arXiv:0705.0540
- Miniutti G., Fabian A. C., Goyder R., Lasenby A. N., 2003, MNRAS, 344, L22
- Miniutti G., Fabian A. C., 2004, MNRAS, 349, 1435
- Miniutti G., Fabian A.C., Miller J.M., 2004, MNRAS, 351, 466
- Miyamoto M. , Kitamoto S., 1989, Natur, 342, 773.
- Nandra K., George I.M., 1994, MNRAS, 267, 974
- Narayan R., Yi I., 1994, ApJl, 428, L13
- Nayakshin S., Melia F., 1998, ApJS, 114, 269
- Nayakshin S., 2000, ApJ, 534, 718
- Neronov A., Aharonian F., 2007, ApJ in press, arXiv:0704.3282
- Papadakis I. E., Petrucci P. O., Maraschi L., McHardy I. M., Uttley P., Haardt F., 2002, ApJ, 573, 92
- Park B., Petrosian V., 1996, ApJ, 103, 255
- Pelletier G., Sol H., 1992, MNRAS, 254, 635
- Petrucci P. O., et al., 2001, ApJ, 556, 716
- Petrucci P. O., et al., 2007, A&A, 470, 889
- Ponti G., Miniutti G., Cappi M., Maraschi L., Fabian A. C., Iwasawa K., 2006, MNRAS, 368, 903
- Porquet D., 2006, A&A, 445, L5
- Poutanen J., Svensson R., 1996, ApJ, 470, 249
- Poutanen J., Krolik J. H., Ryde F., 1997, MNRAS, 292, L21
- Pringle J. E., 1976, MNRAS, 177, 65
- Remillard R., Morgan E., Smith D., Smith E., 2000, IAU Circ., 7389, 2
- Rees M. J., Phinney E. S., Begelman M. C., Blandford R. D., 1982, Nature, 295, 17
- Rees M.J., 1987, MNRAS, 228, P47
- Rees M.J., Netzer H., Ferland G.J., 1989, MNRAS, 347, 640
- Revnivtsev M., Sunyaev R., Borozdin K., 2000, A&A, 361, L37
- Ross R. R., Fabian A. C., 1993, MNRAS, 261, 74
- Ross R. R., Fabian A. C., Young A. J., 1999, MNRAS, 306, 461
- Ross R. R., Fabian A. C., 2005, MNRAS, 358, 211
- Rossi S., Homan J., Miller J.M., Belloni T., 2005, MNRAS, 360, 763
- Rykoff E. S., Miller J. M., Steeghs D., Torres M. A. P., 2007, ApJ, 666, 1129
- Schurch N. J., Done C., 2006, MNRAS, 371, 81
- Schurch N. J., Done C., 2007, MNRAS in press, arXiv:0706.1885
- Shakura N. I., Sunyaev R. A., 1973, A&A, 24, 337
- Shapiro S. L., Lightman A. P., Eardley D. M., 1976, ApJ, 204, 187
- Sol H., Pelletier G., Asseo E., 1989, MNRAS, 237, 411
- Sobolewska M. A., Done C., 2007, MNRAS, 374, 150
- Spruit H. C., Kanbach G., 2002, A&A, 391, 225
- Stern B. E., Begelman M. C., Sikora M., Svensson R., 1995a, MNRAS, 272, 291

- Stern B. E., Poutanen J., Svensson R., Sikora M., Begelman M. C., 1995b, *ApJ*, 449, L13
- Suebsuwong T., Malzac J., Jourdain E., Marcowith A., 2006, *A&A*, 453, 773
- Sunyaev R. A., Titarchuk L. G., 1980, *A&A*, 86, 121
- Stirling, A. M., Spencer, R. E., de la Force, C. J., Garrett, M. A., Fender, R. P., Ogle, R. N. 2001, *MNRAS*, 327, 1273
- Svensson R., Zdziarski A. A., 1994, *ApJ*, 436, 599
- Tagger M., Pellat R., 1999, *A&A*, 349, 1003
- Tagger M., Varnière P., Rodriguez J., Pellat R., 2004, *ApJ*, 607, 410
- Tananbaum, H., Gursky, H., Kellogg, E., Giacconi, R., Jones, C. 1972, *ApJL*, 177, L5
- Turner N. J., Stone J. M., Sano T., 2002, *ApJ*, 566, 148
- Turner N.J., Stone J.M., Krolik J.H., Sano T., 2003, *ApJ*, 593, 992
- Turner N.J., 2004, *ApJL*, 605, L45
- Turner N.J., Blaes O., Socrates A., Begelman M.C., 2005, *ApJ*, 624, 267
- van der Klis M., 2006, in *compact Stellar X-ray sources*, Eds. W.H.G. Lewin and M. van der Klis, Cambridge University Press, 39-112, [ [astro-ph/0410551](#) ]
- Wardziński G., Zdziarski A. A., 2000, *MNRAS*, 314, 183
- Yuan F., 2001, *MNRAS*, 324, 119
- Yuan F., 2003, *ApJL*, 594, L99
- Yuan F., Cui W., Narayan R., 2005, *ApJ*, 620, 905
- Yuan F., Zdziarski A. A., Xue Y., Wu X.-B., 2007, *ApJ*, 659, 541
- Zdziarski A. A., Lubinski P., Smith D. A., 1999, *MNRAS*, 303, L11
- Zdziarski A. A., Poutanen J., Paciesas W. S., Wen L., 2002, *ApJ*, 578, 357
- Zdziarski A. A., Lubiński P., Gilfanov M., Revnivtsev M., 2003, *MNRAS*, 342, 355
- Zdziarski A. A., Gierliński M., 2004, *Progress of Theoretical Physics Supplement*, 155, 99
- Zdziarski A. A., Gierliński M., Mikołajewska J., Wardziński G., Smith D. M., Alan Harmon B., Kitamoto S., 2004, *MNRAS*, 351, 791
- Zycki P. T., Krolik J. H., Zdziarski A. A., Kallman T. R., 1994, *ApJ*, 437, 597